General Disclaimer

One or more of the Following Statements may affect this Document

- This document has been reproduced from the best copy furnished by the organizational source. It is being released in the interest of making available as much information as possible.

- This document may contain data, which exceeds the sheet parameters. It was furnished in this condition by the organizational source and is the best copy available.

- This document may contain tone-on-tone or color graphs, charts and/or pictures, which have been reproduced in black and white.

- This document is paginated as submitted by the original source.

- Portions of this document are not fully legible due to the historical nature of some of the material. However, it is the best reproduction available from the original submission.

NATIONAL AERONAUTICS AND SPACE ADMINISTRATION

The Deep Space Network

Progress Report 42-24

September and October 1974

(NASA-CR-141147) THE DEEP SPACE NETWORK Progress Report, Sep. - Oct. 1974 (Jet Propulsion Lab.) 174 p HC $6.25 CSCL 17B

N75-14010

Unclas G3/32 05039

JET PROPULSION LABORATORY
CALIFORNIA INSTITUTE OF TECHNOLOGY
PASADENA, CALIFORNIA

December 15, 1974

NATIONAL AERONAUTICS AND SPACE ADMINISTRATION

The Deep Space Network

Progress Report 42-24

September and October 1974

JET PROPULSION LABORATORY
CALIFORNIA INSTITUTE OF TECHNOLOGY
PASADENA, CALIFORNIA

December 15, 1974

Prepared Under Contract No. NAS 7-100
National Aeronautics and Space Administration

Preface

Beginning with Volume XX, the Deep Space Network Progress Report changed from the Technical Report 32- series to the Progress Report 42- series. The volume number continues the sequence of the preceding issues. Thus, Progress Report 42-20 is the twentieth volume of the Deep Space Network series, and is an uninterrupted follow-on to Technical Report 32-1526, Volume XIX.

This report presents DSN progress in flight project support, tracking and data acquisition (TDA) research and technology, network engineering, hardware and software implementation, and operations. Each issue presents material in some, but not all, of the following categories in the order indicated:

Description of the DSN

Mission Support
- Ongoing Planetary/Interplanetary Flight Projects
- Advanced Flight Projects

Radio Science
- Radio Science Support
- Special Projects

Supporting Research and Technology
- Tracking and Ground-Based Navigation
- Communications–Spacecraft/Ground
- Station Control and Operations Technology
- Network Control and Data Processing

Network Engineering and Implementation
- Network Control System
- Ground Communications
- Deep Space Stations

Operations
- Network Operations
- Network Control System Operations
- Ground Communications
- Deep Space Stations

Planning and Facilities
- TDA Planning
- Facility Engineering

In each issue, the part entitled "Description of the DSN" describes the functions and facilities of the DSN and may report the current configuration of one of the five DSN systems (Tracking, Telemetry, Command, Monitor and Control, and Test and Training).

The work described in this report series is either performed or managed by the Tracking and Data Acquisition organization of JPL for NASA.

Contents

Network Control and Data Processing

NETWORK ENGINEERING AND IMPLEMENTATION

Deep Space Stations

OPERATIONS

Network Operations

DSN Functions and Facilities

N. A. Renzetti
Office of Tracking and Data Acquisition

The objectives, functions, and organization of the Deep Space Network are summarized. Deep space station, ground communication, and network operations control capabilities are described.

The Deep Space Network (DSN), established by the National Aeronautics and Space Administration (NASA) Office of Tracking and Data Acquisition (OTDA) under the system management and technical direction of the Jet Propulsion Laboratory (JPL), is designed for two-way communications with unmanned spacecraft traveling approximately 16,000 km (10,000 mi) from Earth to the farthest planets of our solar system. It has provided tracking and data acquisition support for the following NASA deep space exploration projects, for which JPL has been responsible for the project management, development of the spacecraft, and conduct of mission operations:

(1) Ranger.

(2) Surveyor.

(3) Mariner Venus 1962.

(4) Mariner Mars 1964.

(5) Mariner Venus 1967.

(6) Mariner Mars 1969.

(7) Mariner Mars 1971.

(8) Mariner Venus/Mercury 1973.

The DSN has also provided tracking and data acquisition support for the following projects:

(1) Lunar Orbiter, for which the Langley Research Center carried out the project management, spacecraft development, and mission operations functions.

(2) Pioneer, for which the Ames Research Center carried out the project management, spacecraft development, and mission operations functions.

(3) Apollo, for which the Lyndon B. Johnson Space Center was the project center and the Deep Space Network supplemented the Spaceflight Tracking and Data Network (STDN), which is managed by the Goddard Space Flight Center (GSFC).

(4) Helios, a joint United States/West Germany project.

(5) Viking, for which the Langley Research Center provides the project management and Lander spacecraft, and conducts mission operations, and for which JPL provides the Orbiter spacecraft.

The Deep Space Network is one of two NASA networks. The other, the Spaceflight Tracking and Data Network, is under the system management and technical direction of the Goddard Space Flight Center. Its function is to support manned and unmanned Earth-orbiting and lunar scientific and advanced technology satellites. Although the DSN was concerned with unmanned lunar spacecraft in its early years, its primary objective now and into the future is to continue its support of planetary and interplanetary flight projects.

A development objective has been to keep the network capability at the state of the art of telecommunications and data handling and to support as many flight projects as possible with a minimum of mission-dependent hardware and software. The DSN provides direct support to each flight project through that project's tracking and data systems. This management element is responsible for the design and operation of the hardware and software in the DSN which are required for the conduct of flight operations.

As of July 1972, NASA undertook a change in the interface between the network and the flight projects. Since January 1, 1964, the network, in addition to consisting of the Deep Space Stations and the Ground Communications Facility, had also included the Mission Control and Computing Facility and had provided the equipment in the mission support areas for the conduct of mission operations. The latter facilities were housed in a building at JPL known as the Space Flight Operations Facility (SFOF). The interface change was to accommodate a hardware interface between the network operations control functions and the mission control and computing functions. This resulted in the flight project's picking up the cognizance of the large general-purpose digital computers, which were used for network processing as well as mission data processing. It also assumed cognizance of all of the equipment in the flight operations facility for display and communications necessary for the conduct of mission operations. The network has already undertaken the development of hardware and computer software necessary to do its network operations control and monitor functions in separate computers. This activity became known as the Network Control System implementation. A characteristic of the new interface is that the network provides direct data flow to and from the stations via appropriate ground communications equipment to Mission Operations Centers, wherever they may be; namely, metric data, science and engineering telemetry, and such network monitor data as are useful to the flight project. It accepts command data from the flight project directly into the ground communications equipment for transmission to the station and thence to the spacecraft in a standardized format.

In carrying out its functions, the network activities can be divided into two general areas. The first includes those functions which are associated with the in-flight support and in tracking the spacecraft; its configuration can be characterized as follows:

(1) *DSN Tracking System.* Generates radio metric data; i.e., angles, one- and two-way doppler and range, and transmits raw data to mission control.

(2) *DSN Telemetry System.* Receives, decodes, records, and retransmits engineering and scientific data generated in the spacecraft to Mission Control.

(3) *DSN Command System.* Accepts coded signals from Mission Control via the Ground Communications Facility (GCF) and transmits them to the spacecraft in order to initiate spacecraft functions in flight.

The second category of activity supports testing, training, and network operations control functions and is configured as follows:

(1) *DSN Monitor and Control System.* Instruments, transmits, records, and displays those parameters of the DSN necessary to verify configuration and validate the network. Provides operational direction and configuration control of the network and primary interface with flight project mission control personnel.

(2) *DSN Test and Training System.* Generates and controls simulated data to support development, test, training, and fault isolation within the DSN. Participates in mission simulation with flight projects.

The capabilities needed to carry out the above functions have evolved in three technical areas:

(1) The Deep Space Stations that are distributed around Earth and which, prior to 1964, formed part of the Deep Space Instrumentation Facility. The technology involved in equipping these stations is strongly related to the state of the art of telecommunications and flight/ground design considerations and is almost completely multimission in character. Table 1 gives a description of the Deep Space Stations and the Deep Space Communications Complexes (DSCCs) they comprise.

(2) Ground communications. This technology supports the Earth-based point-to-point voice and data communications from the stations to the Network Operations Control Area at JPL, Pasadena, and to the Mission Operations Centers, wherever they may be. It is based largely on the capabilities of the common carriers throughout the world which are engineered into an integrated system by the Goddard Space Flight Center for support of all NASA programs. The term "Ground Communications Facility" is used for the sets of hardware and software needed to carry out the functions.

The Network Operations Control Center is the functional entity for centralized operational control of the network and interfaces with the users. It has two separable functional elements; namely, Network Operations Control and Network Data Processing.

The functions of the Network Operations Control Center are:

(1) Control and coordination of network support to meet commitments to network users.

(2) Utilization of the network data processing computing capability to generate all standards and limits required for network operations.

(3) Utilization of network data processing computing capability to analyze and validate the performance of all network systems.

The personnel who carry out the above functions are on the first floor of Building 230, wherein mission operations functions are carried out by certain flight projects. Network personnel are directed by an Operations Control Chief. The functions of the Network Data Processing are:

(1) Processing of data used by Network Operations Control for the control and analysis of the network.

(2) Display in Network Operations Control Area of data processed in Network Data Processing Area.

(3) Interface with communications circuits for input to and output from Network Data Processing Area.

(4) Data logging and production of the intermediate data records.

The personnel who carry out these functions are located in Building 202, which is approximately 200 m from Building 230. The equipment consists of minicomputers for real-time data system monitoring, two XDS Sigma 5's, display, magnetic tape recorders, and appropriate interface equipment with the ground data communications.

Table 1. Tracking and data acquisition stations of the DSN

DSCC	Location	DSS	DSS serial designation	Antenna		Year of initial operation
				Diameter, m (ft)	Type of mounting	
Goldstone	California	Pioneer	11	26(85)	Polar	1958
		Echo	12	26(85)	Polar	1962
		(Venus)[a]	13	26(85)	Az-El	1962
		Mars	14	64(210)	Az-El	1966
Tidbinbilla	Australia	Weemala	42	26(85)	Polar	1965
		Ballima	43	64(210)	Az-El	1973
—	Australia	Honeysuckle Creek	44	26(85)	X-Y	1973
Madrid	Spain	Robledo	61	26(85)	Polar	1965
		Cebreros	62	26(85)	Polar	1967
		Robledo	63	64(210)	Az-El	1973

[a]A maintenance facility. Besides the 26-m (85-ft) diam Az-El mounted antenna, DSS 13 has a 9-m (30-ft) diam Az-El mounted antenna that is used for interstation time correlation using lunar reflection techniques, for testing the design of new equipment, and for support of ground-based radio science.

Mariner Venus/Mercury 1973 Mission Support

E. K. Davis
DSN Systems Engineering Office

This report covers the period from March 1, 1974, through April 15, 1974. April 15, 1974, marked the end of the Mariner Venus/Mercury 1973 (MVM'73) Project's primary mission and the beginning of the Mariner 10 Extended Mission Project. Consequently, this is the final report in the MVM'73 series; however, future reports will continue to summarize DSN support for the extended mission. March 1974 proved to be the most dynamic and critical period of this rather eventful mission. DSN preparations for trajectory correction maneuver (TCM) 3 and for Mercury encounter were completed, and support was provided in a near-flawless manner. In addition, this period saw the correction of some spacecraft problems and the occurrence of new problems requiring the DSN to respond rapidly with appropriate changes in plans, procedures, configurations, and schedules.

I. Planning Activities

During early March 1974, the DSN gave priority to preparations for TCM 3 and to development of the final sequence of events for Mercury encounter. TCM 3 was planned to occur over Deep Space Station (DSS) 14 on March 16, and the encounter TV sequence was planned around a 22.5-kbps data rate, rather than 117.6 kbps, because of the spacecraft antenna feed problem. However, two significant events during the first week of March 1974 required significant changes to these near-final arrangements.

On March 4, 1974, the spacecraft antenna problem corrected itself, thus reopening the possibility of real-time (117.6-kbps) TV operations at Mercury encounter. Further, on March 6, 1974, the spacecraft lost lock on Canopus, and gyros came on to provide attitude stability. However, the roll gyro began oscillating, which resulted in high consumption of attitude control gas. Gas usage effects on the orbit were such as to shift TCM 3 from the DSS 14 to the DSS 43 view period. Further orbit refinements again shifted the TCM to occur over DSS 63.

These problems and changes resulted in a heavy, unanticipated replanning load at a time when plans should have been in the final stage for the approaching encounter with Mercury. Revival of the 117-kbps TV sequence required development of special telecommunications link performance measurement tests, changes to planned DSS configurations, and schedule negotiations to accommodate MVM'73 and Pioneer during encounter. Orbit uncertainties due to nongravitational forces necessitated development and execution of special procedures for generation of simultaneous doppler data and near-simultaneous ranging data to accurately redefine the orbit following TCM 3. Furthermore, to preclude excessive gas consumption during any future loss-of-Canopus event, the spacecraft was placed into a "free-drift" mode using solar pressure on solar panels as an assist to attitude stabilization. In this mode, automatic gyro turn-on was inhibited. Consequently, loss of Canopus would result in the spacecraft's high-gain antenna drifting off the earth line, and 64-m DSS support would be needed for reacquisition. Therefore, special agreements were negotiated with the Pioneer Project, and new DSN procedures were developed wherein one telemetry string at the 64-m stations would always be configured for immediate MVM'73 support.

The introduction of these late but necessary changes shortly before the critical encounter period caused a great deal of DSN concern regarding the Network's ability to avoid operational errors which would be detrimental to the primary mission objectives. DSN Operations planners and advisors provided close support during this high-risk situation to help assure that required results were achieved.

II. Program Control

Weekly status meetings continued throughout this reporting period. Open implementation tasks and problem areas were tracked until appropriate closures were accomplished. Reports included weekly status messages via teletype and monthly inputs to the Project Management Report.

On March 7, 1974, the DSN conducted a special review of various discrepancy areas in the Network, particularly those which represented continuing problems and those which had a potential to impact Mercury encounter support. The Discrepancy Report (DR) Review Board consisted of representatives from DSN Operations and Engineering. Following is a summary of the significant items discussed.

A. Planetary Ranging

The recently implemented planetary ranging capability soon logged a number of discrepancies. Many of these problems were traceable to a lack of operational experience, which significantly improved with time. However, error dispersions continued to be larger than anticipated, and frequent biases and offsets were observed between and within station passes. DSS 63 exhibited a rather consistent 20-m bias. The consensus was that this ranging performance would meet MVM'73 navigation requirements and that ranging assemblies should not be perturbed by any rework prior to end of the mission. Recommended areas for on-going study included: (1) recalculate and verify the 64-m antenna Z-height, (2) check for timing errors as a possible cause, (3) resurvey the DSS 63 site location, and (4) evaluate calibration accuracies using the zero-delay device, and as a function of antenna angle position.

B. DSS Command Subcarrier-Frequency and Bit-Rate Error Alarms

Alarms of this nature occur periodically and account for a large percentage of open DRs in the system; 30 were open at the time of the review. It is important to note that these are alarms, not aborts. The DSN has experienced only one command abort for MVM'73, which was due to an erroneous bit rate. Standard practice is to set the subcarrier-frequency alarm limit tighter than the Project abort limit; e.g., alarm at ±0.2 Hz, abort at ±0.3 Hz deviation. Analysis of DSS analog tape readouts disclosed that 80% of the bit-rate error alarms were false alarms resulting from bit-rate detection circuitry errors rather than actual bit-rate errors.

Two approved engineering change orders which would correct a clock-counter interface problem were available for implementation. However, it was decided that installation would be delayed until after Mercury encounter. Also, a widening of the subcarrier frequency tolerance can be accommodated easily during prepass initialization, but the Project requested that the present alarm limits be maintained.

When these alarms occur, they usually clear immediately, and normal commanding is continued. Infrequently, alarms persist, requiring switch to the backup command string. In either case, short delays have had little or no effect on mission operations, since Mariner 10 is an automated spacecraft. However, concern increases with the number of spacecraft emergencies requiring critical ground command activity.

C. Data Decoder Assembly

Although installation of new selector channels and other modifications significantly improved data decoder assembly (DDA) performance, problems continued throughout the Network. A number of discrepancies were grouped into two categories: DDA external and DDA internal.

(1) DDA external: This category includes those events involving DDA halts and alarms. These problems are intermittent and are usually cleared in less than 10 min by DDA reinitialization or reload. Cause analysis has been difficult because of a lack of data. Deep Space Stations need to dump the DDA memory when a halt/alarm occurs in order to get useful trouble-shooting data; however, most projects are reluctant to approve an additional 15–20 min data outage while this is done. Post-review coordination with the MVM'73 Project resulted in an agreement and procedure for DDA memory dumps as required when critical data were not being handled.

(2) DDA internal: This category includes those discrepancies involving bit errors, improper data sequences, and timing errors. Telemetry data timing errors are now being worked around by special operational procedures involving front panel restarts when errors are observed. Of more concern is the mixing of data in the DDA through a linear combination of bits. This was observed on some of the Venus encounter digital original data records. All bits were recorded but were out of sequence in a systematic interleaving pattern. It was suggested that this was an initialization procedure problem. Actions were assigned for special testing to verify the specific cause and obtain a solution. Results of these tests are discussed in Section III-A2.

The DSN Operations Status Review for Mercury encounter was conducted on March 21, 1974. The purpose was to evaluate the final status of encounter preparations and review potential problem areas. Subjects covered included: test and training, documentation updates, encounter time lines, occultation strategy, configurations, configuration freeze plans, data shipment plans, staffing, and discrepancy report status. All items exhibited a satisfactory readiness posture for the start of encounter operations.

III. Implementation Activities

A. Deep Space Stations

Previous Progress Reports have tracked DSS subsystem implementation progress for MVM'73. All major work was completed prior to Venus encounter in February 1974; consequently, this section continues to diminish, reflecting only tasks to resolve problem areas.

1. Antenna microwave subsystem. An earlier article reported on DSN initiation of emergency implementation of linear polarization tracking capabilities in the 64-m subnet to match the changed polarization in the spacecraft due to high-gain antenna problems. Although this spacecraft problem corrected itself on March 4, 1974, implementation of linear polarization was continued as a contingency against future recurrences. This task, including performance verification tracking tests, was completed by mid-March 1974 as planned.

2. Telemetry and command data subsystem. Return of the spacecraft telecommunications link to normal gain and polarity again made real-time 117.6-kbps TV data possible at Mercury encounter. Consequently, the previously reported problem in digital original data records of 117-kbps data was given priority attention. Special tests were conducted at DSS 14 and Compatibility Test Area (CTA) 21 to determine the cause of recorded data being out of sequence. As suspected, the problem was operationally induced and could be corrected by changes in operational procedures. To avoid having pre-pass countdown simulated data on the record delivered to Project, the original procedure called for loading of virgin tapes following countdown activities. This apparently left the DDA pointers out of phase with the high-density recorder tape position. The high-density cycle at 117 kbps resulted in a linear combination of bits in about 25% of the test cases. Reinitialization of the DDA following loading of new tapes was required to avoid this problem. Special operational instructions to this effect were issued to the DSS. No further indications of the problem were observed in the Mercury encounter data.

3. S/X-band equipment. The special team effort for improvement of the R&D S/X-band performance at DSS 14 was continued throughout this reporting period. Receiver control work, cable replacements, and other trouble-shooting analysis produced an acceptable level of data quality for encounter operations. Previously reported problems with the command modulator assembly switch were not completely resolved prior to Mercury encounter. Therefore, operations were continued in the Block III

exciter rather than the desired Block IV exciter mode. This configuration was acceptable to the MVM'73 Project.

B. DSN Ground Communications

There was no significant DSN communications implementation during this period. However, per NASA request, the DSN did coordinate the planning, configuration, test, and schedules for establishing a video circuit capability from JPL to Goddard Space Flight Center and NASA Headquarters. This service was employed for about 7 h during Mercury encounter to transmit real-time encounter TV and public information broadcasts to these NASA viewers.

IV. Operations Summary

As planned, increasing use was made of the 64-m subnet during March–April 1974 for the trajectory correction maneuver and encounter support. However, Pioneer Project tracking requirements limited the configuration freeze for MVM'73 to an 8-day period around encounter. Standard DSN encounter readiness tests were completed by mid-March 1974. However, special telecommunications link performance and S/X-band performance tests were continued until encounter day. DSN support continued to be satisfactory, with excellent performance demonstrated during the critical encounter sequence and during the occurrence of some additional spacecraft problems.

On March 31 (GMT), at the start of an outgoing TV mosiac sequence, a spacecraft power subsystem problem occurred which resulted in large power dissipations in the spacecraft bus. One of the resulting effects was intermittent reduction of the X-band transponder output power by 27 dB and the development of sidebands on the carrier. A special effort was made at DSS 14 to detect sidebands and analyze their character.

April 15, 1974, marked the end of the successful MVM'73 primary mission. An extended mission for a return to Mercury has been approved. Work on DSN plans for continuing support has been initiated. Future articles will address the Mariner 10 Extended Mission Project.

Summary Report on the Deep Space Network/Viking Flight Project Telecommunications Compatibility

A. I. Bryan
DSN Systems Engineering Section

The Viking Flight Project/Deep Space Network (DSN) Telecommunications Compatibility Test Program consists of three phases: subsystem design, system design, and system verification tests to be performed at the Jet Propulsion Laboratory and at the Air Force Eastern Test Range/Kennedy Space Center complexes. Subsystem design tests were performed with the Viking Orbiter (VO) and the Viking Lander (VL) during 1973. System design compatibility tests were performed with the Viking Orbiter, Viking Lander, and a multiple Viking spacecraft configuration during the summer of 1974. This article describes the system design tests and test results that provided the basis for the establishment of telecommunications system design compatibility between the DSN and the Viking Lander, Viking Orbiter, and a simulated DSN/multiple spacecraft configuration for the Mars planetary orbital operations.

I. Introduction

In order to avoid the difficulty previously experienced by the DSN and Flight Project in establishing and verifying the system interfaces, an overall compatibility test plan, the Viking 1975 Master Integrated Test Plan (MITP) PL-3710005, was developed and agreed to by all major Viking Project systems. The test plan specifies that telecommunications design compatibility would be established at the subsystem and system levels and conclude with a final verification test at Cape Canaveral, Florida, prior to launch. The test plan also specifies the ground and Flight Project equipment/software configuration pretest requirements and the test objectives in all phases.

Results of Phase I testing (subsystem level) have been documented in JPL internal memorandums and are not discussed in this article.

Phase II, system level testing, of the DSN/Viking Project Telecommunications Compatibility Test Program was performed in the summer of 1974, and the results are reported in detail in this summary report. The general objective of this series of tests was to establish the telecommunications system design compatibility between the Orbiter, Lander, a multiple (Orbiter/Lander) spacecraft configuration, and the DSN.

Phase III (system verification) of the test program is to be performed at Cape Canaveral, Florida, between the DSN and each flight Orbiter, Lander, and spacecraft (combined Orbiter and Lander) configuration. The objectives of these tests are to verify continued DSN/Flight Project interface compatibility with flight spacecraft.

Procedures for conducting the compatibility tests for the DSN ground station, as well as test design criteria and test parameters for the ground station hardware and software were prepared by the DSN. Spacecraft telecommunications design performance criteria and test parameters to establish Project nominal and threshold telecommunication conditions were provided by the respective Orbiter/Lander telecommunications teams. The test criteria were included as part of the test procedure to provide real-time assessment of performance. All test procedures, which include test parameters and performance criteria, were approved jointly by the DSN and Flight Project representatives.

II. Phase II Test Report

The Phase II test report includes the DSN/Flight Project compatibility testing between a simulated operational Deep Space Station (CTA 21) and the Viking proof test Orbiter, the Viking spacecraft test Lander, and a simulated multiple spacecraft configuration. For the multiple spacecraft configuration, the proof test Orbiter and spacecraft test Lander were located in the Spacecraft Assembly Facility (SAF). An RF test transmitter, located in the screen room of CTA 21, was used to simulate the second Orbiter S-band downlink.

Each of the three tests is discussed with regard to test objectives, conditions, and results. In addition, Tables 1, 2, and 3 present detailed information on the DSN and Viking spacecraft configurations, test parameters, test criteria, and test results. Table 4 defines the terms used in these tables.

A. DSN/Viking Spacecraft Test Lander Compatibility Testing

1. Test objectives. The objectives of this test were:

(1) To prove telecommunications design compatibility between the DSN and the Viking spacecraft test Lander in accordance with the Master Integrated Test Plan (PL-3710005).

(2) To prove DSN/single spacecraft performance prior to the conducting of the multiple spacecraft RF compatibility tests.

(3) To provide prerequisite data bases for performing the data compatibility tests (DCT 1 through 5) which establish data flow system interface compatibility from the spacecraft via the DSN to the Viking Mission Control and Computing Center (VMCCC).

2. Test conditions. The spacecraft test Lander (S/C TL) was configured to represent a flight spacecraft telecommunications subsystem, and CTA 21 was configured to represent a DSN 64-m antenna station. The S/C TL was located in the screen room of Building 179 (Spacecraft Assembly Facility) at JPL, and CTA 21 is located in Building 125. An S-band RF air link was established between the S/C TL and the ground station. The DSN established a pretest calibration of this air link to an amplitude stability of ±0.2 dB. The ground station software utilized in these tests was the released version of telemetry and command data (TCD) DOI-5050-OP-C, which will be used to support the mission.

3. Test descriptions. Table 1 provides a listing of the tests performed; detailed test descriptions are contained in Ref. 1 for each test listed. In general, nominal and threshold tests are performed in the areas of S-band RF, telemetry, command, and metric data.

4. Test results. The results of the 60 h of tests established telecommunications system design compatibility between the Viking Lander spacecraft and the DSN. Table 1 provides the test data in summary form.

B. DSN/Viking Proof Test Orbiter Compatibility Testing

1. Test objectives. The objectives of this test were:

(1) To establish DSN/Viking Orbiter telecommunications compatibility for telemetry, command, tracking, and metric data in accordance with the Viking Project Master Integrated Test Plan (PL-3710005).

(2) To provide baseline criteria for analysis of the multiple carrier interference effects in the multiple spacecraft RF compatibility tests.

(3) To provide prerequisite data bases for performing data compatibility tests.

2. Test conditions. The Orbiter proof test spacecraft was located in JPL Building 150 (Space Simulator), and S/X-band RF links were established to CTA 21 in Building 125. Both the S-band and X-band links were calibrated by the DSN, and RF amplitude stability was established for a 3-sigma measurement of 0.2 dB for S-band and 1.0 dB for X-band.

With the exception of the Block IV receiver/exciter (an engineering prototype), CTA 21 was configured to simulate a DSN 64-m antenna station utilizing operational hardware and TCD software (DOI-5050-OP-C).

Coordination between the spacecraft and CTA 21 was excellent, and testing was well coordinated considering the Project spacecraft priorities in the Space Simulator, which placed compatibility testing as a second priority.

3. Test descriptions. Table 2 provides a listing of the tests performed; detailed test descriptions are contained in Ref. 1 for each test listed. In general, nominal and threshold tests were performed in the areas of S-band RF, telemetry, command, and metric data.

4. Test results. The results of the 90 h of tests established telecommunications system design compatibility between the Viking Orbiter spacecraft and the DSN. Table 2 summarizes the test results.

C. DSN/Viking Multiple Spacecraft Compatibility testing

1. Test objectives. The objectives of the compatibility tests were as follows:

(1) To verify the performance and operational capability of the DSN in a multiple downlink carrier environment

(2) To ascertain the performance of the Orbiter and Lander under predicted RF interference conditions

(3) To provide baseline criteria as a prerequisite to conducting the multiple spacecraft data compatibility tests (DCT-5)

All tests were accomplished in accordance with Refs. 1 and 2, as revised by VICs 621 and 658.

2. Test conditions. The spacecraft, Orbiter, and Lander, were located in the Spacecraft Assembly Facility. A test transmitter, to simulate the second Orbiter with an S-band RF downlink capability only, was installed in the screen room of CTA 21. S/X-band RF air links were established between the Orbiter spacecraft and CTA 21. Interface with the Lander was established with an S-band RF air link between CTA 21 and SAF. To support these tests, CTA 21 provided two simultaneous S-band uplinks and received and processed telemetry data from three simultaneous downlinks.

3. Test descriptions. In addition to the standard compatibility tests with all RF frequencies at their nominal rest values, the following tests were performed to simulate the potential frequencies of the flight spacecraft under expected doppler effects and S-band power levels during Mars orbital operations. These special RF interference tests are described in detail below, as they are not discussed in Ref. 1. The proof test Orbiter was on RF Channel 9, the spacecraft test Lander was on RF Channel 13, and the test transmitter was assigned to RF Channel 20.

a. False uplink acquisition with ranging. With S-band RF Channels 13 and 20 uplinks adjusted to expected Orbiter RF received levels at Mars distances, ranging modulation was applied to Channel 13 uplink, and the uplink was swept through the assigned Lander channel. The Orbiter was observed for acquisition of a ranging sideband, with subsequent loss of downlink RF lock.

b. False command acquisition with ranging. A single Channel 20 uplink was tuned to a specified offset from the assigned channel frequency. Command and ranging modulation were then applied, and the carrier was swept through Channel 20. The Orbiter was observed for RF and command acquisition, and the Lander was observed for RF acquisition.

c. Radio metric degradation with ranging. With the Orbiter and Lander both in the two-way mode, the Lander uplink was set to an expected Orbiter RF received level, and ranging acquisitions of the Orbiter were conducted to obtain reference performance data. The Lander uplink (Channel 13) was then tuned to a specified offset from the assigned channel frequency. Ranging modulation was applied to the Channel 13 uplink, and the uplink was swept through the frequency band. During the sweep of Channel 13 uplink, continuous ranging acquisitions of the Orbiter were obtained, and data were analyzed for variations in range delay.

d. Viking Lander telemetry degradation by the Viking Orbiter high-rate telemetry. With the Orbiter and Lander both in the two-way mode, a baseline telemetry performance test was conducted. The Orbiter uplink was then tuned to specified frequency offsets, and all telemetry channels, at each frequency offset, were observed for performance degradation.

e. Command and telemetry degradation with ranging. With the Orbiter and Lander both in the two-way mode, the Lander uplink was set to an expected RF Orbiter received level, and continuous commands were sent to the Orbiter to obtain reference performance data. The Lander uplink (Channel 13) was then tuned to a specified offset from the assigned channel frequency. Ranging modulation was applied to the Channel 13 uplink, and the uplink was swept through the frequency band. The Orbiter was observed for loss-of-uplink lock, command anomalies, and telemetry degradation.

4. Test results. The results of the 40 h of tests established telecommunications system design compatibility between the Viking multiple spacecraft and the DSN. Table 3 provides a summary of the test results. The following comments describe test results from the series of special RF interference tests (3a–e above). The RF channels and their center frequencies for these tests are shown in Table 5.

In the special tests, RF frequencies selected to generate RF interference represent considerable offsets from assigned center frequency (ACF) values. However, each of those frequencies is considered possible during the mission. The total offset from ACF was derived from consideration of the VCO rest frequency offset from ACF, VCO drift, temperature effects, and orbital doppler shift. The absolute value of the frequency offset for each test is provided in the discussion below.

Interference from ranging sidebands will occur only during range acquisitions. Immediately following a range acquisition, the code is advanced to the clock component (C_1) only, and all sidebands around higher-order components disappear.

a. False uplink RF acquisition with ranging. The following are the results from the special test described in 3a. The Orbiter uplink (Channel 9) was acquired by the fifth sideband of the second ranging component on the Lander uplink (Channel 13) at a signal level of –137 dBm. The Orbiter was also acquired by the tenth sideband of the third ranging component at a signal level of –150 dBm. These results were as predicted from theoretical analysis. For this test, the Channel 13 uplink was inadvertently set 9 dB below the expected value. The expected interfering levels are, therefore, 9 dB higher than those observed in the test. The frequency offset of Channel 13 was 77.3 kHz below ACF.

Proof Test Orbiter System Problem/Failure Report (P/FR) No. 34395 was generated to document the Orbiter acquisitions observed in this special test.

All tests were successfully completed, and no degradation of downlink thresholds was observed.

b. False command acquisition with ranging. The following are the results from the special test described in 3b. The Orbiter uplink was acquired by the 29th sideband of the third ranging component on a Channel 20 uplink. For this test, the frequency of Channel 20 was set 9.75 kHz below ACF. During the sweep, a command detector in-lock indication was observed.

Proof Test Orbiter System P/FR No., 34395 was generated to document the Orbiter acquisitions observed during this special test.

c. Radio metric degradation with ranging. The following data were obtained from the special test described in 3c: VO reference delay, 5330.1 range units (RU) ± 3.67 (1 sigma); 1 RU = 0.947 ns. VO delay with VL ranging, 5327.3 RU ± 6.64 (1 sigma); 1 RU = 0.947 ns. The data indicated a degradation of the Orbiter ranging function under the established test conditions. The frequency offset on Channel 13 was 77.3 kHz below ACF.

d. Viking Lander telemetry degradation by the Viking Orbiter high-rate telemetry. The following are the results from the special test described in 3d. For this test, two VO (Channel 9) offsets were set. The first offset was established at 27.3 kHz above the Channel 9 ACF, which placed a VO telemetry harmonic on the VL downlink carrier. The second offset was set at 49.4 kHz above the ACF of Channel 9. For this condition, the fifth harmonic of the VO high-rate telemetry channel coincided with the third harmonic of the VL high-rate telemetry channel. In this test, discrepant test data on VL high-rate telemetry were obtained. The low signal-to-noise ratio (SNR) reading remained constant throughout the entire test. This discrepancy was attributed to an intermittent subcarrier demodulator assembly (SDA 2), which had caused anomalies in previous tests. Verification of the cause of the test discrepancy was obtained in the conduct of DCT-5, as the same test parameters were established and the test data obtained were within the established criteria.

A spurious signal (spur) was observed in the VO X-band downlink spectrum during all tests under the conditions of having the Channel 13 uplink transmitter and the VO ranging channel ON. The spur was seen on the spectrum analyzer associated with the Orbiter X-band transmitter support equipment. With the Channel 13 uplink signal

level established at the predicated mission value, the spur was observed to be located ±1.4 MHz (approximately) about the carrier at a level of –20 dB relative to the carrier. No spurs were observed in the S-band downlink spectrum. Since a difference in the Channel 9 and 13 uplink frequencies of 1.36 MHz is within the ranging bandwidth (1.5 MHz) of the VO, the presence of a spur in the X-band downlink is to be expected under these test conditions. The presence of a 1.4-MHz spurious signal under the established test conditions is documented in Proof Test Orbiter System P/FR No. 34392.

e. Command and telemetry degradation with ranging. The following are the results from the special test described in 3e. No degradation in the Orbiter telemetry and command performance was caused by the Lander ranging sidebands. For this test, Lander Channel 13 was offset 77.3 kHz below ACF.

III. Conclusions

The successful completion of the DSN/Viking Flight Project telecommunications system design compatibility tests at JPL represents a significant Project event. It can be assumed with high probability that the system design tests established that the DSN and the Viking spacecraft telecommunications links will satisfy mission objectives and that, when an RF link interference occurs during operations, the interference effects will be reasonably well understood.

The formal compatibility test program developed jointly by the DSN and the Viking Flight Project has been successfully performed on schedule and at anticipated cost. This success has been achieved because of the close coordination and cooperation of the multiple organizations involved.

Phase III of the compatibility test program, to establish the continued telecommunications interface compatibility following transportation of the flight spacecraft to Florida, is scheduled to commence in late January 1975 and will continue until the summer launch in 1975.

References

1. *Deep Space Network/Flight Project Interface Compatibility Test Design Handbook*, 810-8, Rev. A, DSN Standard Practice (JPL internal document).
2. *Viking 1975 Master Integrated Test Plan*, NASA Document PL-3710005.

Test date (1974)	Test title	Test No.	Deep Space Network									
			RCV	EXC	RNG	CMD	Uplink doppler, Hz/s	Uplink offset	CMA SUBC offset	SDA SUBC offset	Mode	RM
7/8	D/L threshold one-way	1A	−145.0 (2)	N/A	OFF	OFF	N/A	N/A	N/A	N/A	5B	
		1B	−149.0 (2)	N/A	OFF	OFF	N/A	N/A	N/A	N/A	6B	
		1C	−149.0 (2)	N/A	OFF	OFF	N/A	N/A	N/A	N/A	7B	
7/9	U/L threshold	2A	−100.0 (2)	−139.5 (1)	OFF	OFF	N/A	N/A	N/A	N/A	3	
			−100.0 (2)	−142.0 (1)	OFF	ON	N/A	N/A	N/A	N/A	3	
7/8		2B	−100.0 (2)	−140.0 (1)	OFF	OFF	N/A	N/A	N/A	N/A	5	
			−100.0 (2)	−142.13 (1)	OFF	ON	N/A	N/A	N/A	N/A	5	
7/8	D/L threshold two-way	3A	−145.0 (2)	−142.5 (1)	OFF	OFF	N/A	N/A	N/A	N/A	3B	
		3B	−145.0 (2)	−142.5 (1)	OFF	OFF	N/A	N/A	N/A	N/A	5B	
		3C	−145.0 (2)	−142.0 (1)	OFF	OFF	N/A	N/A	N/A	N/A	6B	
		3D	−145.0 (2)	−142.0 (1)	OFF	OFF	N/A	N/A	N/A	N/A	7B	
		3E	−145.0 (2)	−142.2 (1)	OFF	ON	N/A	N/A	N/A	N/A	3B/CMD	
		3F	−145.0 (2)	−119.8 (1)	OFF	ON	N/A	N/A	N/A	N/A	5B/CMD	
		3G	−145.0 (2)	−130.0 (1)	ON	OFF	N/A	N/A	N/A	N/A	5AR	
7/9	S/C RCVR pull in	4A	−100.0 (2)	−120.0 (1)	OFF	OFF	N/A	−480 Hz	N/A	N/A	3	
			−100.0 (2)	−120.0 (1)	OFF	OFF	N/A	+480 Hz	N/A	N/A	3	
	S/C range and rate		−100.0 (2)	−142.6 (1)	OFF	OFF	45	+63 kHz	N/A	N/A	3	
			−100.0 (2)	−142.0 (1)	OFF	OFF	45	−63 kHz	N/A	N/A	3	
	S/C rcvr acquisition and tracking rate		−100.0 (2)	−142.5 (1)	OFF	OFF	45	+63 kHz	N/A	N/A	3	
			−100.0 (2)	−142.0 (1)	OFF	OFF	45	−63 kHz	N/A	N/A	3	
	S/C pull in	4B	−100.0 (2)	−120.0 (1)	OFF	OFF	N/A	−480 Hz	N/A	N/A	8	
			−100.0 (2)	−120.0 (1)	OFF	OFF	N/A	+480 Hz	N/A	N/A	8	
	S/C range and rate		−100.0 (2)	−142.0 (1)	OFF	OFF	45	+63 kHz	N/A	N/A	8	
			−100.0 (2)	−142.0 (1)	OFF	OFF	45	−63 kHz	N/A	N/A	8	
	S/C rcvr acquisition and tracking rate		−100.0 (2)	−142.0 (1)	OFF	OFF	45	None	N/A	N/A	8	
			−100.0 (2)	−142.0 (1)	OFF	OFF	45	None	N/A	N/A	8	
7/10	Carrier residual phase jitter	5A	−100.0 dBm	N/A	N/A	N/A	N/A	N/A	N/A	N/A	3B	
			−100.0 dBm	−100.0 dBm	N/A	N/A	N/A	N/A	N/A	N/A	3B	
			−100.0 dBm	−142.0 dBm	N/A	N/A	N/A	N/A	N/A	N/A	3B	
		5B	−100.0 dBm	N/A	N/A	N/A	N/A	N/A	N/A	N/A	5B	
			−100.0 dBm	−100.0 dBm	N/A	N/A	N/A	N/A	N/A	N/A	5B	
			−100.0 dBm	−141.8 dBm	N/A	N/A	N/A	N/A	N/A	N/A	5B	
		5C	−100.0 dBm	N/A	N/A	N/A	N/A	N/A	N/A	N/A	6B	
			−100.0 dBm	−100.0 dBm	N/A	N/A	N/A	N/A	N/A	N/A	6B	
			−100.0 dBm	−142.0 dBm	N/A	N/A	N/A	N/A	N/A	N/A	6B	
		5D	−100.0 dBm	N/A	N/A	N/A	N/A	N/A	N/A	N/A	7B	
			−100.0 dBm	−100.0 dBm	N/A	N/A	N/A	N/A	N/A	N/A	7B	
			−100.0 dBm	−142.0 dBm	N/A	N/A	N/A	N/A	N/A	N/A	7B	

Notes: 1. Ramped from −63 kHz acquired at rest frequency.
2. Ramped from +63 kHz acquired at rest frequency.
3. Ramped from −63 kHz acquired at rest frequency.
4. Ramped from +63 kHz acquired at rest frequency.

Table 1. DSN/Viking spacecraft test Lander compatibility test results

Spacecraft					Test data					Test time, min.	Test comments
EXC	RCVR	PWR	ANT	TWT	RNG	TMU	CDU	Performance	Criteria		
1	2	HI	N/A	1	OFF	A	2	−160.1 dBm	−160 ± 2 dBm	59	DSN RCV signal levels are
2	2	HI	N/A	2	OFF	A	2	−161.1 dBm	−160 ± 2 dBm	41	starting P_c levels.
1	2	HI	N/A	2	OFF	A	2	−160.8 dBm	−160 ± 2 dBm	31	
1	1	HI	N/A	1	OFF	A	1	−153.3 dBm	−150.3 ± 2.5 dBm	32	DSN EXC signal levels are
1	1	HI	N/A	1	OFF	A	1	−152.8 dBm	−150.3 ± 2.5 dBm		starting P_c levels.
1	2	HI	N/A	1	OFF	A	2	−152.4 dBm	−149.2 ± 2.5 dBm	57	
1	2	HI	N/A	1	OFF	A	2	−152.1 dBm	−149.2 ± 2.5 dBm		
1	1	HI	N/A	1	OFF	A	1	−161.9 dBm	−162 ± 2 dBm	37	DSN RCV signal levels are
1	2	HI	N/A	1	OFF	A	2	−161.4 dBm	−162 ± 2 dBm	38	starting P_c levels.
2	2	HI	N/A	2	OFF	A	2	−161.1 dBm	−162 ± 2 dBm	31	
1	2	HI	N/A	2	OFF	A	2	−162.2 dBm	−160 ± 2 dBm	44	
1	1	HI	N/A	1	OFF	A	1	−161.8 dBm	−162 ± 2 dBm	32	
1	2	HI	N/A	1	OFF	A	2	−162.1 dBm	−160 ± 2 dBm	31	
1	2	HI	N/A	1	OFF	A	2	−162.4 dBm	−160 ± 2 dBm	25	
1	1	HI	N/A	1	OFF	A	1	45 s	S/C rcvr must lock		
1	1	HI	N/A	1	OFF	A	1	6 s	to U/L.		
1	1	HI	N/A	1	OFF	A	1	+63.1 kHz	+63.0 kHz	150	
1	1	HI	N/A	1	OFF	A	1	−63.1 kHz	−63.0 kHz		
1	1	HI	N/A	1	OFF	A	1	Acq/trk to +63 kHz	Acq/trk to +63 kHz		See Note 1.
1	1	HI	N/A	1	OFF	A	1	Acq/trk to −63 kHz	Acq/trk to −63 kHz		See Note 2.
2	2	HI	N/A	1	OFF	A	2	6 s	S/C must lock		
2	2	HI	N/A	1	OFF	A	2	6 s	to U/L.		
2	2	HI	N/A	1	OFF	A	2	+63.2 kHz	+63.0 kHz	176	
2	2	HI	N/A	1	OFF	A	2	−63.0 kHz	−63.0 kHz		
2	2	HI	N/A	1	OFF	A	2	Acq/trk to +63 kHz	Acq/trk to +63 kHz		See Note 3.
2	2	HI	N/A	1	OFF	A	2	Acq/trk to −63 kHz	Acq/trk to −63 kHz		See Note 4.
1	1	HI	N/A	1	OFF	A	1	1.97 deg rms	5.0 deg rms		Blk III RCVR and EXC.
1	1	HI	N/A	1	OFF	A	1	3.0 deg rms	5.0 deg rms	60	
1	1	HI	N/A	1	OFF	A	1	14.68 deg rms	None given.		
1	2	HI	N/A	1	OFF	A	2	1.63 deg rms	5.0 deg rms		
1	2	HI	N/A	1	OFF	A	2	2.96 deg rms	5.0 deg rms	40	
1	2	HI	N/A	1	OFF	A	2	17.23 deg rms	None given.		
2	2	HI	N/A	2	OFF	A	2	1.28 deg rms	5.0 deg rms		Blk III RCVR and EXC.
2	2	HI	N/A	2	OFF	A	2	2.74 deg rms	5.0 deg rms	40	
2	2	HI	N/A	2	OFF	A	2	15.99 deg rms	None given.		
1	2	HI	N/A	2	OFF	A	2	1.69 deg rms	5.0 deg rms		
1	2	HI	N/A	2	OFF	A	2	3.56 deg rms	5.0 deg rms	39	
1	2	HI	N/A	2	OFF	A	2	17.52 deg rms	None given.		

Test date (1974)	Test title	Test No.	Deep Space Network RCV	EXC	RNG	CMD	Uplink doppler, Hz/s	Uplink offset	CMA SUBC offset	SDA SUBC offset	Mode	RM
7/9	D/L spectrum analysis	6A	−83.0 dBm	N/A	OFF	OFF	N/A	N/A	N/A	N/A	3B	
			−83.0 dBm	−140.0 dBm	OFF	OFF	N/A	N/A	N/A	N/A	3B	
		6B	−83.0 dBm	−140.0 dBm	OFF	ON	N/A	N/A	N/A	N/A	3B/CMD	
		6C	−83.0 dBm	N/A	OFF	OFF	N/A	N/A	N/A	N/A	5B	
			−83.0 dBm	−120.9 dBm	OFF	OFF	N/A	N/A	N/A	N/A	5B	
		6D	−83.0 dBm	−120.7 dBm	OFF	ON	N/A	N/A	N/A	N/A	5B/CMD	
		6E	−83.0 dBm	N/A	OFF	OFF	N/A	N/A	N/A	N/A	6B	
			−83.0 dBm	−120.0 dBm	OFF	OFF	N/A	N/A	N/A	N/A	6B	
		6F	−83.0 dBm	N/A	OFF	OFF	N/A	N/A	N/A	N/A	7B	
			−83.0 dBm	−120.5 dBm	OFF	OFF	N/A	N/A	N/A	N/A	7B	
		6G	Same as Test 15G. See 15G for results.									
7/10	False lock	7A	−100.0 (2)	−120.0 (1)	OFF	OFF	N/A	+63 kHz	N/A	N/A	N/A	
			−100.0 (2)	−120.0 (1)	OFF	OFF	N/A	−63 kHz	N/A	N/A	N/A	
	U/L spectrum analysis spectrum sweep rate = 200 kHz		−100.0 (2)	−120.0 (1)	OFF	OFF	N/A	N/A	N/A	N/A	N/A	
			−100.0 (2)	−120.0 (1)	OFF	ON	N/A	N/A	N/A	N/A	N/A	
			−100.0 (2)	−120.0 (1)	ON	ON	N/A	N/A	N/A	N/A	N/A	
			−100.0 (2)	−120.0 (1)	ON	OFF	N/A	N/A	N/A	N/A	N/A	
	Spectrum sweep rate = 10 MHz		−100.0 (2)	−120.0 (1)	OFF	OFF	N/A	N/A	N/A	N/A	N/A	
			−100.0 (2)	−120.0 (1)	OFF	ON	N/A	N/A	N/A	N/A	N/A	
			−100.0 (2)	−120.0 (1)	ON	ON	N/A	N/A	N/A	N/A	N/A	
			−100.0 (2)	−120.0 (1)	ON	OFF	N/A	N/A	N/A	N/A	N/A	
7/9	Transponder rest frequency	8A	−100.0 (2)	N/A	OFF	OFF	N/A	N/A	N/A	N/A	3	
			−100.0 (2)	−103.0 (1)	OFF	OFF	N/A	N/A	N/A	N/A	3	
		8B	−100.0 (2)	N/A	OFF	OFF	N/A	N/A	N/A	N/A	5	
			−100.0 (2)	−100.7 (1)	OFF	OFF	N/A	N/A	N/A	N/A	5	
7/10	Auxiliary oscillator frequency	9A	−100.0 (2)	N/A	OFF	OFF	N/A	N/A	N/A	N/A	5	
		9B	−100.2 (2)	N/A	OFF	OFF	N/A	N/A	N/A	N/A	6	
7/12	Command performance	10A	−100.0 (2)	−142.5 (1)	N/A	ON	N/A	N/A	N/A	N/A	3	
			−100.0 (2)	−144.5 (1)	N/A	ON	N/A	N/A	N/A	N/A	3	
		10B	This test was not performed. Test criteria and parameters are contained in Test 10C.									

Notes: 5. Lock obtained by approaching best lock frequency from a +63 kHz offset.
6. Lock obtained by approaching best lock frequency from a −63 kHz offset.

Table 1 (contd)

Spacecraft								Test data		Test time, min.	Test comments
EXC	RCVR	PWR	ANT	TWT	RNG	TMU	CDU	Performance	Criteria		
1	1	HI	N/A	1	OFF	A	1			40	Blk III RCVR and EXC. Photos were taken. There were no apparent spurious components.
1	2	HI	N/A	1	OFF	A	1	To be determined.	No spurious components.		
1	2	HI	N/A	1	OFF	A	1			15	
1	2	HI	N/A	1	OFF	A	2			29	
1	2	HI	N/A	1	OFF	A	2				
1	2	HI	N/A	1	OFF	A	2			11	Discrete Fourier analysis will be performed at a later date.
2	2	HI	N/A	2	OFF	A	2			30	
2	2	HI	N/A	2	OFF	A	2				
1	2	HI	N/A	2	OFF	A	2			21	
1	2	HI	N/A	2	OFF	A	2				
						A		No false lock. The bias doppler did equal 1 MHz whenever an in-lock indication existed.	No false lock. The bias doppler must equal 1 MHz whenever an in-lock condition exists.		See Note 5.
						A					See Note 6.
						A		To be determined.	No spurious components.	60	Photos were taken. There were no apparent spurious components.
						A					
1	1	HI	N/A	1	OFF	A	1	D/L VCO freq = 2112970.156 kHz	2112971.451 ± 30 kHz	51	S/C VCO temp = 14.33 mV at start, 13.88 mV at end.
1	1	HI	N/A	1	OFF	A	1	S/C locked to U/L.	S/C locked to U/L.		
1	2	HI	N/A	1	OFF	A	2	D/L VCO freq = 2112965.659 kHz	2112971.451 ± 30 kHz	61	S/C VCO temp = 14.69 mV at start, 14.06 mV at end.
1	2	HI	N/A	1	OFF	A	2	S/C locked to U/L.	S/C locked to U/L.		
1	2	HI	N/A	1	OFF	A	2	D/L VCO freq = 2294626.4 kHz	2294629.630 ± 20 kHz	44	S/C VCO temp = 14.33 mV at end, 14.42 mV at start.
2	2	HI	N/A	2	OFF	A	2	D/L VCO freq = 2294632.256 kHz	2994629.630 ± 20 kHz	46	S/C VCO temp = 14.06 mV at start, 13.88 mV at end.
1	1	HI	N/A	1	OFF	A	1	Ten 32-word cmds were successfully detected and executed by the S/C. Five 32-word cmds were successfully detected by the S/C.	All commands successfully detected and executed by the S/C.	121	

Test date (1974)	Test title	Test No.	Deep Space Network									
			RCV	EXC	RNG	CMD	Uplink doppler, Hz/s	Uplink offset	CMA SUBC offset	SDA SUBC offset	Mode	RM
7/12	Command performance with and without ranging	10C	−100.0 (2)	−141.5 (1)	OFF	ON	N/A	N/A	N/A	N/A	5AR	
			−100.0 (2)	−141.5 (1)	ON	ON	N/A	N/A	N/A	N/A	5AR	
			−100.0 (2)	−144.0 (1)	OFF	ON	N/A	N/A	N/A	N/A	5AR	
			−100.0 (2)	−143.5 (1)	ON	ON	N/A	N/A	N/A	N/A	5AR	
7/11	Command capability under doppler conditions	11A	−100.0 (2)	−142.5 (1)	OFF	ON	None	+20 kHz	N/A	N/A	3	
			−100.0 (2)	−143.0 (1)	OFF	ON	None	−20 kHz	N/A	N/A	3	
		11B	See Note 7.									
7/10	Ranging channel delay, threshold, and polarity verification	12A	−100.0 (2)	−100.0 (1)	ON	OFF	N/A	N/A	N/A	N/A	5AR	
			−135.0 (2)	−120.2 (1)	ON	OFF	N/A	N/A	N/A	N/A	5AR	
			−135.0 (2)	−120.2 (1)	ON	OFF	N/A	N/A	N/A	N/A	5AR	
			−135.0 (2)	−120.2 (1)	ON	OFF	N/A	N/A	N/A	N/A	5AR	
			−135.0 (2)	−120.3 (1)	ON	OFF	N/A	N/A	N/A	N/A	5AR	
			−135.0 (2)	−130.5 (1)	ON	OFF	N/A	N/A	N/A	N/A	5AR	
			−135.0 (2)	−130.5 (1)	ON	OFF	N/A	N/A	N/A	N/A	5AR	
			−135.0 (2)	−130.5 (1)	ON	OFF	N/A	N/A	N/A	N/A	5AR	
7/11		12B	−99.5 (2)	−99.5 (1)	ON	OFF	N/A	N/A	N/A	N/A	6AR	
			−135.0 (2)	−119.8 (1)	ON	OFF	N/A	N/A	N/A	N/A	6AR	
			−135.0 (2)	−129.5 (1)	ON	OFF	N/A	N/A	N/A	N/A	6AR	
		12C	−100.5 (2)	−100.0 (1)	ON	OFF	N/A	N/A	N/A	N/A	7AR	
			−135.0 (2)	−120.0 (1)	ON	OFF	N/A	N/A	N/A	N/A	7AR	
			−135.0 (2)	−129.5 (1)	ON	OFF	N/A	N/A	N/A	N/A	7AR	
7/11	Ranging acquisition and capability with doppler	13	−135.0 (2)	−120.0 (1)	ON	OFF	None	−20 kHz	N/A	N/A	5AR	
			−135.0 (2)	−130.5 (1)	ON	OFF	None	−20 kHz	N/A	N/A	5AR	
			−135.0 (2)	−120.5 (1)	ON	OFF	None	+20 kHz	N/A	N/A	5AR	
			−135.0 (2)	−130.0 (1)	ON	OFF	None	+20 kHz	N/A	N/A	5AR	
7/9	Modulation index and spectrum analyses	15A	Test 15A was not performed. Test criteria are contained in Test 6A.									
		15B	−83.0 (2)	OFF	OFF	OFF	N/A	N/A	N/A	N/A	8C	
			−83.0 (2)	−14.0 (1)	OFF	ON	N/A	N/A	N/A	N/A	8C	
		15C	−83.0 (2)	OFF	OFF	OFF	N/A	N/A	N/A	N/A	8D	
			−83.0 (2)	−140.0 (1)	OFF	ON	N/A	N/A	N/A	N/A	8D	
		15D	Test 15D was not performed. Test criteria are contained in Test 6E.									

Notes:

7. Command capability under doppler conditions. Test 11B was not performed. The test criteria contained in Test 11B were accomplished in Test 11A; therefore, 11B was deleted as an overtest. A waiver request to delete Test 11B from the MITP was approved during the VL-RF compatibility pretest review.

8. Zero-delay tests have yet to be performed. Thus, at this time, absolute spacecraft delay cannot be determined. Zero-delay tests will be run upon completion of the dual-spacecraft compatibility testing and the spacecraft delay verified.

Table 1 (contd)

Spacecraft								Test data		Test time, min.	Test comments
EXC	RCVR	PWR	ANT	TWT	RNG	TMU	CDU	Performance	Criteria		
1	2	HI	N/A	1	OFF	A	2	Ten 32-word cmds were successfully detected and executed by the S/C. Five 32-word cmds were successfully detected and executed by the S/C. Aborted one cmd.	All commands successfully detected and executed by the S/C.	201	The first of five 32-word cmds aborted. The remaining four 32-word cmds were successfully transmitted.
1	2	HI	N/A	1	OFF	A	2				
1	1	HI	N/A	1	OFF	A	1	All cmds sent were detected and executed by the S/C.	S/C detected and executed 2 cmd series. Ten 32-word cmds dropped lock, reacquired and performed. Five, 10-word cmds.	479	Cmd mod was turned off while at both the + and − offset. U/L was reacquired by the S/C with no problem.
1	1	HI	N/A	1	OFF	A	1			None	
1	2	HI	N/A	1	ON	A	2	5057.3 ns	See Note 9.		
1	2	HI	N/A	1	ON	A	2	5049.7 ns	See Note 9.		
1	2	HI	N/A	1	ON	A	2	5036.5 ns	See Note 10.		
1	2	HI	N/A	1	ON	A	2	5054.4 ns	See Note 11.	178	See Note 8.
1	2	HI	N/A	1	ON	A	2	5049.7 ns	See Note 12.		
1	2	HI	N/A	1	ON	A	2	5031.7 ns	See Note 13.		
1	2	HI	N/A	1	ON	A	2	5054.4 ns	See Note 12.		
1	2	HI	N/A	1	ON	A	2	5060.1 ns	See Note 14.		
2	2	HI	N/A	2	ON	A	2	5023.2 ns	See Note 9.		
2	2	HI	N/A	2	ON	A	2	5023.2 ns	See Note 12.	89	See Note 8.
2	2	HI	N/A	2	ON	A	2	5016.6 ns	See Note 15.		
1	2	HI	N/A	2	ON	A	2	5040.2 ns	See Note 9.		
1	2	HI	N/A	2	ON	A	2	5029.8 ns	See Note 12.	94	See Note 8.
1	2	HI	N/A	2	ON	A	2	5010.0 ns	See Note 15.		
1	2	HI	N/A	1	ON	A	2	5036.5 ns	See Note 12.		
1	2	HI	N/A	1	ON	A	2	5055.4 ns	See Note 15.	189	See Note 8.
1	2	HI	N/A	1	ON	A	2	5033.6 ns	See Note 12.		
1	2	HI	N/A	1	ON	A	2	5033.6 ns	See Note 15.		
1	1	HI	N/A	1	OFF	A	1	To be determined.	No spurious components.	91	Photos were taken. There were no spurious components. Discrete Fourier analysis will be performed at a later date.
1	1	HI	N/A	1	OFF	A	1				
1	1	HI	N/A	1	OFF	A	1			21	
1	1	HI	N/A	1	OFF	A	1				

9-15. Ranging parameters

	Note 9	Note 10	Note 11	Note 12	Note 13	Note 14	Note 15
Discrete spectrum components	15	15	15	15	15	15	15
Continuous spectrum code	N/A	N/A	N/A	N/A	N/A	N/A	N/A
Clock acquisition time	10	15	20	30	25	35	40
Code component acquisition time	1	2	3	5	5	10	10
DRVID averaging time	10	15	20	30	25	35	40

Test date (1974)	Test title	Test No.	Deep Space Network									
			RCV	EXC	RNG	CMD	Uplink doppler, Hz/s	Uplink offset	CMA SUBC offset	SDA SUBC offset	Mode	RM
7/9	Modulation index and spectrum analyses (continued)	15E	−83.0 (2)	OFF	OFF	OFF	N/A	N/A	N/A	N/A	6C	
			−83.0 (2)	−139.5 (1)	OFF	ON	N/A	N/A	N/A	N/A	6C	
		15F	−83.0 (2)	OFF	OFF	OFF	N/A	N/A	N/A	N/A	6D	
			−83.0 (2)	−140.0 (1)	OFF	ON	N/A	N/A	N/A	N/A	6D	
		15G	−83.0 (2)	OFF	OFF	OFF	N/A	N/A	N/A	N/A	6D	
			−83.0 (2)	−141.1 (1)	OFF	ON	N/A	N/A	N/A	N/A	6D	
7/10	Telemetry performance	16A	Y-factor = 6.77 −134 dBm	−142.6 dBm	OFF	OFF	N/A	N/A	N/A	N/A	3B	
			Y-factor = 4.6 −137.5 dBm	−142.6 dBm	OFF	OFF	N/A	N/A	N/A	N/A	3B	
			−137.5 dBm	−142.6 dBm	OFF	OFF	N/A	N/A	N/A	−2.125 Hz −0.350 Hz	3B	
			−137.5 dBm	−142.5 dBm	OFF	OFF	45	−20 kHz	N/A	−2.125 Hz −0.350 Hz	3B	
			−137.5 dBm	N/A	OFF	OFF	N/A	N/A	N/A	−2.125 Hz −0.350 Hz	3B	
7/11		16B	Y-factor = 6.77 −134 dBm	−142.5 dBm	OFF	OFF	N/A	N/A	N/A	N/A	3C	
			Y-factor = 4.6 −137.5 dBm	−142.5 dBm	OFF	OFF	N/A	N/A	N/A	N/A	3C	
			−137.5 dBm	N/A	OFF	OFF	N/A	N/A	N/A	N/A	3C	
		16C	Y-factor = 6.77 −134 dBm	−142.5 dBm	OFF	OFF	N/A	N/A	N/A	N/A	3D	
			−134 dBm	N/A	OFF	OFF	N/A	N/A	N/A	N/A	3D	
7/12		16D (A)	Y-factor = 13.723 −140 dBm	−120 dBm	OFF	OFF	N/A	N/A	N/A	N/A	6B	
			−140.5 dBm	−120 dBm	OFF	OFF	N/A	N/A	N/A	−2.125 Hz −0.350 Hz	6B	
			−140.5 dBm	−120 dBm	OFF	OFF	250	−20 kHz	N/A	−2.125 Hz −0.350 Hz	6B	
			−140.1 dBm	N/A	OFF	OFF	N/A	N/A	N/A	−2.125 Hz −0.350 Hz	6B	

Table 1 (contd)

Spacecraft								Test data				
EXC	RCVR	PWR	ANT	TWT	RNG	TMU	CDU	Performance		Criteria	Test time, min.	Test comments
2	2	HI	N/A	2	OFF	A	2					Photos were taken. There were
2	2	HI	N/A	2	OFF	A	2				18	no spurious components.
2	2	HI	N/A	2	OFF	A	2				18	Discrete Fourier analysis will
2	2	HI	N/A	2	OFF	A	2	To be determined.		No spurious components.		be performed at a later date.
2	2	HI	N/A	2	OFF	A	2				40	
2	2	HI	N/A	2	OFF	A	2					
1	1	HI	N/A	1	OFF	A	1	12.1 dB	HR	10.9 ± 1.5 dB		250 bps coded HR.
								17.56 dB	LR	17.7 ± 1.5 dB		8.33 bps coded LR.
1	1	HI	N/A	1	OFF	A	1	9.0 dB	HR	7.9 ± 1.5 dB		
								15.6 dB	LR	14.7 ± 1.5 dB		
1	1	HI	N/A	1	OFF	A	1	9.0 dB	HR	7.9 ± 1.5 dB	84	SDAs offset.
								15.6 dB	LR	14.7 ± 1.5 dB		
1	1	HI	N/A	1	OFF	A	1	8.5 dB	HR	7.9 ± 1.5 dB		SDAs offset and doppler.
								15.71 dB	LR	14.7 ± 1.5 dB		
1	1	HI	N/A	1	OFF	A	1	9.25 dB	HR	7.9 ± 1.5 dB		One-way mode.
								15.82 dB	LR	14.7 ± 1.5 dB		
1	1	HI	N/A	1	OFF	A	1	9.0 dB	HR	7.9 ± 1.5 dB		500 bps coded HR.
								17.7 dB	LR	17.7 ± 1.5 dB		8.33 bps coded LR.
1	1	HI	N/A	1	OFF	A	1	6.0 dB	HR	4.9 ± 1.5 dB		
								16.25 dB	LR	14.7 ± 1.5 dB		One-way mode.
1	1	HI	N/A	1	OFF	A	1	6.0 dB	HR	4.9 ± 1.5 dB	40	
								15.9 dB	LR	14.7 ± 1.5 dB		
1	1	HI	N/A	1	OFF	A	1	6.0 dB	HR	4.9 ± 1.5 dB		1000 bps coded HR.
								17.6 dB	LR	17.7 ± 1.5 dB	30	8.33 bps coded LR.
1	1	HI	N/A	1	OFF	A	1	6.0 dB	HR	4.9 ± 1.5 dB		One-way mode.
								18.4 dB	LR	17.7 ± 1.5 dB		
2	2	HI	N/A	2	OFF	A	2	4.85 dB	HR	This was an additional		250 bps coded HR.
										test. The criteria were		8.33 bps coded LR.
								12.05 dB	LR	established as	105	SDAs offset.
2	2	HI	N/A	2	OFF	A	2	3.94 dB	HR	4.9 ± 1.5 dB(HR)		SDAs offset and doppler.
								11.85 dB	LR	12.7 ± 1.5 dB(HR)		
2	2	HI	N/A	2	OFF	A	2	4.86 dB	HR	for each element of this		One-way mode.
								12.38 dB	LR	test.		
2	2	HI	N/A	2	OFF	A	2	4.58 dB	HR			
								11.85 dB	LR			

Test date (1974)	Test title	Test No.	Deep Space Network									
			RCV	EXC	RNG	CMD	Uplink doppler, Hz/s	Uplink offset	CMA SUBC offset	SDA SUBC offset	Mode	RM
7/10	Telemetry performance (continued)	16D	Y-factor = 6.77 −135.0 dBm	−120 dBm	OFF	OFF	N/A	N/A	N/A	N/A	6B	
			Y-factor = 4.6 −137.5 dBm	−120 dBm	OFF	OFF	N/A	N/A	N/A	N/A	6B	
			−137.5 dBm	−120 dBm	OFF	OFF	N/A	N/A	N/A	−2.125 Hz −0.350 Hz	6B	
			−137.5 dBm	−120.5 dBm	OFF	OFF	250	−20 kHz	N/A	−2.125 Hz −0.350 Hz	6B	
			−137.5 dBm	N/A	OFF	OFF	N/A	N/A	N/A	−2.125 Hz −0.350 Hz	6B	
7/10		16E	Y-factor = 6.77 −134 dBm	−120 dBm	OFF	OFF	N/A	N/A	N/A	N/A	6C	
			Y-factor = 4.6 −136 dBm	−120 dBm	OFF	OFF	N/A	N/A	N/A	N/A	6C	
			−136 dBm	N/A	OFF	OFF	N/A	N/A	N/A	N/A	6C	
7/10		16F	Y-factor = 6.77 −134 dBm	−120.5 dBm	OFF	OFF	N/A	N/A	N/A	N/A	6D	
			−134 dBm	N/A	OFF	OFF	N/A	N/A	N/A	N/A	6D	
7/11		16G	Y-factor = 4.63 −137.5 dBm	−128.5 dBm	ON	OFF	N/A	N/A	N/A	N/A	5A	
			−137.5 dBm	−128.5 dBm	ON	OFF	N/A	N/A	N/A	−0.350 Hz	5A	
			−137.5 dBm	−128.5 dBm	ON	OFF	100	−20 kHz	N/A	−0.350 Hz	5A	

Table 1 (contd)

Spacecraft								Test data			Test time, min	Test comments
EXC	RCVR	PWR	ANT	TWT	RNG	TMU	CDU	Performance		Criteria		
2	2	HI	N/A	2	OFF	A	2	11.1 dB	HR	10.9 ± 1.5 dB		250 bps coded HR.
								16.8 dB	LR	17.7 ± 1.5 dB		8.33 bps coded LR.
2	2	HI	N/A	2	OFF	A	2	8.5 dB	HR	7.9 ± 1.5 dB		
								15.2 dB	LR	14.7 ± 1.5 dB		
2	2	HI	N/A	2	OFF	A	2	8.5 dB	HR	7.9 ± 1.5 dB	110	SDAs offset.
								15.5 dB	LR	14.7 ± 1.5 dB		SDAs offset and doppler.
2	2	HI	N/A	2	OFF	A	2	8.1 dB	HR	7.9 ± 1.5 dB		One-way mode.
								15.6 dB	LR	14.7 ± 1.5 dB		
2	2	HI	N/A	2	OFF	A	2	8.1 dB	HR	7.9 ± 1.5 dB		
								14.77 dB	LR	14.7 ± 1.5 dB		
2	2	HI	N/A	2	OFF	A	2	8.5 dB	HR	7.9 ± 1.5 dB		500 bps coded HR.
								17.7 dB	LR	17.7 ± 1.5 dB		8.33 bps coded LR.
2	2	HI	N/A	2	OFF	A	2	6.29 dB	HR	4.9 ± 1.5 dB	55	
								16.08 dB	LR	14.7 ± 1.5 dB		
2	2	HI	N/A	2	OFF	A	2	6.5 dB	HR	4.9 ± 1.5 dB		One-way mode.
								16.25 dB	LR	14.7 ± 1.5 dB		
2	2	HI	N/A	2	OFF	A	2	5.4 dB	HR	4.9 ± 1.5 dB		1000 bps coded HR.
								17.8 dB	LR	17.7 ± 1.5 dB		8.33 bps coded LR.
2	2	HI	N/A	2	OFF	A	2	5.4 dB	HR	4.9 ± 1.5 dB	81	One-way mode.
								17.65 dB	LR	17.7 ± 1.5 dB		
1	2	HI	N/A	1	ON	A	2	20.95 dB		20.8 ± 1.5 dB		8.33 LR only.
											50	
1	2	HI	N/A	1	ON	A	2	20.05 dB		20.8 ± 1.5 dB		
1	2	HI	N/A	1	ON	A	2	19.9 dB		20.8 ± 1.5 dB		

Test date (1974)	Test title	Test No.	Deep Space Network									
			RCV	EXC	RNG	CMD	Uplink doppler, Hz/s	Uplink offset	CMA SUBC offset, Hz	SDA SUBC offset, Hz	Mode	RM
6/26	D/L threshold one-way	1A	Blk III RCV 2	N/A	OFF	OFF	N/A	N/A	N/A	N/A	1A	304
6/27		1B	Blk IV RCV 3	N/A	OFF	OFF	N/A	N/A	N/A	N/A	1A	312
6/30		1C	Blk IV RCV 3	N/A	OFF	OFF	N/A	N/A	N/A	N/A	1A	204
6/28		1D	Blk III RCV 2	N/A	OFF	OFF	N/A	N/A	N/A	N/A	16A	370
6/28		1E	Blk IV RCV 3	N/A	OFF	OFF	N/A	N/A	N/A	N/A	16A	370
7/2		1F	Blk IV RCV 3	N/A	OFF	OFF	N/A	N/A	N/A	N/A	16A	374
6/28	U/L threshold	2A	−107.0 dBm	−140.0 dBm Starting level	OFF	OFF	N/A	N/A	N/A	N/A	1	304
					OFF	ON	N/A	N/A	N/A	N/A	1	
					ON	OFF	N/A	N/A	N/A	N/A	1	
					ON	ON	N/A	N/A	N/A	N/A	1	
		2B	−107.0 dBm	−140.0 dBm Starting level	OFF	OFF	N/A	N/A	N/A	N/A	2	376
					OFF	ON	N/A	N/A	N/A	N/A	2	
					ON	OFF	N/A	N/A	N/A	N/A	2	
					ON	ON	N/A	N/A	N/A	N/A	2	
6/27	D/L threshold two-way	3A	Blk III RCV 2	−129.8 dBm	OFF	OFF	N/A	N/A	N/A	N/A	1A	302
6/27		3B	Blk IV RCV 3	−129.8 dBm	OFF	OFF	N/A	N/A	N/A	N/A	1A	302
6/30		3C	Blk IV RCV 3	−127.0 dBm	OFF	OFF	N/A	N/A	N/A	N/A	1A	304
6/27		3D	Blk III RCV 2	−129.8 dBm	ON	OFF	N/A	N/A	N/A	N/A	1AR	303
6/28		3E	Blk IV RCV 3	−129.8 dBm	ON	OFF	N/A	N/A	N/A	N/A	1AR	303
6/30		3F	Blk IV RCV 3	−131.0 dBm	ON	OFF	N/A	N/A	N/A	N/A	1AR	305
6/28		3G	Blk III RCV 2	−130.5 dBm	OFF	ON	N/A	N/A	N/A	N/A	1A/CMD	302
6/28		3H	Blk III RCV 2	−130.0 dBm	OFF	OFF	N/A	N/A	N/A	N/A	16A	370
6/26	S/C rcvr pull in	4A	−107.0 dBm	−110.0 dBm	OFF	OFF	N/A	+500 Hz	N/A	N/A	1	304
	S/C rcvr pull in		Blk III RCV 2	−110.0 dBm	OFF	OFF	N/A	−500 Hz	N/A	N/A	1	
	S/C rcvr range and rate			−120.0 dBm	OFF	OFF	500	+40 kHz	N/A	N/A	1	
	S/C rcvr range and rate			−120.0 dBm	OFF	OFF	500	−40 kHz	N/A	N/A	1	
	S/C rcvr acquisition and tracking rate			−120.0 dBm	OFF	OFF	500	+ 7 kHz	N/A	N/A	1	
	S/C rcvr acquisition and tracking rate			−120.0 dBm	OFF	OFF	500	− 7 kHz	N/A	N/A	1	
6/26	S/C rcvr pull in	4B	−107.0 dBm	−110.0 dBm	OFF	OFF	N/A	+500 Hz	N/A	N/A	2	376
	S/C rcvr pull in		Blk III RCV 2	−110.0 dBm	OFF	OFF	N/A	−500 Hz	N/A	N/A	2	
	S/C rcvr range and rate			−120.0 dBm	OFF	OFF	500	+40 kHz	N/A	N/A	2	
	S/C rcvr range and rate			−120.0 dBm	OFF	OFF	500	−40 kHz	N/A	N/A	2	
	S/C rcvr acquisition and tracking rate			−120.0 dBm	OFF	OFF	500	+ 7 kHz	N/A	N/A	2	
	S/C rcvr acquisition and tracking rate			−120.0 dBm	OFF	OFF	500	− 7 kHz	N/A	N/A	2	
7/2	Carrier residual phase jitter	5A	− 99.0 dBm	N/A	OFF	OFF	N/A	N/A	N/A	N/A	1A	304
			− 99.0 dBm	− 75.0 dBm	OFF	OFF	N/A	N/A	N/A	N/A	1A	
			− 99.0 dBm	−130.0 dBm	OFF	OFF	N/A	N/A	N/A	N/A	1A	
		5B	−100.0 dBm	N/A	OFF	OFF	N/A	N/A	N/A	N/A	16A	374
			−100.0 dBm	− 70.0 dBm	OFF	OFF	N/A	N/A	N/A	N/A	16A	
			−100.0 dBm	−130.0 dBm	OFF	OFF	N/A	N/A	N/A	N/A	16A	
6/27	U/L spectrum and false lock	6A	Blk III RCV 2	−115.5 dBm	OFF	OFF	15	±2 kHz	N/A	N/A	1	300
		6B	Blk III RCV 2	−112.0 dBm	OFF	OFF	15	±2 kHz	N/A	N/A	2	372
6/28	D/L spectrum analysis	7A	Blk III RCV 1,2	N/A	OFF	OFF	N/A	N/A	N/A	N/A	1A	300
			−110.0 dBm	−115.0 dBm	ON	OFF	N/A	N/A	N/A	N/A	1A/1AR	300/301
		7B	Test not performed.									
6/28		7C	Blk III RCV 1,2	N/A	OFF	OFF	N/A	N/A	N/A	N/A	16A	370
			−110.0 dBm	−115.0 dBm	OFF	OFF	N/A	N/A	N/A	N/A	16A	370
			−110.0 dBm	−115.0 dBm	ON	OFF	N/A	N/A	N/A	N/A	16AR	371

Table 2. DSN/Viking proof test Orbiter compatibility test results

Spacecraft								Test data		Test time, min	Test comments
EXC	RCVR	PWR	ANT	TWT	RNG	TMU	CDU	Performance	Criteria		
1	1	HI	HI	1	OFF	1	1	−160.1 dBm	−158.0 ± 2 dBm	34	None.
1	2	LO	LO	1	OFF	1	1	−161.0 dBm	TBD	10	S-band test.
1	1	HI	HI	1	OFF	1	1	−146.2 dBm	−145.0 ± 3 dBm	5	X-band test.
2	2	LO	HI	2	OFF	2	2	−156.3 dBm	−158.0 ± 2 dBm	16	None.
2	2	LO	HI	2	OFF	2	2	−159.0 dBm	TBD	30	S-band test.
2	2	HI	HI	2	OFF	2	2	−147.8 dBm	−145.0 ± 3 dBm	45	X-band test.
1	1	HI	HI	1	OFF	1	1	−154.5 dBm −154.0 dBm −154.0 dBm −154.5 dBm	−152.3 ± 2 dBm −152.3 ± 2 dBm −152.3 ± 2 dBm −152.3 ± 2 dBm	70	RCVR2, EXC 1.
2	2	HI	LO	2	OFF	2	2	−155.0 dBm −155.5 dBm −156.0 dBm −154.0 dBm	−151.8 ± 2 dBm −151.8 ± 2 dBm −151.8 ± 2 dBm −151.8 ± 2 dBm	70	RCVR2, EXC 1.
1	1	LO	LO	1	OFF	1	1	−159.2 dBm	−158.0 ± 2 dBm	38	EXC1 used all tests.
1	1	LO	LO	1	OFF	1	1	−160.0 dBm	TBD	28	S-band test.
1	1	HI	HI	1	OFF	1	1	−148.8 dBm	TBD	28	X-band test.
1	1	LO	LO	1	ON	1	1	−159.8 dBm	−158.0 ± 2 dBm	21	None.
1	1	LO	LO	1	ON	1	1	−160.8 dBm	TBD	28	S-band test.
1	1	HI	HI	1	ON	1	1	−148.3 dBm	TBD	25	X-band test.
1	1	LO	LO	1	OFF	1	1	−160.0 dBm	−158.0 ± 2 dBm	34	None.
2	2	LO	HI	2	OFF	2	2	−155.2 dBm	−158.0 ± 2 dBm	28	None.
1	1	HI	HI	1	OFF	1	1	5.0 s 3.0 s +40.0 kHz −40.0 kHz Acq/trk Acq/trk	<60 s <60 s +40.0 kHz −40.0 kHz Acq/trk to +7 kHz Acq/trk to −7 kHz	69	None.
2	2	HI	LO	2	OFF	2	2	21.0 s 7.0 s +40.2 kHz −39.9 kHz Acq/trk Acq/trk	<60 s <60 s +40.0 kHz −40.0 kHz Acq/trk to +7 kHz Acq/trk to −7 kHz	30	None.
1	1	HI	HI	1	OFF	1	1	2.58 deg rms 2.69 deg rms 10.22 deg rms	<3.6 deg rms <2.8 deg rms TBD	71	EXC 1.
2	2	HI	HI	2	OFF	2	2	1.39 deg rms 2.69 deg rms 10.55 deg rms	<3.6 deg rms <2.8 deg rms TBD	60	EXC 1.
1	1	LO	HI	1	OFF	1	1	No false lock	No false lock	44	Photos of U/L taken.
2	2	LO	LO	2	OFF	2	2	No false lock	No false lock	47	
1	1	LO	HI	1	OFF	1	1	TBD	No spurious components	61	Photos of D/L taken show no apparent spurious components.
1	1	LO	HI	1	OFF/ON	1	1				
2	2	LO	HI	2	OFF	2	2			38	Fourier analysis will be provided at a later time.
2	2	LO	HI	2	OFF	2	2				
2	2	LO	HI	2	ON	2	2				

Test date (1974)	Test title	Test No.	Deep Space Network RCV	EXC	RNG	CMD	Uplink doppler, Hz/s	Uplink offset	CMA SUBC offset, Hz	SDA SUBC offset, Hz	Mode	RM
		7D	Test not performed.									
7/10		7E	−90.0 dBm	−115.0 dBm	OFF	OFF	N/A	N/A	N/A	N/A	9G	324
7/10		7F	−93.0 dBm	−115.0 dBm	OFF	OFF	N/A	N/A	N/A	N/A	10K	344
7/3		7G	−106.0 dBm	−115.0 dBm	ON	ON	N/A	N/A	N/A	N/A	1FR/CMD	305
6/28		7H	Blk III RCV 1,2	N/A	OFF	OFF	N/A	N/A	N/A	N/A	2A	372
			−110.0 dBm	−126.5 dBm	ON	ON	N/A	N/A	N/A	N/A	2AR/CMD	373
6/26	Transponder rest frequency	8A	−107.0 dBm	−140.3 dBm	OFF	OFF	N/A	N/A	N/A	N/A	1	304
		8B	−108.5 dBm	−140.3 dBm	OFF	OFF	N/A	N/A	N/A	N/A	2	376
6/28	Auxiliary oscillator frequency	9A	−110.0 dBm	N/A	OFF	OFF	N/A	N/A	N/A	N/A	1	200
		9B	−110.0 dBm	N/A	OFF	OFF	N/A	N/A	N/A	N/A	16	370
7/1	Command performance w/wo ranging	10A	−110.0 dBm	−142.5 dBm	OFF	ON	N/A	N/A	N/A	N/A	1	304
			−110.0 dBm	−142.5 dBm	ON	ON	N/A	N/A	N/A	N/A	1R	305
		10B	−110.0 dBm	−142.0 dBm	OFF	ON	N/A	N/A	N/A	N/A	2	376
			−110.0 dBm	−142.0 dBm	ON	ON	N/A	N/A	N/A	N/A	2R	377
6/29	Command capability under doppler	11A	−100.0 dBm	−130.0 dBm	OFF	ON	N/A	±40 kHz	±0.10	N/A	1	304
		11B	−109.5 dBm	−129.5 dBm	OFF	ON	N/A	±40 kHz	±0.10	N/A	2	376
7/1	Ranging delay, threshold, and polarity	12A	−110.0 dBm	−108.0 dBm	ON	OFF	N/A	N/A	N/A	N/A	1FR	305
			−136.0 dBm	−137.0 dBm	ON	OFF	N/A	N/A	N/A	N/A	1FR	305
7/2		12B	−115.0 dBm	−108.0 dBm	ON	ON	N/A	N/A	N/A	N/A	16FR	375
			−134.0 dBm	−137.0 dBm	ON	ON	N/A	N/A	N/A	N/A	16FR	375
7/2		12C	−131.0 dBm	−108.5 dBm	ON	ON	N/A	N/A	N/A	N/A	2AR	377
			−136.0 dBm	−137.5 dBm	ON	ON	N/A	N/A	N/A	N/A	2AR	377
7/3		12D	−112.0 dBm	−106.0 dBm	ON	OFF	N/A	N/A	N/A	N/A	1R	305
7/1	Ranging acquisition capability with doppler	13A	−107.0 dBm	−107.5 dBm	ON	ON	N/A	−40 kHz	N/A	N/A	1FR	305
			−137.0 dBm	−118.0 dBm	ON	ON	N/A	−40 kHz	N/A	N/A	1FR	305
7/2		13B	−117.0 dBm	−108.5 dBm	ON	ON	N/A	−40 kHz	N/A	N/A	16FR	375
			−137.0 dBm	−118.0 dBm	ON	ON	N/A	−40 kHz	N/A	N/A	16FR	375
7/12	DRVID test	14	−116.0 dBm	−108.0 dBm	ON	ON	N/A	N/A	N/A	N/A	1FR	301
6/30	Modulation index and spectrum analysis	15A	Blk III RCV 1,2	−115.0 dBm	OFF/ON	OFF	N/A	N/A	N/A	N/A	1F/1FR	304/305
7/2		15B	−90.0 dBm	−115.0 dBm	OFF	OFF	N/A	N/A	N/A	N/A	2E	376
7/2		15C	−90.0 dBm	−115.0 dBm	OFF/ON	OFF	N/A	N/A	N/A	N/A	2A/2AR	376/377
6/30		15D	−90.0 dBm	−115.0 dBm	OFF	OFF	N/A	N/A	N/A	N/A	1S	304
7/24		15E	−90.0 dBm	−115.0 dBm	OFF	OFF	N/A	N/A	N/A	N/A	14A	336
7/24		15F	−90.0 dBm	−115.0 dBm	OFF	OFF	N/A	N/A	N/A	N/A	13P	306
7/10		15G	−90.0 dBm	−115.0 dBm	OFF	OFF	N/A	N/A	N/A	N/A	12W	354
6/30		15H	−90.0 dBm	−115.0 dBm	OFF	OFF	N/A	N/A	N/A	N/A	1U	304
6/30		15I	−90.0 dBm	−115.0 dBm	OFF	OFF	N/A	N/A	N/A	N/A	1N	304
7/6		15J	−90.0 dBm	−100.0 dBm	OFF	OFF	N/A	N/A	N/A	N/A	11V	330
7/10		15K	−90.0 dBm	−115.0 dBm	OFF	OFF	N/A	N/A	N/A	N/A	9G	324
7/10		15L	−90.0 dBm	−115.0 dBm	OFF	OFF	N/A	N/A	N/A	N/A	10K	334
7/6		15M	−90.0 dBm	−115.0 dBm	OFF	OFF	N/A	N/A	N/A	N/A	2H	332
7/6		15N	−90.0 dBm	−115.0 dBm	OFF	OFF	N/A	N/A	N/A	N/A	2Q	332
		15O	Test not performed.									
6/30		15P	−90.0 dBm	−115.0 dBm	OFF	OFF	N/A	N/A	N/A	N/A	1M	304

Notes:
1. Spacecraft VCO drift prevented normal acquisition on average of 30-min runs.
2. Test was performed with command modulation off.
3. Spacecraft range delay could not be determined. The zero-delay measurements were not performed due to spacecraft configuration in the chamber. Relative delay measurements may be determined by calculating the spacecraft cable configuration. This step has not been accomplished yet. All acquisitions good.

Table 2 (contd)

Spacecraft								Test data		Test time, min	Test comments
EXC	RCVR	PWR	ANT	TWT	RNG	TMU	CDU	Performance	Criteria		
2	1	HI	HI	1	OFF	1	1			46	Tests 7B and 7D were
1	1	HI	HI	2	OFF	2	1			43	not performed because
1	1	HI	HI	1	ON	1	1			20	of insufficient gain from
2	2	LO	LO	2	OFF	2	2			39	Blk IV coupled with
2	2	LO	LO	2	ON	2	2				excessive X-band RF loss.
1	1	HI	HI	1	OFF	1	1	505 s	<30 s	149	See Note 1.
2	2	HI	LO	2	OFF	2	2	66 s	<30 s	140	
1	1	LO	HI	1	OFF	1	1	23.366177 MHz	N/A	36	Readings are D/L
2	2	LO	HI	2	OFF	2	2	23.366268 MHz	N/A	38	frequency.
1	1	HI	HI	1	OFF	1	1	S/C verified all cmds	S/C verified all cmds	90	None.
1	1	HI	HI	1	ON	1	1	S/C verified all cmds	S/C verified all cmds		Acquired ranging code.
2	2	HI	LO	2	OFF	2	2	S/C verified all cmds	S/C verified all cmds	182	None.
2	2	HI	LO	2	ON	2	2	S/C verified all cmds	S/C verified all cmds		Acquired ranging code.
1	1	HI	HI	1	OFF	1	1	S/C verified all cmds	S/C verified all cmds	52	None.
2	2	HI	LO	2	OFF	2	2	S/C verified all cmds	S/C verified all cmds	115	
1	1	HI	HI	1	ON	1	1	5451 RU, ns	980 ± 180 ns	93	See Note 2.
1	1	HI	HI	1	ON	1	1	5445 RU, ns	980 ± 180 ns		See Note 3.
2	2	HI	HI	2	ON	2	2	5446 RU, ns	1000 ± 100 ns	63	All good acquisitions.
2	2	HI	HI	2	ON	2	2	5476 RU, ns	1000 ± 100 ns		
2	2	HI	LO	2	ON	2	2	5450 RU, ns	1000 ± 180 ns	56	Good acquisitions.
2	2	HI	LO	2	ON	2	2	5443 RU, ns	1000 ± 180 ns		6G, 4B acquisitions.
1	1	HI	HI	1	ON	1	1	5064 RU, ns	TBD	30	X-band, Blk IV RCV.
1	1	HI	HI	1	ON	1	1	5448 RU, ns	980 ± 180 ns	37	None.
1	1	HI	HI	1	ON	1	1	5454 RU, ns	980 ± 180 ns		All good acquisitions.
2	2	HI	HI	2	ON	2	2	5452 RU, ns	980 ± 180 ns	49	None.
2	2	HI	HI	2	ON	2	2	5455 RU, ns	980 ± 180 ns		All good acquisitions.
1	1	LO	HI	1	ON	1	1	<1 ns	< 108 ns	480	3-sigma variations.
1	1	HI	HI	1	OFF/ON	1	1	TBD	Verify modification	55	Photographs taken of all
2	2	HI	LO	2	OFF	2	2		indices	23	spectrums.
2	2	HI	LO	2	OFF/ON	2	2			39	Discrete Fourier
1	1	HI	HI	1	OFF	1	1			22	analysis of baseband
2	2	HI	LO	1	OFF	2	2			91	telemetry spectrum will
1	1	HI	LO	1	OFF	2	2			24	be performed later.
1	2	HI	HI	2	OFF	1	2			25	
1	1	HI	HI	1	OFF	1	1			37	
1	1	HI	HI	1	OFF	1	1			18	
2	2	LO	HI	1	OFF	1	2			29	
2	1	HI	HI	1	OFF	1	1			46	
1	1	HI	HI	2	OFF	2	1			43	
2	2	LO	LO	1	OFF	2	2			29	
2	2	LO	LO	1	OFF	2	2			22	
1	1	HI	HI	1	OFF	1	1			18	

Test date (1974)	Test title	Test No.	Deep Space Network									
			RCV	EXC	RNG	CMD	Uplink doppler, Hz/s	Uplink offset	CMA SUBC offset, Hz	SDA SUBC offset, Hz	Mode	RM
7/6	Telemetry performance	16A	Y-factor = 10.05	EXC 1	OFF	OFF	N/A	N/A	N/A	N/A	2A	332
			Y-factor = 10.05	−138.0 dBm	ON	OFF	N/A	N/A	N/A	N/A	2AR	333
			Y-factor = 12.64		OFF	OFF	N/A	N/A	N/A	N/A	2A	332
			Y-factor = 12.64		OFF	OFF	13	36.8 kHz	N/A	+0.22	2A	332
			Y-factor = 12.64		OFF	OFF	N/A	36.8 kHz	N/A	+0.22	2A	332
6/30	Telemetry performance (continued)	16B	Y-factor = 9.62	−127.0 dBm	OFF	OFF	N/A	N/A	N/A	N/A	1N	304
7/24		16C	Y-factor = 9.62	−125.0 dBm	OFF	OFF	N/A	N/A	N/A	N/A	1N	304
7/24		16D	Y-factor = 8.46	−136.0 dBm	OFF	OFF	N/A	N/A	N/A	N/A	14A	336
7/10		16E	Y-factor = 6.42	−127.0 dBm	OFF	OFF	N/A	N/A	N/A	N/A	12W	354
7/10		16F	Y-factor = 6.93	−127.0 dBm	OFF	OFF	N/A	N/A	N/A	N/A	9G	324
		16G	Test not performed.									
7/4		16H	Y-factor = 4.91	−138.0 dBm	OFF	OFF	N/A	N/A	N/A	N/A	2H	332
7/24		16I	Y-factor = ST/NO = 6.2	−126.0 dBm	OFF	OFF	N/A	N/A	N/A	N/A	13P	306
6/30		16J	Y-factor = 6.42	−127.0 dBm	OFF	OFF	N/A	N/A	N/A	N/A	1S	304
7/2		16K	Y-factor = 10.48	−127.0 dBm	OFF	OFF	N/A	N/A	N/A	N/A	2E	376
6/30		16L	Y-factor = 9.53	−127.0 dBm	OFF	OFF	N/A	N/A	N/A	N/A	1U	304
			Y-factor = 6.57	−127.0 dBm	OFF	OFF	N/A	N/A	N/A	N/A	1U	304
7/24		16M	Y-factor = 9.71	−126.0 dBm	OFF	OFF	N/A	N/A	N/A	N/A	1U	304
			Y-factor = 6.57	−126.0 dBm	OFF	OFF	N/A	N/A	N/A	N/A	1U	304
7/24		16N	Y-factor = 12.52	−125.0 dBm	OFF	OFF	N/A	N/A	N/A	N/A	2Q	336
7/6		16O	Y-factor = 4.83	−125.0 dBm	OFF	OFF	N/A	N/A	N/A	N/A	1F	304
			Y-factor = 4.83	−127.0 dBm	ON	OFF	N/A	N/A	N/A	N/A	1FR	305
7/10	Telemetry performance (continued)	16P	Y-factor = 10.74	−127.0 dBm	OFF	OFF	N/A	N/A	N/A	N/A	10K	344
			Y-factor = 6.34	−127.0 dBm	OFF	OFF	N/A	N/A	N/A	N/A	10K	344
7/6		16Q	Y-factor = 12.33	−127.0 dBm	OFF	OFF	N/A	N/A	N/A	N/A	11V	330
			Y-factor = 6.8	−127.0 dBm	OFF	OFF	N/A	N/A	N/A	N/A	11V	330
7/24		16R	Y-factor = 7.55	−125.0 dBm	OFF	OFF	N/A	N/A	N/A	N/A	1M	304
			Y-factor = 7.55	−125.0 dBm	OFF	OFF	N/A	N/A	N/A	N/A	1M	304
			Y-factor = 7.55	−125.0 dBm	OFF	OFF	25.8	36.8 kHz	N/A	+2.20 +0.22	1M	304

Note: 4. Strong SNR due to multipath addition from low-gain antenna cabling.

Table 2 (contd)

Spacecraft								Test data			
EXC	RCVR	PWR	ANT	TWT	RNG	TMU	CDU	Performance	Criteria	Test time, min	Test comments
2	2	LO	LO	1	OFF	2	2	LR = 6.4 dB	LR = 6.3 ± 1.6 dB	339	Blk III, RCV 2 Used for all tests except 16C, 16M, 16Q.
2	2	LO	LO	1	ON	2	2	LR = 5.45 dB	LR = 5.4 ± 1.8 dB		
2	2	LO	LO	1	OFF	2	2	LR = 9.5 dB	LR = 8.6 ± 1.6 dB		
2	2	LO	LO	1	OFF	2	2	LR = 8.8 dB	LR = 7.7 ± 2.0 dB		
2	2	LO	LO	1	OFF	2	2	LR = 9.6 dB	LR = 8.5 ± 1.8 dB		
1	1	HI	HI	1	OFF	1	1	HR = 3.40 dB LR = 9.20 dB	HR = 3.2 ± 0.9 dB LR = 8.8 ± 2.6 dB	33	
1	1	HI	HI	1	OFF	1	1	HR = 2.60 dB LR = 8.80 dB	HR = 3.2 ± 0.9 dB LR = 8.8 ± 2.6 dB	39	Blk IV, RCV 3.
2	2	HI	LO	1	OFF	2	2	LR = 5.00 dB	LR = 4.5 ± 1.6 dB	25	
1	2	HI	HI	2	OFF	1	2	HR = 6.20 dB LR = 6.05 dB	HR = 5.4 ± 0.9 dB LR = 5.5 ± 2.6 dB	54	5.85 with low-gain antenna terminated in load (see Note 4).
2	1	HI	HI	1	OFF	1	1	HR = 3.60 dB LR = 12.10 dB	HR = 3.3 ± 0.9 dB LR = 11.7 ± 2.6 dB	41	
2	2	LO	LO	1	OFF	2	2	LR = 4.50 dB	LR = 5.6 ± 1.6 dB	54	
1	1	HI	LO	1	OFF	2	2	HR = 5.94 dB LR = 6.34 dB	HR = 5.1 ± 1.0 dB LR = 6.2 ± 2.8 dB	43	
1	1	HI	HI	1	OFF	1	1	HR = 6.00 dB LR = 10.75 dB	HR = 5.4 ± 0.9 dB LR = 11.3 ± 2.6 dB	58	
2	2	HI	LO	2	OFF	2	2	HR = 3.40 dB LR = 6.23 dB	HR = 3.3 ± 1.0 dB LR = 6.6 ± 2.8 dB	52	
1	1	HI	HI	1	OFF	1	1	HR = 5.62 dB	HR = 5.1 ± 0.9 dB	44	
1	1	HI	HI	1	OFF	1	1	HR = 11.92 dB LR = 5.90 dB	HR = 11.5 ± 0.9 dB LR = 5.8 ± 2.6 dB		
1	1	HI	HI	1	OFF	1	1	HR = 5.30 dB	HR = 5.1 ± 0.9 dB	42	Blk IV, RCV 3.
1	1	HI	HI	1	OFF	1	1	HR = 11.50 dB LR = 5.67 dB	HR = 11.5 ± 0.9 dB LR = 5.8 ± 2.6 dB		
2	2	HI	LO	1	OFF	2	2	HR = 5.80 dB LR = 8.53 dB	HR = 5.5 ± 1.0 dB LR = 8.8 ± 2.8 dB	65	
1	1	HI	HI	1	OFF	1	1	HR = 3.50 dB LR = 9.10 dB	HR = 3.3 ± 0.9 dB LR = 8.9 ± 2.6 dB	98	
1	1	HI	HI	1	ON	1	1	HR = 1.68 dB LR = 8.20 dB	HR = 2.4 ± 1.1 dB LR = 8.0 ± 2.8 dB		
1	1	HI	HI	2	OFF	2	1	HR = 3.75 dB	HR = 3.3 ± 1.0 dB	110	
1	1	HI	HI	2	OFF	2	1	HR = 8.85 dB LR = 6.27 dB	HR = 7.7 ± 0.9 dB LR = 5.8 ± 2.8 dB		+.25 dB out of tolerance.
2	2	LO	HI	1	OFF	1	2	HR = 5.80 dB	HR = 5.5 ± 0.9 dB	64	Performed with Blk IV RCV.
2	2	LO	HI	1	OFF	1	2	HR = 9.10 dB LR = 5.55 dB	HR = 8.9 ± 0.9 dB LR = 5.7 ± 2.6 dB		
1	1	HI	HI	1	OFF	1	1	HR = 4.00 dB LR = 7.26 dB	HR = 4.0 ± 0.9 dB LR = 6.4 ± 2.6 dB	151	Narrow-bandwidth LR.
1	1	HI	HI	1	OFF	1	1	LR = 7.10 dB	LR = 6.1 ± 2.6 dB		Medium-bandwidth LR.
1	1	HI	HI	1	OFF	1	1	HR = 3.85 dB LR = 6.63 dB	HR = 3.8 ± 1.0 dB LR = 5.6 ± 2.9 dB		

Test date (1974)	Test title	Test No.	Deep Space Network						
			RCV	EXC	RNG	CMD	Uplink doppler, Hz/s	Uplink offset	CMA SUBC offset
7/27	False U/L RF acquisition with ranging	1	−137.5(2) −130.5(1) −111.0(3) −137.5(2) −130.5(1) −111.0(3)	−117.0(1) N/A −128.5(2) −117.0(1) N/A −128.5(2)	ON(1) N/A OFF(2) ON(1) N/A OFF(2)	OFF OFF 	13 EXC 1 NO 	(72.623 kHz) 2112.894097 MHz EXC 1 (72.623 kHz) 2112.894097 MHz EXC 1	N/A N/A N/A N/A N/A N/A
7/27	False command acquisition with ranging	2	−135.5(2) −131.8(1) −111.0(3)	N/A N/A −113.0(1)	N/A N/A ON(1)	N/A N/A ON(1)	NO	−10.055 kHz −2115.348090 MHz EXC 1	N/A
7/27	Command and telemetry degradation with ranging	3	−137.0(2) −131.8(1) −111.0(3)	−117.5(2) −123.0(1) N/A	ON(2) OFF(1) N/A	OFF(2) ON(1) N/A	1 EXC 2	2112.894347 MHz EXC 2	N/A
7/29	Radio metric degradation with ranging	4	−137.0(2) −132.0(1) −116.0(3)	−108.0(2) −120.0(1) N/A	ON(2) ON(1) N/A	OFF(2) OFF(1) N/A	1 EXC 2	2112.894447 MHz EXC 2 75.888 kHz	N/A
7/29	VL telemetry degradation by VO HRT	5	−137.0(2) −132.0(1) −116.0(3)	−120.0(1) −121.5(2) N/A	OFF	OFF	N/A	N/A	N/A
		5	−137.0(2) −132.0(1) −116.0(3)	−120.0(1) −121.5(2) N/A	OFF	OFF	N/A	2111.634558 MHz +28.75 kHz (2)	N/A
			−137.0(2) −132.0(1) −116.0(3)	−120.0(1) −121.5(2) N/A	OFF	OFF	N/A	2111.656658 MHz +50.732 kHz (2)	N/A
7/29	Multiple S/C telemetry performance	6	−137.0(2) −134.5(1) −118.5(3)	−121.5(1) −111.5(2) N/A	OFF(1) ON(2) N/A	OFF	N/A	N/A	N/A
			−137.0(2) −134.5(1) −118.5(3)	−121.5(1) −111.5(2) N/A	OFF(1) ON(2) N/A	OFF	250 (1) 13 (2)	+20 kHz	N/A

Table 3. DSN/Viking PTO/SCTL compatibility test results

Spacecraft				Test data			Test time, min	Test comments
SDA SUBC offset	Mode	RM	S/C	Performance		Criteria		
N/A N/A N/A N/A N/A N/A	5AR 1F TLM-G	304	Lander Orbiter Test XMTR	No false RF and CDU acquisition with ramp			146	U/L levels set for Orbiter. With ramp, no false acq. At static offset, both RF acq and CDU lock. However, unable to repeat CDU lock.
	5AR 1F TLM-G	304	Lander Orbiter Test XMTR	Both RF and CDU false acq with static offset. −137.0 2nd RNG component −150.0 3rd RNG component RF and CDU lock				
N/A	3B 1F TLM-G	304	Lander Orbiter Test XMTR	Orbiter False U/L RF lock (−150 dBm) RCVR VCO 23,3661000 Orbiter 2111.604907 −150.0 dBm 3rd RNG comp RF and CDU lock 29th harmonic			75	U/L levels set for Orbiter. False acq of both carrier and CDU occurred as expected.
N/A	5AR 1F TLM-G	304	Lander Orbiter Test XMTR	No apparent CMD degrad No significant TLM degrad SNRs during ramp 7.83 dB HR 12.68 dB LR	Ref. SNRs 7.77 dB HR 13.02 dB LR		129	Orbiter TLM. 4000 bps coded HR. 8.33 bps coded LR. U/L levels set for Orbiter.
N/A	5AR 1FR TLM-G	305	Lander Orbiter Test XMTR	TBD		TBD	189	Orbiter ranging: Code comp = 10 Clock acq = 120 s Component acq = 2 s DRVID acq = 120 s, 5 points
N/A	5B 1F TLM-F	304	Lander Orbiter Test XMTR	16.4 dB LR 2.5 dB HR 13.19 dB LR 7.62 dB HR 15.75 dB LR 6.5 dB HR	Lander Orbiter Test XMTR	Reference data.		Lander HR data low (6 dB). Suspect SDA.
N/A	5B 1F TLM-F	304	Lander Orbiter Test XMTR	16.21 dB LR 2.52 dB HR 13.0 dB LR 7.5 dB HR 15.2 dB LR 6.44 dB HR	Lander Orbiter Test XMTR	No degradation from reference data.	124	
N/A	5B 1F TLM-F	304	Lander Orbiter Test XMTR	16.31 dB LR 2.47 dB HR 13.1 dB LR 7.14 dB HR 15.07 dB LR 6.48 dB HR	Lander Orbiter Test XMTR			
N/A	5B 1FR 1C	305	Lander Orbiter Test XMTR	9.52 dB HR 16.98 dB LR 4.24 dB HR 9.71 dB LR 3.44 dB HR 15.33 dB LR	Lander A2 Lander B1 Orbiter A3 Orbiter A1 Test XMTR B3 Test XMTR B2	7.9 ± 1.5 dB 14.7 ± 1.5 dB 3.4 ± 1.6 dB 8.0 ± 3.3 dB 3.3 ± 1.6 dB 11.7 ± 3.3 dB	385	
1:0.350 Hz 2:2.125 Hz 3:2.2 Hz 4:0.225 Hz 5:0.225 Hz 6:2.2 Hz				9.3 dB HR 17.54 dB LR 4.3 dB HR 10.1 dB LR 3.7 dB HR 16.98 dB LR	Lander Orbiter Test XMTR	7.9 ± 1.5 dB 14.7 ± 1.5 dB 3.1 ± 1.7 dB 7.3 ± 3.6 dB 3.0 ± 1.7 dB 11.2 ± 3.3 dB		

Test date (1974)	Test title	Test No.	Deep Space Network						
			RCV	EXC	RNG	CMD	Uplink doppler, Hz/s	Uplink offset	CMA SUBC offset
7/29	Multiple S/C telemetry performance (contd)	6	−137.0(2) −134.5(1) −118.5(3)	−121.5(1) −111.5(2) N/A	OFF(1) ON(2) N/A	OFF	N/A	+20 kHz	N/A
7/27	Multiple S/C telemetry performance	7	−137.0(2) −134.3(1) −111.0(3)	−120.0(1) −110.0(2) N/A	ON(1) OFF(2) N/A	OFF	N/A	N/A	N/A
			−137.0(2) −134.3(1) −111.0(3)	−120.0(1) −110.0(2) N/A	ON(1) OFF(2) N/A	OFF	250(1) 13(2)	+20 kHz (1) +20 kHz (2)	N/A
			−137.0(2) −134.3(1) −111.0(3)	−120.0(1) −110.0(2) N/A	ON(1) OFF(2) N/A	OFF	N/A	+20 kHz (1) +20 kHz (2)	N/A
7/26	Multiple S/C command with doppler	8	−137.5(2) −129.5(1)	−120.0(1) −114.0(2)	OFF(1) ON(2)	ON(1) ON(2)	N/A	N/A	N/A
			−130.5(3)	N/A	N/A	N/A			
			−137.5(2) −129.5(1)	−119.5(1) −115.5(2)	OFF(1) ON(2)	ON(1) ON(2)	N/A	+20 kHz (1) +20 kHz (2)	−0.1 Hz −0.1 Hz
			−130.5(3)	N/A	N/A	N/A			
7/25	Multiple carrier D/L carrier analysis	9	− 93.5(2) − 95.5(1) − 91.5(3)	−120.0(1) −115.0(2) N/A	OFF(1) ON(2)	OFF	N/A	N/A	N/A
			− 93.5(2) − 96.0(1) − 89.0(3)	N/A (one-way)	OFF	OFF	N/A	N/A	N/A
7/25	Multiple carrier U/L spectrum analysis	10	N/A N/A N/A N/A N/A N/A N/A N/A N/A N/A	−115 (2) −121.5(1) −115 (2) −121.5(1) −126.5(2) −133.0(1) −126.5(2) −130.5(1) −124.0(2) −133.0(1)	OFF OFF OFF OFF ON ON ON ON ON ON	OFF OFF OFF OFF ON ON ON OFF OFF ON	N/A N/A N/A N/A N/A N/A N/A N/A N/A N/A	N/A N/A N/A N/A N/A N/A N/A N/A N/A N/A	N/A N/A N/A N/A N/A N/A N/A N/A N/A N/A
7/25	Multiple carrier D/L threshold and acquisition	11	−139.6(2) −138.0(1) −135.0(3)	−119.7(1) −130.5(2) N/A	OFF(1) ON(2) N/A	OFF OFF	N/A	N/A	N/A
			−139.6(2) −138.0(1) −135.0(3)	N/A N/A N/A	OFF(1) OFF(2) N/A	OFF	N/A	N/A	N/A

Notes: 1. RF channel assignments for all tests
Lander: Channel 13
Orbiter: Channel 9
Test XMTR: Channel 20

2. Orbiter X-band D/L turned on for Tests 1, 2, 3, 4, 5.

Table 3 (contd)

Spacecraft				Test data			Test time, min	Test comments
SDA SUBC offset	Mode	RM	S/C	Performance		Criteria		
1:0.350 Hz				9.06 dB HR	Lander	7.9 ± 1.5 dB		
2:2.125 Hz				16.54 dB LR		14.7 ± 1.5 dB		
3:2.2 Hz				4.32 dB HR	Orbiter	3.2 ± 1.7 dB		
4:0.225 Hz				10.2 dB LR		7.7 ± 3.3 dB		
5:0.225 Hz				3.64 dB HR	Test XMTR	3.1 ± 1.7 dB		
6:2.2 Hz				15.52 dB LR		11.5 ± 3.3 dB		
N/A	5AR		Lander	17.51 dB LR	Test XMTR A2	N/A	171	Blk IV RCV threshold degraded; TLM criteria for Test XMTR not applicable.
	1F		Orbiter	23.1 dB LR	Lander B1	20.8 ± 1 dB LR		
	1G		Test XMTR	5.36 dB HR	Orbiter A3	3.4 ± 1.6 dB HR		
				11.28 dB LR	A1	8.0 ± 3.3 dB LR		
				9.0 dB HR	Test XMTR B3	N/A		
LE 1:0.350 Hz	5AR		Lander	17.6 dB LR	Test XMTR	N/A	171	Blk IV RCV threshold degraded; TLM criteria for test transmitter not applicable.
LS 2:N/A	1F		Orbiter	22.55 dB LR	Lander	20.8 ± 1.5 dB		
OS 3:2.2 Hz	1G		Test XMTR	5.42 dB HR	Orbiter	3.1 ± 1.7 dB		
OE 4:0.225 Hz				11.38 dB LR		7.3 ± 3.6 dB		
TTE 5:0.225 Hz				9.0 dB HR	Test XMTR	N/A		
TTS 6:2.2 Hz								
1:0.350 Hz	5AR		Lander	17.96 dB LR	Test XMTR	N/A		
2:N/A	1F		Orbiter	22.7 dB LR	Lander	20.8 ± 1.5 dB		
3:2.2 Hz	1G		Test XMTR	5.39 dB HR	Orbiter	3.2 ± 1.7 dB		
4:0.225 Hz				11.14 dB LR		7.7 ± 3.3 dB		
5:0.225 Hz				9.0 dB HR	Test XMTR	N/A		
6:2.2 Hz								
N/A	5B		Lander	Ranging acquisition			187	Ranging:
	1FR		Orbiter	CMDs to Orbiter (5)				10 components
				CMDs to Lander (three 32-word)				Clock acq time = 120
								Code comp acq = 2
	1G		Test XMTR	No degrad to either S/C				DRVID averaging = 120
N/A	5B		Lander	CMDs to Orbiter (5)				
	1FR		Orbiter	CMDs to Lander (three 32-word)				
	1G		Test XMTR	No degrad to either S/C				
N/A	5B	305	Lander	TBD		TBD	178	Photos taken of Lander, Orbiter, and test XMTR.
	1FR		Orbiter					
	1G		Test XMTR					
N/A	5B	305	Lander	TBD		TBD		Fourier analysis of D/L spectra will be provided at a later date.
	1FR		Orbiter					
	1G		Test XMTR					
N/A	N/A	N/A	Orbiter	TBD		TBD	90	Photos taken of all configurations. U/L frequencies at Orbiter and Lander best locks.
N/A	N/A	N/A	Lander					
N/A	N/A	N/A	Orbiter					
N/A	N/A	N/A	Lander					
N/A	N/A	N/A	Orbiter					
N/A	N/A	N/A	Lander					
N/A	N/A	N/A	Orbiter					
N/A	N/A	N/A	Lander					
N/A	N/A	N/A	Orbiter					
N/A	N/A	N/A	Lander					
N/A	5B	305	Lander	−162.4 dBm		−160.0 ± 2 dBm	212	Two-way.
	1FR		Orbiter	−158.7 dBm		−158.0 ± 2 dBm		Two-way.
	1G		Test XMTR	−156.7 dBm		−158.0 ± 2 dBm		One-way.
N/A	5B	305	Lander	−161.9 dBm		−158.0 ± 2 dBm		One-way.
	1FR		Orbiter	−159.4 dBm		−158.0 ± 2 dBm		One-way.
	1G		Test XMTR	−156.5 dBm		−158.0 ± 2 dBm		One-way.

3. All dBm settings for uplink and downlink are carrier power (P_c). Uplink levels established before RNG/CMD modulation applied, except in Tests 1, 2, 3.

4. SDA assignments for tests

Lander ENG:	1	Orbiter ENG:	4
Lander SCI:	2	Test XMTR ENG:	5
Orbiter SCI:	3	Test XMTR SCI:	6

Table 4. Definition of terms for Tables 1, 2, and 3

Term	Definition
Bit rate	Clock frequency of the telemetry bit information
Car. sup.	Downlink carrier suppression due to telemetry modulation
CMA SUBC offset	Command modulation assembly subcarrier frequency offset relative to nominal
D/L	S-band RF downlink
DSN CMD	Telemetry and command data handling command modulation
DRVID	Differenced range versus integrated doppler
DSN EXC	The standard DSN Block III S-band exciter equipment
DSN RCVR	The standard DSN Block III S-band receiving equipment
HR	High rate
LR	Low rate
P_c	Power in carrier
DSN RNG	Planetary ranging assembly modulation
S/C ant	Spacecraft antenna
S/C CDU	Spacecraft command detector unit
S/C EXC	Spacecraft S-band exciter equipment
S/C mode	Spacecraft telemetry mode
S/C PWR	Spacecraft transmitter power mode
S/C RCVR	Spacecraft S-band receiving equipment
S/C RNG	Spacecraft ranging channel—ON/OFF
S/C RM	Spacecraft radio mode
S/C TMU	Spacecraft telemetry modulation unit
S/C TWT	Spacecraft traveling wave tube amplifier
SDA SUBC offset	Subcarrier demodulator assembly subcarrier frequency offset relative to nominal
TBD	To be determined
TLM	Telemetry
U/L	S-band RF uplink
Uplink doppler	Ramp rate of the uplink carrier frequency
Uplink offset	Uplink carrier frequency offset relative to the spacecraft receiver rest frequency

Table 5. RF channels and center frequencies for special RF interference tests

	Orbiter Channel 9, MHz	Lander Channel 13, MHz	Test transmitter Channel 20, MHz
DSN receive	2293.148148	2294.629630	2297.222222
DSN transmit	2111.607253	2112.971451	Not Applicable

Pioneer 10 and 11 Mission Support

R. B. Miller
DSN Systems Engineering Office

Preparations for the Pioneer 11 Jupiter encounter are described, including changes in the DSN implementation from that used for the Pioneer 10 encounter. The reliability of the Ground Data System with respect to commanding the spacecraft is discussed.

I. Introduction

The closest approach of Pioneer 11 to the planet Jupiter will occur on December 3, 1974, at 0522 GMT. The spacecraft will pass within 1.6 Jupiter radii (114,000 km) of the center of the planet with a velocity at closest approach of 48 km/s. The spacecraft will be 732 million km (4.9 AU) from earth. The encounter support period is defined as closest approach ±30 days, which is from November 3, 1974, through January 3, 1975. The 60-day encounter period corresponds to ±380 Jupiter radii from the planet. This may seem like an excessively long encounter period until it is compared with a Venus or Mercury encounter. The time period around Venus or Mercury in a typical flyby trajectory, which would correspond to ±380 planetary radii, would be only ±2 days.

The 60 days around Pioneer 11 Jupiter periapsis passage will have very much the same level of activity as did the period around the Pioneer 10 Jupiter encounter last year. In the 60-day time span, there will be on the order of 8 h a day of critical commanding until the critical encounter phase, which extends from −95 to +95 Jupiter radii (corresponding to November 26 through December 9, 1974), when there will be 24 h a day of critical command activity. The spacecraft will enter the bow shock of Jupiter as early as November 25 and depart the bow shock as late as December 11. The magnetopause will be crossed inbound as early as November 27 and outbound as late as December 8. There will be both a solar and earth occultation. There will again be viewing of the Galilean satellites with several of the onboard instruments; however, there will not be a satellite radio occultation as there was of Io during the Pioneer 10 mission. A smaller number of commands should be necessary for the Pioneer 11 than for the Pioneer 10 Jupiter encounter because several of the problems in the Pioneer 10 imaging photopolarimeter discovered after launch were corrected prior to the Pioneer 11 launch. This means that the total number of commands transmitted in the 60 days of encounter will be somewhere in the region of 12,000 to 15,000.

II. DSN Preparation

After the success of the Pioneer 10 Jupiter encounter, it was agreed with the Pioneer Project that the Pioneer 11 Jupiter encounter should be supported in as identical a fashion as practical. No new implementation was required for the Pioneer 11 encounter. However, some changes were necessitated in the Deep Space Network between the Pioneer 10 and 11 encounters.

First, before the Pioneer 10 Jupiter encounter, there were serious reliability problems with the 400-kW transmitter at DSS 14. Because of reliability concerns, a 100-kW transmitter was installed at DSS 14 prior to the Pioneer 10 encounter. Subsequent to the encounter, the 400-kW transmitter was returned to the vendor and reworked. It was reinstalled at DSS 14 in September 1974. Testing has shown the reworked 400-kW transmitter to be considerably improved in reliability; therefore, the 400- instead of the 100-kW transmitter will serve as the emergency transmitting capability for the Pioneer 11 Jupiter encounter.

In order to prepare for the Viking mission and to support a Saturn radar experiment in December 1974, it was necessary to replace all of the feed cones at DSS 14. The feed cone used for the Pioneer 10 encounter was the polarization diversity S-band (PDS) cone. This cone was replaced in September 1974 with an S-band polarization diversity (SPD) cone, which is more nearly identical to the operational cones at DSS 43 and DSS 63. After temporary installation of the X-band receive only (XRO) cone and associated dichroic plate and ellipsoid required for Viking X/S-band, the XRO cone was removed and the S-band megawatt transmit cone (SMT) reinstalled so that Pioneer would have a backup S-band capability in the event of a failure in the newly installed PDS cone.

During the Pioneer 10 encounter, a problem was discovered with the elevation drive motor gear boxes at DSS 43. The symptom was an extremely noisy operation of the boxes. It was seriously debated at that time whether or not the antenna should be taken off-line during the 60-day encounter period in order to investigate the problem. Instead, to avoid impact on the encounter, it was decided to continue to operate the antenna until after encounter, and emergency procedures were given to the station with instructions on how to cut the shaft on a particular motor if it should happen to freeze up during the encounter. Rework of the elevation drive motor gear boxes was then accomplished at DSS 43 in January and finished in July 1974.

Similar symptoms were also discovered in DSS 63 elevation gear boxes. A meeting was held in late November with Network Operations, the cognizant operations engineer (COE), and the cognizant sustaining engineer (CSE) to assess the risk to the Pioneer 11 encounter if the elevation drive motor gear boxes at DSS 63 were not opened up and repaired. It was decided at that time that, even though it was undesirable to have DSS 63 out of service the month before the actual encounter, the risk was unacceptable to the encounter if the work was not accomplished. DSS 63 was therefore taken off-line for the entire month of October so that the remaining elevation drive motor gear boxes could be removed and reworked.

One of the major activities in preparation for the Pioneer 10 encounter was seeking means of providing the most reliable Command System possible for the encounter period. One part of that effort was an attempt to get command confirmation external to the command modulator assembly operational prior to the Pioneer 10 encounter. Technical difficulties were encountered in the external command confirmation related to phase stability problems in the confirmation loop. For that reason, the external confirmation was not put into operation for Pioneer 10, and instead, a special cable audit was performed of all cables in the command critical path in which the cables were inspected and sealed prior to the Pioneer 10 encounter. Subsequently, the external command confirmation problems were solved, and the external command confirmation which involves feedback from the exciter to the command modulator assembly was put into operation on September 1, 1974; therefore, no special cable audit was performed for Pioneer 11 encounter.

The only change in telemetry or command software at the Deep Space Stations between the Pioneer 10 and 11 encounters was required in order to accommodate a change in equipment numbering at the conjoint stations, DSS 42 and DSS 61. This software change involved using a paper-tape overfill whenever loading the telemetry and command processor (TCP) software for Pioneer support at DSSs 42 and 61.

The configuration control and freeze plan for the Pioneer 11 encounter was essentially identical to that for Pioneer 10, with the dates adjusted to match the change in the time of encounter. A modified configuration control will be put into effect from October 29 (the date of the operational readiness test for the encounter) through January 3, 1975. This modified configuration control involves approval by the DSN Managers, Network Operations Project Engineers, and station directors of any

engineering change order (ECO) work to be continued during the encounter period. The configuration of the 64-m stations will be frozen from November 26 through December 9, which coincides with the 24-h critical operations.

III. DSN Command Reliability

The principal concern of the Pioneer Project prior to the Pioneer 10 encounter was the reliability of the total Ground Data System with respect to commanding. This Project concern culminated in a complaint to JPL upper management in February 1973. In response, a JPL "Tiger Team" was formed to study the problem of command reliability. The principal outcome of that activity, rather than any design changes in hardware or software, was an improvement in the procedures associated with the operation of the Command System. Better communications between Project personnel and Mission Control and Computing Center (MCCC) and DSN operators, and the use of timed commands instead of priority commands by the Project, were the major factors that resulted in improved command performance.

Prior to February 1973, the mean time between failure of the Command System was on the order of 24 h. Heavy commanding occurred for only about 4 h every 2 days. At that time, about every other command sequence the Project tried to execute was interrupted by a command failure. After the extensive activity to seek ways of improving command reliability, it was predicted that the mean time between failures for the Pioneer 10 Jupiter encounter period would be on the order of 25 h. These mean-time-between-failure figures are computed based on total track time and not normalized to periods of heavy command activity. The Command System tends to fail or be detected as failed more often when it is under heavy use. Since the encounter period represented almost continuous heavy commanding, and the ordinary cruise activity involved heavy commanding perhaps only 4 to 8 h every 2 days, the prediction of a mean time between failures of 25 h, compared to a prior history of 24 h during cruise, actually represented predicting something like 5 times better performance.

The actual performance during the 60-day encounter was a mean time between failures of 49 h. The total number of commands transmitted during the 60-day Pioneer 10 encounter period was 17,286, and of these commands only seven failed to be transmitted on time. Thus, the mean time between aborts was 205.7 h during the 60 days of encounter. This was achieved even though the mean time between failures was 49 h because of the special procedures that were used during encounter to ensure rapid switchover, in the event of a failure, to redundant system elements. None of the seven failed commands during encounter caused a loss of science data.

In the time period from January 1974 to July 1974, the mean time between failures of the Command System was 66 h. This does not mean that the performance has been better than during the encounter because of the fact that the command activity is much lower. However, it does indicate that the improved command reliability achieved during encounter has not been totally lost in the cruise period since encounter. For this reason, the DSN has confidence that a similar command reliability can be achieved during the Pioneer 11 Jupiter encounter.

Another measure of command reliability is statistics on the total number of system aborts, where an abort is defined as a failure of a command to transmit at the scheduled time of transmission. This does not represent the total number of system failures in that, once an abort occurs, it usually interrupts a sequence of commands, which then have to be replanned and rescheduled. The number of aborts is, however, still a good indication of the Command System performance. Table 1 gives the statistics from launch to August 1974 for both Pioneer 10 and Pioneer 11 and compares them to the commands transmitted during the Pioneer 10 60-day encounter. It can be noted from these statistics that the average command rate in cruise for Pioneer 10 is on the order of 1700 commands per month, and for Pioneer 11 on the order of 1400, while the 60-day encounter period averaged 8643 commands per month.

IV. Test and Training in Preparation for Encounter

Since the Pioneer 11 encounter Ground Data System support would be almost identical to that provided for Pioneer 10, a much smaller number of test and training exercises were planned leading up to Pioneer 11 encounter. A total of 78 h in six tests, including the Operational Readiness Test, was planned in preparation for the Pioneer 11 encounter. These tests were run during actual Pioneer 11 tracks, using the spacecraft as a simulation source in exactly the same fashion as for the Pioneer 10 encounter. Some parts of the tests and the operational readiness test involved the actual commanding of the spacecraft in executing portions of the real encounter sequence. No significant Deep Space Network problems were encountered in any of the tests and training for the Pioneer 11 Jupiter encounter.

Particular items that were of training concern for the Pioneer 10 encounter were the digitally controlled oscillators at DSSs 14 and 43. These are the devices which replaced the vacuum-controlled oscillators and enabled precision tuning of the transmitters and receivers at DSSs 14 and 43 to allow for the tremendous doppler experienced during the Jupiter periapsis passage. There has now been a year and a half of operational experience with these devices, which are used for all tuning, including handovers of missions tracked at DSSs 14 and 43. For this reason, there is more confidence in successful operational use of these devices for the Pioneer 11 encounter than there was for Pioneer 10. Of interest is the fact that ranging data accuracy from 1 to 10 km has been achieved using these devices to do sawtooth ramping and observing the effects of the ramping a round-trip light time after transmission. Such ranging data have been taken once a month and will help achieve the navigation accuracy required for Pioneer 11 to successfully fly past Jupiter and on to Saturn.

Table 1. DSN command reliability

	Pioneer 10	Pioneer 11
Total comm nds transmitted	65,163	23,266
Total number of system aborts[a]	61	22
Total command reliability, %	99.91	99.90
Data base (launch to August 1974), months	30	17
During Pioneer 10 60-day encounter		
Total commands transmitted	17,286	
Total number of system aborts	5	
Total number of procedural aborts	2	
Total command reliability, %	99.96	

[a]Represents failure of a command to transmit at time of transmission.

S/X-Band Experiment: A Study of the Effects of Multipath on Group Delay

T. Y. Otoshi
Communications Elements Research Section

An analytical expression is presented for calculating the effects of multipath on group delay. The expression was experimentally verified by tests made at the Telecommunications Development Laboratory using the Mariner Venus/Mercury 1973 Radio Frequency Subsystem, Block 3 receiver and the Mu 1 ranging machine.

I. Introduction

With the exception of DSS 14, all stations of the Deep Space Network use the conventional zero-delay ranging configuration, in which the zero-delay device (ZDD) is mounted on the dish surface. A zenith range measurement via the airpath to a dish-mounted ZDD and a Z-height correction (Ref. 1) provide needed ground station information for determining the true range to the spacecraft.

Results of airpath tests at DSS 14 showed that large changes in range occurred as a function of antenna elevation angle when a ZDD was mounted on the 64-m antenna dish surface (Ref. 2). This characteristic was also observed on the 64-m antenna systems at DSS 43 and DSS 63 (Ref. 3). Since the range dependence on elevation angle could be due to a multipath phenomenon, one cannot assume that a zenith measured value is the correct value.

Other airpath tests made on the 64-m antenna S/X system at DSS 14 showed that large-range changes also occurred when small changes were made in axial focusing of the hyperbola. Another unexplained airpath phenomenon observed was a 53-ns discrepancy between the theoretical and experimental values of S-band zero delay range when the dichroic plate/ellipsoid assembly was retracted and the system was operated for S-band only (Ref. 4). Because of the described airpath problems, the ZDD configuration at DSS 14 has been operated in a cable configuration (Ref. 5) since January 12, 1974.

Although it had been suspected that some of the airpath problems could be due to multipath, other system testing priorities made it difficult to perform further airpath tests to isolate the source of the problems. It was also thought that multipath could not generate errors of the magnitudes which were observed. Recently, the study of the multipath effect was reinitiated and resulted in the

derivations of two theoretical expressions which showed that surprisingly large errors on range measurements could be caused by multipath. One expression derived by J. R. Smith (Refs. 6, 7) is based on the phase shift produced on the envelope of a carrier that is phase-modulated with a square-wave. The analysis was done for the range-clock modulation and detection processes actually employed by the Planetary and Mu-Ranging systems. The second expression, which was derived independently by this author, is based on the conventional definition of group delay where the output phase of a carrier wave is differentiated with respect to frequency. It was shown by Smith (Ref. 7) that for low range-clock modulation frequencies, the two independent derivations reduced to the same mathematical expression.

This article presents the theoretical expression derived by this author and the test data obtained at the Telecommunications Development Laboratory (TDL), showing good agreement between theory and experiment.

II. Summary of Theoretical Expressions

Figure 1 shows the multipath configuration for which the theory was derived. Path 1 is the primary path, and path 2 is the leakage path. The group delay (in seconds) for a signal to travel from the input port to the output port can be expressed as

$$t_g = t_{g1} + \epsilon_g \tag{1}$$

where t_{g1} is the group delay which would be observed in the absence of multipath, and ϵ_g is the deviation from t_{g1} caused by multipath. As derived in the Appendix, this error term is given by

$$\epsilon_g = A(t_{g2} - t_{g1})\left[\frac{A + \cos\theta}{1 + 2A\cos\theta + A^2}\right] \tag{2}$$

where

$$\theta = -(\beta_2 \ell_2 - \beta_1 \ell_1) \tag{3}$$

and where

A = ratio of the magnitude of the leakage wave to the magnitude of the primary wave

β_1, β_2 = phase constants, respectively, of paths 1 and 2, rad/m

ℓ_1, ℓ_2 = physical path lengths, respectively, of paths 1 and 2, m

t_{g1} = group delay of the primary wave traveling through path 1 only, s

t_{g2} = group delay of the leakage wave traveling through path 2 only, s

It is also shown in the Appendix that the carrier phase delay in seconds is

$$t_p = t_{p1} + \epsilon_p \tag{4}$$

where

$$\epsilon_p = -\frac{1}{\omega}\tan^{-1}\left[\frac{A\sin\theta}{1 + A\cos\theta}\right] \tag{5}$$

The differenced range versus integrated doppler (DRVID) can be calculated from (See Ref. 8)

$$\text{DRVID} = t_g - t_p \tag{6}$$

and relative carrier amplitude in dB from

$$20\log_{10}\left|\frac{E_{out}}{E_{in}}\right| = 20\log\left|\frac{E_1}{E_{in}}\right| + 20\log_{10}|1 + A\,e^{j\theta}| \tag{7}$$

Assuming that $t_{g2} > t_{g1}$, and $\theta = -2\pi m$ where m is a positive integer, the group delay and amplitude errors simultaneously reach their upper bounds while the phase delay error given by Eq. (5) goes to zero. When $\theta = -(2n-1)\pi$ where n is a positive integer, the group delay and amplitude errors simultaneously go to their lower bounds while the phase delay error goes to zero. However, in the case where $t_{g2} < t_{g1}$, the group delay error and carrier amplitude simultaneously reach *opposite* bounds. The expressions for upper and lower bounds on phase delay, group delay, and carrier amplitude are given in the Appendix.

Figure 2 shows plots of the upper and lower bounds of group delay in a free-space media for cases where $t_{g2} > t_{g1}$. The upper bound is obtained when the leakage and primary waves are in phase. The lower bound is obtained when the signals are out of phase. If $t_{g2} < t_{g1}$, the opposite polarity must be assigned to the $\Delta\ell$ and error-bound values of Fig. 2. For this latter case, the new upper bound will be reached when the signals are out of phase rather than in phase. (See Case 2 in the Appendix.) The signal level ripple shown on the plot is the peak-to-peak carrier signal level change as observed when θ is varied 360 deg or less. The ripple was calculated from

$$\Delta_{dB} = 20\log_{10}\frac{|E_{out}|_{max}}{|E_{out}|_{min}} = 20\log_{10}\left(\frac{1+A}{1-A}\right) \tag{8}$$

The curves shown on Fig. 2 may be useful for isolating possible sources of leakage waves on the 64-m antenna. Possible leakage can result from scattering of waves from the quadripod legs, tricone, or the dichroic plate/ellipsoid assembly support structures. Some of the differential path lengths of leakage and primary waves on the 64-m antenna can be of the order of 30 m.

III. Experimental Setup

Figure 3 shows a multipath device that was fabricated for purposes of verifying the theoretical equations presented above. Figure 4 is a block diagram of this device. To obtain the desired differential delay between path 1 and path 2, appropriate length cables can be inserted into either path 1 or path 2. The amplitude and phase of the signal in path 2 is adjusted with the variable attenuator and phase shifter, respectively. Repeatable coaxial switches were used to permit measurements of the amplitude and group delay of the signals in the individual paths.

The ranging tests were performed at the TDL in JPL Building 161. The TDL tests were performed with a 516-kHz square wave phase-modulating the uplink signal of 2113 MHz that was transmitted to an MVM'73 Radio Frequency Subsystem (RFS). After receiving the range-coded uplink, the RFS then generated a coherent 2295-MHz downlink signal that was transmitted to the Block 3 receiver through coaxial cables. The multipath device was inserted into this downlink path and therefore, adjustments made on the multipath device resulted in one-way range changes only. Measurements of absolute two-way range as well as one-way range changes were achieved with the Mu-1 ranging machine.

The initial TDL test parameters were as follows:

MVM'73 Radio Frequency Subsystem
Radio mode 022
Uplink signal level total power = −115 dBm
Block 3 Receiver
Mu-1 ranging machine
Carrier suppression = 9 dB
Integration time = 30 s

IV. Test Results

Table 1 shows a summary of the ranging test results obtained with the multipath device. Appropriate length cables were inserted into path 2 of the multipath device to create differential path lengths of 23 ns (Case A) and 93.2 ns (Case B). For each case, the signal in path 2 was adjusted to be approximately −21, −11, and −6 dB relative to the primary signal. More precise post-calibration measurements showed the leakage and primary signals to be at the relative dB levels indicated in the table. The maximum and minimum received signal levels shown in Table 1 are in reasonably good agreement with those predicted by Eqs. (A-10a) and (A-10b). The tabulated received signal levels as obtained from automatic gain control (AGC) calibrations are estimated to be accurate to ±0.2 dB.

Theoretical range change values were calculated from Eqs. (A-23a) and (A-23b). The agreement between theory and experimental range change value was typically within 1 ns. The large discrepancy of 14 ns for the last case in Part B of Table 1 could possibly be due to an error in setting the attenuator so that the relative signal level was actually −6 dB instead of the relative level of −5.5 dB on which the theoretical calculations were based. It is also possible that the discrepancy was caused by the fact that the theoretical value is valid only at a single frequency. The measured value applies to a carrier wave that is phase-modulated with a 516 kHz square wave. Therefore, for severe multipath cases it might be more appropriate to make comparisons with a theoretical value that is averaged over an effective finite bandwidth. For example, see Footnote b in Table 1.

V. Summary and Conclusions

Theoretical equations have been derived for studying the effects of multipath (or leakage) on group delay measurements. The theory was developed for group delay but is applicable to analysis of envelope delay when distortion is small. In general, very good agreement was obtained between theory and experiment.

The theory can be applied to ZDD test data to help isolate possible sources of leakage waves on the 64-m antenna. This type of analysis was done by J. R. Smith (Refs. 6, 7) for the Mariner 10 spacecraft antenna system. He showed a correlation of range change to amplitude change and isolated one of the major causes as being a multipath signal reflecting from a solar panel on the Mariner 10 spacecraft.

In this article, only one-way range error was analyzed. In a telecommunications system, the range change can be

caused by a two-way effect (uplink and downlink). The two-way range error analysis is somewhat more involved and too lengthy to include in this article. Test data on the effects of multipath on two-way range has been obtained and will be reported in a subsequent issue of this publication.

Acknowledgements

This experimental work at TDL was supported and made possible by D. L. Brunn of the Spacecraft Radio Section. M. M. Franco of the Communications Elements Research Section fabricated the multipath device.

References

1. *TRK-2-8 Module of DSN System Requirements Detailed Interface Design Document 820-13, Rev. A*, Jet Propulsion Laboratory, July 1, 1973 (JPL internal document).

2. Stelzried, C. T., Otoshi, T. Y., and Batelaan, P. D., "S/X Band Experiment: Zero Delay Device Antenna Location," in *The Deep Space Network Progress Report 42-20*, Jet Propulsion Laboratory, Pasadena, Calif., Apr. 15, 1974, pp. 64–68.

3. Schlaifer, R., "Planetary Ranging Station Delays," IOM 421-PF-TRK040, March 4, 1974 (JPL internal document).

4. Otoshi, T. Y., "Operational Support for Proposed Ranging Experiment to Resolve Range Anamolies in DSS-14 S/X System," IOM 3333-74-106, May 14, 1974 (JPL internal document).

5. Otoshi, T. Y., and Stelzried, C. T., "S/X Experiment: A New Configuration for Ground System Range Calibrations With the Zero Delay Device," in *The Deep Space Network Progress Report 42-20*, pp. 57–63, Jet Propulsion Laboratory, Pasadena, Calif., Apr. 15, 1974.

6. Smith, J. R., "Viking Ranging Investigation Team," IOM 3382-74-064, July 22, 1974 (JPL internal document).

7. Smith, J. R., "Viking Ranging Investigation Team," IOM 3382-74-076, July 30, 1974 (JPL internal document).

8. MacDoran, P. F., "A First-Principles Derivation of the Differenced Range Versus Integrated Doppler (DRVID) Charged-Particle Calibration Method," in *The Deep Space Network, Space Programs Summary 37-62, Vol. II*, pp. 28–34. Jet Propulsion Laboratory, Pasadena, Calif., Mar. 31, 1970.

9. Ramo, S., and Whinnery, J. R., "Fields and Waves in Modern Radio," John Wiley & Sons, Inc., New York, N.Y., 1953, pp. 46–48.

10. Collin, R. E., "Foundations for Microwave Engineering," pp. 132–137, McGraw-Hill Book Company, New York, N.Y., 1966.

Table 1. Results of one-way range tests with the multipath device (frequency = 2.295 GHz)

Test conditions	Phase shifter setting, deg	Approx. received signal level, dBm	Range change, ns		
			Average measured value[a]	Theoretical value	Measured minus theoretical
A. Measured delay via path 2 alone is 23.0 ns longer than path 1 alone					
1. Attenuator adjusted to make leakage signal be −21 dB relative to primary signal					
Phase shifter adjusted to obtain maximum received signal	−224.9	−89.6	1.7	1.9	− 0.2
Phase shifter adjusted to obtain minimum received signal	− 45.9	−91.2	− 2.5	− 2.3	− 0.2
2. Attenuator adjusted to make leakage signal be −10.8 dB relative to primary signal					
Phase shifter adjusted to obtain maximum received signal	−224.9	−88.1	4.8	5.1	− 0.3
Phase shifter adjusted to obtain minimum received signal	− 45.9	−93.5	−10.1	− 9.3	− 0.8
3. Attenuator adjusted to make leakage signal be −5.65 dB relative to primary signal					
Phase shifter adjusted to obtain maximum received signal	−224.9	−86.7	7.3	7.9	− 0.6
Phase shifter adjusted to obtain minimum received signal	− 45.9	−97.0	−26.4	−25.1	− 1.3
B. Measured delay via path 2 alone is 93.2 ns longer than path 1 alone					
1. Attenuator adjusted to make leakage signal be −20.7 dB relative to primary signal					
Phase shifter adjusted to obtain maximum received signal	−397.0	−89.5	7.6	7.8	− 0.2
Phase shifter adjusted to obtain minimum received signal	−218.0	−91.1	− 9.2	− 9.4	0.2
2. Attenuator adjusted to make leakage signal be −10.7 dB relative to primary signal					
Phase shifter adjusted to obtain maximum received signal	−397.0	−88.0	20.5	21.1	− 0.6
Phase shifter adjusted to obtain minimum received signal	−218.0	−93.3	−36.6	−38.7	2.1
3. Attenuator adjusted to make leakage signal be −5.5 dB relative to primary signal					
Phase shifter adjusted to obtain maximum received signal	−397.0	−86.6	31.1	32.3	− 1.2
Phase shifter adjusted to obtain minimum received signal	−218.0	−97.0	−91.2	−105.2[b]	14.0

[a]Number of 30-sec integration data points used to obtain average value was typically 20. The calculated standard error associated with the average was typically ± 0.2 ns.

[b]The average theoretical range change over the frequency range of 2295.0 ± 0.5 MHz is −98.4 ns.

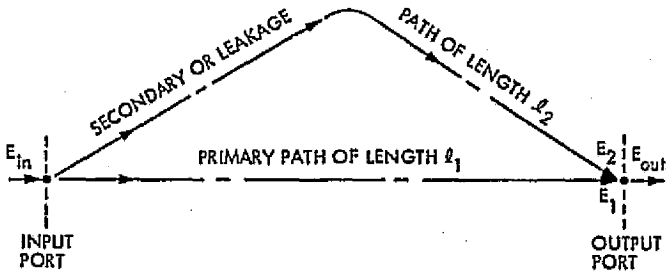

Fig. 1. Geometry for multipath analysis

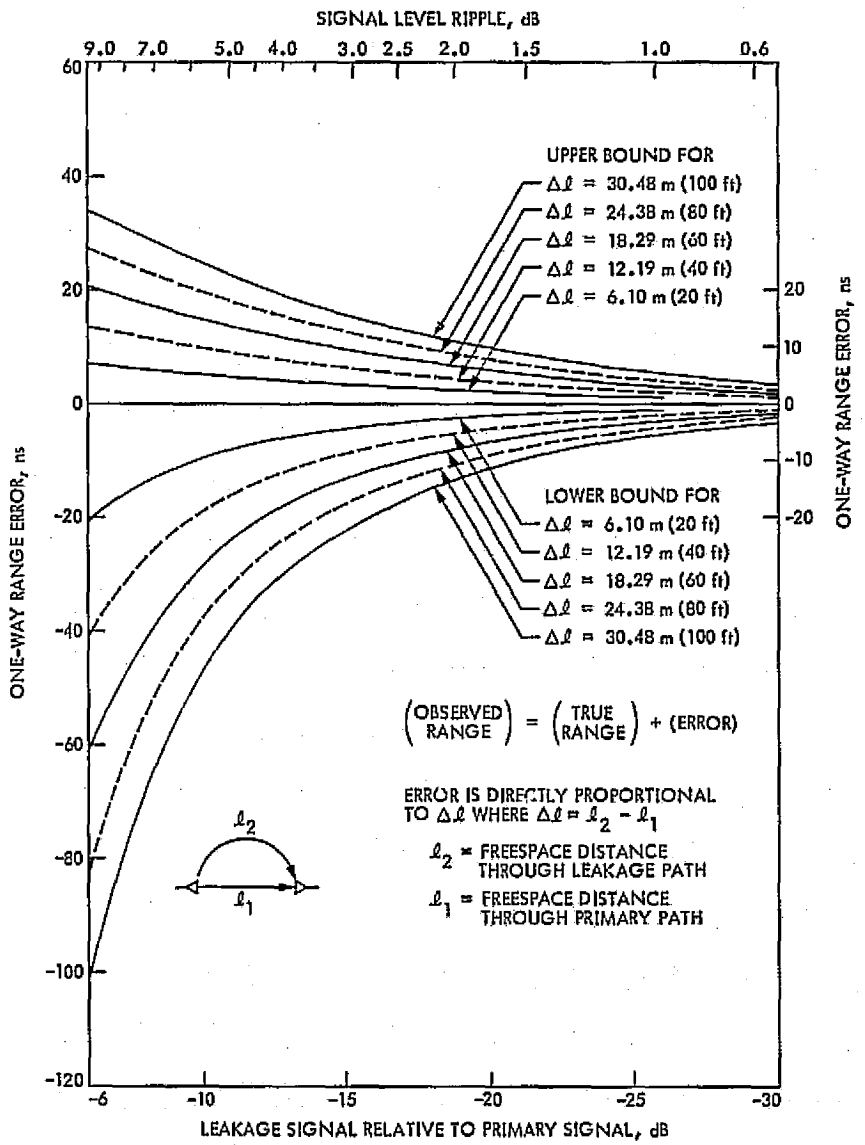

Fig. 2. Limits of one-way range error due to multipath in a free-space media

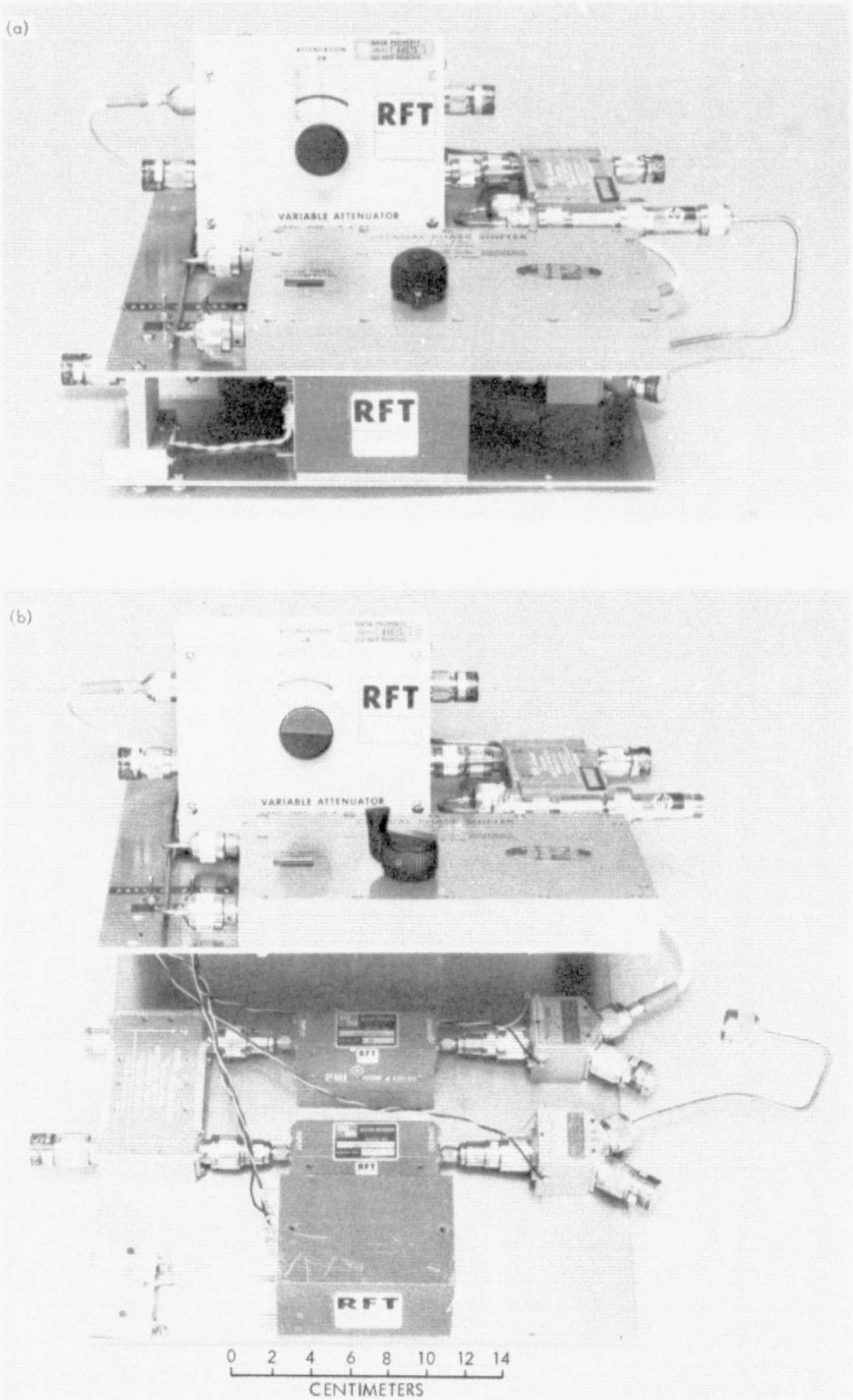

Fig. 3. Multipath device for experimental verification of theoretical derivations: (a) completely assembled, (b) partially disassembled

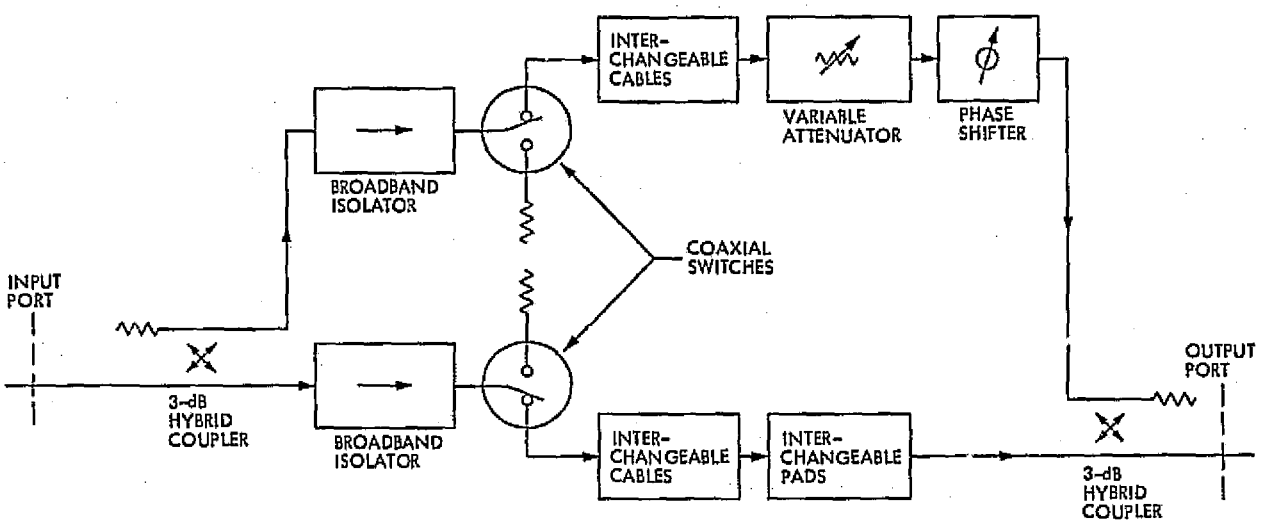

Fig. 4. Multipath device block diagram

Appendix

Derivation of Equations for Phase and Group Delay Errors Caused by Multipath

Figure 1 shows the basic multipath configuration under study where two waves combine after traveling through two separate paths. This basic case can be generalized to include more waves and more paths, but it is sufficient to consider the basic case to show the effect of interference on group delay. Let the wave at the input port be expressed as

$$E_{in} = |E_{in}| \exp(j\phi_0) \tag{A-1}$$

and the wave at the output port be the phasor sum of the primary path wave E_1 and the secondary path wave E_2 so that

$$\begin{aligned} E_{out} &= E_1 + E_2 \\ &= |E_1| \exp(j\phi_1) + |E_2| \exp(j\phi_2) \end{aligned} \tag{A-2}$$

Then from Eqs. (A-1) and (A-2)

$$\frac{E_{out}}{E_{in}} = \left|\frac{E_1}{E_{in}}\right| \exp j(\phi_1 - \phi_0) + \left|\frac{E_2}{E_{in}}\right| \exp[j(\phi_2 - \phi_0)] \tag{A-3}$$

Let

$$\phi_1 - \phi_0 = -\beta_1 \ell_1 \tag{A-4}$$

$$\phi_2 - \phi_0 = -\beta_2 \ell_2 \tag{A-5}$$

where

ℓ_1 = physical length of path 1, m

ℓ_2 = physical length of path 2, m

β_1, β_2 = phase constants, respectively, of paths 1 and 2, rad/m

Substitution of Eqs. (A-4) and (A-5) into Eq. (A-3) gives

$$\frac{E_{out}}{E_{in}} = \left|\frac{E_1}{E_{in}}\right| \exp(-j\beta_1\ell_1)\left[1 + \left|\frac{E_2}{E_1}\right| \exp[-j(\beta_2\ell_2 - \beta_1\ell_1)]\right] \tag{A-6}$$

The ratio $|E_2/E_1|$ is a parameter that is generally of interest so that it is convenient to let

$$A = \left|\frac{E_2}{E_1}\right| \tag{A-7}$$

Furthermore, let

$$\theta = -(\beta_2\ell_2 - \beta_1\ell_1) \tag{A-8}$$

and

$$F = 1 + A e^{j\theta} \tag{A-9}$$

so that substitution into Eq. (A-6) gives the output signal magnitude ratio of

$$\left|\frac{E_{out}}{E_{in}}\right| = \left|\frac{E_1}{E_{in}}\right| |1 + A e^{j\theta}| \tag{A-10}$$

and relative phase of

$$\arg\left(\frac{E_{out}}{E_{in}}\right) = -\beta_1\ell_1 + \arg F \tag{A-11}$$

where

$$\arg F = \tan^{-1}\left[\frac{A \sin\theta}{1 + A\cos\theta}\right] \tag{A-12}$$

From substitution of Eq. (A-11) into the definition of phase delay (Refs. 9, 10) given as

$$t_p = \frac{-1}{\omega}\left[\arg\left(\frac{E_{out}}{E_{in}}\right)\right] \tag{A-13}$$

we obtain

$$t_p = t_{p1} + \epsilon_p \tag{A-14}$$

where

$$t_{p1} = \frac{\beta_1\ell_1}{\omega} \tag{A-15}$$

$$\epsilon_p = -\frac{1}{\omega}\tan^{-1}\left[\frac{A\sin\theta}{1 + A\cos\theta}\right] \tag{A-16}$$

From setting the differential of ϵ_p with respect to ℓ_2 equal to zero, one finds that ϵ_p becomes maximum when $\theta = \pm\cos^{-1}(-A)$ so that the upper and lower bounds of phase delay error are

$$(\epsilon_p)_U = +\frac{1}{\omega}\tan^{-1}\left(\frac{A}{\sqrt{1 - A^2}}\right) \tag{A-17}$$

$$(\epsilon_p)_L = -\frac{1}{\omega}\tan^{-1}\left(\frac{A}{\sqrt{1-A^2}}\right) \qquad \text{(A-18)}$$

The worst possible case occurs when $A \to 1$ and the error bounds become $\pm 1/(4f)$. For example, at 2.0 GHz the worst-case phase delay error that can be caused by multipath is ± 0.125 ns.

The definition of group delay (Refs. 9, 10) is

$$t_g = -\frac{d}{d\omega}\left[\arg\left(\frac{E_{out}}{E_{in}}\right)\right] \qquad \text{(A-19)}$$

From substitution of Eq. (A-11) into Eq. (A-19), we obtain

$$t_g = t_{g1} + \epsilon_g \qquad \text{(A-20)}$$

where

$$t_{g1} = \frac{d\beta_1}{d\omega}\ell_1 \qquad \text{(A-21)}$$

$$\epsilon_g = -\frac{d}{d\omega}\arg F \qquad \text{(A-22)}$$

where $\arg F$ was given by Eq. (A-12). Note that t_{g1} is the group delay that would be obtained in the absence of multipath and ϵ_g is the group delay error or deviation from t_{g1}.

Performing the operation of Eq. (A-22) and assuming that over the frequency interval of interest

$$\frac{\partial A}{\partial \omega} = 0$$

we obtain

$$\epsilon_g = A(t_{g2} - t_{g1})\left(\frac{A + \cos\theta}{1 + 2A\cos\theta + A^2}\right) \qquad \text{(A-23)}$$

where

$$t_{g2} = \left(\frac{d\beta_2}{d\omega}\right)\ell_2$$

$$t_{g1} = \left(\frac{d\beta_1}{d\omega}\right)\ell_1$$

Note that t_{g1} is the delay through path 1 only in the absence of the multipath signal, while t_{g2} is the delay through path 2 only.

Performing a differentiation[1] of Eq. (A-23) with respect to ℓ_2 and setting the results equal to zero leads to the solutions of the values of θ which give upper and lower bounds of ϵ_g for two different cases. These are given as follows.

Case 1 Upper Bound

Assume $t_{g2} > t_{g1}$ and $\theta = -2\pi m$ where θ was given by Eq. (A-8) and m is a positive integer. In practice, m will usually be an integer greater than 10.

For these conditions, the leakage and primary waves are in phase and the group delay as given by Eq. (A-23) reaches an upper bound of

$$(\epsilon_g)_{U1} = (t_{g2} - t_{g1})\left(\frac{A}{1+A}\right) \qquad \text{(A-23a)}$$

At the same time, note from Eqs. (A-10) and (A-16) that the output signal magnitude ratio and phase delay error become

$$\left|\frac{E_{out}}{E_{in}}\right| = \left|\frac{E_1}{E_{in}}\right|(1 + A) \qquad \text{(A-10a)}$$

$$\epsilon_p = 0 \qquad \text{(A-16a)}$$

It is interesting to note that both the group delay and magnitude of the output signal reach an upper bound simultaneously while the phase delay error goes to zero.

Case 1 Lower Bound

Assume $t_{g2} > t_{g1}$ and $\theta = -(2n-1)\pi$ where θ is defined by Eq. (A-8) and n is a positive integer. In practice, n will usually be an integer greater than 10.

For these conditions, the leakage and primary waves are out of phase and the group delay error as given by Eq. (A-23) reaches a lower bound of

$$(\epsilon_g)_{L1} = -(t_{g2} - t_{g1})\left(\frac{A}{1-A}\right) \qquad \text{(A-23b)}$$

and the output signal magnitude ratio as given by Eq. (A-10) also reaches a lower bound of

$$\left|\frac{E_{out}}{E_{in}}\right| = \left|\frac{E_1}{E_{in}}\right|(1 - A) \qquad \text{(A-10b)}$$

[1] In the differentiation, it is assumed that the radian frequency ω is sufficiently large so that large changes of θ occur with small changes of ℓ_2. Then in the interval over which θ undergoes a 360-deg change, $\partial t_{g2}/\partial \ell_2 \simeq 0$. For those special cases where these assumptions are not valid or where more accuracy is required, one can obtain the exact bounds from incrementing ℓ_2 and performing numerical computations of Eq. (A-23).

while the phase delay error as given by Eq. (A-16) is zero.

Case 2 Upper Bound

Assume $t_{g1} > t_{g2}$ and $\theta = (2n-1)\pi$ where θ is defined by Eq. (A-8) and n is a positive integer. In practice, n will usually be an integer greater than 10.

Under these conditions, the leakage and primary waves are out of phase, but in contrast to Case 1, the group delay error reaches an upper bound of

$$(\epsilon_g)_{U2} = (t_{g1} - t_{g2})\left(\frac{A}{1-A}\right) \tag{A-23c}$$

when the output signal magnitude ratio reaches a *lower* bound of

$$\left|\frac{E_{out}}{E_{in}}\right| = \left|\frac{E_1}{E_{in}}\right|(1-A) \tag{A-10c}$$

and the phase delay error as calculated from Eq. (A-16) is zero.

Case 2 Lower Bound

Assume $t_{g1} > t_{g2}$ and $\theta = 2\pi m$ where θ is given by Eq. (A-8) and m is a positive integer. In practice, m will usually be an integer greater than 10.

Under these conditions the leakage and primary waves are in phase, but the group delay error goes to its lower bound of

$$(\epsilon_g)_{L2} = -(t_{g1} - t_{g2})\left(\frac{A}{1+A}\right) \tag{A-23d}$$

Simultaneously, the output signal magnitude ratio reaches an upper bound of

$$\left|\frac{E_{out}}{E_{in}}\right| = \left|\frac{E_1}{E_{in}}\right|(1+A) \tag{A-10d}$$

and the phase delay error goes to zero.

Differenced Range Versus Integrated Doppler

A parameter which is of primary importance to radio science experiments with a spacecraft is differenced range versus integrated doppler which can be expressed as (Ref. 8)

$$\text{DRVID} = t_g - \hat{t}_p \tag{A-24}$$

Then substitutions of Eqs. (A-14) to (A-16) and Eqs. (A-20) to (A-23) give

$$\begin{aligned}\text{DRVID} = &\left(\frac{d\beta_1}{d\omega} - \frac{\beta_1}{\omega}\right)\ell_1 \\ &+ A(t_{g2} - t_{g1})\left(\frac{A + \cos\theta}{1 + 2A\cos\theta + A^2}\right) \\ &+ \frac{1}{\omega}\tan^{-1}\left[\frac{A\sin\theta}{1 + A\cos\theta}\right]\end{aligned} \tag{A-25}$$

Note that in a dispersionless system

$$\frac{d\beta_1}{d\omega} = \frac{\beta_1}{\omega}$$

and in the absence of multipath, $A = 0$, so that

$$\text{DRVID} = 0$$

Pioneer Venus 1978: Telemetry Performance Predicts

B. K. Levitt
Communications Systems Research Section

The Pioneer Venus 1978 probe-to-Earth telemetry links will be degraded by fading in the atmosphere of Venus. The severity of this fading is characterized by the variance σ_x^2, where the amplitude fading is represented by the lognormal random variable e^x. For the convolutionally encoded/sequentially decoded telemetry modes, the link performance depends on σ_x^2, the total received signal-to-noise ratio P_T/N_0, the modulation index θ, and the decoder computational capacity N. Using nominal values for anticipated system losses, and assuming a maximum deletion rate requirement of 10^{-2}, the minimum required P_T/N_0 and optimum θ are profiled as functions of N and σ_x^2 for the 256-bps large probe telemetry mode. These predictions are based on a recently developed theoretical model for the combined effects of lognormal fading and noisy carrier reference on sequentially decoded phase-shift-keyed telemetry.

I. Introduction

Current plans call for the Pioneer Venus 1978 (PV'78) large probe to have a 256-bps convolutionally encoded/sequentially decoded telemetry mode. Attention has been focused on this particular mode because initial calculations based on a recently developed theoretical model for the combined effects of atmospheric fading and noisy carrier reference (Ref. 1) predict a marginal link performance with available system parameters. The 256-bps link is examined further to determine the effects of system losses, and variations in the fading level and the sequential decoder computational capacity.

II. Objectives

A standard DSN sequential decoder can perform about 25,000 computations/second in real-time operation at 256 bps, this is equivalent to a computational capacity N of roughly 100 computations/bit. However, since a frame deletion is a block of *detected* bit errors, whenever a real-time deletion does occur, we do have the option of storing the soft-quantized received data for that frame and attempting to decode it later at a scaled-down rate with a correspondingly higher N. In this article, we will investigate the dependence of the sequential decoding performance for the 256-bps link on N.

The PV'78 probe-to-Earth telemetry links will be degraded by fading in the atmosphere of Venus. The severity of this fading is characterized by the variance σ_x^2, where the amplitude fading is represented by the lognormal random variable e^x. Our previously published link performance predictions (Ref. 1) were based on a supposed worst case fading level of $\sigma_x^2 = 0.014$, a value computed by Woo (Ref. 2, Eq. 14) in his study of the Venus atmosphere. A more careful examination of Woo's report revealed that the value $\sigma_x^2 = 0.014$ applied to the special case of a probe on the surface of Venus transmitting *vertically* through the atmosphere; the atmosphere was assumed to be 55 km in depth. However, the probe-to-Earth telemetry links may be as much as 60° off the vertical, with an atmospheric path length L that could greatly exceed 55 km. Furthermore, during a probe's approximately 2-hour descent to the surface of Venus, L increases from zero initially to a maximum value at the surface. Using experimental data from the Russian Venera space probes, Woo has derived the following relationship between σ_x^2 and L (Ref. 2, Eqs. 12 and 13):

$$\sigma_x^2 = 0.0142\left(\frac{L}{55}\right)^{11/6};\ L \text{ in km} \qquad (1)$$

The range of σ_x^2 applicable to the probe telemetry links is roughly $0 \leq \sigma_x^2 \leq 0.06$; the variation in the performance of the 256-bps link over this range of fading is determined below.

The previously published link performance analysis assumed an ideal communication system, with no losses other than noisy carrier reference and fading. In fact, however, at 256 bps, the data channel is expected to have a nominal total loss $L_D = 2.08$ dB due to predetection recording (1.00 dB), multipath interference (0.50 dB), waveform distortion (0.20 dB), symbol synchronizer assembly (0.20 dB), and subcarrier demodulator assembly (0.18 dB); the carrier tracking channel loss $L_C = 1.00$ dB is entirely due to predetection recording. The idealized noisy reference/fading model for sequential decoding performance can be adapted to incorporate these system losses by making two equation modifications (Ref. 1, Eqs. 7 and A-17):

$$\rho \equiv \frac{E_B}{N_0} = \left(\frac{1}{L_D}\right)\left(\frac{P_T}{N_0}\right)\left(\frac{\sin^2\theta}{R_B}\right) \qquad (2)$$

$$\eta \equiv \frac{P_c}{N_0 2B_{Lo}} = \left(\frac{1}{L_C}\right)\left(\frac{P_T}{N_0}\right)\left(\frac{\cos^2\theta}{2B_{Lo}}\right) \qquad (3)$$

In these equations, P_T/N_0 is the total received signal-to-noise ratio, θ is the modulation index, the data rate $R_B = 256$ bps, and the two-sided threshold loop noise bandwidth $2B_{Lo} = 12$ Hz. For given values of N and σ_x^2, this modified model is used to compute the minimum P_T/N_0 and optimum θ required to achieve a frame deletion rate of 10^{-2}.

III. Results

Using the formulas for the modified noisy reference/fading model discussed above, a complete telemetry performance profile for the 256-bps sequentially decoded mode was developed. The results of this theoretical study are presented below in a series of graphs. These computations use Layland's formula for the characteristic decoder memory time T_m (Ref. 3, Eq. 6), in which $T_m \sim 2T_B$ (bit time) for sufficiently large N. The validity of this formula is suspect, and it has been identified as a weak link in the modeling efforts (see "Commentary," Ref. 1, p. 60). Stolle (Ref. 4) has suggested that better agreement between the theoretical model and experimental results is obtained when T_m/T_B is increased to about 4 or 5 at 256 bps: this corresponds to more averaging of the fading and noisy reference random processes (Ref. 1, Eq. 11), which should lower the P_T/N_0 requirement for a given system. To investigate the sensitivity of the model to the value of T_m, the sequential decoding performance of several telemetry systems at 256 bps was computed with $T_m/T_B = 2$ and $T_m/T_B = 4$: the difference in required P_T/N_0 in each comparison was small, amounting to about 0.2 dB on the average. The conclusion is that the model is fairly insensitive to refinements in the value of T_m; and the P_T/N_0 requirements presented in this report are reasonably accurate, although they may be interpreted as worst case (slightly high) predictions.

In Fig. 1, the received bit energy-to-noise ratio ρ, required to achieve a frame deletion rate of 10^{-2}, is plotted against the sequential decoder computational capacity N, for the idealized case of perfect carrier reference, no system losses, and no fading ($\sigma_x^2 = 0$). We see that increasing N from 100 computations/bit (real-time decoding) to 1000 or 2000 computations/bit only lowers the required ρ by about 0.5 dB. This special case is intended as a reference point for telemetry design control table (DCT) applications in order to gauge losses (increases in required P_T/N_0) attributed to noisy carrier reference, fading, etc.

Figure 2 still neglects atmospheric fading, but incorporates the noisy reference and non-ideal system losses L_D and L_C. For a given N, the required P_T/N_0 curves have broad minima over the modulation index θ. Increasing N from 100 to 1000 and 2000 computations/bit only lowers the minimum required P_T/N_0 (at the optimal modulation indices, θ_{opt}) by 0.32 and 0.40 dB, respectively.

Figure 3 shows how the minimum required P_T/N_0 and the corresponding θ_{opt} increase with the fading parameter σ_x^2, for $N = 100$ computations/bit. As an example, suppose that the probe has descended to the surface of Venus and is transmitting to Earth in a direction 60° off the vertical; if we assume a spherical atmospheric envelope 55 km in depth, and take the radius of Venus to be 6050 km, we compute an atmospheric path length L of 109 km. Using Eq. (1), this yields a fading parameter $\sigma_x^2 = 0.049$. From the figure, we see that this amount of fading degrades the link by 2.9 dB. Of course, σ_x^2 would only reach 0.49 at the end of the probe's 2-hour descent; initially, $\sigma_x^2 = 0$. For simplicity, we would not want to design the probe telemetry system to permit the modulation index θ to vary continually so as to be always optimized over variations in σ_x^2. Since the required P_T/N_0 is highest at maximum σ_x^2, suppose we fix $\theta = 64.3°$ corresponding to θ_{opt} at $\sigma_x^2 = 0.049$. Because the required P_T/N_0 varies slowly with θ near its minimum for a given σ_x^2, the resulting required P_T/N_0 (dashed curve in Fig. 3) is not significantly higher than in the optimal case (e.g., less than 0.2-dB loss at $\sigma_x^2 = 0$).

Figures 4 and 5 are the same as Fig. 3, except that $N = 1000$ and 2000 computations/bit, respectively. At $\sigma_x^2 = 0.049$, the P_T/N_0 requirement drops by 0.35 dB and 0.42 dB, respectively, due to the increase in N.

Finally, we will discuss the interpretation of these results for telecommunications design control table (Table 1) applications. As an example, we will use information obtained from Figs. 1–3 to form the DCT (shown below) for the real-time decoding case ($N = 100$ computations/bit) with a system optimized for $\sigma_x^2 = 0.049$.

Parameter 1 is a current estimate by the PV'78 Project of the available P_T/N_0, based on the indicated transmitter power, receiver noise temperature, and receiving antenna elevation; this estimate is also based on an assumed probe-to-Earth range of 5.75×10^7 km, transmitting and receiving antenna gains of 1.5 and 61.7 dB (64-m antenna), respectively, and some estimated system losses (e.g., transmitter circuit and pointing losses, polarization loss, etc.). This quoted value is subject to change as the design develops, and this will cause a corresponding change in the performance margins.

Next consider the DCT telemetry performance entries. From Fig. 1 we find that the ρ required to achieve a deletion rate of 10^{-2} in the absence of fading, noisy reference, and system losses is 2.58 dB: this is item 9. Figure 3 tells us that we should set $\theta = 64.3°$ to minimize the required P_T/N_0 when $\sigma_x^2 = 0.49$. Figure 2 shows that if we neglect the fading, a system with $\theta = 64.3°$ (suboptimal) requires $P_T/N_0 = 31.74$ dB, including system losses L_D and L_C. Using Eq. (2), we find that the effect of the noisy reference is to increase ρ to 4.68 dB: the noisy reference loss (item 10) is then given by 4.68−2.58 = 2.10 dB. Returning to Fig. 3, we see that the fading increases the required P_T/N_0 to 34.49 dB (item 15), so that the fading loss is simply 34.49−31.74 = 2.75 dB (item 11). The telemetry performance margin is the difference between the available and required values of P_T/N_0, or 2.45 dB.

Now consider the carrier performance entries in the DCT. Item 2 is the required signal-to-noise ratio in the (two-sided) threshold loop bandwidth $2B_{Lo}$, in the absence of fading and system (predetection recording) losses. For telemetry purposes, this parameter has already been fixed: using Eq. (3) with $P_T/N_0 = 31.74$ dB, we find that $\eta = 12.69$ dB. If we entered this value in item 2, and a 2.75-dB fading loss in item 3, we would have 34.49 dB as the required P_T/N_0 in item 7 and a 2.45-dB margin in item 8. However, instead of gauging the performance of the tracking loop according to its noisy reference telemetry requirements, we will use this section of the DCT to examine it from another point of view. The very long baseline interferometry (VLBI) experiment requires a very clean received carrier, with low phase jitter σ_ϕ^2. Suppose an η of 10 dB in the absence of fading will yield an acceptable σ_ϕ^2: enter this value of η in item 2. Using Eq. (A-3) from the Appendix, we find that $\eta = 10$ dB results in $\sigma_\phi^2 = 0.1416$ rad², with $\sigma_x^2 = 0$. To achieve this same σ_ϕ^2 for arbitrary σ_x^2, we can deduce from Eq. (A-3) that we need

$$\eta \cong (10 + 14.1\,\sigma_x^2)\ \text{dB} \qquad (4)$$

at $\sigma_x^2 = 0.049$, this reduces to $\eta = 10.69$ dB. Therefore, the fading loss is 0.69 dB (item 3). To achieve this performance level, the DCT indicates a required P_T/N_0 of 29.74 dB (item 7), yielding a margin of 7.20 dB (item 8).

Telemetry performance margins for other values of N and σ_x^2 can be computed from the values of required P_T/N_0 in Figs. 3–5, and the equation

$$\text{margin} = 36.94\ \text{dB} - (\text{required } P_T/N_0)\ \text{dB} \qquad (5)$$

References

1. Levitt, B. K., "Performance Degradation of Uncoded and Sequentially Decoded PSK Systems Due to Log-Normal Fading," in *The Deep Space Network Progress Report 42-23*, pp. 58-67, Jet Propulsion Laboratory, Pasadena, Calif., Oct. 15, 1974.

2. Woo, R., et al., *Effects of Turbulence in the Atmosphere of Venus On Pioneer Venus Radio—Phase 1*, Technical Memorandum 33-644, Jet Propulsion Laboratory, Pasadena, Calif., June 30, 1973.

3. Layland, J. W., "A Model for Sequential Decoding Overflow Due to a Noisy Carrier Reference," *Proceedings of the International Telemetering Conference* (ITC), Oct. 15–17, 1974, Los Angeles, Calif.

4. Stolle, E., Deutsche Forschungs Versuchsanstalt fur Luft und Raumfahrt, Private communication given at Helios Working Group Splinter Session, September 27, 1973.

5. Tausworthe, R. C., *Theory and Practical Design of Phase-Locked Receivers*, Vol. 1, Technical Report 32-819, Jet Propulsion Laboratory, Pasadena, Calif., Feb. 15, 1966.

Table 1. Telecommunications design control table

	Item	Parameter	Nominal value, dB	Comments
	1	Available P_T/N_0	36.94	XMTR: 41.9 watts RCVR: 26.1 K, 30° elevation
Carrier performance	2	Threshold SNR, η	10.00	VLBI requirement
	3	Fading loss	0.69	$\sigma_x^2 = 0.049$
	4	System loss, L_G	1.00	
	5	$2B_{Lo}$	10.79	12 Hz
	6	$\cos^2\theta$	−7.26	$\theta = 64.3°$
	7	Required P_T/N_0	29.74	Item 2 + item 4 + item 5 − item 6
	8	Margin	7.20	Item 1 − item 7
Telemetry performance	9	Ideal ρ (lossless)	2.58	Deletion rate = 10^{-2}
	10	Noisy reference	2.10	
	11	Fading loss	2.75	$\sigma_x^2 = 0.049$
	12	System loss, L_D	2.08	
	13	Rate, R_B	24.08	256 bps
	14	$\sin^2\theta$	−0.90	$\theta = 64.3°$
	15	Required P_T/N_0	34.49	Item 9 + item 10 + item 11 + item 12 + item 13 − item 14
	16	Margin	2.45	Item 1 − item 15
Telemetry mode: PV'78 large probe real-time telemetry link (N = 100 computations/bit) at 256 bps, using sequential decoding.				

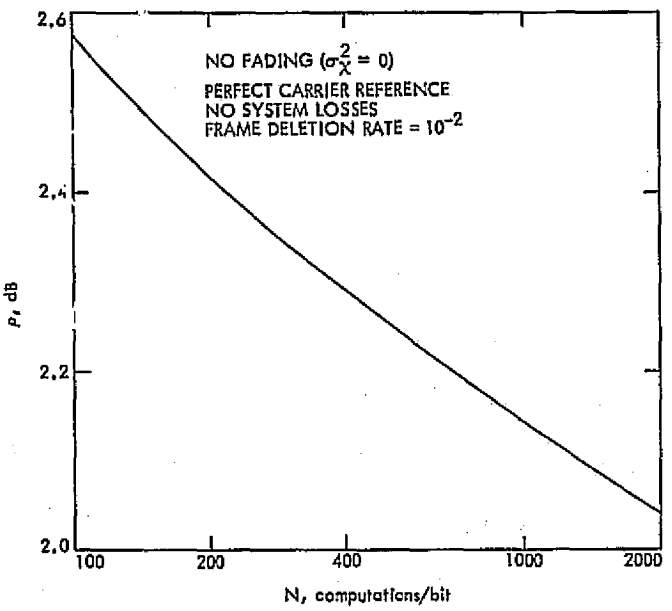

Fig. 1. Received bit energy-to-noise ratio ρ, required to achieve a frame deletion rate of 10^{-2}, as a function of sequential decoder computational capacity N, neglecting fading, noisy carrier reference, and system losses

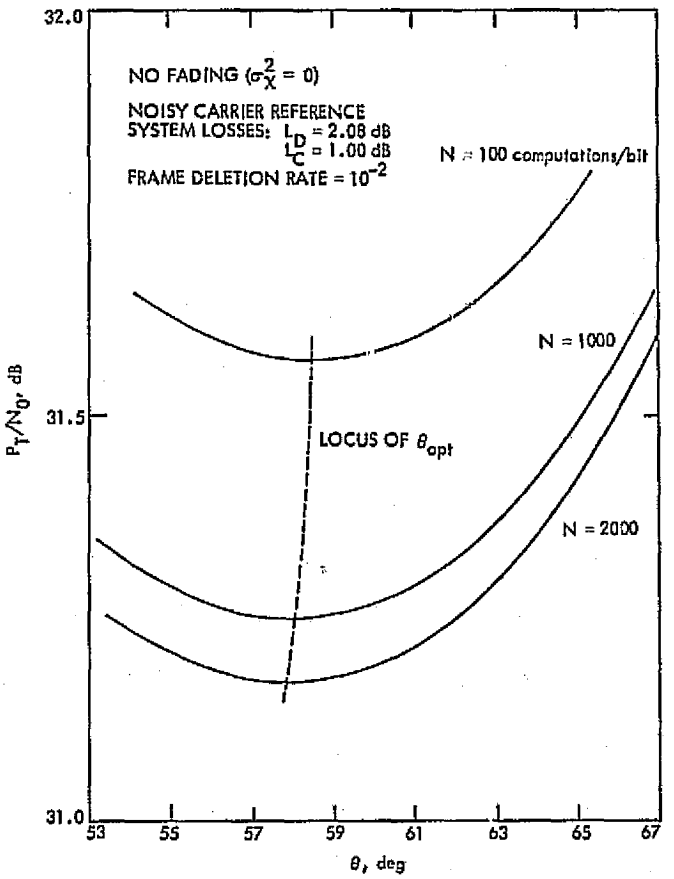

Fig. 2. Total received signal power-to-noise ratio P_T/N_0, required to achieve a deletion rate of 10^{-2}, as a function of modulation index θ, for a given computational capacity N, neglecting atmospheric fading

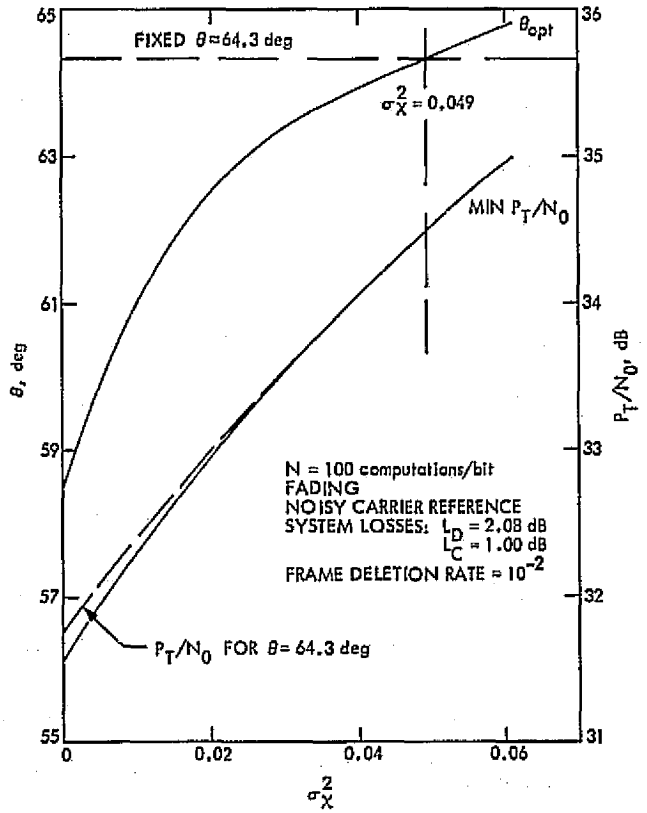

Fig. 3. Minimum received signal-to-noise ratio P_T/N_0 and corresponding optimum modulation index θ, required to achieve a deletion rate of 10^{-2}, as a function of fading variance σ_x^2, when computational capacity $N = 100$ computations/bit

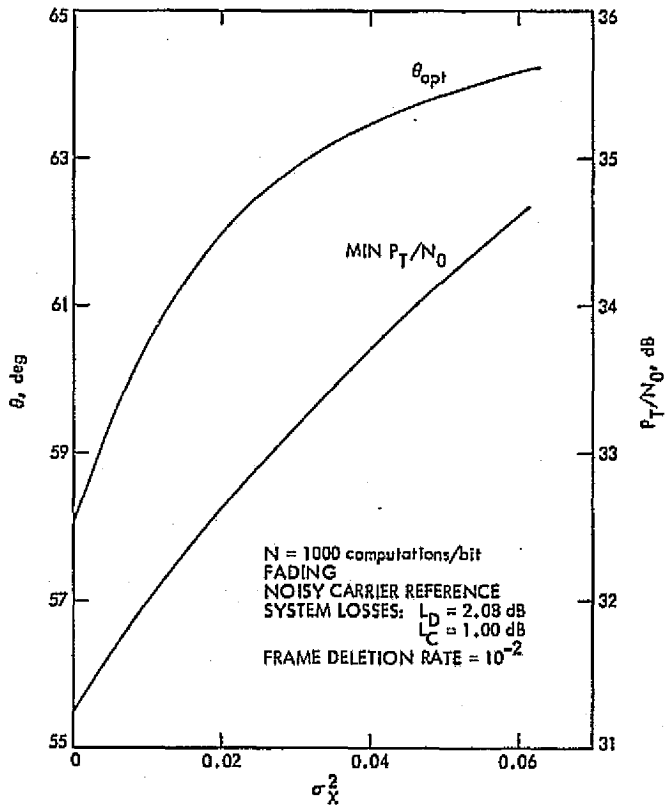

Fig. 4. Same as Fig. 3, except $N = 1000$ computations/bit

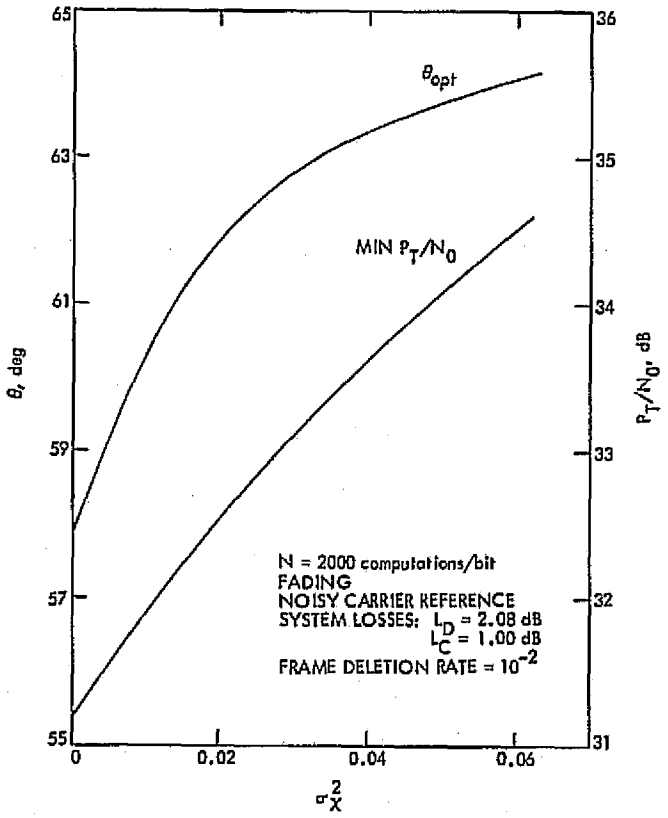

Fig. 5. Same as Fig. 3, except N = 2000 computations/bit

Appendix

Phase Jitter of a Linearized Second-Order Phase-Locked Loop Preceded by a Bandpass Limiter in the Presence of Lognormal Fading

Suppose the input to a second-order phase-locked loop receiver is degraded by lognormal amplitude fading, represented by the random variable e^{χ} at some instant of time. It is assumed that the threshold loop parameter ratio $r_0 = 2$, and the bandpass limiter preceding the phase-locked loop is operating in the limiter suppression region (limiter input signal-to-noise ratio $\eta_i << 1$). Then, linear phase-locked loop theory has shown (Ref. 1, Eq. A-15) that the effective signal-to-noise ratio in the (one-sided) operating loop bandwidth B_L has the form

$$\rho_L \cong \frac{5.172\,\eta\,e^{2\chi}}{2\sqrt{\eta}\,e^{\chi} + 1} \tag{A-1}$$

where η is the signal-to-noise ratio in the (two-sided) threshold loop bandwidth $2B_{L0}$.

Conditioned on ρ_L, the variance of the loop phase error, called phase "jitter," is approximated by (Ref. 5, Eq. 8–17)

$$\sigma_\phi^2 \cong \frac{1}{\rho_L} \tag{A-2}$$

using the linear model for the loop. If the mean of the Gaussian random variable χ is the negative of its variance σ_χ^2 (Ref. 2, Eq. 8), the expected phase jitter is then given by

$$\begin{aligned}\overline{\sigma_\phi^2} &\cong \frac{2\sqrt{\eta}\,\overline{e^{-\chi}} + \overline{e^{-2\chi}}}{5.172\eta} \\ &= \frac{2\sqrt{\eta}\exp(3\sigma_\chi^2/2) + \exp(4\sigma_\chi^2)}{5.172\eta}\end{aligned} \tag{A-3}$$

Convolutional Codes for *M*-ary Orthogonal and Simplex Channels

R. F. Lyon
Communications Systems Research Section

Convolutional codes chosen for greatest free distance or lowest error probability on a binary channel are not necessarily good codes for an M-ary channel. A rate k/ν coder generates a 2^ν-ary output symbol for each k input bits. If a binary channel is used, the appropriate measure of distance between these symbols is Hamming distance (number of bit disagreements). But if either a 2^ν-ary orthogonal channel, or a 2^ν-ary simplex channel is used, the distance between any two different symbols is unity (number of symbol disagreements). Other distance measures are appropriate on other M-ary channels. Good rate 1/2 and 1/3 codes have been found by computer search for the orthogonal 4-ary and 8-ary channels. The result is a reduction of error probabilities by about a factor of two below previously tabulated codes. The computer technique used is described. At a fixed constraint length, further performance improvement results from increasing ν, up to a limit at ν = K (constraint length) on the orthogonal 2^ν-ary channel.

I. Introduction

Good codes have codewords that are "far apart" in signal space. When a codeword is a sequence of antipodal signals designed for a binary channel, the Hamming distance defines "far apart." Convolutional codes with the largest possible minimum Hamming distance between any pair of codewords (free distance) have been tabulated for rate 1/2, 1/3, and 1/4, for constraint lengths up to 14 (Ref. 1). But Hamming distance is not the correct measure of distance in many signal spaces; those systems that use a larger number of symbols, $M > 2$, have a wide variety of distance measures. The simplest of these are the orthogonal and simplex distance measures—the distance from a symbol to any other symbol is one, and the distance to itself is zero. Other possibilities are biorthogonal, where the distance from a symbol to its negative is twice all other distances; phase shift keying, where two dimensional Euclidian distances between points on a circle are used; and combined phase and amplitude keyed systems, with more complicated distance measure. We will concern ourselves only with symmetric systems; that is, the set of distances of all symbols from symbol x_i is independent of i.

II. The Convolutional Coder

A convolutional coder consists of a shift register to hold a short history of the input, and a group of mod-2 adders (parity generators) to compute output symbols as a function of past and present inputs (see Fig. 1). Inputs are shifted into the register in groups of k bits; the register holds K such groups, where K is called the constraint length of the coder. The number of binary symbols generated per input of k bits is termed ν. We extend the concept of the coder to let these ν bits select one of $M = 2^\nu$ channel symbols. We make no attempt to generalize the relation between ν and M.

The coder rate is k/ν bits per binary symbol, or k bits per M-ary symbol; that is, each k input bits result in the output of one $2^\nu = M$-ary channel symbol. Then an input of length L (groups of k bits) causes an output of length $L + K - 1$ (symbols).

III. Distance Between Code Words

Since the coder uses only linear mod-2 adders, an all-zero input corresponds to an all-zero output of binary symbols, which selects a symbol sequence all-x_0. Each codeword corresponding to a length L input (with zeroes before and after) differs from a sequence of x_0's in at most $L + K - 1$ places. Then, with $L = 1$, an immediate upper bound on the minimum distance between codewords is

$$d_f \leq K \cdot d_{\max} \tag{1}$$

where $d_{\max}$ is the greatest distance from x_0 to another codeword. This bound is often quite loose. For example, using $M = 4$ with distances 0, 1, 1, 2 corresponds to the familiar Hamming distance on a binary channel with symbols grouped in pairs. Since $d_{\max} = 2$, our simple bound is

$$d_f \leq 2K$$

A much better well-known bound (Ref. 2) for a binary channel is

$$d_f \leq \min_{L>0} \left[\frac{2^\nu}{2^\nu - 1} (K + L - 1) \right] \tag{2}$$

For example, at $K = 8$ the bounds are 16 and 10, respectively.

We can informally estimate d_f by assuming the coder generates K outputs which are random and equally likely to be either (a) any of M symbols, or (b) any of $M - 1$ symbols different from x_0. That is,

$$\left.\begin{aligned} &\text{(a)} \quad d_f \approx K \cdot \left[\sum_{i=0}^{M} |x_0 - x_i| \right] \Big/ M \\ &\text{(b)} \quad d_f \approx K \cdot \left[\sum_{i=1}^{M} |x_0 - x_i| \right] \Big/ (M-1) \end{aligned}\right\} \tag{3}$$

Then in our example ($K = 8$, distances 0, 1, 1, 2) we would estimate

$$\text{(a)} \quad d_f \approx \frac{0+1+1+2}{4} \cdot K = 8$$

$$\text{(b)} \quad d_f \approx \frac{1+1+2}{3} \cdot K = 10.7$$

We conjecture that for any symmetric distance measure, and large enough K, (3b) is an upper bound on d_f, though for small K (e.g., $K = 1$) it is obvious that the greater bound $d_f \leq K \cdot d_{\max}$ can be achieved. We further conjecture that a d_f at least as great as (3a) can always be achieved, even for large K.

IV. Finding Codes With Large Free Distance

In the last section we showed how to estimate the free distance of a good code. In this section we describe a computer technique for finding codes that meet or nearly meet this estimate. We will consider only orthogonal and simplex symbols—all distances are one, and the estimate (3b) is the same as the bound (1); $d_f \leq K$.

We will represent the connections from the shift register to the adders by ν vectors of kK bits; these are called connection vectors $g_1, g_2, \cdots, g_\nu$. A one in bit i of g_j represents a connection from the ith shift register stage, $1 \leq i \leq kK$, to the jth adder. The output of the jth adder after the nth bit of data input $x(n)$ is

$$S_j(n) = g_j * x = \sum_{i=1}^{kK} g_j(i) \cdot x(n - i + 1) \pmod 2 \tag{4}$$

The data are convolved with the connection vectors (code generators or generating polynomials), hence the name convolutional code.

To find good codes of short constraint length, we propose to test all possible values of the connection vectors.

For $K = 8$, $k = 1$, $\nu = 2$ (code rate $R_c = 1/2$), the number of possibilities is

$$N = 2^{K\nu} = 2^{16} = 65536$$

However, many of these are duplications. We may wish to check each possibility to see if its reflections have already been considered before proceeding to evaluate the free distance and other properties.

An obvious way to measure free distance is to compute the distance of all codewords from the zero codeword, and take the minimum. This procedure is not effective, however, because there are an infinite number of codewords to test. We can modify the procedure to check distances of all codewords generated by inputs of length $\ell \leq L_{max}$. But then we have to consider what value of L_{max} is sufficient; a proven bound on the sufficient L_{max} is prohibitively large (Ref. 3). But experience shows that $L_{max} = kK$ (bits) is probably sufficient (at least for orthogonal distance measure). Then there are $2^{L_{max}-1} = 128$ inputs to consider for each code in our example. For all codes, the total number of inputs to check is $2^{K\nu+L_{max}-1} = 2^{23}$. Each requires the calculation of up to $\nu(kK + L_{max} - 1) = 30$ output bits, by adding $kK = 8$ bits modulo 2. This makes about $2^{31} \approx 2$ billion elementary operations. For $K = 12$ this figure becomes about $2^{44} \approx 10^{13}$.

But all is not hopeless. Suppose we wish to search for codes with $d_f \geq d_{min}$. Use a program that starts checking with short inputs, and gives up on a code as soon as any distance is less than d_{min}. For example, we hope to meet the bound $d_f = 8$ in the $K = 8$ example, so set $d_{min} = 8$. The first input to try is a single one ($\cdots 010 \cdots$). The output will just be K groups of ν bits, one from each connection vector. If any group of ν bits is all zero, the distance will not equal K, otherwise it will. So there are $(2^\nu - 1)^K$ codes that pass this first step, out of $2^{\nu K}$ total tested. In our example, 6561 codes survive (about 10%). In $2^{\nu K} \cdot kK \cdot kK = 2^{22} = 4$ million elementary operations, the bulk of the task has been eliminated. Less dramatic reductions are made for successively longer inputs. To eliminate a large memory requirement, the loop on input lengths should be within the loop on codes. Any code that survives through $\ell = L_{max}$ is printed. Comparisons can then be made between the codes generated to determine which are better by some other criteria.

Rather than continuing the procedure through a large L_{max} which is felt to be sufficient, it may be useful to stop with a moderately small L_{max}, and send the surviving codes to a true free distance computing algorithm; several effective algorithms are known (Refs. 1, 4, and 5).

V. Evaluating Other Code Properties

Associated with every convolutional code is a transfer function[1] (Ref. 6)

$$T(D, N, L) = \sum_{i=1}^{\infty} \sum_{j=1}^{\infty} \sum_{l=1}^{j} a_{ijl} D^i N^j L^l \qquad (5)$$

where each term represents a_{ijl} inputs of length ℓ, with codewords at distance i from the all-zero codeword, and differing from the all-zero input in j bits. The transfer function is useful for evaluating bounds on the first event error probability P_E and the bit error probability P_B (Ref. 6). It is shown that

$$P_E \leq T(D, N, L)\big|_{N=1,\, L=1,\, D=D_0}$$
$$P_B \leq \frac{\partial T(D, N, L)}{\partial N}\bigg|_{N=1,\, L=1,\, D=D_0} \qquad (6)$$

where for a stationary channel

$$D_0 = \sum_{y_r} P(y_r|x_r)^{1/2} P(y_r|x'_r)^{1/2} < 1 \qquad (7)$$

for $\{y_r\}$ the set of channel outputs, and x_r and x'_r the correct and incorrect input symbols, separated by a unit distance.

The computer procedure described in the preceding section is useful in that all coefficients of terms of $T(D, N, L)$ with exponents of L less than or equal to L_{max} can be exactly calculated with little extra computation. Then P_E and P_B can be estimated, though not necessarily bounded.

Since there are several codes with a maximum value of d_f, we must choose between them by other considerations, such as: (a) minimum P_E as $D_0 \to 0$; (b) minimum P_B as $D_0 \to 0$; (c) minimum P_E at some chosen value of D_0; (d) minimum P_B at some chosen value of D_0. It is often possible to find a code which is best or almost best on all these conditions over a wide range of D_0.

FORTRAN subroutines, listed in the appendix, have been written to carry out the evaluation of $T(D, N, L)$, and P_E and P_B, for a list of values of D_0. The subroutine

[1] Differs from Viterbi's representation in the meaning of the exponent of L.

EVAL is set up to return without output as soon as any distance is less than the supplied value of M, or to return the new d_f in variable M if $d_f \geq M$; so in checking a list of possible codes, M can be initially set small (even zero) and the program will print all codes with d_f at least as great as the d_f of the previously printed code.

VI. Results

For $K \leq 8$ there are many rate 1/2 codes with $d_f = K$ on the 4-ary orthogonal channel. For $K \geq 9$, there are none with $d_f = K$.

Table 1 lists the best codes found (in terms of P_B for $D_0 < 0.4$), along with some previously known codes (designed for the binary channel). The leading terms of the error probability estimates are also listed in Table 1. Figure 2 is a graph of the estimates of P_B versus D_0 for all the codes in Table 1. Notice that the previously known $K = 11$ code is worse than either of the $K = 10$ codes.

Codes with $d_f = K$ are much more abundant for $\nu > 2$; but the number of codes to check is also much greater. At $K = 8$, $\nu = 3$ (rate 1/3) there are $2^{\nu K} = 16$ million codes to check; the first distance check with input $\cdots 010 \cdots$ only brings this down to $(2^\nu - 1)^K = 5.8$ million. But we can find plenty of good codes without checking these by building on the rate 1/2 codes. If g_1 and g_2 form a rate 1/2 code with free distance d_f, then the addition of any g_3 forms a rate 1/3 code with free distance $\geq d_f$ on the 8-ary channel. If the bound was met at $\nu = 2$, it will be met at $\nu = 3$; if it was not met at $\nu = 2$, it may be improved at $\nu = 3$. And many good rate 1/3 codes will also be good rate 2/3 codes. Similarly, good codes are easily found for the 16-ary orthogonal channel at rates 1/4, 2/4, and 3/4.

The rate 1/3 codes in Table 2 were found by taking g_1 and g_2 from the best rate 1/2 code, then trying all values of g_3 to find the best. The resulting bit error probabilities are compared with those of previously tabulated codes (Ref. 1) in Fig. 3. Notice that the best $K = 4$ code found by this procedure is not quite as good as the one from Ref. 1.

We can hypothesize a best possible rate $1/\nu$ code by assuming that every non-zero data sequence in the coder will result in an output different from the zero output. Then the distance of any codeword caused by a length ℓ input ($\ell \leq K$) will be $K + \ell - 1$. Thus the transfer function of the code will be

$$\begin{aligned} T(D,N,L) &= D^K NL + D^{K+1}N^2L^2 + D^{K+2}(N^2 + N^3)L^3 \\ &\quad + D^{K+3}(N^3 + 2N^4 + N^5)L^4 + \cdots \\ &= D^K\left[NL + \sum_{l=2}^{K} D^{l-1}L^l \sum_{j=2}^{l}\binom{l-2}{j-2}N^j\right] \\ &\quad + \text{terms with higher } \ell \end{aligned} \tag{8}$$

We can continue to estimate P_E and P_B by truncating the transfer function to $\ell \leq L_{\max} = K$; thus we will have a comparison between our codes and these ideal codes. We see that

$$\begin{aligned} P_B &\approx D_0^K\left[1 + \sum_{l=2}^{K} D_0^{l-1} \sum_{j=2}^{l}\binom{l-2}{j-2}\right] \\ &= D_0^K\left[1 + D_0\sum_{l=2}^{K}(2D_0)^{l-2}\right] \\ &\approx D_0^K[1 + D_0 + 2D_0^2 + 4D_0^3 + 8D_0^4 + \cdots] \end{aligned} \tag{9}$$

and

$$\begin{aligned} P_B &\approx D_0^K\left[1 + \sum_{l=2}^{K} D_0^{l-1} \sum_{j=2}^{l} j\binom{l-2}{j-2}\right] \\ &= D_0^K\left[1 + \sum_{l=2}^{K}(2D_0)^{l-2}\cdot\left(\frac{l+2}{2}\right)\right] \\ &\approx D_0^K[1 + 2D_0 + 5D_0^2 + 12D_0^3 + 28D_0^4 + \cdots] \end{aligned} \tag{10}$$

For a fixed constraint length K, these codes can actually be achieved if ν is allowed to increase sufficiently (this corresponds to an exponential increase in bandwidth when using an orthogonal signal set of size 2^ν). In fact, these codes are the "orthogonal tree codes" of Ref. 7 with $\nu = K$. Each connection vector has a single one; that is, the ν-bit symbol number is just taken from the last K input bits, with no mod-2 adders needed (see Fig. 4).

Figure 5 shows how close our rate 1/2 and 1/3 codes come to this idealization, on the basis of P_B. Notice that at $K = 3$, $\nu = 3$ these achieve the idealization, but for large K, miss by more than 10% of D_0.

VII. Application to Noncoherent MFSK

A channel with random phase disturbances used with multi-frequency-shift-keying is described in the literature (Refs. 8, 9, and 10). From the channel output statistics

we can calculate D_0 as a function of the predetection signal-to-noise ratio, $ST/N_0 = \alpha^2/2$. When frequency m is transmitted, the receiver outputs are $r_1, r_2, \cdots, r_M$, where

$$p(r_j) = \begin{cases} r_j \exp\left(-\frac{r_j^2}{2}\right), & \text{if} \quad j \neq m \\ r_m \exp\left(-\frac{r_m^2}{2} - \frac{\alpha^2}{2}\right) I_0(\alpha r_m), & \text{if} \quad j = m \end{cases} \tag{11}$$

Then we can calculate D_0 from Eq. (7):

$$\begin{aligned} D_0 &= \int\int p(r_j)^{1/2} p(r_m)^{1/2} dr_j dr_m, \qquad j \neq m \\ &= \left\{ \int_0^\infty r \exp\left(-\frac{r^2}{2}\right) \left[\exp\left(-\frac{\alpha^2}{2}\right) I_0(\alpha r) \right]^{1/2} dr \right\}^2 \end{aligned} \tag{12}$$

Notice that D_0 does not depend on M, the number of frequencies (symbols). By using Taylor series we can compute an asymptotic value for small α:

$$D_0 \approx \exp\left(-\frac{\alpha^4}{16}\right) \approx \exp\left[-\left(\frac{ST}{2N_0}\right)^2\right], \qquad \frac{ST}{N_0} \ll 1$$

Using $I_0(x) \to \exp(x)/\sqrt{2\pi x}$, we find for large α:

$$D_0 \approx \frac{\sqrt{\pi}}{2} \alpha \exp\left(-\frac{\alpha^2}{4}\right) = \sqrt{\frac{\pi ST}{2N_0}} \exp\left(-\frac{ST}{2N_0}\right), \qquad \frac{ST}{N_0} \gg 1$$

A numerically calculated curve of D_0 versus ST/N_0 is shown in Fig. 6. When using this channel with small ST/N_0, we will repeat each symbol n times (extend the tone duration to nT), to bring D_0 down to

$$D_0' = D_0^n \approx \exp\left[-n\left(\frac{ST}{2N_0}\right)^2\right], \qquad \frac{ST}{N_0} < 1 \tag{13}$$

We will use a rate $1/\nu$ coder to send one bit per branch, at a bit rate of $1/(nT)$ bps. From a specification of acceptable bit error rate and a chosen code, we can choose D_0, and hence determine the required value of the product $n(ST/2N_0)^2$.

For example, if we need $P_B \leq 10^{-3}$, and we wish to use $M = 4$ frequencies and constraint length $K = 7$, Fig. 2 indicates that $D_0 \leq 0.25$ will suffice. This requires $n(ST/2N_0)^2 \geq 1.39$. Now if we are constrained by power to $ST/N_0 = 0.2$, then we must use $n = 139$ or more. The resulting data rate is $R = 1/139T$ bps, compared to the wideband capacity (Ref. 8)

$$C = \frac{S}{N_0 \ln 2} \cdot \frac{ST/N_0}{2 + (ST/N_0)} = 0.0262/T \text{ bps}$$

for an estimated code efficiency of

$$\frac{R}{C} = \frac{1}{139 \cdot 0.0262} = 0.275$$

(See Ref. 9 for some actual simulated code efficiencies.)

Can we improve on this? Suppose we keep $K = 7$ fixed and allow ν to increase to K, and M to increase to $2^\nu = 128$ frequencies. The ideal code ($\nu = K$) performance from Fig. 5 indicates that $D_0 \leq 0.324$, or $n(ST/2N_0)^2 \geq 1.13$ will suffice. Keeping $ST/N_0 = 0.2$, we need $n = 113$, for $R = 1/113T$, and $R/C = 0.338$. Thus, by allowing bandwidth expansion, without necessitating a more complicated decoder, we improve the rate by $139/113 = 1.22$. Furthermore, the coder is simplified to just a K-bit shift register, with parallel outputs going to an M-ary transmitter. However, the increased bandwidth necessitates a more complicated receiver and demodulator.

VIII. Conclusions

The bounds on P_E and P_B from Ref. 6 do not converge for $D_0 \geq 0.5$, and are very difficult to evaluate in any case. But the estimates presented in this paper, based on error sequences of length $\ell \leq L_{max}$ are easily formed finite sums. These estimates are useful in finding good convolutional codes, and in predicting error statistics.

Good codes are needed for each different measure of distance on a channel. These good codes can look surprisingly different from codes designed for binary channels—the best code of fixed constraint length for the very noisy wideband noncoherent MFSK channel simply sends each input bit to the transmitter K times in K positions.

More work is needed to compile a list of good codes for all commonly used M-ary channels.

References

1. Larsen, K. J., "Short Convolutional Codes with Maximal Free Distance for Rates 1/2, 1/3, and 1/4," *IEEE Trans. Inform. Theory*, Vol. IT-19, pp. 371–372, May 1973.

2. Heller, J. A., "Sequential Decoding: Short Constraint Length Convolutional Codes," in *Supporting Research and Advanced Development*, Space Programs Summary 37-54, Vol. III, pp. 171–177, Jet Propulsion Laboratory, Pasadena, Calif., Dec. 31, 1968.

3. Costello, D. J., *Construction of Convolutional Codes for Sequential Decoding*, Technical Report EE-692, Department of Elec. Eng., Univ. of Notre Dame, Notre Dame, Ind., Aug. 1969.

4. Forney, G. D., Jr., "Use of a Sequential Decoder to Analyze Convolutional Code Structure," *IEEE Trans. Inform. Theory*, Vol. IT-16, pp. 793–795, Nov. 1970.

5. Bahl, L. R., Cullum, C. D., Frazer, W. D., and Jelinek, F., "An Efficient Algorithm for Computing Free Distance," *IEEE Trans. Inform. Theory*, Vol. IT-18, pp. 437–439, May 1972.

6. Viterbi, A. J., "Convolutional Codes and Their Performance in Communication Systems," *IEEE Trans. Commun. Technol.*, Vol. COM-19, pp. 751–772, Oct. 1971.

7. Viterbi, A. J., "Orthogonal Tree Codes," in *Supporting Research and Advanced Development*, Space Programs Summary 37-39, Vol. IV, pp. 204–209, Jet Propulsion Laboratory, Pasadena, Calif., June 30, 1966.

8. Bar-David, I., and Butman, S., "Performance of Coded, Noncoherent, Hard-Decision MFSK Systems," Technical Report 32-1526, Vol. XIII, pp. 82–91, Jet Propulsion Laboratory, Pasadena, Calif., Nov. 1972.

9. Butman, S., and Klass, M. J., "Capacity of Noncoherent Channels," Technical Report 32-1526, Vol. XVIII, pp. 85–93, Jet Propulsion Laboratory, Pasadena, Calif., Sept. 1973.

10. Butman, S. A., and Lyon, R. F., "Performance of Noncoherent MFSK Channels with Coding," *International Telemetering Conference Proceedings*, Los Angeles, October 15-17, 1974, Vol. X, pp. 142–150.

Table 1. Best known rate 1/2 convolutional codes (a) and previously tabulated codes (b) with error probability estimates based on error sequences with $\ell \leq K$, on the orthogonal 4-ary channel

K	Code (hexadecimal)		P_E estimate	P_B estimate	Type
2	2	3	$D^2 + D^3$	$D^2 + 2D^3$	a, b
3	5	7	$D^3 + 2D^4 + \cdots$	$D^3 + 4D^4 + \cdots$	a, b
4	A	D	$D^4 + 4D^5 + \cdots$	$D^4 + 10D^5 + \cdots$	a
4	D	F	$2D^4 + 3D^5 + \cdots$	$3D^4 + 8D^5 + \cdots$	b
5	12	1F	$2D^5 + 3D^6 + \cdots$	$3D^5 + 7D^6 + \cdots$	a
5	13	1D	$3D^5 + 2D^6 + \cdots$	$6D^5 + 7D^6 + \cdots$	b
6	2E	3D	$2D^6 + 8D^7 + \cdots$	$3D^6 + 25D^7 + \cdots$	a
6	2B	3D	$4D^6 + 8D^7 + \cdots$	$10D^6 + 21D^7 + \cdots$	b
7	52	6D	$4D^7 + 8D^8 + \cdots$	$7D^7 + 27D^8 + \cdots$	a
7	5B	79	$D^6 + 4D^7 + 7D^8 + \cdots$	$D^6 + 10D^7 + 24D^8 + \cdots$	b
8	AD	DF	$6D^8 + 12D^9 + \cdots$	$17D^8 + 49D^9 + \cdots$	a
8	A7	F9	$2D^7 + 3D^8 + 12D^9 + \cdots$	$5D^7 + 6D^8 + 43D^9 + \cdots$	b
9	172	19F	$D^8 + 7D^9 + \cdots$	$2D^8 + 22D^9 + \cdots$	a
9	171	1EB	$2D^8 + 5D^9 + \cdots$	$4D^8 + 16D^9 + \cdots$	b
10	2DD	812	$2D^9 + 8D^{10} + \cdots$	$3D^9 + 37D^{10} + \cdots$	a
10	277	365	$D^8 + 3D^9 + 8D^{10} + \cdots$	$D^8 + 7D^9 + 27D^{10} + \cdots$	b
11	5AD	73F	$3D^{10} + 18D^{11} + \cdots$	$5D^{10} + 70D^{11} + \cdots$	a
11	4DD	7B1	$D^8 + D^9 + 8D^{10} + 20D^{11} + \cdots$	$3D^8 + 2D^9 + 6D^{10} + 95D^{11} + \cdots$	b
12	A4F	DAD	$9D^{11} + 20D^{12} + \cdots$	$27D^{11} + 113D^{12} + \cdots$	a
12	8DD	BD3	$3D^{10} + 8D^{11} + 26D^{12} + \cdots$	$6D^{10} + 42D^{11} + 128D^{12} + \cdots$	b

Table 2. Rate 1/3 convolutional codes and error probability estimates: (a) best codes found by procedure in text, (b) previously known codes

K	Code (hexadecimal)			P_E estimate	P_B estimate	Type
3	5	7	4	$D^3 + D^4 + 2D^5$	$D^3 + 2D^4 + 5D^5$	a
3	5	7	7	$D^3 + 2D^4 + D^5$	$D^3 + 4D^4 + 8D^5$	b
4	A	D	9	$D^4 + D^5 + 3D^6 + \cdots$	$D^4 + 2D^5 + 8D^6 + \cdots$	a
4	B	D	F	$D^4 + D^5 + 3D^6 + \cdots$	$D^4 + 2D^5 + 7D^6 + \cdots$	b
5	12	1F	14	$D^5 + D^6 + 4D^7 + \cdots$	$D^5 + 2D^6 + 11D^7 + \cdots$	a
5	15	1B	1F	$D^5 + 2D^6 + 2D^7 + \cdots$	$D^5 + 4D^6 + 6D^7 + \cdots$	b
6	2E	3D	24	$D^6 + D^7 + 5D^8 + \cdots$	$D^6 + 2D^7 + 13D^8 + \cdots$	a
6	27	2B	3D	$D^6 + 2D^7 + 3D^8 + \cdots$	$D^6 + 5D^7 + 10D^8 + \cdots$	b
7	52	6D	46	$D^7 + 2D^8 + 4D^9 + \cdots$	$D^7 + 4D^8 + 15D^9 + \cdots$	a
7	5B	65	7D	$2D^7 + 2D^8 + 5D^9 + \cdots$	$3D^7 + 7D^8 + 18D^9 + \cdots$	b
8	AD	DF	99	$D^8 + 2D^9 + 7D^{10} + \cdots$	$D^8 + 5D^9 + 22D^{10} + \cdots$	a
8	95	D9	F7	$D^8 + 3D^9 + 5D^{10} + \cdots$	$D^8 + 7D^9 + 15D^{10} + \cdots$	b
9	172	19F	134	$D^9 + 2D^{10} + 8D^{11} + \cdots$	$D^9 + 5D^{10} + 22D^{11} + \cdots$	a
9	16F	1B3	1C9	$D^9 + 2D^{10} + 8D^{11} + \cdots$	$D^9 + 5D^{10} + 26D^{11} + \cdots$	b
10	2DD	312	27B	$D^{10} + 5D^{11} + 4D^{12} + \cdots$	$D^{10} + 14D^{11} + 14D^{12} + \cdots$	a
10	24F	2F5	39B	$D^{10} + 6D^{11} + 3D^{12} + \cdots$	$D^{10} + 19D^{11} + 10D^{12} + \cdots$	b
11	5AD	73F	474	$D^{11} + 5D^{12} + 8D^{13} + \cdots$	$D^{11} + 14D^{12} + 28D^{13} + \cdots$	a
11	56B	5B9	67D	$2D^{11} + 8D^{12} + 4D^{13} + \cdots$	$4D^{11} + 28D^{12} + 15D^{13} + \cdots$	b
12	A4F	DAD	959	$D^{12} + 6D^{13} + 9D^{14} + \cdots$	$D^{12} + 16D^{13} + 37D^{14} + \cdots$	a
12	9F7	BD3	CB5	$D^{11} + 6D^{13} + 9D^{14} + \cdots$	$D^{11} + 16D^{13} + 32D^{14} + \cdots$	b

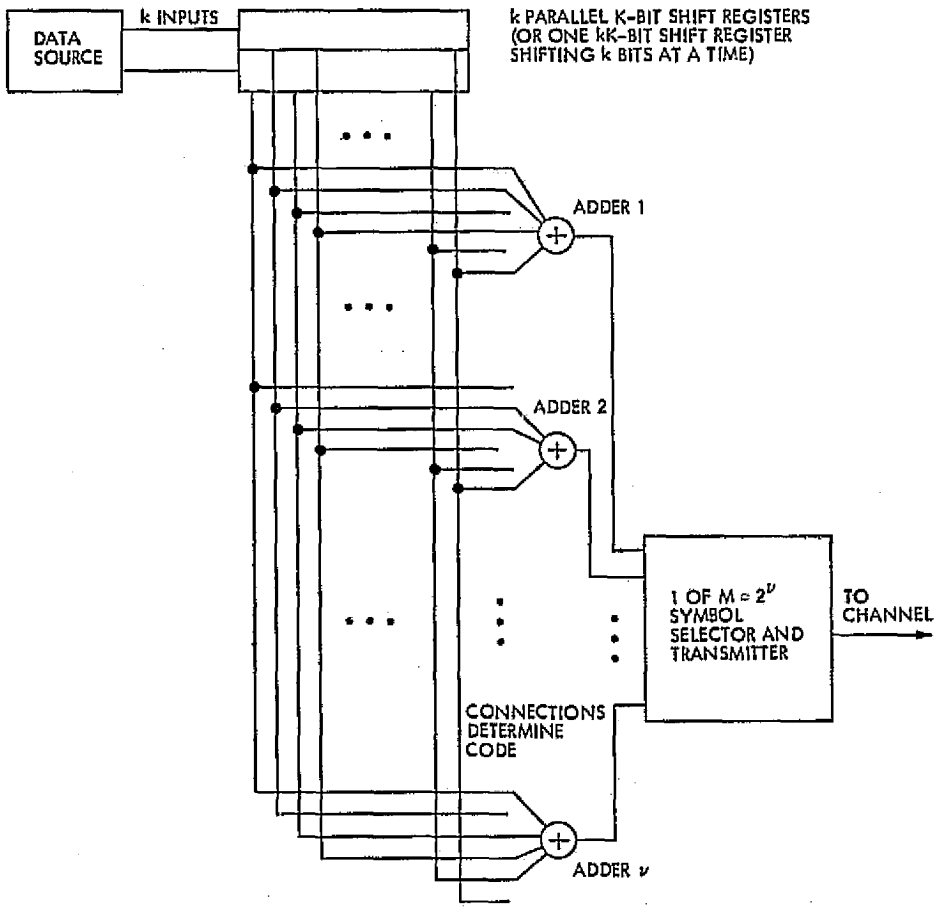

Fig. 1. A rate k/ν convolutional coder for the M-ary channel with $M = 2^{\nu}$, drawn for $k = 2$

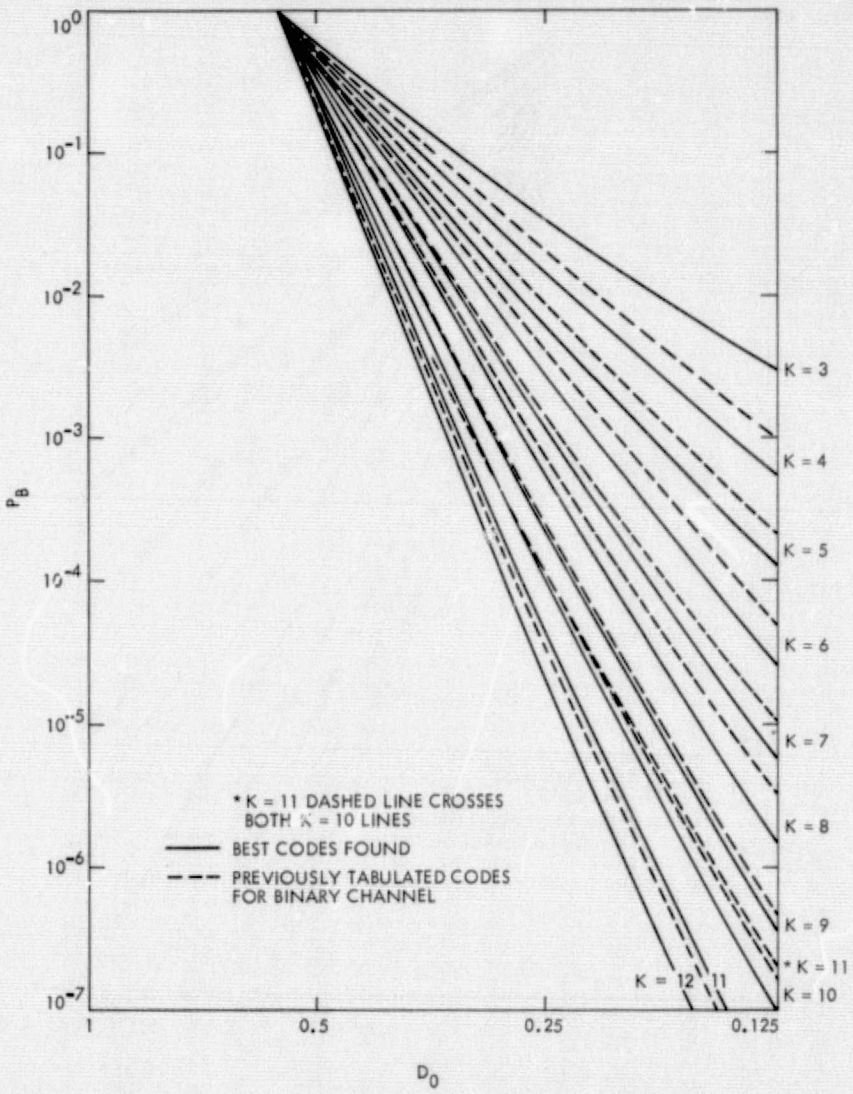

Fig. 2. Estimates of P_B vs D_0 for rate 1/2 codes on 4-ary channel

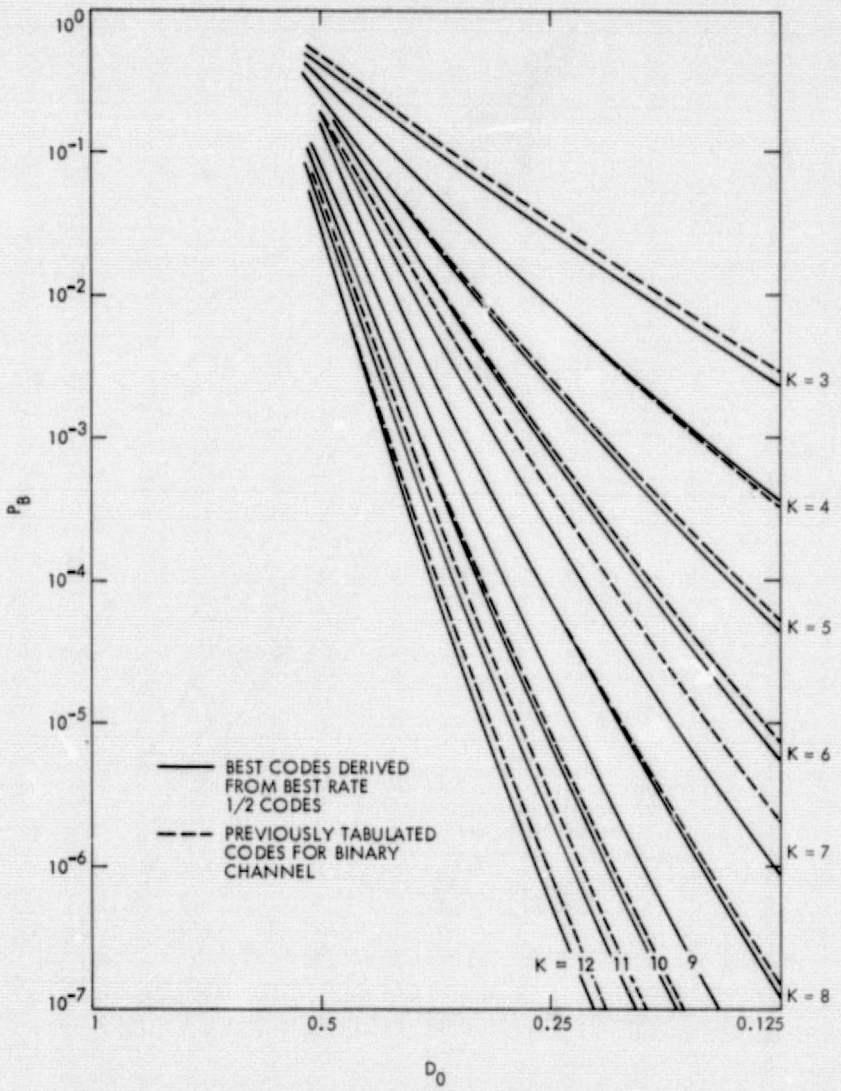

Fig. 3. Estimates of P_B vs D_0 for rate 1/3 codes on 8-ary channel

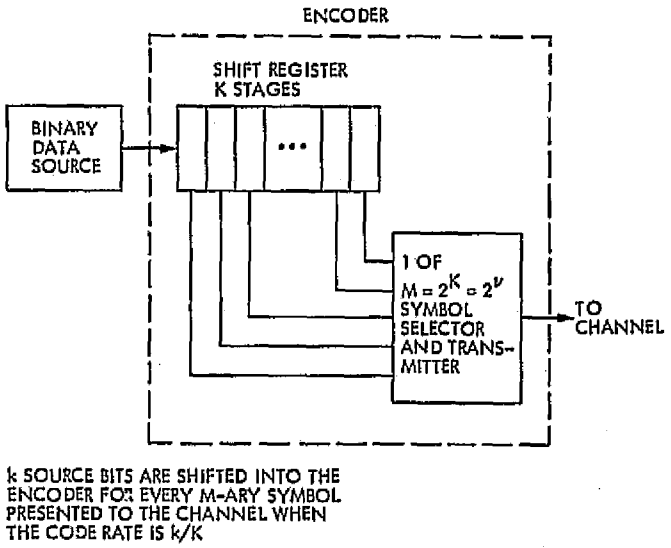

Fig. 4. The best convolutional codes of constaint length K on the M-ary orthogonal channel, achieved by allowing ν to increase to $\nu = K$, while $M = 2^\nu$

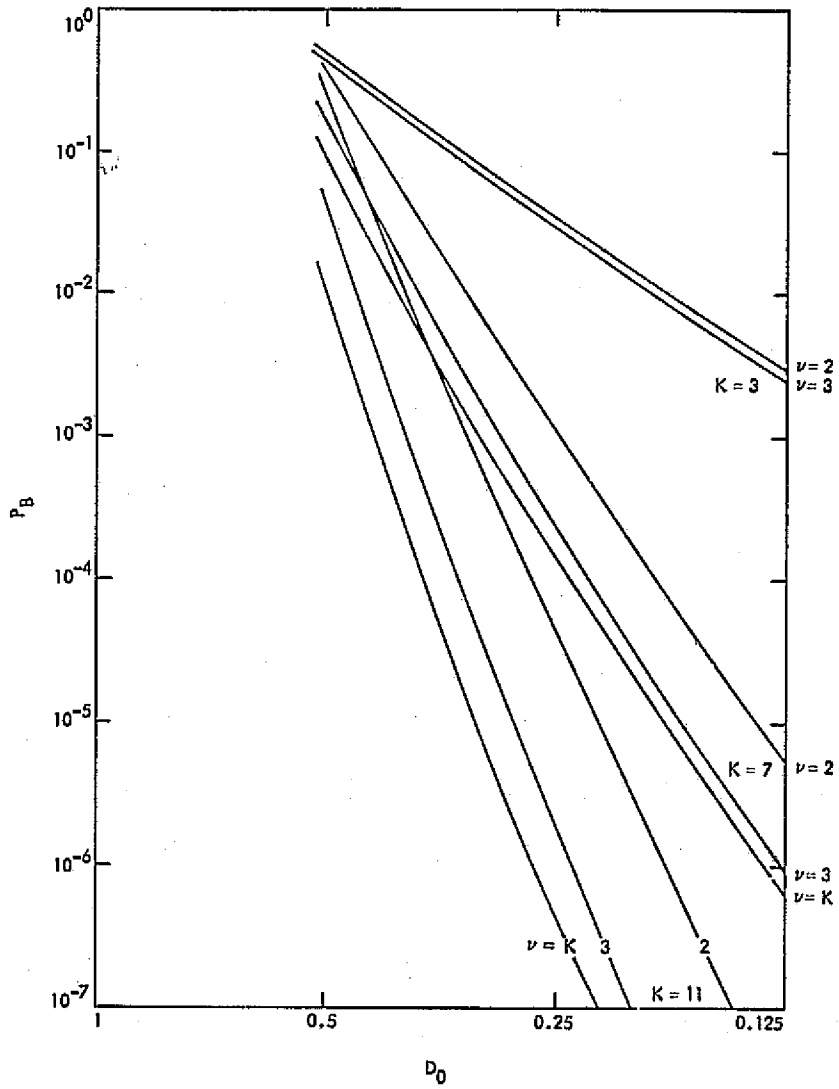

Fig. 5. Dependence of best P_B vs D_0 curves on ν, with $M = 2^{\nu}$, for $K = 3, 7, 11$

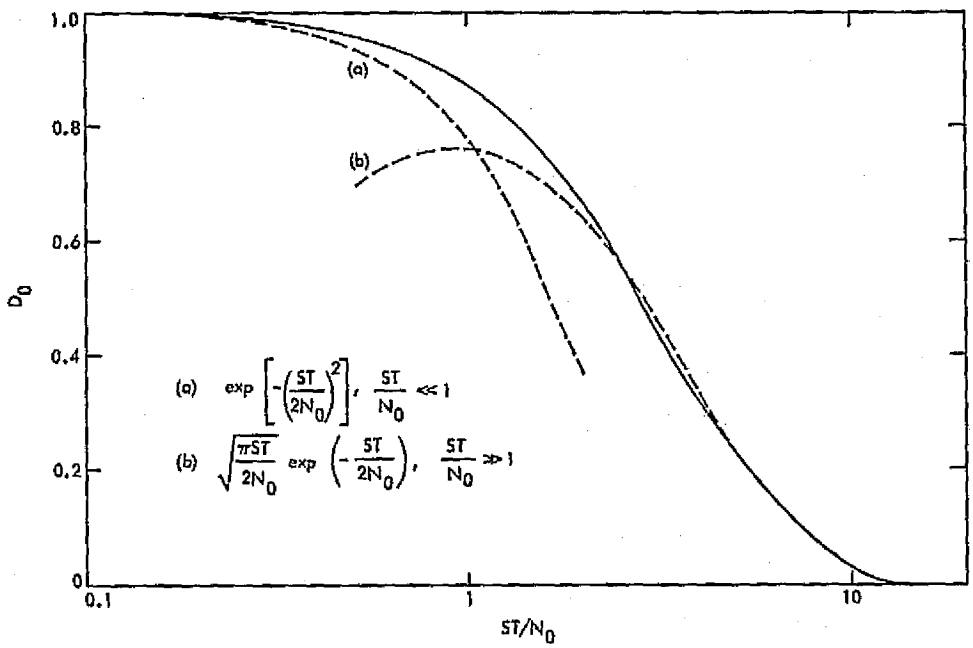

Fig. 6. D_0 vs signal-to-noise ratio ST/N_0 for noncoherent MFSK and the two asymptotic approximations

Appendix

```
C   SUBROUTINE TO EVALUATE CONVOLUTIONAL CODES
C   R F LYON    JPL 238-420   SEC 331   X2766
C
C   LG(1)  FIRST CONNECTION VECTOR
C    - - -
C   LG(N2) LAST CONNECTION VECTOR
C   K      CONSTRAINT LENGTH
C   N1/N2  RATE IN BITS/SYMBOL
C   M      MINIMUM DISTANCE
C   LM     MAXIMUM INPUT LENGTH TO TEST
C   FLAG   PRINT CONTROL
C          FLAG>0 PRINT ALL COEFFS OF T(D,N,L)
C          FLAG<0 PRINT ALL COEFFS OF T(D,N)
C          FLAG=0 PRINT HEADER ONLY
C   DISY   EXTERNAL SUBROUTINE DEFINING DISTANCE MEASURE
C   DISB   EXTERNAL SUBROUTINE GIVING A DISTANCE BOUND
C   ERR    EXTERNAL SUBROUTINE TO ESTIMATE ERROR PROBABILITY
C   ERROT  ENTRY POINT TO PRINT ERROR ESTIMATES
      SUBROUTINE EVAL(LG,K,N1,N2,M,LM,FLAG)
      DIMENSION KOUNT(12,12,15),KSUM(12,15)
      DIMENSION LG(4),LC(4),ND(4)
C     CLEAR COUNTERS TO BE USED
      KMIN=0
      DO 1 L=1,LM
      DO 1 N=1,L
      CALL DISB(NDB,K,L,N1)
      DO 1 ND1=M,NDB
C     COEFFICIENT OF T(D,N,L)
    1 KOUNT(L,N,ND1-M+1)=0
      DO 21 N=1,LM
      DO 21 ND1=M,NDB
C     COEFFICIENT OF T(D,N)
   21 KSUM(N,ND1-M+1)=0
C     MINIMUM DISTANCE INITIALIZE
      MD=1000000
C     LOOP ON INPUT LENGTHS UP TO LM
      DO 11 L=1,LM
C     LOOP ON INPUTS OF LENGTH L
      DO 10 IN=IOR(2**(L-1),1),2**L,2
C     WEIGHT INITIALIZE
      N=0
C    CONVOLVE INPUT WITH CODE GENERATORS
C     LOOP ON N2 CODE GENERATORS
      DO 2 I=1,N2
C     CLEAR SPACE FOR CONVOLUTION
    2 LC(I)=0
C     LEFT JUSTIFY INPUT
      II=ISL(IN,31-L)
C     LOOP ON CODE GENERATORS
    3 DO 4 I=1,N2
C     SHIFT OUTPUTS
    4 LC(I)=ISL(LC(I),1)
C     SHIFT INPUT
      II=ISL(II,1)
```

```
      C     TEST 0F LEFTM0ST BIT
            IF(II) 5,7,3
      C     L00P 0N GENERAT0RS
    5       D0 6 I=1,N2
      C     ADD GENERAT0RS T0 0UTPUTS, M0D 2
    6       LC(I)=IE0R(LC(I),LG(I))
      C     C0UNT INPUT WEIGHT
            N=N+1
            G0 T0 3
      C     EVALUATE DISTANCES 0F C0NV0LVED SEQUENCES FR0M ZER0
    7       CALL  DIST(ND,LC,N1,N2)
      C     L00P 0N SHIFTED VERSI0NS 0F INPUT
    3       D0 8 I=1,N1
      C     UPDATE NIMIMUM DISTANCE
            IF(ND(I).LT.M0) M0=ND(I)
      C     AB0RT IF DISTANCE T00 SH0RT
    8       IF(ND(I).LT.M) RETURN
      C     L00P 0N SHIFTED INPUTS
            D0 9 I=1,N1
            ND1=ND(I)-M+1
      C     INCREMENT C0UNTERS
            KSUM(N,ND1)=KSUM(N,ND1)+1
            K0UNT(L,N,ND1)=K0UNT(L,N,ND1)+1
            IF(ND1.EQ.1) KMIN=KMIN+1
    9       C0NTINUE
      C     MAKE INCREMENTAL CHANGE IN ERR0R ESTIMATES
            CALL ERR(N,ND,N1)
   10       C0NTINUE
      C     FINISH L00PS 0N INPUTS
   11       C0NTINUE
      C     PRINT HEADER
            PRINT 100,FLAG,K,N1,N2,N2,(I,LG(I),I=1,N2),M0,KMIN
      C     CHECK PRINT C0NTR0L
            IF(FLAG) 13,16,15
      C     LIST ALL C0UNTERS
   15       D0 12 L=1,LM
            CALL DISB(NDB,K,L,N1)
            PRINT 101,L,NDB-M0+1,(ND1,ND1=M0,NDB)
            D0 12 N=MIN(L,2),L
            PRINT 102,N,(K0UNT(L,N,ND1-M+1),ND1=M0,ND0)
   12       C0NTINOE
      C     LIST C0UNTERS WITH0UT LENGTH FACT0R
   13       C0NTINUE
      X     PRINT 101,LM,NDB-M0+1,(ND1,ND1=M0,NDB)
      X     D0 14 N=1,LM
      X14   PRINT 102,N,(KSUM(N,ND1-M+1),ND1=M0,ND0)
      C     PRINT ERR0R ESTIMATES
            CALL ER0UT
      C     RETURN MINIMUM DISTANCE
   16       M=M0
            RETURN
  100   F0RMAT(I1,'K=',I2,'  RATE',I2,'/',I1,',N(',' G',I1,'=',23),'  DF=',I2,/5)
  101   F0RMAT('0L=',I2,X,' N(2X,D=',I2,')
  102   F0RMAT(' N=',I2,15(I7))
            END
```

```
      SUBROUTINE TO COMPUTE UNION BOUND ESTIMATE OF PE AND PB
C     N    INPUT WEIGHT (EXPONENT OF N IN T(D,N))
C     N1   NUMBER OF SHIFTED VERSIONS OF INPUT
C     ND   SET OF DISTANCES (EXPONENTS OF D IN T(D,N))
C          FOR EACH SHIFTED VERSION OF INPUT
      SUBROUTINE ERR(N,ND,N1)
      DIMENSION ND(4),DO(8),PE(8),PB(8)
C     PE= T(DO)
C     PB= DT(DO,N)/DN|N=1
      DO 1 I=1,N1
      DO 1 J=1,K
      PB(J)=PB(J)+N*DO(J)**ND(I)
      PE(J)=PE(J)+  DO(J)**ND(I)
    1 CONTINUE
      RETURN
C     ENTRY TO SET UP VALUES OF DO AND CLEAR PB AND PE
C     KK   NUMBER OF VALUES TO DO SUPPLIED
C     DD   VALUES OF DO,STARTING AT INDEX 1
      ENTRY ERSET(DD,KK)
      DIMENSION DD(8)
      K=KK
      DO 2 J=1,K
      DO(J)=DD(J)
      PB(J)=0
      PE(J)=0
    2 CONTINUE
      RETURN
C     ENTRY TO PRINT RESULTS
      ENTRY EROUT
      PRINT 4
C     THREE COLUMNS; DO, PE, PB
C     FOR K VALUES OF DO
      DO 3 J=1,K
      PRINT 5,DO(J),PE(J),PB(J)
    3 CONTINUE
      RETURN
    4 FORMAT('0      DO          PE          PB')
    5 FORMAT(F8.4,2F9.7)
      END
```

```
C     SUBROUTINE DEFINING DISTANCE MEASURE ON M-ARY SYMMETRIC CHANNEL
C     ND  LIST OF N1 DISTANCES TO RETURN
C     LC  LIST OF N2 CODER OUTPUTS
C     N1/N2  CODE RATE
C     ONLY ONE OF EACH N1 OUTPUT POSITIONS IS ACTUALLY OUTPUT FOR EACH
C      OF N1 SHIFTED VERSIONS OF THE INPUT
      SUBROUTINE DIST(ND,LC,N1,N2)
      DIMENSION ND(4),LC(4)
      L=0
C     DIST= NUMBER OF PLACES IN WHICH ANY OF N2 OUTPUTS ARE ONE
      DO 1 I=1,N2
C     'OR' OUTPUTS TOGETHER
    1 L=IOR(L,LC(I))
      DO 2 I=1,N1
    2 ND(I)=0
    3 DO 5 I=1,N1
      L=ISL(L,1)
C     CHECK LEFTMOST BIT
      IF(L) 4,6,5
    4 ND(I)=ND(I)+1
    5 CONTINUE
      GO TO 3
    6 RETURN
C     ENTRY TO COMPUTE DISTANCE BOUND ON M-ARY SYMMETRIC CHANNEL
      ENTRY DISB(NDB,K,LL,N1)
C     BOUND IS INTEGER>=(K+L-1)/N1
C     I.E. LENGTH OF OUTPUT SEQUENCE
      NDB=(K+LL+N1-2)/N1
      RETURN
      END
```

DSN Research and Technology Support

E. B. Jackson and A. L. Price
R. F. Systems Development Section

The activities of the Development Support Group in operating and maintaining the Venus Station (DSS 13) and the Microwave Test Facility (MTF) are discussed and progress noted. Major activities discussed include equipment modifications required for the planned automation demonstration, measurements made of radiation from the planet Jupiter and various radio sources, testing and installation of the 400-kW X-band planetary system, efficiency measurements on a DSN 20-kW transmitter, a brief summary of initial testing of microwave power transmission over a distance of 1.5 km, clock synchronization transmissions, and various interferometric observations of radio sources. Additionally, a discussion of the phased array video enhancement experiment on the Mariner 10 second Mercury encounter and DSS 13's role in that experiment is given.

During the four-month period ending October 15, 1974, the Development Support Group, in its operation of the Venus Station (DSS 13) and the Microwave Test Facility (MTF), made progress on various projects as discussed below.

I. In Support of Section 331

A. Station Automation (Pulsars)

As part of the overall DSN Station Automation Project (Research and Technology Operating Plan (RTOP) 68 "Station Monitor and Control"), a demonstration is planned using the Venus Station to perform a pulsar track under remote control from JPL in Pasadena. There are three "control" computers installed within DSS 13: a dedicated SDS-910 which operates the Clock Synchronization Transmitting System, including positioning of the 9-m antenna; another dedicated SDS-910 which positions the 26-m antenna; and a more general-purpose machine, an SDS-930, which does general control and computation work.

The two SDS-910 computers, which are internally referred to as "A" and "B," have had "intercomputer communications links," of Section 331 design, installed between them and the SDS-930 computer. Additionally, the SDS-910B (26-m control) has rewired clock and timing circuits, two modified interrupts to function with the intercomputer communications link, and has had the PIN-

POT capability expanded. In order to provide positive antenna control as well as positioning, the SDS-910B has also been interconnected with the 26-m servo/positioning system so as to *control* (1) brakes, (2) HIGH/LOW-speed switching in both azimuth and elevation, and (3) the movement warning horn mounted near the antenna. Additionally, the SDS-910B *monitors* (1) brakes ON/OFF, (2) AZ/EL drive in HIGH/LOW speed, (3) mode of computer control, (4) hydraulic pressure ON/OFF, (5) azimuth cable wrap-up warning, both left and right, and (6) AZ/EL prelimit position warnings.

The SDS-930 has also been altered for the planned demonstration. Changes include expansion of the interrupt and PIN–POT capability, expansion of central memory, and addition of a "Pulsar Data Collector" consisting of an A/D converter, timing and control logic, auxiliary memory (8192 × 24-bit words), and necessary power supply.

The current capabilities of the computers are summarized in Table 1. However, without additional wiring, additional interrupts are available by installing additional cards as follows: (1) SDS-910A—10, (2) SDS-910B—0, (3) SDS-930—6.

Testing of these various additional automated features, along with the necessary software, was performed for 54-1/4 hours, while actual observation at 2388 MHz, left-circular polarization (LCP), with the 26-m antenna was performed for 114 hours. The pulsars observed are tabulated in Table 2.

B. Phased Array Experiment on Mariner 10

In an effort to provide higher resolution picture data from the Mariner 10 second Mercury encounter, an experiment was proposed which utilized the signals from three DSN stations, in realtime, with the signals properly phased to achieve an overall signal-to-noise ratio (SNR) improvement whose absolute magnitude was a function of the individual station SNRs, but for this experiment was predicted to be 0.7 dB. The three stations chosen for arraying were DSSs 12, 13, and 14. The data were microwaved to DSS 14 for appropriate phasing and combining, where they were used as the input signal to the second (beta) telemetry detection "string" and were subsequently transmitted by high-speed data line to JPL. During pre-encounter testing, improvements within 0.1 dB of predicted were achieved; during encounter, the arrayed stations' receiving systems performed well. DSS 13 provided a total of 19-1/2 hours of pre-encounter testing and encounter data collection tracking.

Certain modifications to DSS 13 equipment were necessary for performance of this experiment. The Mod IV R&D receiver was modified for use during the Mariner 10 second Mercury encounter. The normal 2295-MHz portion of the receiver provided phased-lock-loop operation with an 8-Hz loop bandwidth. To provide for subcarrier detection, an additional channel was implemented. This was comprised of a phase detector along with appropriate bandwidth, gain, and phasing components (Fig. 1). The first conversion intermediate frequency (30 MHz) of the Mod IV receiver was fed through a bandpass amplifier to the input of a phase detector. The reference input for the phase detector was obtained from the station central frequency synthesizer. The phase shifter in the reference line provided phasing capability to optimize phase detection of the subcarrier (177.6 kHz). The output of the phase detector was fed through an amplifier, for level setting, to the signal combiner equipment at DSS 14 via the microwave link.

Tracking predicts were furnished in the standard DSN format, and some minor conversions were necessary to obtain receiver tuning frequencies for DSS 13.

All equipment worked well during the preceding tests as well as during the encounter sequence.

II. In Support of Section 333

A. Source Observation

During the 61 hours devoted to observing weak radio sources, the sources tabulated in Table 3 were measured at 2295 kHz, with the 26-m antenna adjusted to receive right-circular polarization (RCP), with data processing being done by the noise adding radiometer (NAR).

B. Radio Star Calibration

With the receiver tuned to 2278.5 MHz, and the 26-m antenna adjusted to receive RCP, flux measurements were made of radio sources 3C123, 3C218, Cygnus A, and Virgo A during 91-1/4 hours of observation.

C. 26-m Antenna Sidelobe Measurements

In completion of this measurement of antenna sidelobes (Ref. 1), a short observation period was devoted to reaffirmation of the baseline data with the quadripod legs covered; the covering was then removed, and additional observation was done to obtain "after" baseline data. Total observation was 8-1/4 hours, at 2278.5 MHz, RCP, with data collection being performed by the NAR. This completed this program at DSS 13.

D. Sky Survey

With the 26-m antenna fixed in azimuth at 180 deg and progressively positioned in 0.1-deg increments between 86.5- and 88.2-deg elevation, 1210 hours of data were automatically collected during the night and weekend hours when the station was not manned. Additionally, 19-1/4 hours of data were collected by the NAR with the 26-m antenna positioned to point at the pole star, Polaris.

III. In Support of Section 335

A. X-Band Planetary Radar

The modification to the DSS 13 Transmitter Control System to enable simultaneous operation of the two klystrons to be used in this system has been completed. Satisfactory testing of the dual klystron configuration (installed into the feedcone to be used at DSS 14) at sustained powers of 300 kW (150 kW per klystron) has been achieved. These tests included the complete waveguide/feed system to be employed in the final configuration at DSS 14.

After testing, the feedcone and dual klystron, waveguide system, and feed were moved to DSS 14 and installed onto the 64-m antenna during the week ending September 29, 1974. Modification of the DSS 14 Transmitter Control System to operate this system has been completed and control function testing is underway. Radio frequency (RF) testing will commence as soon as water is available for cooling klystrons and waveguide/feed systems.

Due to late delivery of the buffer amplifier system, and failure of the traveling wave tube amplifiers that are to be used in that system, a temporary, substitute system is being locally fabricated so that normal testing, including phased operation under automatic phase lock control, can proceed at DSS 14, striving for a December 1, 1974, operational date.

B. DSS 63/43 100-kW Transmitter Testing

The DSS 63 100-kW transmitter system testing has been completed, and all components have been shipped to Spain for installation. The JPL/contractor team scheduled to go to Spain to effect installation on-site is now engaged in additional technical training and Spanish language classes, with an anticipated departure date of November 15–28, 1974.

The DSS 43 system testing has progressed to the crowbar cabinet, which has the new dual-ignitron (series arrangement of two ignitrons) setup. The local control cabinet has been checked out, an 8-hour heat run at 1 MW has been made on the power supply and filter configuration and modification of the control logic cards has been completed.

C. 26-m Antenna Maintenance

Some difficulty has been experienced with intermittent fuse blowing in the servo system. An analysis of the existing circuitry indicated that, probably as a result of several modifications in the past, the clutch and brake circuits were incorrectly wired. The wiring was revamped and the problem was solved.

Observation of the valve drive current required during track, as well as some "brake off" testing, indicated the antenna was out-of-balance in elevation. Measurements using a dynamometer in series with an anchor cable indicated that an additional 9072 kg (10 tons) of counterweight would be required to rebalance. Section 332 personnel fabricated this weight in two modules of lead weights mounted in steel supports. These modules were then positioned on the antenna and welded into place. Subsequent testing indicates significant reduction in valve drive current, and less tendency to "fall" when brakes are released.

D. 20-kW Transmitter Efficiency Measurement

In anticipation of installing 20-kW transmitters at all 26-m DSN stations, it was desirable to know, by actual measurement, whether or not a nominal 50 kW (62.5 kVA) 60- to 400-Hz frequency changer was capable of furnishing the required operating power. After retuning according to current DSN practices, the 20-kW transmitter at DSS 11 was measured to have an ac-to-RF efficiency of 38.9% at 20-kW RF output, and an HV dc to RF efficiency of 50.5% at 20-kW RF output power. The measured power factor was 0.9, which places operation at these power levels well within the capabilities of the standard 50-kW frequency changer.

E. Kapton Feedhorn Cover Testing

In anticipation of installing thicker (0.127 mm (0.005 inch)) feedhorn covers, made of Kapton,[1] onto DSN antennas, a determination of power handling capability was necessary. Testing was first accomplished on the 26-m antenna, at a power output of 400 kW at 2388 MHz, for a period of 2 hours. Testing was also accomplished on the 9-m antenna, at a power output of 100 kW at 7149.9 MHz. (The power density in the 9-m feedhorn is 2-1/4 times that of the 26-m antenna.) In both cases, subsequent visual examination did not reveal any damage. Both

[1] Trademark of Dupont Corp.

feedhorn covers remained in service and are used for routine operations. Testing is planned at 8495 MHz, 400 kW, when the X-band radar at DSS 14 goes into service. However, testing thus far has given ample indication that the new covers are safe for DSN use at S-band.

F. Microwave Power Transmission Testing

To demonstrate feasibility and to develop RF-to-dc power conversion devices of appropriate efficiency, a contract has been awarded to the Raytheon Corporation to demonstrate microwave power transmission from the DSS 13 26-m antenna to the DSS 13 near-field collimation tower, a slant range of 1546 m. Contract requirements specify a minimum recovered power of 12,500 W, at an efficiency (incident RF power-to-recovered dc) of at least 75%.

After field probing at low level (10 W radiated) to determine field distribution, high-power testing of a prototype device was performed with the device mounted on the collimation tower. Testing was accomplished at various incident power levels, up to 150 mW/cm^2 calculated (total radiated power of 275 kW at 2388 MHz, vertical polarization). The prototype demonstrated dc recovery at efficiencies greater than 75%.

IV. In Support of Section 421

A. VLBI

Paired with DSS 43, DSS 13 participated in interferometric measurements of 69 radio sources, including Pioneer 11. Source switching was accomplished on an average of every 13 minutes, and actual observation consumed 15 hours, with an additional 2-1/2 hours for data testing and calibrations. Data were recorded on a special video tape recorder temporarily installed for this purpose.

B. Scintillation Experiment

In an experiment proposed and conducted by Drs. W. A. Coles and E. A. Ricketts of the University of California at San Diego, and approved by the Radio Astronomy Experiment Selection (RAES) Panel as RA-157, 33-1/2 tracking hours and 7 non-tracking hours of support have been provided. These measurements of radio sources 3C273, 3C279, and PKS 1148-00 were made in the interferometric mode; the paired station was another DSN station. Measurements were made at 2290 MHz, with the antenna adjusted to receive RCP. The output data, converted to a frequency of 2.5 MHz, were microwaved to DSS 14 for realtime data reduction during some of the experiments. During others, the other station(s) microwaved their data to DSS 13 for realtime data reduction.

V. In Support of Section 422

Clock Synchronization Transmissions

Continuing with transmissions as scheduled by DSN scheduling, clock synchronization signals were provided to other DSN stations as tabulated in Table 4. Total transmission time was 12-1/4 hours.

VI. In Support of Section 825

A. Pioneer 10 and 11 Science Support

DSS 13 continued to provide an average of 8-1/4 hours per week of routine observation. Measurements of the radiation from Jupiter and the radio source calibrators tabulated in Table 5 were made at 2295 MHz with the 26-m antenna adjusted to receive RCP. Observations were made for a total of 140-3/4 hours, with the data being collected by the NAR.

B. Interstellar Molecular Line Search

In a continuing experiment (Ref. 2), observations designed to detect recombination lines of carbon were made at DSS 13 for total observing time of 32 hours. Observations, using the 26-m antenna, were made at 2273 MHz, directed at an area in the vicinity of NGC 2023, in an effort to detect emission lines from $C_{142}\alpha$. In addition to the tracking support, an additional 8-1/4 hours of non-tracking support was provided for data analysis and program checkout. This experiment was performed by Drs. G. R. Knapp, Owens Valley Radio Observatory, and T. B. H. Kuiper, Jet Propulsion Laboratory.

References

1. Jackson, E. B., "DSN Research and Technology Support," in *The Deep Space Network Progress Report 42-20*, p. 125, Jet Propulsion Laboratory, Pasadena, Calif., Apr. 15, 1974.

2. Jackson, E. B., "DSN Research and Technology Support," in *The Deep Space Network Progress Report 42-22*, p. 111, Jet Propulsion Laboratory, Pasadena, Calif., Aug. 15, 1974.

Table 1. Current computer capabilities

Computer	PIN available	POT available	Interrupt available	Memory size (24-bit)
SDS-910A	6	8	22	8,192
SDS-910B	6	7	32	8,192
SDS-930	9	11	10	16,384

Table 2. Pulsars selected for test observation at DSS 13 (6/16–10/15)

0031−07	0833−45	1818−04
0329+54	1133+16	1911−04
0355+54	1237+25	1929+10
0525+21	1604−00	1933+16
0628−28	1642−03	2021+51
0736−40	1706−16	2045−16
0823+26	1749−28	2111+46
		2218+47

Table 3. Weak radio sources observed at DSS 13 (6/16–10/15)

3C218	3C286	NGC 7027
3C273	3C309.1	Virgo A
3C274	3C348	W33
3C279	3C353	

Table 4. Clock synchronization broadcasts from DSS 13

DSS 42	DSS 43	DSS 51	DSS 62	DSS 63
3	4	1	3	1

Table 5. Radio source calibrators used for Pioneer science support (6/16–10/15)

3C17	3C123	3C348
3C48	3C274	3C353
3C66	3C309.1	PKS 0237-23
		Virgo A

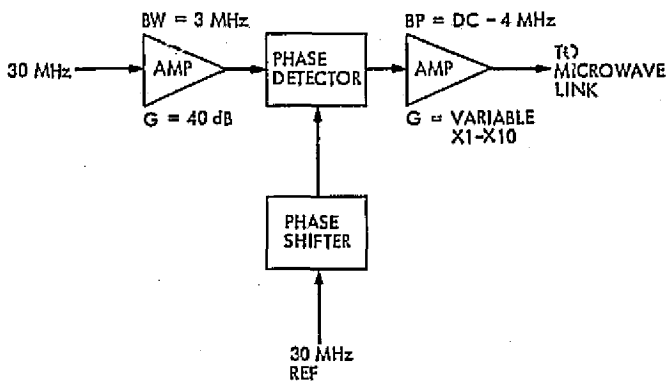

Fig. 1. DSS 13 receiver connection for phased array experiment

Automatic Microwave Configuration

J. G. Leflang
R. F. Systems Development Section

Work has been completed on the design and fabrication of hardware which provides computer access to the microwave subsystem configuration control group. Testing is nearly complete.

I. Introduction

A computer interface logic assembly has been developed as part of the automation effort which is being applied to the microwave configuration control equipment. The logic assembly provides computer access, through a DSN 14-line standard interface, to part of the configuration control equipment.

At the time of the last report (Ref. 1), the standard interface was being changed to include a priority structure. All of the changes have been completed, and the hardware has been tested at DSS 14. This article briefly describes the standard interface design and the test results.

II. Interface Design

One section of the logic assembly acts as a standard interface adapter. As indicated in Fig. 1, the adapter can be considered as a converter from 14 lines (12 bilateral and 2 unilateral) to 25 unilateral lines. The "response" and "ready" lines are transfer interlocks, and the two function lines are used to establish transmission direction priority for opposing requests.

The standard interface adapter contains all of the logic necessary to correctly condition the interface to receive or transmit, as well as containing line drivers, receivers, line terminations, and noise rejection circuits.

The logic is synchronous, sequential, and uses clocked storage. Random logic functions are accomplished by two 256 × 4 (1024-bit) read-only memories. The use of memory reduces the package count by 20 and improves operation speed by eliminating buildup of gate delays.

III. Testing

Tests were conducted at DSS 14 during the recent cone change. The logic assembly was inserted into the cabling of the module II/III switch control panel. Using the 14-line interface test fixture (Ref. 1), position control and indication were verified for all of the RF switches in the tricone, modules II and III. No problems or failures were encountered in the logic assembly. All of the information

required for control and verification of correct operation was easily sent through the 14-line interface.

Noise margins within the logic assembly were checked after the equipment was connected to the long cables which run from the control room to the antenna. Unfortunately, the test was run at a time when the station was not operating, and the only noise observed on the cabling was a differential voltage of approximately 400 mV at 60 Hz and its harmonics. This noise did not feed through the output buffers into the logic assembly.

IV. Conclusion

Two tests are still required. One is a noise margin test in a station which is conducting tracking operations; the other is operation using a DSN computer instead of the standard interface test fixture. Even though the testing is not complete, enough has been done to provide confidence that there are no remaining problems associated with controlling or monitoring the position of switches within the microwave subsystem. When the two remaining tests are successfully completed, the design of the implementation prototype can begin.

Reference

1. Leflang, J. G., "Automation of Microwave Configuration Control," in *The Deep Space Network Progress Report 42-21*, pp. 59–64, Jet Propulsion Laboratory, Pasadena, California, June 15, 1974.

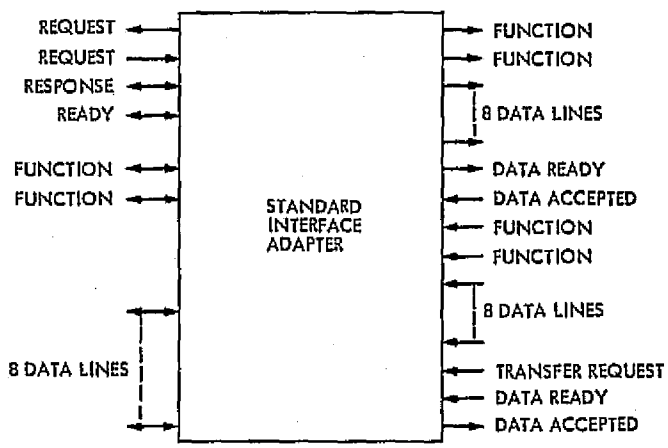

Fig. 1. Interfaces on the standard interface adapter

FORTRAN Implementation of Tutorial Input

K. Moyd
Communications Systems Research Section

This article describes the FORTRAN implementation of "Tutorial Input," a computer/human interface for real-time control programs. The emphasis is on the communication between the standardized input routine and a real-time FORTRAN control program. Changes made to the Tutorial Input specifications are explained, and samples of the use of this implementation are given.

I. Introduction

"Tutorial Input" is a standardized computer/human interface for real-time control programs. It was developed by A. I. Zygielbaum (Ref. 1), who has implemented an assembly language version for the PDP 11/20. A version has been written in real-time FORTRAN II for the XDS 930 computer, to be used in the pulsar automation demonstration. Some additions were made to the Tutorial Input specifications to increase the interface flexibility; some modifications were made to permit the input routine to be written entirely in FORTRAN. Much of the input routine could be used for other computers and projects.

A summary of Tutorial Input is given in Section II; the communication between the control program and the input routine is described in Section III; the changes to the original specifications are summarized in Section IV; and examples of the use of Tutorial Input are given in Section V. A description of the Tutorial Input routine and the flowcharts are presented in the Appendix.

II. Summary of Tutorial Input

Tutorial Input is a method by which an operator enters parameters and control information into a real-time control program written by a user. It allows the operator to determine how much help he needs in entering information rather than having a completely preprogrammed series of messages or requiring him to memorize the entry sequence. The input is divided into commands and parameters. A command is a name associated with a specific set of numeric and/or alphanumeric parameters. A control command does not have any parameters. Once the operator enters a command, he may enter as many of its parameters in order as he knows. If one or more parameters are not entered, the computer will prompt the operator by typing out the name of the next parameter. The process continues until all the parameters are entered.

If the operator determines that he made an error, he may cancel the input, causing an abnormal exit from the

input routine; he may backspace over the incorrect character(s); he may delete the entire line; or he may retype the incorrect command. An asterisk typed in place of a parameter value causes the previously accepted value of that parameter to be used. Certain errors are detected by the computer. An error indication is typed out, and operator correction is expected. The input routine is terminated normally when no new command follows on the same line as the last parameter of the previous command, if there have been no uncorrected errors.

III. Interfacing with the User's Program

All communication between the user's program and the input routine is by means of tables in COMMON. These tables must be initialized by the user before the input routine is entered the first time. The names used below to define the tables are those used in the input routine.

A set of four tables defines the commands, and a set of three tables defines the parameters. Each command table must be dimensioned at least NCOM (in COMMON), the number of commands. The ordering of commands is not important. ICOM(I) gives the four-character name of the I^{th} command. INPAR(I) is the number of parameters, and INDEX(I) is the index in the parameter tables of the first parameter associated with that command. IFLAG(I) is set to 1 upon normal exit from the input routine if the I^{th} command was successfully entered. Each parameter table must be dimensioned at least NPAR (in COMMON), the total number of parameters. The parameters for the I^{th} command have indices from INDEX(I) to INDEX(I) + INPAR(I) − 1. One parameter may be included in several commands. Control commands (no parameters) have no entries in the parameter tables. INAME(J) is the four-character name typed out if the J^{th} parameter is the next one to be entered. ICODE(J) specifies how the parameter is to be decoded. In this version ICODE(J) = −1 for floating point, 0 for integer, and 1 for alphanumeric. Because floating point numbers take two words on the XDS 930 while integers take only one, there are two tables for returning parameter values, PARAM and IPARAM. IPIND(J) is the index in the appropriate parameter storage table; ICODE(J) determines which table is to be used. Alphanumeric parameters are stored in the integer table and are therefore limited to four characters on the XDS 930.

Both the flag table (IFLAG) and the parameter storage tables are buffered in the input routine. The internal parameter buffer is entirely floating point. The values in the parameter storage tables are moved to the internal parameter buffer upon entry to the input routine, and the updated values are moved from the internal buffer to the storage tables upon normal exit. Therefore, any change made in the parameter storage tables by the user's program while the input routine is active may be overwritten when the input routine is done. The flag table is buffered differently. An internal buffer is zeroed upon entry to the input routine. As each command is successfully processed, the corresponding flag is set in the buffer. Upon normal exit from the input routine, those flags corresponding to new input are set in the flag table. The other flags are not affected at all. Therefore, the user may safely reset flags even when the input routine is active.

The use of the parameters and flags is left to the user. In cases in which parameter changes may occur at any time, the value in the parameter storage table may be used as the parameter value in the user's program. In cases in which the timing of parameter changes is critical, the appropriate flag(s) can be checked and the values transferred from the storage tables to the active locations at the proper time. The flags corresponding to control commands can be tested and acted upon in a background loop or in appropriate interrupt routines. A flag should be reset as soon as its command is acted upon to decrease the probability of not recognizing a new set of parameters.

At the present time, the user determines how entry to the input routine is initiated. Two possible methods are console interrupt and breakpoint control. The user must make sure that operator input/output (I/O) does not interfere with any other I/O. This may be a problem if either the operator I/O or other I/O is interrupt controlled.

IV. Additions and Modifications

The original Tutorial Input did not contain the flag table. Its inclusion allows parameter changes to be detected more easily and permits the timing of operator input to be made independent of the basic user program (with the exception of I/O interference). By means of the flag table, commands with no parameters can be used for program control. The only effect of such a control command is to set the corresponding flag.

The remaining tables are basically the same as in the assembly language implementation except that array indices are used in place of addresses. The internal parameter buffer is entirely floating point.

A method for indicating errors was established. Because a new line is not accepted until the previous line is

completely processed, any recognizable error must be on the last line typed. Λ Δ on the line below marks the first character of the command or parameter in error. All commands and parameters preceding the Δ have been accepted by the input routine; everything following the Δ will be ignored. In the case of a command error, input is to be continued with the typing of a new command. In case of a parameter error, the message corresponding to that parameter is typed out, and input is to be continued with the entering of that parameter. An error message is typed on the line following the error indicator. The possible messages are:

ILLEGAL COMMAND—longer than four characters.

UNRECOGNIZED COMMAND—not in the table of command names.

ILLEGAL PARAMETER—longer than four characters for an alphanumeric parameter, illegal character for a numeric parameter.

The control characters R^c, C^c and E^c described in Ref. 1 do not exist on the 930 typewriters. They have been replaced by ǂ , <, and ⧺, respectively. The ǂ causes immediate exit from the input routine without transferring any parameters from the internal buffer to the storage tables and without changing any flags. The < causes the previous character to be deleted. As many characters will be deleted as there are <s until the beginning of the line is reached. Excess <s will be ignored. The ⧺ causes the entire line to be deleted. A carriage return may be done before retyping the line.

V. Sample of Tutorial Input

A program was written to test the Tutorial Input routine. It set up the necessary tables in COMMON. The command and parameter definitions are given in Table 1. In this case, NCOM = 4 and NPAR = 5. Three of the parameters are stored in the integer table IPARAM; two, in the floating point table PARAM. Both tables were zeroed at the beginning of the test program.

The input routine was called whenever a specific breakpoint was set. The flag table was zeroed before each call. Upon return to the main program, the tables IFLAG, IPARAM, and PARAM were typed out.

Typewriter output from the test program is shown in Figs. 1 and 2. The entry numbers were added later. The underlined characters were typed out by the computer; the rest were entered by the operator. Figure 1 gives examples of normal use of Tutorial Input. Entries 1, 2, and 3 show the command POSN being entered in three ways: with no prompting, with complete prompting, and with partial prompting. The use of the asterisk, the effect of a no-parameter command (STOW), and the combining of several commands are shown in entries 4, 5, and 6, respectively. Figure 2 gives examples of the error indications and shows the use of the operator correction features. The parameters at the beginning of the generation of Fig. 2 were the same as at the end of Figure 1. Entry 1 shows two illegal commands (more than four characters). Entry 2 shows a command, STW, that is not in the command list. In this case, the parameters for RECV were accepted. Entry 3 shows an illegal parameter (a letter in a numeric parameter). In this case, the first parameter for RECV was accepted; only the second parameter (ATTN) had to be entered. The use of the input cancellation (ǂ), backspace (<), and line delete (⧺) are shown in entries 4, 5, and 6, respectively. In entry 6, a carriage return was typed before the line was reentered.

Reference

1. Zygielbaum, A. I., "Tutorial Input—Standardizing the Computer/Human Interface", in *The Deep Space Network Progress Report 42-23*, pp. 78-86, Jet Propulsion Laboratory, Pasadena, California, October 15, 1974.

Table 1. Tutorial input command and parameter definitions

Command definitions		
Name	Number of parameters	Index of first parameter
POSN	3	1
TMCN	1	4
STOW	0	—
RECV	2	4

Parameter definitions			
Index	Message	Decoding type	Storage index
1	RA	0 (integer)	1
2	DEC	0	2
3	TYPE	1 (alphanumeric)	3
4	TMCT	−1 (floating point)	1
5	ATTN	−1	2

C-2

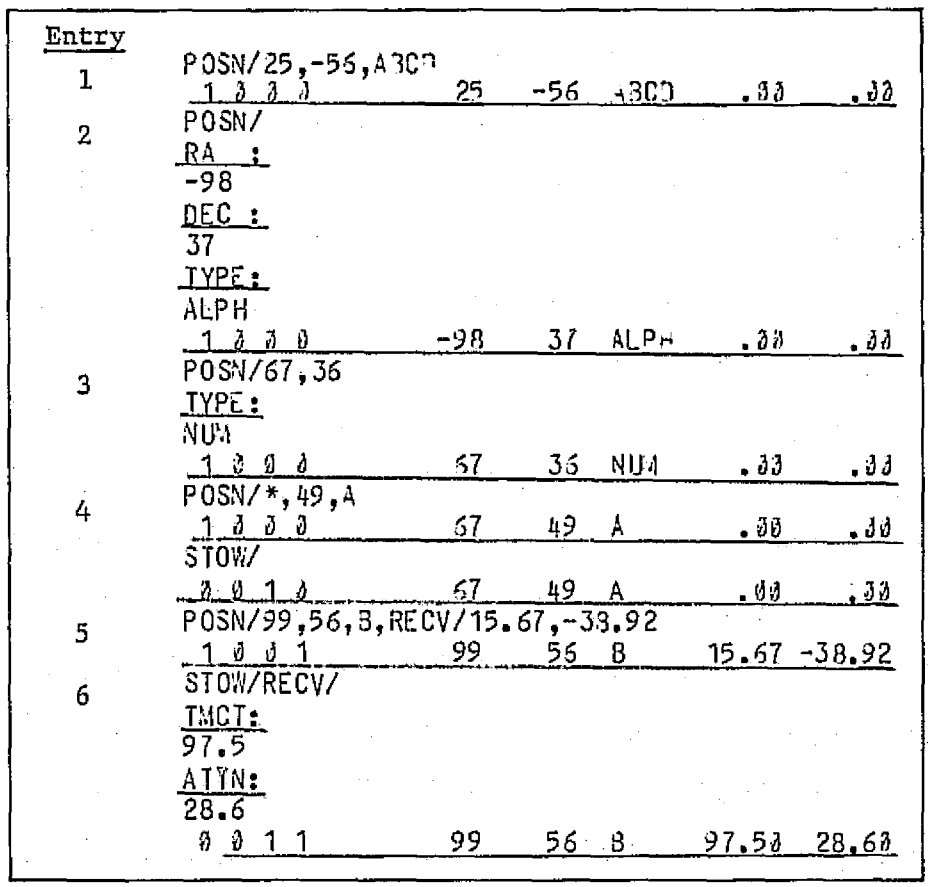

Entry						
1	POSN/25,-56,ABCD					
	1 0 0 0	25	-56	ABCD	.00	.00
2	POSN/					
	RA :					
	-98					
	DEC :					
	37					
	TYPE:					
	ALPH					
	1 0 0 0	-98	37	ALPH	.00	.00
3	POSN/67,36					
	TYPE:					
	NUM					
	1 0 0 0	67	36	NUM	.00	.00
4	POSN/*,49,A					
	1 0 0 0	67	49	A	.00	.00
	STOW/					
	0 0 1 0	67	49	A	.00	.00
5	POSN/99,56,B,RECV/15.67,-38.92					
	1 0 0 1	99	56	B	15.67	-38.92
6	STOW/RECV/					
	TMCT:					
	97.5					
	ATTN:					
	28.6					
	0 0 1 1	99	56	B	97.50	28.60

Fig. 1. Normal Input

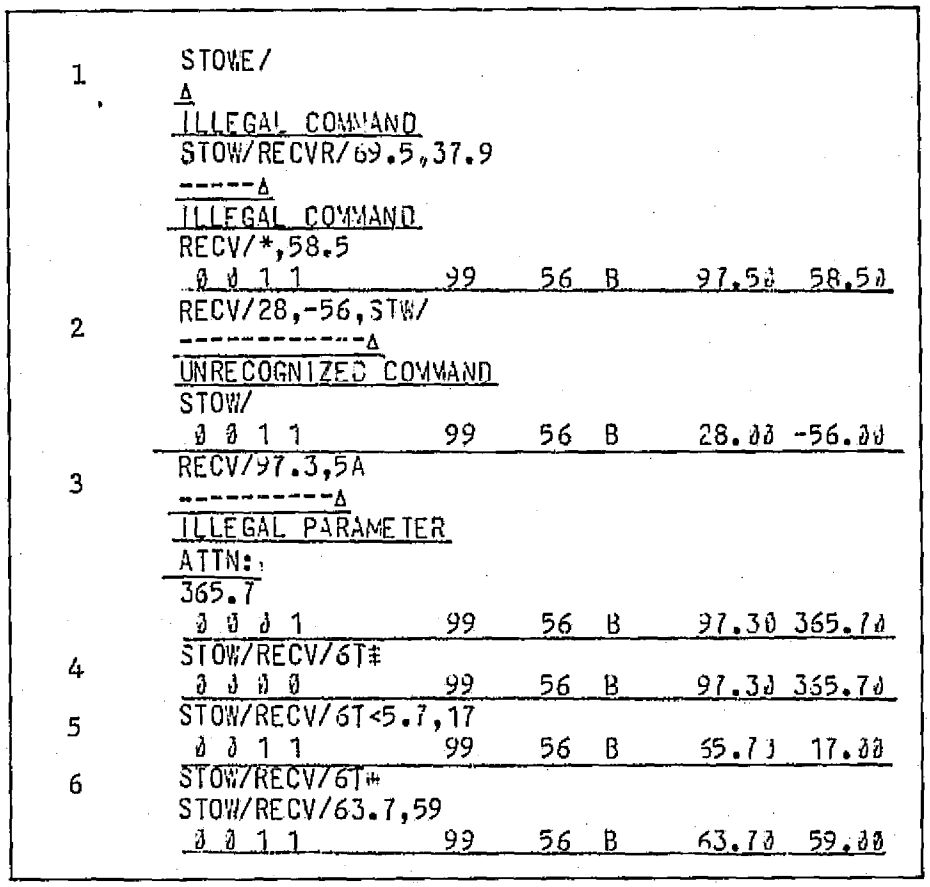
1
STOWE/
Δ
ILLEGAL COMMAND
STOW/RECVR/69.5,37.9
-----Δ
ILLEGAL COMMAND
RECV/*,58.5
0 0 1 1 99 56 B 97.50 58.50
2
RECV/28,-56,STW/
----------Δ
UNRECOGNIZED COMMAND
STOW/
0 0 1 1 99 56 B 28.00 -56.00
3
RECV/97.3,5A
----------Δ
ILLEGAL PARAMETER
ATTN:
365.7
0 0 0 1 99 56 B 97.30 365.70
4
STOW/RECV/6T#
0 0 0 0 99 56 B 97.30 365.70
5
STOW/RECV/6T<5.7,17
0 0 1 1 99 56 B 55.70 17.00
6
STOW/RECV/6T*
STOW/RECV/63.7,59
0 0 1 1 99 56 B 63.70 59.00

Fig. 2. Errors

Appendix

The Tutorial Input routine consists of a main routine named TUTOR and four subroutines named TYPEIN, AFIELD, NFIELD, and ERRIND. There is no additional COMMON needed for communication among these routines.

TYPEIN accepts one line of input, edits out backspaces, counts the resulting number of input characters, and sets a flag if the input cancellation character was entered. The input line is stored in an array with one character per word.

AFIELD takes the next field of the input line, terminated by a slash, comma, or blank (end of line), and packs it into one four-character word (blank filled to the right if necessary). The terminator is not included in the resulting word. If there are more than four characters, a flag is set to −1. If an asterisk occurs in the field, the flag is set to 1. Otherwise, the flag is 0.

NFIELD takes the next field of the input line, terminated by a comma or blank, and packs it into three words, four characters per word (blank filled at the end if necessary). A comma is included as the last non-blank character if there are fewer than 12 characters. A flag is set to −1 if there are more than 12 characters or if there is a character other than an asterisk, number, sign, or decimal point. If an asterisk occurs in the field, the flag is set to 1. Otherwise the flag is 0.

ERRIND causes the error indicator to be typed out. It sets the indicator at the actual point of the error, even if the line included backspaces.

TUTOR takes care of the entire input procedure, including the accepting of input, processing of commands and parameters, error indications, and buffer transfers. The detailed procedures have been covered in previous sections of the article and will not be repeated here.

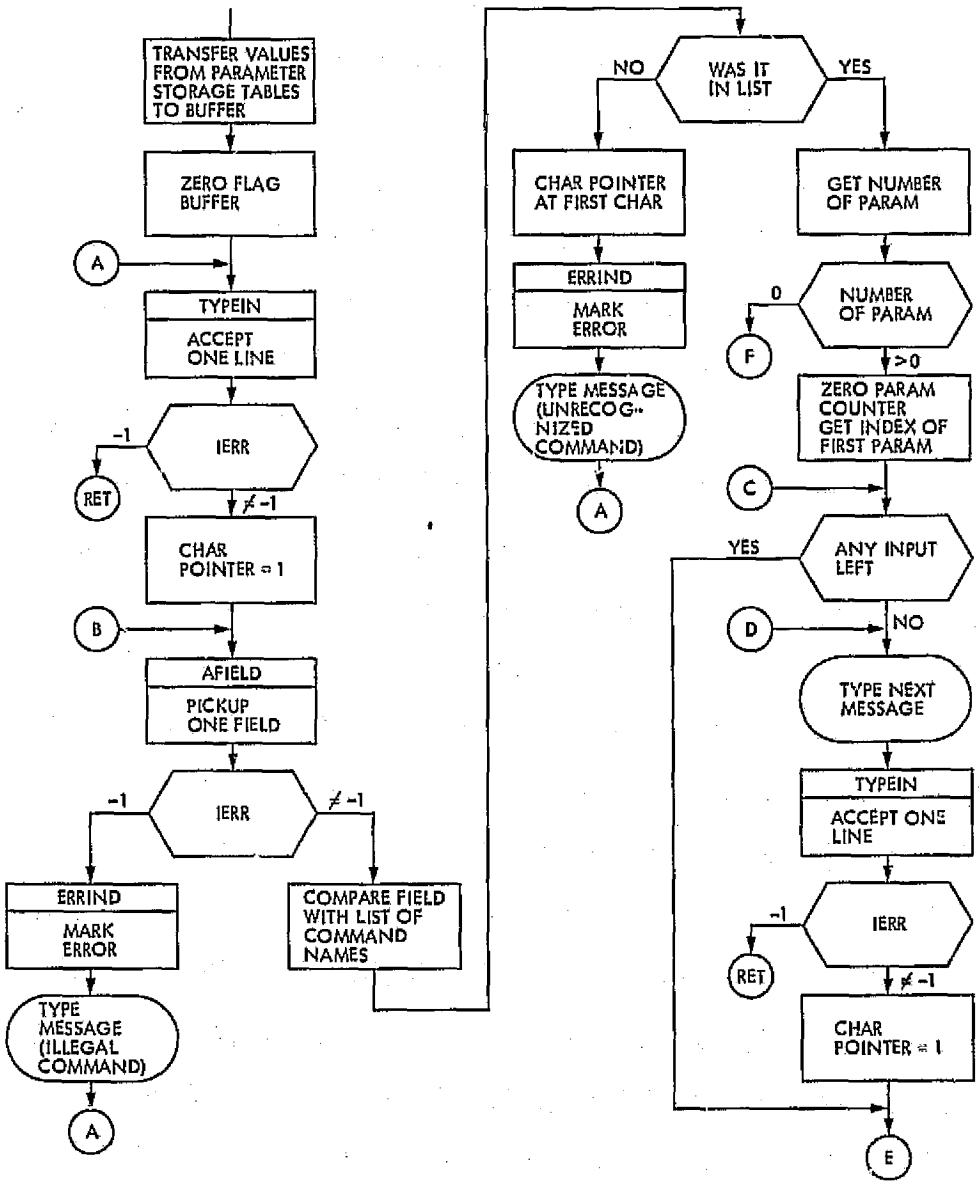
TRANSFER VALUES FROM PARAMETER STORAGE TABLES TO BUFFER
ZERO FLAG BUFFER
A
TYPEIN
ACCEPT ONE LINE
IERR
-1
RET
≠ -1
CHAR POINTER = 1
B
AFIELD
PICKUP ONE FIELD
IERR
-1
≠ -1
ERRIND
MARK ERROR
TYPE MESSAGE (ILLEGAL COMMAND)
A
COMPARE FIELD WITH LIST OF COMMAND NAMES
WAS IT IN LIST
NO
YES
CHAR POINTER AT FIRST CHAR
ERRIND
MARK ERROR
TYPE MESSAGE (UNRECOGNIZED COMMAND)
A
GET NUMBER OF PARAM
NUMBER OF PARAM
0
F
>0
ZERO PARAM COUNTER
GET INDEX OF FIRST PARAM
C
ANY INPUT LEFT
YES
D
NO
TYPE NEXT MESSAGE
TYPEIN
ACCEPT ONE LINE
IERR
-1
RET
≠ -1
CHAR POINTER = 1
E

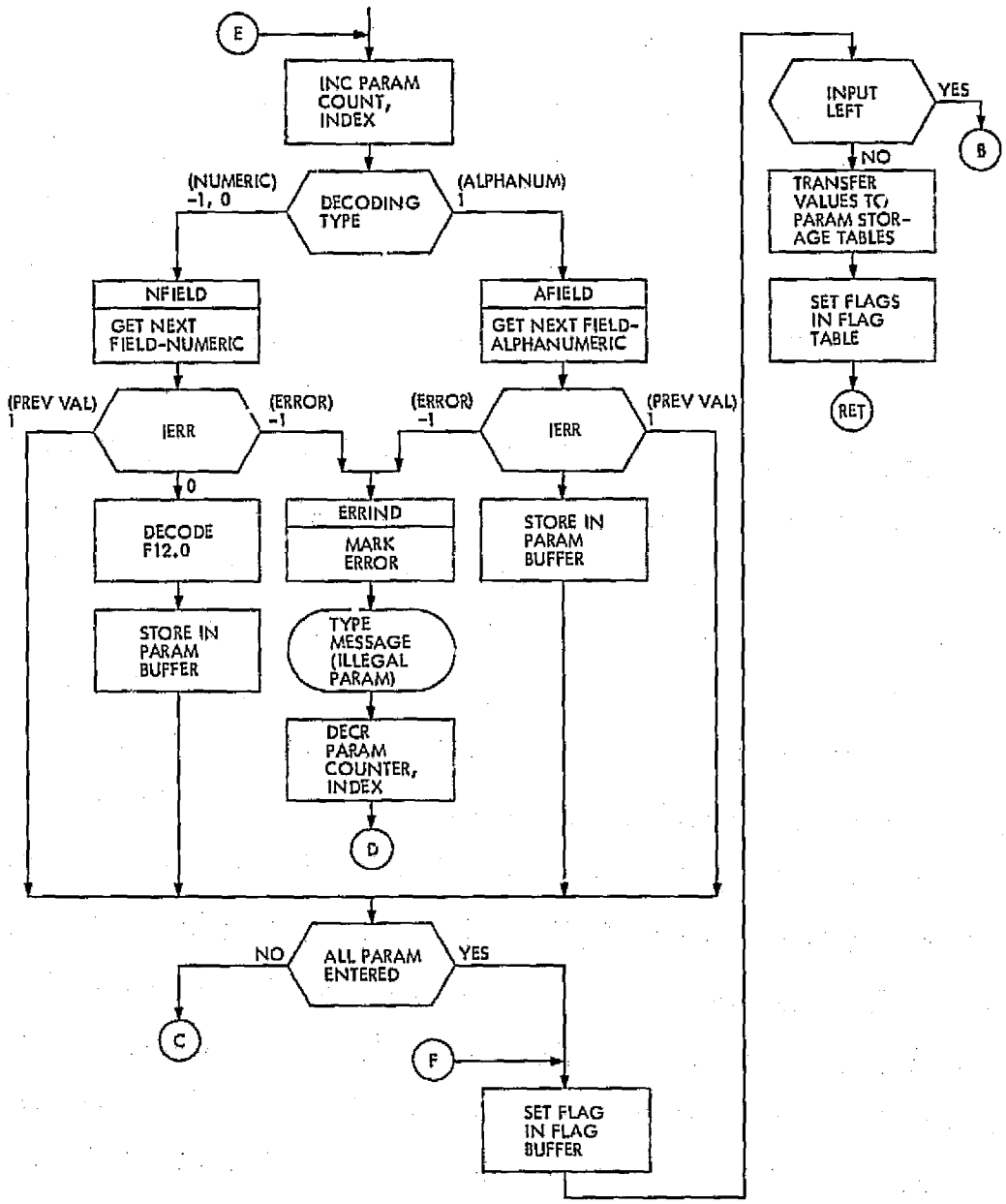
E
INC PARAM COUNT, INDEX
(NUMERIC) -1, 0
DECODING TYPE
(ALPHANUM) 1
NFIELD
GET NEXT FIELD-NUMERIC
AFIELD
GET NEXT FIELD-ALPHANUMERIC
(PREV VAL) 1
IERR
(ERROR) -1
(ERROR) -1
IERR
(PREV VAL) 1
0
DECODE F12.0
ERRIND
MARK ERROR
STORE IN PARAM BUFFER
STORE IN PARAM BUFFER
TYPE MESSAGE (ILLEGAL PARAM)
DECR PARAM COUNTER, INDEX
D
NO
ALL PARAM ENTERED
YES
C
F
SET FLAG IN FLAG BUFFER
INPUT LEFT
YES
B
NO
TRANSFER VALUES TO PARAM STOR-AGE TABLES
SET FLAGS IN FLAG TABLE
RET

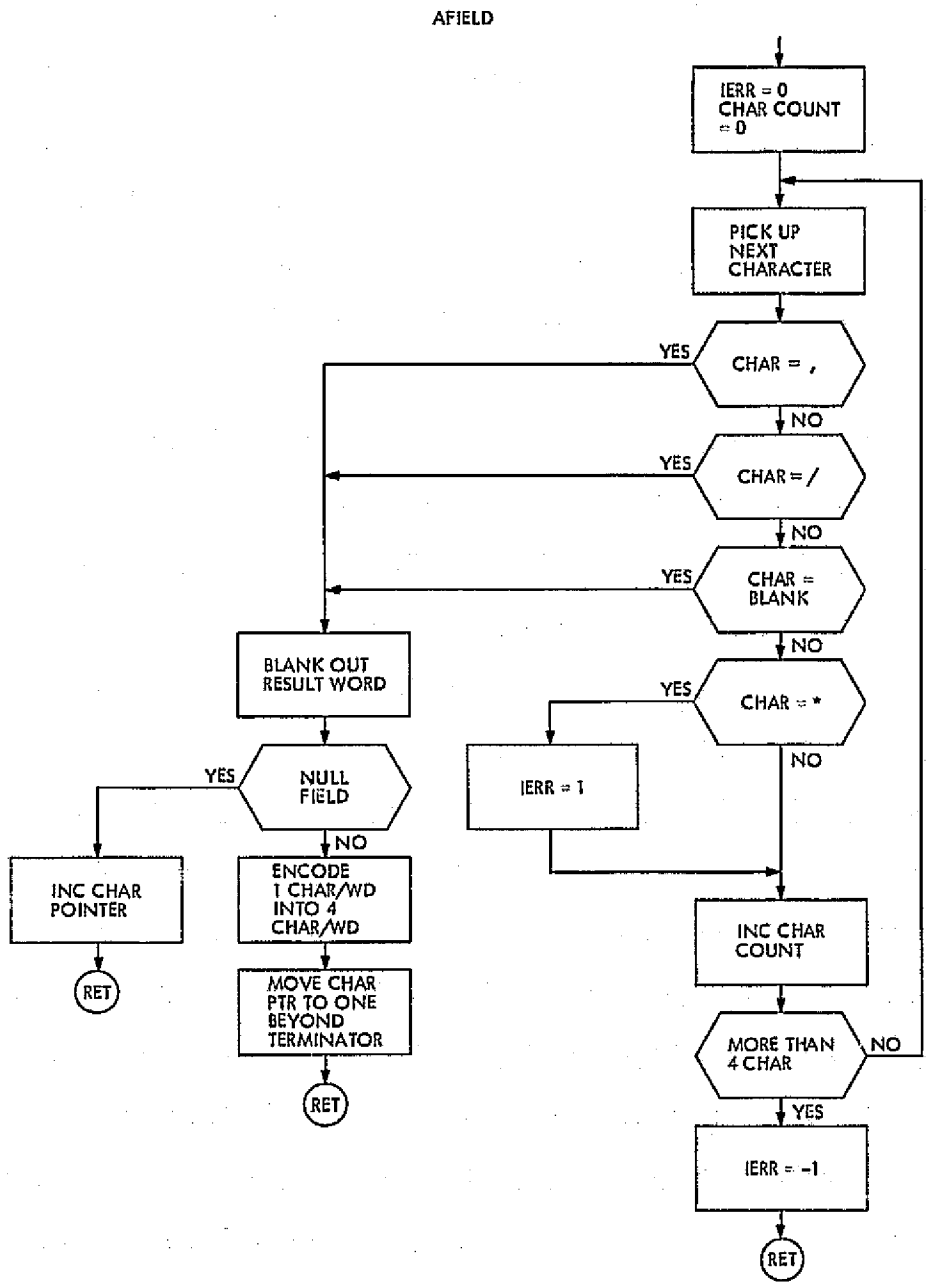
AFIELD
IERR = 0
CHAR COUNT = 0
PICK UP NEXT CHARACTER
CHAR = ,
YES
NO
CHAR = /
YES
NO
CHAR = BLANK
YES
NO
CHAR = *
YES
NO
IERR = 1
BLANK OUT RESULT WORD
NULL FIELD
YES
NO
INC CHAR POINTER
RET
ENCODE 1 CHAR/WD INTO 4 CHAR/WD
MOVE CHAR PTR TO ONE BEYOND TERMINATOR
RET
INC CHAR COUNT
MORE THAN 4 CHAR
NO
YES
IERR = -1
RET

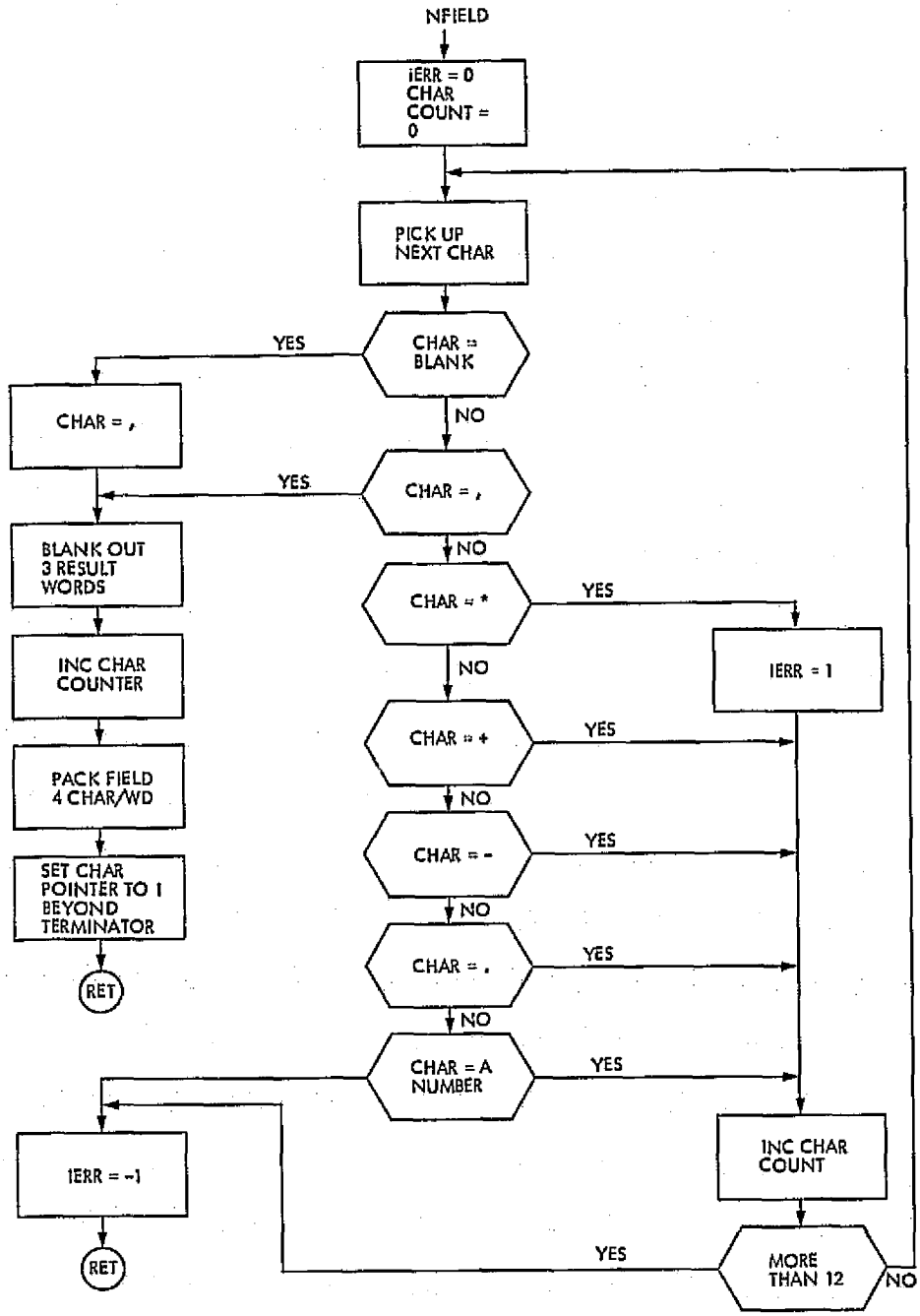
NFIELD
IERR = 0
CHAR COUNT = 0
PICK UP NEXT CHAR
CHAR = BLANK
YES
CHAR = ,
NO
CHAR = ,
YES
BLANK OUT 3 RESULT WORDS
NO
CHAR = *
YES
IERR = 1
INC CHAR COUNTER
NO
CHAR = +
YES
PACK FIELD 4 CHAR/WD
NO
CHAR = -
YES
SET CHAR POINTER TO 1 BEYOND TERMINATOR
NO
CHAR = .
YES
RET
NO
CHAR = A NUMBER
YES
IERR = -1
INC CHAR COUNT
RET
YES
MORE THAN 12
NO

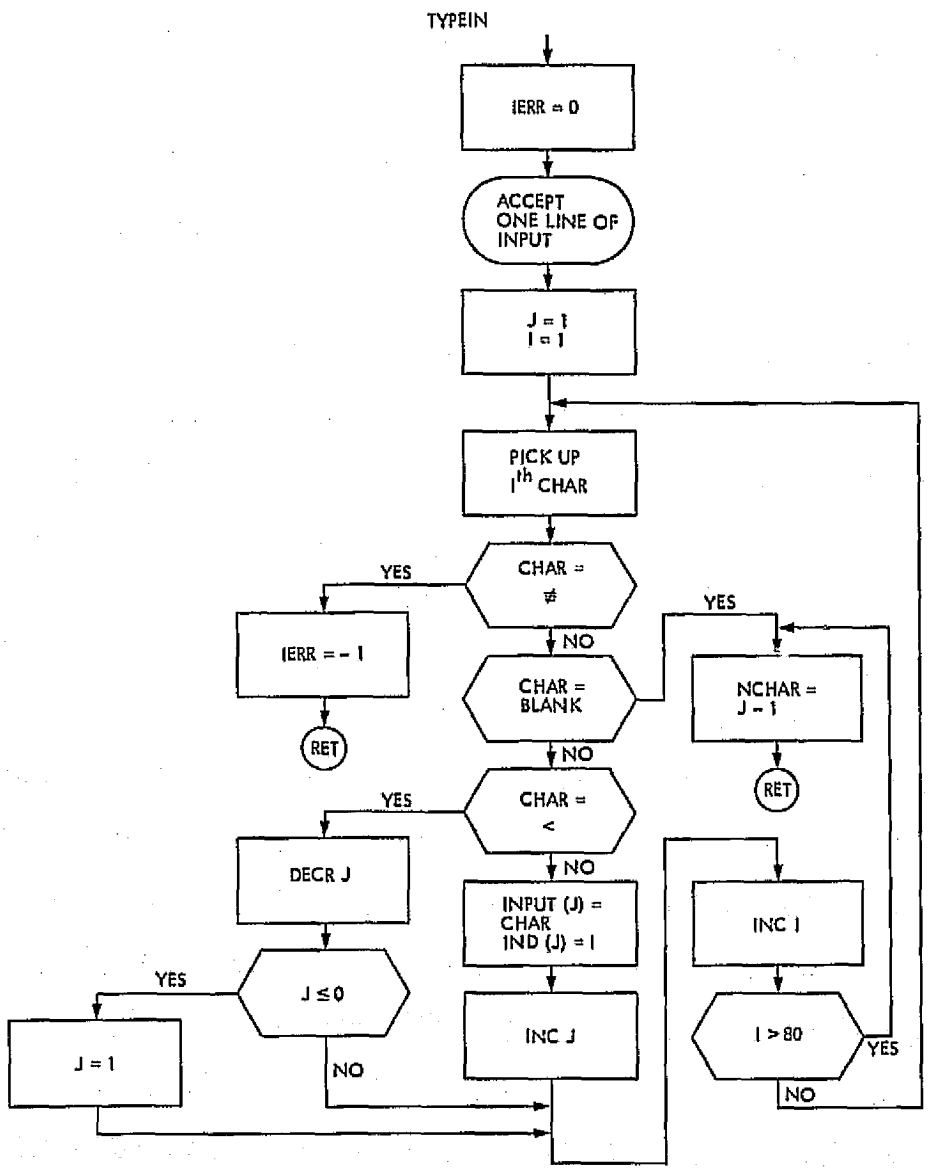
TYPEIN
IERR = 0
ACCEPT ONE LINE OF INPUT
J = 1
I = 1
PICK UP I^th CHAR
CHAR = ≠
YES
IERR = -1
RET
NO
CHAR = BLANK
YES
NCHAR = J - 1
RET
NO
CHAR = <
YES
DECR J
J ≤ 0
YES
J = 1
NO
NO
INPUT (J) = CHAR
IND (J) = I
INC J
INC I
I > 80
YES
NO

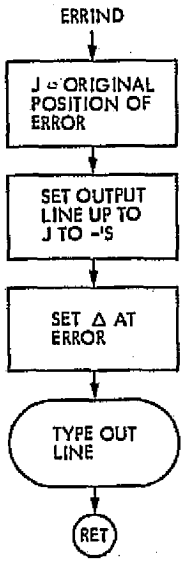
ERRIND
J = ORIGINAL POSITION OF ERROR
SET OUTPUT LINE UP TO J TO -'S
SET Δ AT ERROR
TYPE OUT LINE
RET

Portability of the MBASIC Machine-Independent Design

M. C. Riggins
DSN Data Systems Development Section

Part of the current work of the DSN Software Standards Project concerns the machine-independent design of the MBASIC processor. This article describes a study effort toward a portable implementation of the machine-independent design. The method made use of the STAGE2 portable, general-purpose macro processor, by means of which it was possible to invent a set of seemingly machine-independent macro templates for translation into an arbitrary target assembly language. The conclusions reached by this study are that the macros defined seem to form an adequate program MBASIC processor design language, that it is possible to carry structured programming concepts to the assembly language level, and that implementation by machine-independent macros may not be quite as efficient as hand coding but may yield significantly lower implementation costs.

I. Introduction

This article describes one phase of work done in support of the MBASIC machine-independent design (MID) activity. The purpose of the work was threefold: (1) to validate the MID design, i.e., to verify that the algorithms supplied actually perform as required by the MBASIC Language Specification (Ref. 1); (2) to evaluate whether the design supplied was truly machine-independent; and (3) to investigate methods which promote an orderly and rapid implementation of this design on an arbitrary target computer.

The design criteria specify that the design should be free of characteristics peculiar to specific host computers but should make maximum use of characteristics shared among a defined class of computers. Considerations beyond the set of common basic requirements define the MBASIC environmental interface, which is then to be undertaken as a separate implementation activity for each host computer. Thus, the implementation of an MBASIC processor into a given host computer consists of coding the MID and designing and coding the environmental routines which interface the MID to the system.

If the MID could meet its goals, it seemed reasonable that there would also be a method whereby the implementation of the MID could take place as rapidly and be as error-free as possible. That is, it seemed reasonable to seek a way of coding the MID in a machine-independent language—or at least in a language which requires only relatively minor alteration to transfer that body of code from one machine to another. Such a philosophy severely limits the choice of a programming language, for very few languages are machine-independent, widely available, and suitable for coding language processors. Languages such as FORTRAN and COBOL are largely machine-independent and widely available but inadequate for language implementation. Assembly language makes for efficient programs but is certainly not portable.

II. Macro Languages

The best choice for implementing the MID seemed to be one which would permit coding in a set of machine-independent macros, which could then be translated into an arbitrary target assembly language by merely redefining the macro definition body to fit that host system. This choice presumed that the macros themselves could take a portable form acceptable to various hosts.

Fortunately, STAGE2 (Ref. 2) seemed ideally suited for this purpose. STAGE2 is a general-purpose, readily available, portable macro generator/processor that can be installed in any computer capable of accepting ANSI-FORTRAN. STAGE2 permits its user to define macro "templates", which, when sensed in the source stream, then cause the generation of assembly language code also supplied by the user. Moreover, STAGE2 was already available on the U1108, so no further effort was required to begin in the MBASIC portability study.

Furthermore, even if STAGE2 were not available on another particular computer, the macro instructions, with proper specifications, checked and certified correct by previous implementation on the U1108, could serve as the basis for coding on the envisioned host. In such a case, the programmer himself is a manual macro translator. Further, since the U1108 implementation could be certified correct, any failures in other implementations could be isolated to coding errors on the new host system.

III. Portability of MBASIC

The envisioned process for implementing MBASIC into a given system is illustrated in Fig. 1. The figure shows several levels of documentation and their interrelationships. The MBASIC Language Specification is contained in a set of manuals (Ref. 1), which lead to the MID as a set of flowcharts and environmental interface specifications (Ref. 3). Upon study of the flowcharts, a set of macro specifications can be generated sufficient to encode the MID. An outline of such specifications appears in Appendix A of this article. The specifications, along with the assembly language manuals for the host, lead the programmer to providing proper macro body definitions in the host assembly language. Then, the MID-macro instructions can be translated (either by STAGE2 or manually) into a host assembly language implementation of the MID.

The machine-dependent design (MDD) proceeds similarly, building the capability required by the environmental interface. The figure shows that some of the MID macros may be useful in the MDD and should, of course, be available to the MDD programmer, as well as the assembly language of the host. The resultant MDD assembly language, together with that for the MID, forms the full MBASIC processor.

IV. The MID Macro Set

The MBASIC-MID is contained in a set of flowcharts which follow a structured programming topology. For this reason, a set of CRISP (Ref. 4) control structures, such as IF...THEN...ELSE, LOOP...EXIT...REPEAT, and DO CASE, plus the MBASIC design conventions were determined to be sufficient for the purpose of coding the MID. To implement these macros, a set of *utility macros* was designed and coded for stack manipulation, label generation, and flow-of-control, all of which are for internal use of the macros used to code the MID. The entire set of macros has four subdivisions:

(1) Machine-independent system utility macros

(2) Machine-dependent utility macros

(3) Machine-independent MID macros

(4) Machine-dependent MID macros

These subdivisions are described below:

(1) Machine-independent system utility macros—These macros function as routines to be used by other macros for tasks such as stack manipulation, label generation, and comments.

(2) Machine-dependent utility macros—These routines generate assembly language code for addressing, branching (conditional and nonconditional), subroutine linkage, and carriage control. This set, like the

system utility macros, is for internal use by other macros and will not appear in the code for the MID.

(3) Machine-independent MID macros—These macros are the flow-of-control macros. They do not generate any assembler code directly. Indirectly, through calls to other macros, they generate code and manipulate labels for the control structures IF...THEN ...ELSE, UNLESS...THEN...ELSE, DO CASE, and LOOP...EXIT...REPEAT.

(4) Machine-dependent MID macros—These macros generate code directly and handle procedure and subroutine linkage, variable declaration, arithmetic operations, and MBASIC design conventions.

There are two basic lines of division within this set of macros: independence/dependence and utility/non-utility. Independence/dependence separates the macros that generate assembler code (dependence) directly from those that do not (independence). Utility/non-utility separates the macros that appear in the MID design code (non-utility) from those that do not (utility). Using these macros, the MBASIC MID could be coded using the same structures that the flowcharts were written in. Verification of the translation from flowchart to code was indeed made much easier because of this. Additionally, each non-utility macro generates an assembly code comment that aids in understanding and debugging the assembly code, because it specifies which macro call generated the code that follows that comment.

As the design and implementation of the set of macros proceeded, checking the macros, individually and in groups, was also included. After a preliminary set of macros, as defined by the specifications derived from the MID (except for a few of the MID conventions), was designed, implemented, and tested, a test program was written to exercise all possible macros, directly or indirectly. The test program is shown as Appendix A. Even without a detailed macro specification, the test procedure is fairly readable and understandable—far more so than if the macros were more assembly-language-like.

This test program and the macros were run through the STAGE2 system; the code was generated, assembled, and executed. The output from this run, shown as Appendix B, was verified to be that specified by the design of the test program.

V. Coding the Design

The coding of the MBASIC MID was to take place in multiple phases. However, at this writing, none of these has begun. The first phase was to involve coding and testing the first three tiers of the MID using dummy stubs (Ref. 5) in place of references to modules at tier 4. In succeeding stages, all ten tiers of the MID were to be implemented. The implementation was not necessarily meant to compete with the current operational MBASIC processor on the 1108 in terms of efficiency. The code generated by STAGE2 would, hopefully, be equivalent to the operational processor, but it would probably be somewhat slower because of the limited optimization capability of STAGE2. This was considered to be of minor importance initially, because our aim was to implement the design in a portable fashion even if it were likely to be less efficient than coding the design by hand for a particular machine.

When that design had been macro-coded and the macro-coding verified, it would form a correct, compilable source for multi-implementations. Hand coding or machine translation and optimization could conceivably then make the operation very efficient, and more importantly, could proceed, with the knowledge that any errors detected were not in the design but somewhere in the coding.

VI. Conclusions

The proof of the method described is incomplete, and awaits an actual implementation for validation of the techniques proposed. However, one conclusion can be drawn unequivocally at this point: Carrying top-down structured programming concepts to the assembly language level for a particular computer needs no more support than a macro processor such as STAGE2. Less strongly, but with some degree of assurance, it seems fair to state that the set of macros specified for the complete MID form an adequate program design language (PDL) for the MID which will serve as a better, more definite basis for implementation than do the flowcharts. As a final conclusion, it also seems fair to state, based on the experience here, that portable machine-independent portions of systems appear feasible and desirable but may lead to some lack of efficiency in execution speed and core utilization; however, they may yield significantly lower initial implementation costs.

References

1. *Fundamentals of MBASIC*, Vols. I and II, Jet Propulsion Laboratory, Pasadena, California, March and October 1973 (JPL internal document).
2. Waite, W., *Implementing Software for Nonnumeric Applications*, Prentice-Hall, Inc., Englewood Cliffs, New Jersey, 1973.
3. *Software Specification Document: Machine Independent MBASIC*, Jet Propulsion Laboratory, Pasadena, California, to be published (JPL internal document).
4. Tausworthe, R. C., "Control-Restrictive Instructions for Structured Programming (CRISP)," *The Deep Space Network Progress Report 42-22*, pp. 134–151, Jet Propulsion Laboratory, Pasadena, California, 1974.
5. Baker, F. T., *Chief Programmer Teams: Principles and Procedures*, Report FSC 71-5108, IBM Federal Systems Division, Gaithersburg, Maryland, June 1971.

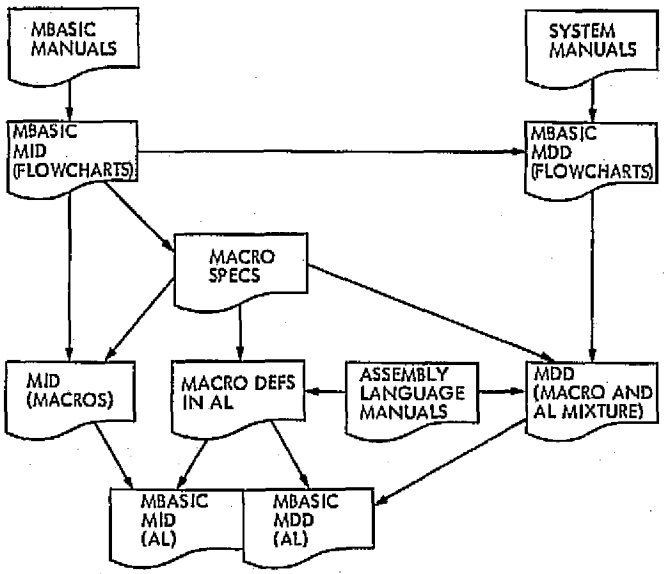

Fig. 1. Implementation of the MBASIC processor by machine-independent macro structures

Appendix A

```
:PROGRAM: MACTST                                                    MOD# 1;
.1   :DECLARE Y1(1);  DECLARE AND INITIALIZE
     :DECLARE Y2(1);  LOOP INDEX VARIABLES
     :DECLARE Y3(1);
     :DECLARE Y4(1);
     :DECLARE DX(1);
     :Y1=(3); ASSIGN POSITIVE LITERAL VALUE
     :Y2=(1);
     :Y3=Y2; ASSIGN VALUE OF VARIABLE (=1)
     :Y4=(3);
     :DX=(-1); ASSIGN NEGATIVE LITERAL VALUE
     :PRINT THE FOLLOWING PRINTOUT SHOULD APPEAR IN NUMERIC ORDER;
.3   :LOOP :DO CASE Y1 OF 1 TO 3;
.4           :CASE 1::PRINT 3. FINAL CASE PRINTS LINES 4-10;
.5                 :DO PROCED; TEST DO,CALL,IF,LOOP,REPEAT
                   :END;
.6           :CASE 2::PRINT 2. UNTIL LOOP AND ADDITION MACRO;
                   :END;
.7           :CASE 3::PRINT 1. FIRST DO-CASE TRANSFER;
                   :ENDBLOCK;
.8       :Y1=Y1 + DX; ADDITION OF VARIABLE VALUE (=-1)
       :EXIT IF (0) >= Y1;
         :REPEAT;
.9   :PRINT MACRO TEST TERMINATED;
     :ENDPROG;


:PROCEDURE: PROCED                                                  MOD# 1.5;
<*  TESTS CALL,IF,UNLESS,LOOP,AND REPEAT MACROS,AND *>;
<*  ALSO INCLUDED UTILITY MACROS UNDER =,#,<,>,>=,<= *>;
.1 :LOOP :EXIT UNLESS Y2 <= (7);
.2      :IF Y2 < (4);
.3        :THEN :IF Y4 > Y2;  TEST VARIABLE VALUES (Y4=2).
.4                    :THEN :IF Y2 = (1);
.5                             :THEN :PRINT 4.  TEST VALUES WITH <,>,=;
                                     :END;
.6                             :ELSE :PRINT 5.  TEST VALUES WITH <,>,#;
                                     :ENDBLOCK;
                          :END;
.7                    :ELSE :LOOP :PRINT 6. THIS LINE WILL BE PRINTED 3 TIMES;
.8                                  :Y3=Y3 + (1);
                                  :EXIT UNLESS Y3 <= (3);
                                    :REPEAT;
                          :ENDBLOCK;
                    :END;
.9/S1     :ELSE :CALL SUBRTN; TEST CALL,UNLESS,REPEAT
                    :ENDBLOCK;
.10       :Y2=Y2 + (1);
          :REPEAT;
     :ENDPROC PROCED;
```

```
:SUBROUTINE: SUBRTN                                                    MOD# S1;
<* TEST SUBROUTINE NESTING, UNLESS  ,REPEAT *>;
.1  :UNLESS (5) < Y2;
.2    :THEN :UNLESS Y2 # (4);
.3            :THEN :PRINT 7. Y2 <= 5 AND Y2 = 4;
                    :END;
.4            :ELSE :PRINT 8. Y2 <= 5 AND Y2 # 4;
.5                  :UNLESS Y2 = (5);
.6                    :THEN :PRINT ***ERROR IN UNLESS Y2=(5);
                            :END,NOELSE;
                    :ENDBLOCK;
              :END;
.7/S2 :ELSE :CALL SUBSUB; TEST NESTING, REPEAT
            :ENDBLOCK;
    :RETURN;



:SUBROUTINE: SUBSUB                                                    MOD# S2;
<*   TEST SUBROUTINE NESTING, REMAINING UNLESS, AND REPEAT *>;
.1   :UNLESS Y2 > (6);
.2     :THEN :PRINT 9. Y2 <= 6;
.3           :IF Y2 # (6);
.4             :THEN :PRINT  ***ERROR IN IF Y2#(6);
                     :END,NOELSE;
              :END;
.5/S3  :ELSE :CALL SBSBSB; TEST NESTING, REPEAT
             :ENDBLOCK;
     :RETURN;



:SUBROUTINE: SBSBSB                                                    MOD# S3;
<*    TEST NESTING, REPEAT  *>;
.1   :LOOP :PRINT 10. THIS LINE WILL BE PRINTED TWICE;
.3       :Y4=Y4 + (-1); ADDITION OF NEGATIVE LITERAL
.4/S4    :CALL SSSS(Y4); TRUTH VALUES + ARGUEMENT PASSING
       :EXIT IF (1) >= Y4;
         :REPEAT;
     :RETURN;



:SUBROUTINE: SSSS                                                      MOD# S4;
.1   :A1=TRUE(#1 = (2)); Y4 IS PASSED PARAMETER
.2   :IF A1 IS TRUE;
.3     :THEN :PRINT 11. Y4 = 2  UPON ENTRY TO SSSS;
             :END;
.4     :ELSE :PRINT 12. THIS PATH TAKEN ON SECOND CALL TO SSSS;
             :ENDBLOCK;
     :RETURN;
$FINISHED;
```

Appendix B

```
THE FOLLOWING PRINTOUT SHOULD APPEAR IN NUMERIC ORDER
1. FIRST DO-CASE TRANSFER
2. UNTIL LOOP AND ADDITION MACRO
3. FINAL CASE PRINTS LINES 4-10
4.  TEST VALUES WITH <,>,=
5.  TEST VALUES WITH <,>,#
6. THIS LINE WILL BE PRINTED 3 TIMES
6. THIS LINE WILL BE PRINTED 3 TIMES
6. THIS LINE WILL BE PRINTED 3 TIMES
7. Y2 <= 5 AND Y2 = 4
8. Y2 <= 5 AND Y2 # 4
9. Y2 <= 6
10. THIS LINE WILL BE PRINTED TWICE
11. Y4 = 2  UPON ENTRY TO SSSS
10. THIS LINE WILL BE PRINTED TWICE
12. THIS PATH TAKEN ON SECOND CALL TO SSSS
MACRO TEST TERMINATED
```

4800-bps High-Speed Data Error Statistics

J. P. McClure
DSN Data Systems Development Section

Analysis of GCF 4800-bps high-speed data error statistics information shows error bursts having a median length of 26 bits, though the range of burst lengths is very wide. Approximately 70% of the bits within a typical burst were error-free. An error block usually contains only one burst. Several burst characteristics are directly related to bit error rate. There is a small time correlation between errors experienced in opposite directions of transmission.

During October–December 1972, a series of high-speed data (HSD) tests were conducted between CTA 21 and DSSs 14, 42, 51, 61, and 71. These tests, which were run at 4800 bps on the Ground Communication Facility's (GCF) conventional HSD circuits, were designed to gather data on the distribution of the bit errors generated in the HSD System.

The configuration used for these tests is shown in Fig. 1. Identical 1200-bit high-speed data test blocks were generated by the DOI-5300-SP-A program operating in the Digital Instrumentation Subsystem (DIS). This continual data stream was forwarded through the block multiplexer. The encoder added the usual 33-bit error detection code. The encoded blocks were transmitted via a 203A List 2 data set at 4800 bps. Conventional back-to-back-data-set regeneration was routinely used at the NASA Communications (NASCOM) overseas switch centers (Madrid and Canberra) and at the central NASCOM switch at Goddard Space Flight Center (GSFC). Data were received by a 203A, decoded to detect errors, and forwarded to the receive section (sensor) of the DOI-5300-SP-A program.

The receive section compared the received block with a known good block on a bit-by-bit basis. The resulting error positions, by block number and bit location, were recorded on magnetic tape and reduced by an 1108 analysis program.

No attempt was made during the tests to specify particular circuits, nor to influence the circuit routing used by NASCOM. The goal was to obtain a realistic sample of the service normally supplied by the GCF.

Thirty-one separate tests were conducted, the total circuit time subtending 66 h. The individual tests were assigned to one of three analysis groups according to the measured bit error rate. The green group consists of individual tests having bit error rates better (less) than 1×10^{-5}. The amber group rates fall between 1×10^{-4} and 1×10^{-5}. The red group rates were all worse than 1×10^{-4}. These three groups, green, amber, and red, represent

excellent, normal, and poor GCF error performance. Normally, the GCF would not utilize red condition circuits (since they are out of limits); however, these tests were continued in order to provide an upper bound on error performance.

Most of the tests were run simultaneously in both directions (full-duplex). This permitted comparison of both sides of the circuit under identical conditions.

Table 1 shows various parameters by color group. A comparison of blocks received versus blocks transmitted shows an increasing block loss as line conditions worsen. This loss was composed of two parts: short line outages and sync recognition failures. The relative magnitude of the two parts could not be measured; only the total was observed. (Sync failure occurs when the 24-bit block synchronization code contains more than three errors. When this happens, the DIS comm buffer does not recognize the sync pattern and the faulty block is not inputted to the computer.)

Error blocks also naturally increase (percentage-wise) as line conditions worsen, and block thruput (a function of error and missed blocks) falls. The total thruput for these tests, 99.55%, is very close to the GCF's long-term average of 99.5%.

Median burst length was 26 bits for the total group, and was surprisingly close to this value for both the green and amber groups. In common with wideband data experiences, a relatively few long bursts cause the average burst length (59 bits) to substantially exceed the median (26 bits) case.

Within a burst, there are roughly 2 error-free bits for each in error. This ratio, in common with other burst parameters, is quite dependent on how a burst is defined. In this analysis, a burst was considered to be a string of good and bad bits which always starts and stops with an error and which was separated from an adjacent burst by 40 or more good bits.

A review of the raw data shows three kinds of bursts:

(1) A single-hit type of error, which produced only a few errors separated by many good bits. The data set scrambler establishes the minimum length of this type of burst, which occurs mostly during good line conditions.

(2) A truly random burst condition, wherein 1's were translated to 0's and 0's to 1's with about equal probability. During such bursts, the number of good bits and error bits were about equal.

(3) A carrier-failure condition due either to a long, heavy noise condition or an actual circuit failure. During this condition, the data set clamped its output to the 1 state until more normal conditions prevailed. This all-1's output causes all data 0's to be changed to 1's.

The bit translations entry in Table 1 shows an increasingly greater preference for 0-to-1 translations as line conditions worsen. This appears to be due solely to the third type of burst outlined above.

Block error rates were determined for the 1200-bit blocks now being used in the GCF and also for 2400- and 4800-bit lengths. During good circuit conditions, the block error rate increases linearly with block length, indicating that the bursts are much more than 4800 bits apart. This proportionality does not quite hold during average (amber) conditions. During red conditions, a significant number of the longer blocks apparently contain more than one burst.

As mentioned earlier, most of the tests were conducted simultaneously in both directions. Since the test start times were accurately recorded to the second, it was often possible to determine how many block errors occurred simultaneously in both directions. The results, shown in Table 2, imply that perhaps one error block in ten is mated with an error block in the opposite direction. Most such dual errors could be expected to be caused by the same error-generating source.

Using a model developed by D.C. Card, the circuit and its delivered bits can be considered to always be in one of two states—burst or error-free. During the error-free state, all bits are delivered without errors. During the burst state, some bits are delivered in error and some are error-free, as noted earlier. Each bit may thus be classified as one of three types:

0 An error-free bit occurring during a non-burst state. (This is the "normal" state which we would like all bits to occupy.)

1 An *error* bit occurring within a burst.

2 An *error-free* bit occurring within a burst.

A burst always starts with an error and ends with an error. This permits a firm determination of the beginning and end of each burst and eliminates the spectre of bursts which contain no errors.

Using the above tags, a 0-to-0 transition occurs between 2 bits, both of which are error-free and outside a burst. A 0-to-1 transition marks the beginning of a burst and is

ultimately followed by a 1-to-0 transition at the end of the burst. A 1-to-2 transition would indicate an error bit followed by a good bit, both within a burst. (0-to-2 and 2-to-0 transitions are not permissible since category 2 bits can occur only within a burst, while 0 bits occur only outside a burst.)

From the transition data, it was possible to construct the Card transition probability matrices shown in Table 3. These matrices depict, for each of the groups and the total, the probability of occurrence of each of the transitions. The bit types across the top represent the state of bit n and the types along the left show the state of the $n + 1$ bit. For instance, in the green group, the probability of a 1-to-2 transition is 0.592, whereas the probability of a 1-to-0 transition is 0.088. As discussed earlier, 0-2 and 2-0 transitions are not permitted and are given a zero probability. The matrices readily show many of the characteristics previously pointed out: the burst nature of the errors, good/bad ratio in a burst, etc.

Figure 2 presents information on the distance between bit errors. In the green group, for instance, there were 305 cases where adjacent bits (distance = 1) were in error, 215 cases where there was one good bit between the error bits (distance = 2), etc.

If the errors were random, the slope of the curve would have been $1/2^n$. In all cases, this slope holds through a distance of 6 to 7 bits. Beyond this point, the presence of many good bits mixed with a few error bits causes the slope to decrease.

The peaks in Fig. 2 at a distance of 5 and 18 were caused by the data set scrambler, a shift register device which makes the transmission spectrum essentially independent of the digital bit sequences. Unfortunately, during very short circuit noise pulses (hits), the scrambler acts as a $\times 3$ error multiplier, inserting extra errors at distances of 5 and 18.

Table 1. Error parameters

Parameter	Group			Total
	Green	Amber	Red	
Test duration, min	1095.2	362.7	2486.6	3944.5
Number of tests	9	19	3	31
Bit error rate:				
Average	3.04×10^{-6}	3.08×10^{-5}	2.52×10^{-4}	4.33×10^{-5}
Median test	2.3×10^{-6}	2.48×10^{-5}	2.54×10^{-4}	1.63×10^{-5}
Number of bursts	84	1167	1462	2713
Bursts per hour	4.6	35.3	193.0	41.3
Blocks transmitted:				
Inbound	181279	275062	85587	541928
Outbound	81374	326682	0	408056
Total	262653	601744	85587	949984
Blocks not received	9	1066	1465	2540
Blocks received in error	78	1184	495	1757
Block thruput, %	99.96	99.63	97.71	99.55
Burst length, bits:				
Shortest	0	1	1	0
Longest	417	869	1071	1
Average	38.9	50.2	71.6	59.1
Median	24	26	54	26
Bits within bursts, %:				
Good bits	70.8	69.6	68.9	69.3
Error bits	29.2	30.4	31.1	30.7
Error bit translations, bits:				
1's translated to 0's	345	7558	8318	16221
0's translated to 1's	527	13298	16180	30005
Block error rate:				
1200 bit blocks	0.00030	0.0020	0.0058	0.00185
2400 bit blocks[a]	0.00058	0.0035	0.0084	0.00315
4800 bit blocks[a]	0.00108	0.0067	0.012	0.00564

[a]Derived from tests conducted with 1200 test blocks.

Table 2. Simultaneous block errors in opposite directions

Tests	Block errors inbound	Block errors outbound	Simultaneous block errors
3,4	37	100	3
5,6	11	22	0
31,32	0	11	0
33,34	176	9	0
1,2	0	24	0
7,8	5	24	2
9,10	1	37	0
35,36	2	19	0
37,38	29	53	9
11,12	221	214	14
22,23	96	112	23
	578	625	51

Table 3. Card transition probability matrices

Green

	0	1	2
0	$1-(2.73\times10^{-7})$	0.088	0
1	2.73×10^{-7}	0.320	0.244
2	0	0.592	0.756

Amber

	0	1	2
0	$1-(2.02\times10^{-6})$	0.065	0
1	2.02×10^{-6}	0.341	0.259
2	0	0.594	0.741

Red

	0	1	2
0	$1-(1.14\times10^{-5})$	0.045	0
1	1.14×10^{-5}	0.355	0.270
2	0	0.600	0.730

Total

	0	1	2
0	$1-(2.40\times10^{-6})$	0.055	0
1	2.40×10^{-6}	0.348	0.265
2	0	0.597	0.735

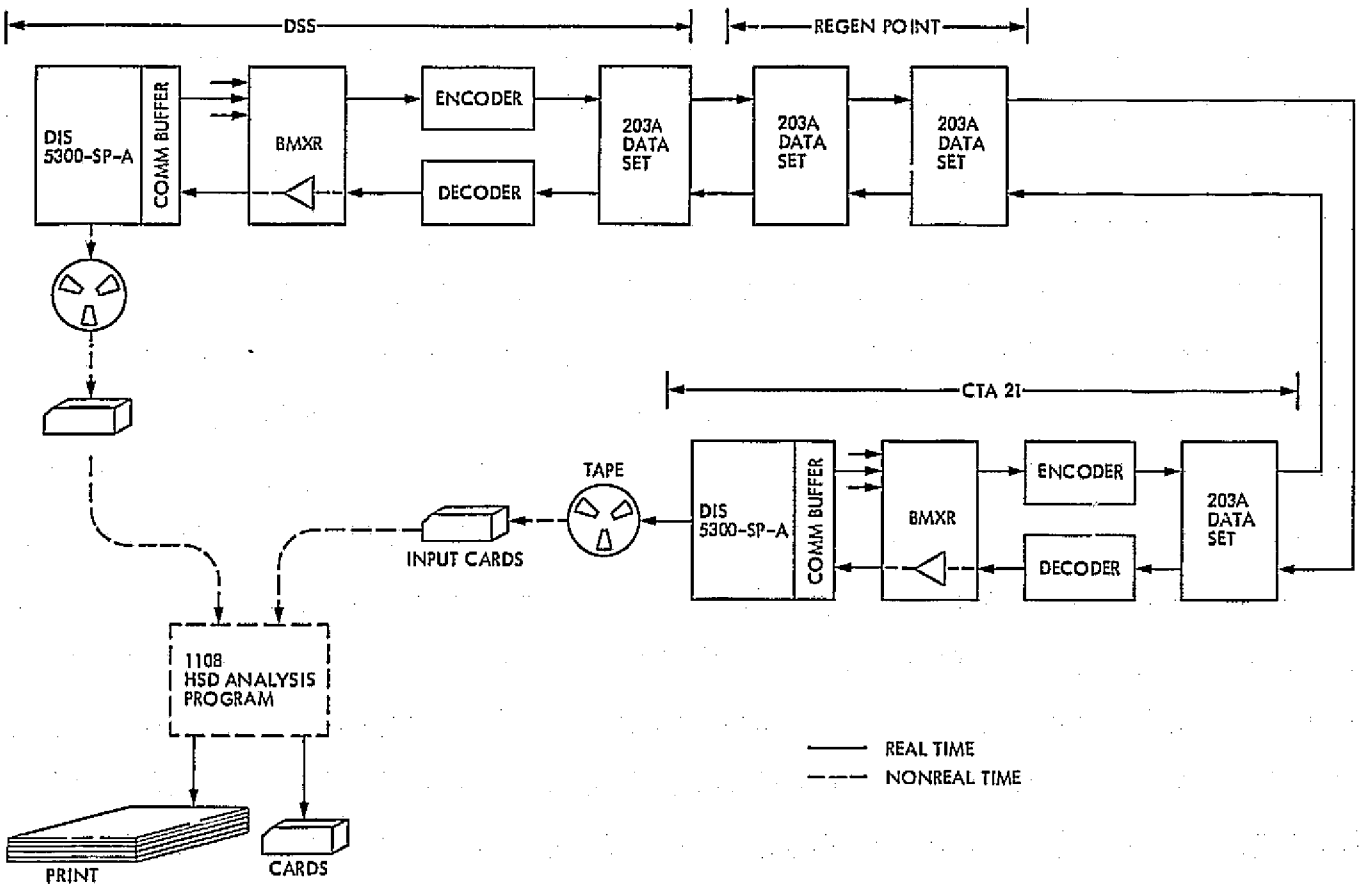

Fig. 1. 4800-bps high-speed data test configuration

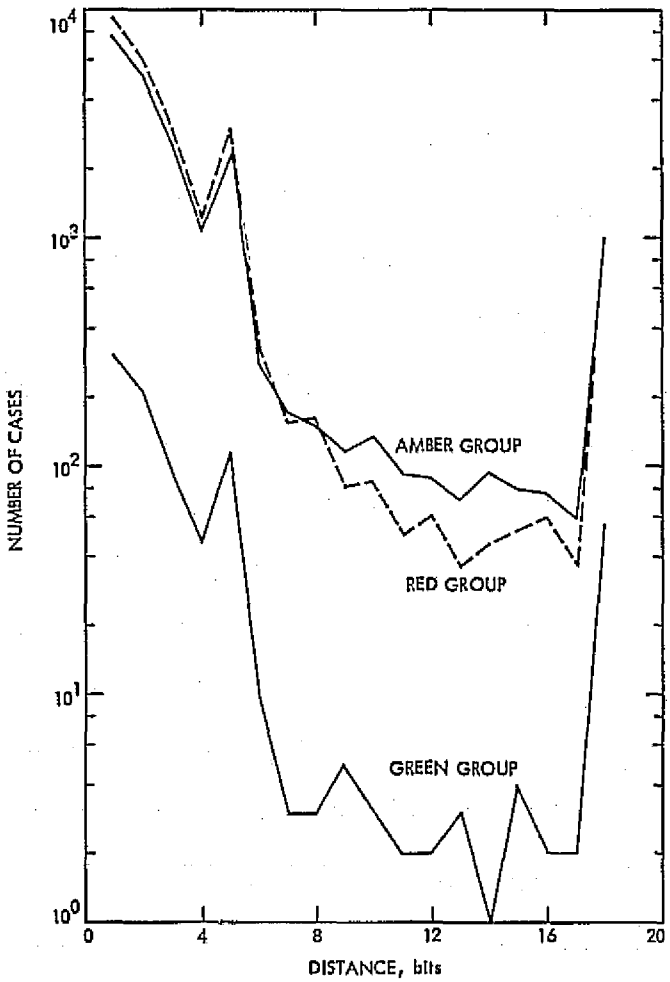

Fig. 2. Distance between bit errors

Modifying an HA/Dec Coordinate Antenna Pointing System to Process Data From an X/Y-Mounted Antenna

W. Davis
DSN Data Systems Development Section

About mid-1972, JPL assumed responsibility for the operation of NASA's STDN station at Canberra. This action was prompted by the decommissioning of DSS 41 at Woomera and increased tracking commitments for the DSN. Although DSS 44 (previously STDN's Honeysuckle Apollo) is a unified S-band 26-m antenna, its coordinate system is X/Y. This article addresses the differences between the X/Y system and that of the DSN's HA/dec, and describes how a functional system was created using subsystem assemblies from both stations.

I. DSN/STDN Configuration

The antenna pointing assembly (APA) and the tracking data handling (TDH) subsystem within a DSN 26-m Deep Space Station (DSS) operate in conjunction with an antenna whose orthogonal axes are oriented in hour angle (HA) and declination (dec). Servo position information is processed by a transmitter-repeater-encoder servo system and routed directly to storage registers within the TDH. This is the distribution point for all angle information such as visual displays, angle information to the APA computer, and angle information to the digital instrumentation subsystem (DIS) for high-speed data line transmission to the Network Operations Control Center (NOCC) and Flight Project.

Such a system (see Fig. 1) was available from DSS 51 for installation at Honeysuckle. It would seem that substituting a complete system would be the most logical approach from the standpoint of conversion requirements. However, mechanical problems involved with the mounting and coupling of the DSN transmitter-repeaters on the axis shafts of the STDN antenna precluded this approach. An approach using parts from both systems was finally employed. The interface was selected at a point following the STDN translator. This then included the STDN transmitters and the servo repeaters on the antenna structure, thus maintaining the integrity of the precision calibrations that are necessary with that portion of a servo system, as well as eliminating the mechanical problems mentioned previously.

II. Problem Areas and Software

Combining portions of both systems created two basic incompatibilities:

1. The data code generated by the STDN translator is in binary rather than binary-coded decimal (BCD) as it is in the DSN.
2. Data processing must operate with an *X/Y* coordinate system rather than an HA/dec system.

The APA computer provided a ready solution to the coordinate conversion problem, and because this approach involved writing a new operational software program, the additional task of converting the coding format was also placed within the software. This second consideration eliminated the need for extensive circuit redesign of the TDH storage registers. These registers accept six packed-decimal digits (4 bits each except for the most significant digit, which has 2 bits) in BCD. Output from the STDN translators is 16 bits of straight binary plus sign.

In its new role, the APA computer will process 16 bits of straight binary data from the translator and deliver them as 21 bits of BCD to the TDH storage buffer. Because there is no sign capability within the buffer, negative angles will be represented by angles within the fourth quadrant. (The STDN antenna delivers + and −90 deg readings in both axes.) The conversion between the coordinate systems is done within the software using trigonometric routines. The unmodified DSN software utilized the HA/dec and azimuth/elevation (az/el) coordinate systems, converting from one to the other as needed. The az/el system is used for refraction corrections, visibility/rise time considerations, angle "stop" tests, position offsets, and rate offsets. The HA/dec system is used for antenna positioning, error display, and position and rate offsets.

In the modified version, the *X/Y* system takes the place of the HA/dec. However, the HA/dec system is still utilized internally for some purposes. For example, right ascension and declination are converted to hour angle and declination, and then a conversion is used to obtain the *X/Y* equivalents.

III. Problem Areas and the Hardware

Logic level requirements and system timing problems were solved using hardware. The APA uses positive logic, as opposed to negative, for both the TDH registers and the STDN translator. Fortunately, the input circuits of the APA were already equipped with negative-to-positive logic conversion circuits; so no modifications were required to handle the input angle data. Output circuits, however, were not buffered for conversion from positive to negative. Two existing spare parallel output channels were cabled to an existing auxiliary chassis within the APA computer. The appropriate buffering was done in this chassis using standard circuit board cards, and the necessary backplane wiring was added. Output cabling to the TDH registers was also added. The new interface as assembled at DSS 44 is shown in Fig. 2.

Another important consideration was that of timing relative to the transfer of data between the interfaces. Communication between the APA and the translator was accomplished by using a system clock pulse from the computer in conjunction with a software mechanized delay in the data sample routine. Both the "read" pulse, required by the translator for sampling its data, and the pulse furnished by the translator, which alerts the reading device (in this case the APA) to take data, required characteristics not inherent in the pulses furnished by the APA.

The read pulse was modified by taking a 50-pps clock pulse from the computer and modifying its width and polarity using existing circuitry within the TDH buffer before sending it to the translator. The translator's "sample ready" to the APA was simulated by a corresponding "built-in" delay within the software routine.

There was also a timing consideration associated with the output data to the TDH storage buffer. As mechanized within the DSN, the APA and TDH either singularly or in unison can command data storage from the DSN translator. The flow of data in this case was from the translator directly to the APA or to the TDH via the storage registers. Essentially, they received data in parallel, the TDH path being buffered by the storage registers. This allowed the TDH longer sample periods for such things as visual displays, but did not hinder the higher rate required by the APA for angle error updates to the servo drive system.

At DSS 44, however, the APA furnishes the input to the storage register rather than the translator. With the TDH requesting data and the APA storing, it is obvious that a priority system had to be designed. This was done by using existing logic within the buffer register. The timing circuits originally used for the DSN requirements furnished all the needed logic, making it possible to accomplish the task by simply restructuring that logic. The new circuit design allows the buffer register to follow data inputs from the APA at a 50-pps rate whenever a

TDH sample pulse is not present. The sample pulse has priority and will hold the buffer register in the store mode, thus guaranteeing the validity of the data output to the TDH.

IV. Operating Personnel Considerations

Station operational requirements had to be considered when data output formats to the station were established. All visual readouts of angles are in values of X and Y, so that station personnel can readily relate them to the observed position of the antenna. This includes all displays serviced by the TDH buffer register, the typewriter printout, and the commanded angle information of the APA remote control panel. Manual inputs to this panel, such as position and rate offsets, are recognized by the APA program as X and Y angles, as are the predicted angles delivered to the station by the Flight Project/NOCC.

V. Conclusion

DSS 44 is unique to the Deep Space Network, and in all probability will remain so. Under the circumstances, lengthy new designs were not considered worthwhile. Adoption of this hybrid system was only the first of several approaches used to minimize the total effort. Relying heavily upon software and restructuring of existing circuit logic accomplished the job in a reasonable amount of time and at low cost.

Bibliography

1. Corliss, W. R., *Space Craft Tracking*, NASA EP-55, Oct. 1, 1968.
2. Davis, W., *MSFN Translator, DSN APS/TDH Interface*, Modification Procedure BP510007A, Sept. 6, 1974 (JPL internal document).
3. McCornock, D., *Modifications to APS Software for Operations at DSS-44*, D01-5069-OP, October 1974 (JPL internal document).
4. Perlman, M., *Description and Evaluation of Angular Encoding Systems Utilized by Goldstone Tracking Antennas*, Technical Memorandum No. 33-25, Nov. 30, 1960 (JPL internal document).

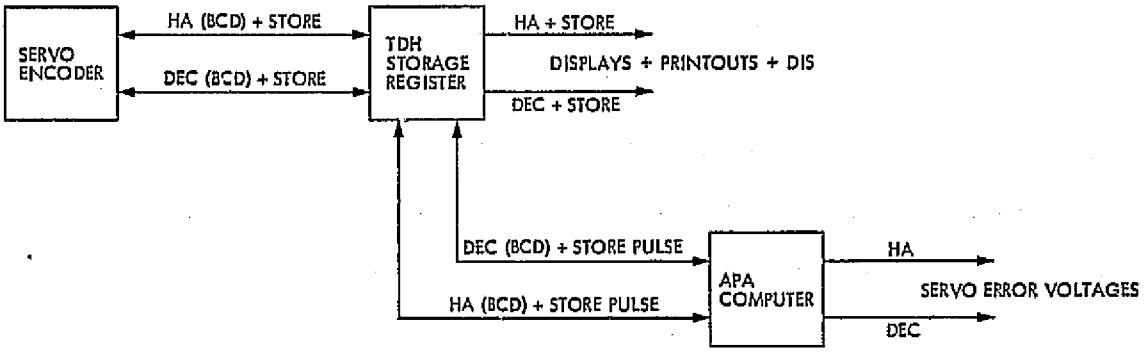

Fig. 1. DSN configuration

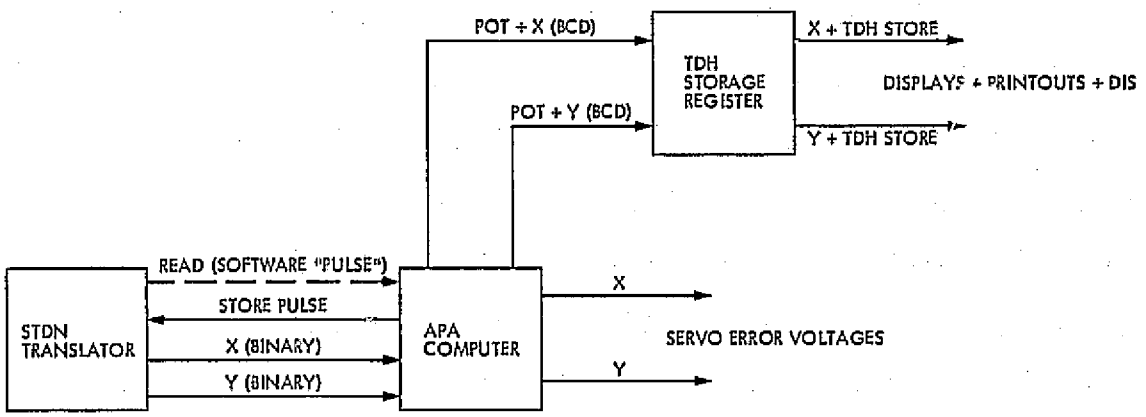

Fig. 2. DSS 44 configuration

Viking 1975 Analog Recording

G. B. Hamilton
DSN Data Systems Development Section

The requirements on the FR1400 analog magnetic tape recorders in the DSN have been increasing in recent years. Viking 1975 requirements appeared particularly stringent. Problems of insufficient tape recording channels or bandwidth were solved by decreasing telemetry requirements and by providing no backup recording for occultation purposes on the standard telemetry recorders.

I. Introduction

An understanding of the potential problems to be faced by the analog telemetry recorders for the Viking 1975 mission may be facilitated by mention of the difficulties involved in the Mariner Venus/Mercury 1973 (MVM'73) mission, particularly at a 64-m antenna site. It was decided by the Deep Space Network (DSN) that since occultation data recorded on the occultation-dedicated analog tape recorders at DSSs 14 and 43 comprised prime radio science data, critical occultation data backup would be provided on the standard telemetry recorders. To this end, two tracks were assigned to occultation, three tracks to telemetry, and two tracks were shared by telemetry and occultation signals. Telemetry recording resources were stressed, particularly by the number of ground signals to be recorded and the large bandwidth which some of them required. Considerable investigation was needed before a workable final recording configuration for MVM'73 was evolved.

II. Viking 1975 Requirements and Changes

Occultation requirements for Viking 1975 will remain approximately the same as for MVM'73, while the number of many of the telemetry requirements will nearly double. It is clear therefore that with the present seven-track recorders, occultation and telemetry cannot share the same tape recorder. All occultation signals are therefore to be recorded on occultation-dedicated FR1400 Analog Magnetic Tape Recorders at DSSs 14 and 43.

At the same time, the DSN has agreed that only four of the 16 possible ground signals must be recorded on the telemetry recorders. In order to obviate interference problems, it is planned to install low-pass (50-Hz) filters in the pre/post detection recording subsystem (PPR) and the analog instrumentation subsystem (AIS), such that the bandwidth of these signals will be limited before they are routed into voltage controlled oscillators (VCOs) and multiplexed with other signals. The bandwidth-restricted

ground signals processed in the PPR are also to be used in the occultation recorder's signal conditioning equipment.

As a result of the above agreements, individual track assignments are relatively uncrowded and are substantially the same as for the Mariner 1971 mission, on a track-for-track basis, with the exception of the necessity for the mixing of speedlock signals with VCO signals containing subcarrier demodulation assembly (SDA) output data. MVM'73 recording successfully made use of speedlock signals mixed with SDA output VCO signals. To ensure success in the playback of data at Compatibility Test Area (CTA) 21, an external bandpass filter was used in MVM'73 and will be used in Viking 1975 to extract speedlock from a multiplex and present it to the servo of the FR2000 analog magnetic tape recorder.

Listed below are the recommended track assignments for a 64-m station:

Cruise Mode, 38.1 cm/s (15 ips)

Track 1. Ground signals, NASA time, commands and voice on VCOs ranging from 1.3 to 93 kHz

Track 2. Baseband Orbiter 1 direct record

Track 3. Orbiter 1 SDA outputs, 13.5-kHz VCO and 108-kHz VCO combined

Track 4. Speedlock 25-kHz direct record

Track 5. Speedlock 25-kHz direct record

Track 6. Baseband Orbiter 2 direct record

Track 7. Orbiter 2 SDA outputs, 13.5/108-kHz VCOs

Planetary Mode, 152.4 cm/s (60 ips)

Track 1. Same as cruise

Track 2. Same as cruise

Track 3. Baseband Lander direct record

Track 4. Speedlock 100-kHz mixed with Orbiter 1 SDA outputs on 13.5/525-kHz VCOs

Track 5. Speedlock 100-kHz mixed with Orbiter 2 SDA outputs on 13.5/525-kHz VCOs

Track 6. Same as cruise

Track 7. Lander SDA outputs, 13.5/108-kHz VCOs

The following are the recommended track assignments for the 26-meter stations, 38.1 cm/s (15 ips), planetary and cruise mode:

Track 1. Vacant

Track 2. Receiver 1 baseband, direct record

Track 3. Ground signal, NASA time, command and voice

Track 4. Speedlock 25-kHz mixed with SDA 1 output, 108-kHz VCO

Track 5. Speedlock 25-kHz mixed with SDA 2 output, 108-kHz VCO

Track 6. Receiver 2 baseband, direct record

Track 7. Vacant

III. Predictions for Data Degradation

Detected data outputs recorded at encounter signal-to-noise ratios should be capable of being reproduced with data degradations of less than 1 dB. Baseband data similarly recorded should be capable of being reproduced with data degradation of less than 1.5 dB. The improvement in the baseband degradation figure from past performance is expected to occur as a result of upgrading the present FR2000s at CTA 21 to FR2000As with improved time base error and skew figures.

IV. Testing Performance

Two tests should be performed in validation of the proposed configuration. One is playback of baseband data using speedlock multiplexed with SDA outputs. This will test interference with speedlock as well as the degradation figure for baseband. The other test is the playback of the track having ground signals, time, and command recorded to check for the efficacy of the low-pass filters. The successful extraction of time would be a good indication of this. Other possible tests may be considered as having already been accomplished by the success experienced in past missions.

Evaluation of a Flutter Compensator for DSN Predetection Recording

J. R. McAllaster
DSN Data Systems Development Section

Results of evaluation tests conducted on an R&D model digital flutter compensator designed to reduce the effects of flutter, or time base error, in an instrumentation-quality magnetic tape recorder/reproducer are presented and discussed. These tests were conducted using machines exhibiting a wide range of transport servo stability in an effort to determine the effectiveness of the flutter compensator as a machine-independent device. The flutter compensation technique is potentially useful in the DSN for improving the reproduce capability of the pre/post detection recording subsystem.

I. Introduction

Tests have previously been conducted to determine the decrease in data degradation using a digital flutter compensator to reduce the effects of flutter, or time base error, in the process of recording and reproducing telemetry baseband data on existing record/reproduce machines in the pre/post detection recording subsystem. References 1 and 2 show that the flutter compensator consistently experienced buffer overflow, and Ref. 1 states that an increased buffer length would eliminate this problem. This article will discuss an evaluation of a later model R&D flutter compensator with a larger buffer length (16K by 6 bits vs 1K by 6 bits).

II. Objective

The purpose of evaluating the expanded buffer flutter compensator was to determine whether the previously experienced overflow problem has been conquered and to ascertain its capability of reducing the effects of transport servo time base error and dynamic skew. In addition, the desirability of formal implementation into the DSN was studied.

III. Test Configuration

Figure 1 is a block diagram of the expanded buffer R&D model flutter compensator. The circuit is operationally the

same as that discussed in Ref. 1, where the circuit and its operation are described; therefore, it will not be repeated here. Figure 2 is a block diagram depicting the record and reproduce test configuration used to acquire the data reported here. The filters F1 through F3, shown in Fig. 2, would be essential and integral elements of a prototype flutter compensator. Since these were not included in the R&D model design, commercial electronic filters were used for this evaluation. And since the transfer function of the device is heavily dependent on the filter characteristics (e.g., phase linearity, harmonic distortion, and amplitude linearity), the scope of this evaluation was limited to determining its capability to correct time base error only; i.e., data degradation attributable to the compensator was not measured.

The two-channel strip chart recorder was used to monitor the behavior of the flutter compensator only: one channel recorded the position of the data in the buffer and the other channel recorded phase shift between input and output data. These data were recorded to observe malfunctions in the flutter compensator: buffer underflow/overflow, as previously reported, and incremental phase shift, which was observed while conducting evaluation tests. The data compiled in Table 1 are time base error plus dynamic skew, measured in accordance with IRIG Document 118-73.

IV. Discussion of Test Results

Considerable difficulty was encountered in obtaining observation repeatability for the data listed in Table 1. Access to the recorders/reproducers used to conduct the tests had to be on a non-interference as-available basis, and in some instances the machine's condition was altered between tests because of intervening usage by the prime user. In addition, the R&D model flutter compensator's erratic performance (primarily incremental phase shift) appeared to change as a function of its environment (e.g., ambient electromagnetic noise and temperature). Therefore, the data reported in Table 1 should be interpreted as an indication of the magnitude of performance improvement that the flutter compensator could be expected to provide over the range of machine servo stability listed. Nevertheless, the test results indicate that the flutter compensation technique significantly reduces the inherent flutter, or time base error, and dynamic skew associated with an instrumentation-quality record/reproduce machine.

Buffer overflow was experienced with the FR1400 and FR1900 machines. The nature of overflow with the FR1400 was random but persistent. Figure 3 is an extreme sample of data indicating the nature of the overflow and the incremental phase shift phenomena. This later problem was observed in all tests conducted. Overflow on the FR1900 occurred only once; however, the strip chart recorder data indicate that it would have occurred consistently given a longer test time. (The FR1900 was available for only 1 day, so more extensive tests were precluded.)

V. Conclusions

The results of tests reported in this article indicate that the flutter compensation technique will reduce the effects of flutter, or time base error, in a record/reproduce machine. However, as can be seen from an analysis of Table 1, the technique produces diminishing marginal returns as a direct function of machine quality. A significant disadvantage of the technique as presently implemented is the loss of bandwidth. In the existing design, the synchronization signal is recorded at the recorder upper bandedge on the same track as the data; therefore, the data and synchronization signal must be interspaced in frequency by at least 1/2 to 1 octave so that they can be separated upon playback without excessive filtering requirements. As a result, 1/3 to 1/2 of the available data bandwidth is sacrificed to the synchronization signal. Any future design effort should consider a more optimal synchronization signal frequency to reduce this loss of bandwidth.

In addition, the buffer overflow/underflow problem remains to be corrected. Reference 3 documents a successful demonstration of an R&D model flutter compensator. The authors of Ref. 3 state that "...the difference between the average writing rate and the average reading rate would inevitably cause the delay line buffer to either overflow or underflow, depending on the direction of the frequency offset." These writers conclude that a long-term read/write clock rate difference correction is mandatory. The flutter compensator developed at JPL does not contain a circuit to accomplish this.

References

1. Slekys, A. G., "Implementation of a Flutter Compensator for DSN Predetection Recording," in *The Deep Space Network Progress Report*, Technical Report 32-1526, Vol. XVI, pp. 132–139, Jet Propulsion Laboratory, Pasadena, Calif., August 15, 1973.
2. Slekys, A. G., "Open-Loop Receiver/Predetection Recording System for the DSN," in *The Deep Space Network Progress Report 42-20*, pp. 139–148, Jet Propulsion Laboratory, Pasadena, Calif., April 15, 1974.
3. Klein, M. S. and Tomback, S., "Digital Time-Base Error Compensator for Wideband Telemetry Recorder/Reproducers," International Telemetering Conference Proceedings, Washington, D. C., pp. 523–531, September 1969.

Table 1. Evaluation data

Tape speed, cm/s	Ampex FR1400			Ampex FR1900			Bell & Howell VR3700B			Ampex FR2000A		
	In	Out	$\frac{\text{In}}{\text{Out}}$	In	Out	$\frac{\text{In}}{\text{Out}}$	In	Out	$\frac{\text{In}}{\text{Out}}$	In	Out	$\frac{\text{In}}{\text{Out}}$
304.8	15	0.20	75	1.5	0.15	10	1.0	0.25	4.0	0.55	0.20	2.8
152.4	15	0.25	60	2.5	0.30	8.3	1.0	0.40	2.5	0.80	0.25	3.2
76.2	50	1.5	33	4.5	1.4	3.2	1.5	1.0	1.5	1.25	0.50	2.5
38.1	150	5.0	30	6.5	1.5	4.3	2.7	2.0	1.4	2.5	0.80	3.1

Notes: 1. The column labeled "In" is the signal at DATA IN and the column labeled "Out" is the signal at DATA OUT shown in Fig. 2.

2. The In and Out numbers are in microseconds.

3. The In and Out numbers are time base error plus dynamic skew measured in accordance with IRIG 118-73.

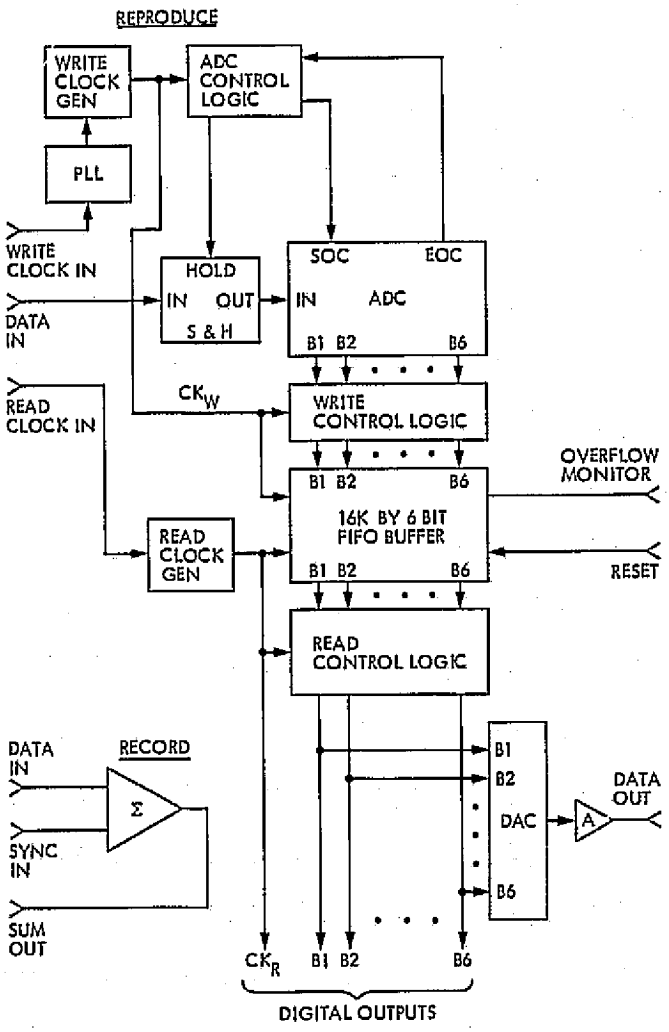

Fig. 1. Block diagram of R&D model flutter compensator

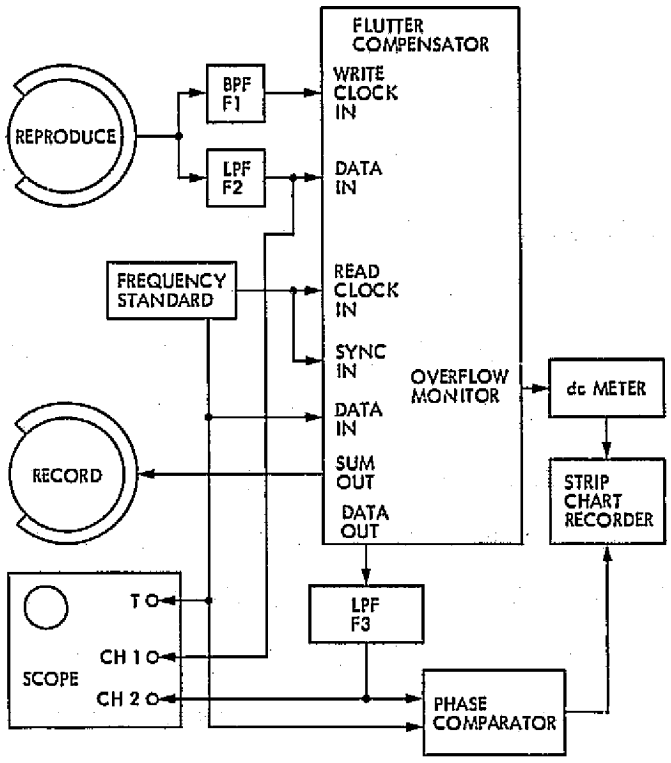

Fig. 2. Block diagram of flutter compensator test configuration

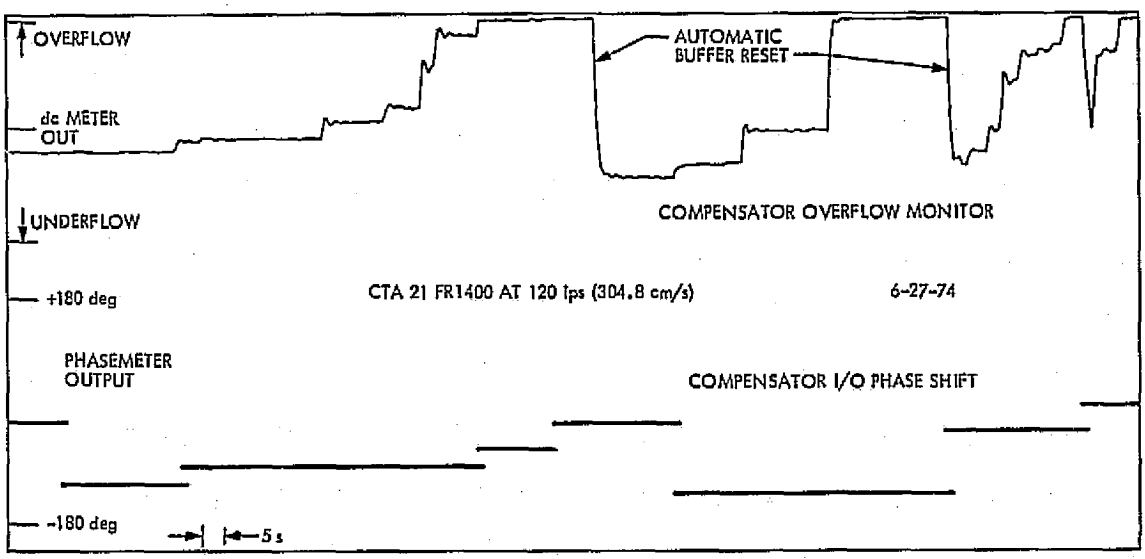

Fig. 3. Sample of compensator behavior

Continuous Spectrum Planetary Ranging Operational Software

G. R. Osborn
DSN Data Systems Development Section

The Planetary Ranging Operational Software has been expanded to provide continuous spectrum ranging in addition to the already existing discrete spectrum mode. The new functions are considered in this article.

I. Introduction

The Planetary Ranging Operational Program has been expanded to provide continuous spectrum ranging. The discrete spectrum version of the program was described earlier (Ref. 1). Either mode can now be selected, depending on mission requirements. Both code types provide high precision range measurements to spacecraft at planetary distances. The equipment is operational at DSSs 14, 43, 63, 71, and CTA 21.

Four continuous spectrum modes are provided. A short code using pseudonoise (PN) components of lengths 2, 7, 11, 15, and 19 or a long code using lengths 2, 7, 11, 15, 19, and 23 can be selected. Either code length can be used with differenced range versus integrated doppler (DRVID) during acquisition, or a faster acquisition with DRVID after acquisition only can be performed.

The short composite code length is $2\times7\times11\times15\times19 = 43{,}890$ bits. With a bit period of approximately one microsecond, the maximum round-trip light time that can be measured without ambiguity is about 43 milliseconds, corresponding to 6500 kilometers in one-way range. Since the spacecraft position is normally known much more accurately than this, the short code is usually adequate to unambiguously refine the range.

If necessary, a longer code containing components of lengths 2, 7, 11, 15, 19, and 23 can be selected. It has an ambiguity interval of about 150,000 kilometers.

The continuous spectrum ranging code has the advantages of a PN code: its spectrum is similar to white noise, hence it is relatively immune to interference from other spacecraft signals; further it does not degrade the other

channels more than white noise would. An exception is the 500-kilohertz clock and its odd harmonics, which appear as sharp spectral lines in the composite signal.

The composite PN from the transmitter coder is transmitted regardless of which component is to be received. The advantage of this approach is that a new acquisition can be started immediately, without having to wait a round-trip light time for the correct component to be received. On the other hand, the ranging power must be shared between all components, so acquisitions take considerably longer. For example, the short code clock correlation is 0.33, which is equivalent to a 9-dB loss compared to a discrete spectrum acquisition.

II. Hardware

The continuous spectrum coders consist of short PN code generators of lengths 2, 7, 11, 15, 19, and 23 bits. The composite code is obtained by a modified majority logic of the PN sequences. The longer components have a higher error probability simply because they have more bit positions to be integrated, hence more opportunities for noise to be misinterpreted as the correlation peak. The longer components are therefore given a larger share of the ranging power, maximizing the acquisition probability for the entire code. The code structure is described in more detail in Ref. 2.

The local reference signals to the two correlators depend on the code type and the acquisition phase. The channel A reference can be any component or the composite code. The channel B reference can be any component or the composite delayed by one bit time, or the clock lagged by 90 degrees.

The entire receiver coder can be shifted in 16 range unit steps for clock phase adjustment. Each component other than the clock can be stepped one bit time, which is equivalent to 1024 range units. Stepping a component affects the composite code, but not the other components.

III. Acquisition Sequence

The acquisition sequence consists of the following steps:

(1) Measure the clock phase, then shift the receiver coder to place the clock at the nearest positive peak. The amount that the clock is shifted, in range units, becomes the least significant 11 bits of the range number.

(2) Determine S_i, the number of bit positions each PN component must be shifted to reach its correlation peak.

(3) Subtract $2^{10}S_iX_i$ from the range number, where X_i is the Chinese number (defined below) for that component.

(4) Evaluate the range number module $2^{10}\Pi_{i=1}^{n} L_i$ if it goes negative. L_i is the length of the ith component.

(5) Return each component to its correlation peak with additional shifts.

Step 1 is the same as for a discrete spectrum acquisition. The equation

$$\tau = 512\left(1 - \frac{A}{|A| + |B|}\right)\frac{B}{|B|} \qquad (1)$$

produces a number between -1024 and 1023, which is the initial clock phase in range units. The correlator local references for the clock integration are in-phase clock to correlator A and clock lagged by 90 degrees to correlator B.

After clock integration the entire receiver coder is shifted to place the correlator A output to a positive peak of the clock. This step insures that one of the PN correlations per component will be exactly at the peak. Since the clock is not shifted more than one PN bit position, no Chinese number need be used.

The execution of step 2 of the above algorithm depends on whether DRVID is being processed or not. If DRVID during acquisition is required, the correlator A local reference is one of the PN components, while the clock delayed by 90 degrees is fed to correlator B for DRVID sensing. The component is stepped one bit per integration interval. The channel A correlation voltage from each bit position is stored in an array. After the last bit position has been integrated the array is scanned to find the most positive entry, which is the correlation peak. The array subscript of the most positive entry is S_i, the number of shifts required to reach the correlation peak.

If there is no DRVID during acquisition, both correlator channels are used to integrate two bit positions simultaneously. This is accomplished by feeding the component delayed by one bit time to correlator B. The

component is stepped two bit positions between integrations in this case. The array of correlation voltages is filled two locations at a time, but the range computation is otherwise the same as when DRVID is being processed.

In step 3, above, the Chinese number is the number of bit positions the composite code is shifted for a single shift of a component. This effect can be easily seen in Fig. 1. If the 7 component is right-shifted one place, the pattern which is shown around bit position zero becomes displaced to position 22. The Chinese number is 22 in this case. An algorithm for determining Chinese numbers is given in Ref. 3.

While it is not obvious, each range between 0 and $\Pi_{i=1}^{n} L_i$ bit positions will result in a different combination of component shifting and the algorithm will produce a unique (and correct) range number from each combination.

Each component is shifted to the correlation peak after the maximum correlation of all positions has been determined. This is accomplished by continuing to step the component in the same direction as was used to search for the maximum. Since the code is cyclic, the effect is the same as backing up the code to the peak. This step does not affect the range determination, but causes unity correlation after acquisition when the composite code is selected. The composite code is used for DRVID after the acquisition is complete.

Figure 1 shows an example of the PN acquisition sequence. A code containing components of lengths 2, 7, and 11 is shown. This abbreviated code is not implemented but is shown here for simplicity.

IV. DRVID

Only one correlator channel is available for DRVID sensing during acquisition. The in-phase clock cannot be measured. Since a single value cannot be used to compute phase, the correlation voltages from the clock integration are used to derive the in-phase voltage by the relationship $A_i \cong |A_c| + |B_c| - |B_i|$, where A_c and B_c are the clock correlations. This derived value of A_i, along with the measured value of B_i, is used in Eq. (1) to compute clock phase.

The derived value of A_i is valid only if the amplitude of the ranging signal remains constant during acquisition. Amplitude variations do not result in large DRVID errors, however, since the clock is servoed to null the quadrature channel. Amplitude variations affect the servo gain. Short-term DRVID variations are not followed as accurately if the amplitude changes, but slow changes are still accurately tracked.

After acquisition the receiver coder is switched to the composite code. All components are then correlated simultaneously, resulting in a stronger detected signal. The receiver coder is also shifted by ¼ clock cycle at this time. DRVID is then derived from the two composite correlations rather than from the clock. The clock correlation is 0.33 for the short code, 0.25 for the long code, and unity for the composite code. DRVID jitter is thus reduced after acquisition.

DRVID after acquisition is computed from the equation $\tau = 512 \cdot (B-A)/(B+A)$. The signals are shown in Fig. 2. The equation is valid only to ±90 degrees of the clock, or ±512 range units. Since the receiver coder is shifted back to the null at each DRVID time, arbitrarily large DRVID excursions can be tracked provided DRVID does not change by more than 512 range units during a single sample interval. Such a large step is unlikely.

The discrete spectrum DRVID performance has been improved by shifting the clock to the 45 degree point after acquisition. Equation (1), which is used also for discrete spectrum DRVID, provides an estimate of phase that is less sensitive to noise when $A = B$. DRVID jitter is reduced by $\sqrt{2}$. Reference 4 indicates that somewhat more improvement will occur with a spacecraft because the transponder attenuates the higher harmonics and shifts their phase.

The discrete and continuous spectrum DRVID signals are shown in Fig. 2. At a given signal level the continuous spectrum mode produces twice as much jitter.

V. Summary

Numerous refinements have been made in the program for the continuous spectrum release, particularly for operator convenience. The rules for entering the initialization parameters have been simplified, and variables are now displayed in a more legible format. Portions of the program were rewritten for greater efficiency, since most of memory is being used.

Much of the code is common to all modes of operation, hence much that was described for the discrete spectrum version (Ref. 1) applies also to the continuous spectrum version.

References

1. Osborn, G. R., "Planetary Ranging Operational Software," in *The Deep Space Network Progress Report 42-21*, pp. 87–91, Jet Propulsion Laboratory, Pasadena, Calif., June 15, 1974.

2. Tappan, R. W., *DSIF Technical Description, Planetary Ranging Equipment, MM'71 Configuration*, TD505943A, Feb. 4, 1972 (JPL internal document).

3. Stewart, B. M., *Theory of Numbers*, The Macmillan Company, New York, 1952.

4. Molinder, J., "Digital Telemetry and Command: Mean-Square Error and Bias of Phase Estimator for the JPL Sequential Ranging System," in *The Deep Space Network*, Space Programs Summary 37-64, Vol. II, pp. 27–28, Jet Propulsion Laboratory, Pasadena, Calif., Aug. 31, 1970.

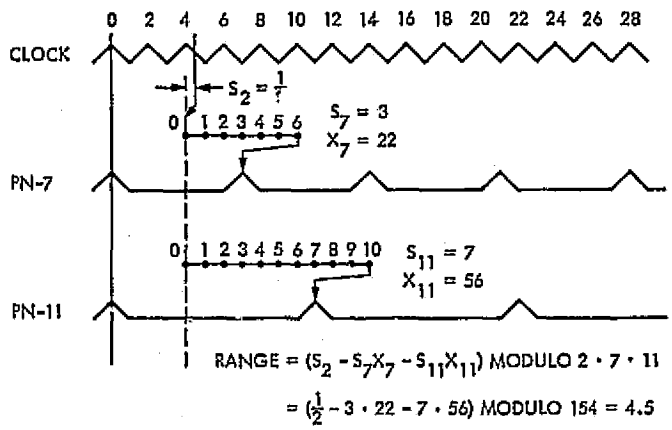

Fig. 1. PN acquisition sequence

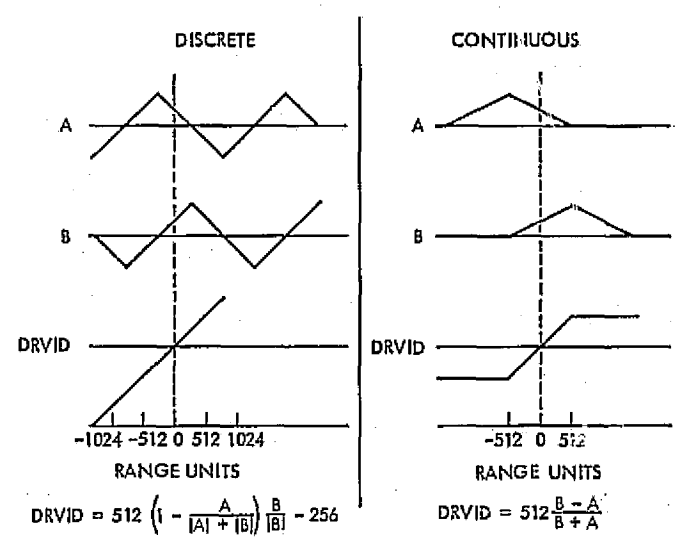

Fig. 2. DRVID waveforms

Resolution of an Inconsistency in Deep Space Station Longitude Solutions

K. H. Rourke and N. A. Mottinger
Tracking and Orbit Determination Section

This article presents analysis and results that lead to the resolution of a discrepancy in Deep Space Station (DSS) longitude estimates that had been obtained in 1971 and 1972 from spacecraft near-encounter radio metric data. A 21-m discrepancy between the Mariner 4 and Mariner 9 DSS longitude solutions is shown to be reduced to within 3 m with the application of improved solution strategies. The resulting agreement between all encounter arc longitude solutions for Mariners 4, 5, 6, and 11 is within 5 m.

I. Introduction

In 1971, during the preparation of DSS location estimates for the Mariner 9 navigation operations, there appeared a large discrepancy between the three distinct longitude estimates that were obtained from processing the Mariner 4, 5 and 6 near encounter data sets (Ref. 1). Specifically, the DSS longitudes that were determined from the Mariner 4 near-encounter data were consistently removed from the Mariner 5- and 6-based solutions, by as much as 14 m, whereas the Mariner 5 and 6 solutions agree to within 1 m. The processing of the subsequently obtained Mariner 9 near-encounter data, instead of clarifying matters, produced DSS longitude solutions that were 7 to 8 m from the Mariner 5 and 6 values in a direction opposite to the Mariner 4 displacement and, hence, roughly 21 m removed from the Mariner 4 determination. A disagreement of this size, of course, shed considerable doubt on the reliability of the current DSS location determination process required by the DSN in its support of the interplanetary flight projects. When these results persisted in the face of conserted analysis a special study team was established in April 1973 to resolve what had then become known as "the longitude problem."

The resolution of the longitude problem was achieved in October 1973. Basically it was found that the Mariner 4 and 9 determinations were subject to a solution instability due to insufficient postencounter radio data coverage. Mariner 9 was, of course, tracked postencounter as it successfully inserted into Mars orbit. The large inser-

tion burn, however, precluded the useful processing of the postencounter data. Mariner 4 was tracked postencounter, although only a relatively small amount of two-way Doppler data were obtained due to required picture playback activity.

With the identification of the possible data deficiencies, strengthened determination strategies could be specified for both data sets. The measures that were applied did, indeed, improve the Mariner 4/Mariner 9 agreement, to a value less than 8 m. The resulting agreement for all the available encounter data sets, Mariners 4, 5, 6 and 9 was reduced to within ±2.5 m.

This article presents the supporting analysis and arguments for the October 1973 longitude problem resolution. This material, however, includes only a part of the entire longitude problem effort and cannot be taken as a summarization of all the effort that contributed to the resolution.[1] Much of the work has unfortunately gone unpublished, principally due to the negative nature of most of the results. These results allowed, nevertheless, a focusing of the effort into the areas that finally produced the resolution.

The contents of this article are organized as follows: In the following two sections the basic characteristics of the longitude problem are described, and the general problem of determining DSS locations from encounter radio metric data is discussed. The role of spacecraft geocentric range rate uncertainty in the determination of station location solutions is introduced as a possible source of solution instability.

In the next sections the Mariner 4 and 9 near-encounter data sets are analyzed. The Mariner 4 solutions are shown to give better agreement with the other encounter solutions as Doppler measurements are added to the conventionally used, encounter ±5-day data set. The credibility of the extended data arc solutions is established by sensitivity analysis. The effect of spacecraft geocentric range rate accuracy on longitude solutions is explicitly shown for the Mariner 9 data set with the use of near-encounter range measurements. A special processing of these measurements is shown to improve the longitude solution agreement by 2 to 3 m. With these adjustments to the Mariner 4 and 9 solutions, the agreement between all the Mariner encounter solutions improves to within ±2.5 m. This range is considered consistent with the expected error in the individual longitude determinations.

II. Character of the Longitude Problem

Figure 1 shows the preresolution state of the DSS longitude disagreement. The station coordinates are shown in terms of spin-axis distance and longitude for each of the encounter data sets, Mariners 4, 5, 6, and 9. The solutions are based on the DE84 ephemeris and are referenced to a post-Mariner 9 encounter station location set, LS37. LS37 is a minor update to the location set LS35 described in Ref. 1.

The Mariner 4/Mariner 9 disagreement is shown to be 14.5 m, a reduction by 6.5 m from the 21-m disagreement that was understood to be the status of the longitude problem in April 1973. The reduction was due to two factors:

(1) A 2.0- to 2.5-m reduction in the Mariner 4 displacement from LS37 when the ephemeris reference was shifted from DE78 to DE84.

(2) The establishment of the Mariner 9 solutions on a consistent ephemeris reference with respect to the Mariner 4, 5 and 6 solutions. As indicated, the reference ephemeris for the solutions shown in Fig. 1 is DE84. When the longitude problem was first identified the solutions were, by error, not consistently referenced: the Mariner 9 solutions were referenced to DE80 whereas the other solutions were referenced to DE78. Thus, approximately 4 m of the 21-m disagreement were nonexistent.

The Mariner 4/Mariner 9 separation is still shown to be an unacceptably large 14 to 15 m. The relative longitudes and spin axis values, however, show good agreement. This fact had been taken as an indication that the longitude problem was due to error in the determinations of the rotation of the Earth, the precession of the equinox, or possible drifts in the planetary ephemeris. Investigations carried out in these areas, however, indicated that the source of the longitude problem should be sought elsewhere.

The investigation was thus narrowed to consider the principal remaining error source—that of the actual station location estimation process—and specifically the

[1]The principal contributors to the effort were D. W. Trask, J. Ellis, H. F. Fliegel, J. F. Jordan, T. Nishimura, S. J. Reinbold, H. N. Royden, M. A. Slade, M. Standish, F. B. Winn, and J. W. Zielenbach.

estimation effects that produce large absolute longitude errors, yet allow the corresponding relative longitude and spin axis values to be well behaved.

III. Conceptual Analysis of Station Location Determination

In this section the determination of DSS locations is considered from the basic Hamilton-Melbourne (Ref. 2) point of view. It is shown that a mechanism exists that can explain the above-stated characteristics of the Mariner 4/Mariner 9 disagreement; specifically, because of uncertainties in the spacecraft range rate, it is shown that station absolute longitude estimates are more sensitive to data errors than spin axis or relative longitude estimates. This point serves as a motivation for the analysis of the Mariner 4 and Mariner 9 encounter data sets presented in the succeeding sections. The value of the approach is not necessarily compelling in the case of Mariner 4 although the longitude estimates do show better agreement if larger data sets are used. The value of the approach is clear from the analysis of the Mariner 9 data set, however, as the treatment of geocentric range rate uncertainties is shown to improve both the longitude agreement and the formal solution accuracies as well.

Figure 2 illustrates the basic geometry of station location determination using encounter radio data, with emphasis on longitude related parameters. Hamilton and Melbourne's well-traveled analysis shows that a very good and instructive approximation to the range rate or Doppler observable can be expressed as follows:

$$\dot{\rho} = \dot{r} + r_s\omega \cos\delta \sin\left[\alpha_{GR}(t) - \alpha_{S/C}(t) + \lambda\right]$$

where

$\dot{\rho}$ = range rate observable

$\dot{r}$ = geocentric range rate of spacecraft

r_s = DSS distance from the Earth spin axis

ω = Earth rotation rate

δ = spacecraft declination

$\alpha_{GR}(t)$ = right ascension of Greenwich

$\alpha_{S/C}(t)$ = right ascension of spacecraft

A convenient time reference for this representation is the nominal time of the spacecraft crossing of the local nominal DSS meridian, i.e., t_0 such that

$$\alpha_{GR}(t_0) + \lambda_0 = \alpha_{S/C}(t_0)$$

where λ_0 is the nominal DSS longitude.

The above expression then reduces to

$$\dot{\rho} = \dot{r} + r_s\omega \cos\delta \sin\left[\omega(t - t_0) - \Delta\alpha_{S/C} + \Delta\lambda\right]$$

with $\pi/2 \leq (t - t_0)\,\pi/2$, approximately, for a single day's pass, where $\Delta\lambda = \lambda - \lambda_0$ and

$$\Delta\alpha_{S/C} = \alpha_{S/C}(t_0) - \alpha_{S/C_0}(t_0)$$

for α_{S/C_0}, the nominal spacecraft right ascension at t_0. The value of the near-encounter radio data is that the spacecraft position coordinates, i.e., α and δ, are accurately determined relative to the encounter planet position. A planetary ephemeris then provides an absolute reference for the spacecraft position near the time of encounter e.g., encounter ± 5 days. Thus assuming no difficulties with the planetary ephemeris or timing standards, the Doppler observable expressed in terms of the remaining uncertain parameters $\dot{r}$, r_s and $\Delta\lambda$ can be given as follows:

$$\dot{\rho} = \dot{r} + r_s\omega \cos\delta \cos\left(\omega t + \Delta\lambda\right)$$

letting $t_0 = 0$.

One may question the addition of $\dot{r}$, the spacecraft geocentric range rate as an uncertainty to be considered along with station longitude and spin axis errors. This is, however, just the point that is to be established: that although spacecraft range rate is well observed by Doppler observations, only small uncertainties in this parameter can still degrade the ability to accurately determine DSS locations. To illustrate this, the observable equation can be used to obtain the following expression for the variation in range rate as a function of variations in $\dot{r}$, r_s, and $\Delta\lambda$:

$$\Delta\dot{\rho} = \Delta\dot{r} + (\omega \cos\delta \sin\omega t)\,\Delta r_s - (r_s\omega \cos\delta \cos\omega t)\,\Delta\lambda$$

Thus, as is shown in Fig. 3, incremental effects in observed range rate take the form of a bias for $\Delta\dot{r}$, a sine curve for Δr_s, and a cosine curve for $\Delta\lambda$. The curves in Fig. 3 serve to illustrate that the $\Delta\dot{r}$ and $\Delta\lambda$ range rate effects are somewhat similar in appearance in that they are even functions about $t = 0$ in contrast to the odd function nature of the Δr_s effect. Due to this similarity, geocentric range rate and longitude are relatively difficult to independently extract from a solution based on a single

pass of DSS data. This fact is pointed out in Ref. 2 and is illustrated quite well in Fig. 4, which is taken from that reference. Note that for increasing pass half widths, down to a practically used 75 deg[2] that $\Delta\dot{r}$ and $\Delta\lambda$ estimation accuracies, given 1 mm/s observation noise, are strongly linked and only approach spin-axis accuracies for low tracking elevations. The accuracy of $\Delta\lambda$ is seen to improve considerably if $\dot{r}$ is perfectly known, i.e., if the spacecraft range rate is fixed or very accurately determined by an alternate information source. This behavior is the result of a high correlation between the $\Delta\lambda$ and $\Delta\dot{r}$ estimation errors, 0.96 for 75 deg half-pass widths, which is due to the similarity of the longitude and range rate effects illustrated in Fig. 3. As long as this correlation is high, DSN longitude can be determined only to the extent that geocentric range rate is known. The correspondence can be expressed approximately as

0.1 mm/s range rate accuracy $\sim$ 1.4 m longitude accuracy

i. e., $\Delta\dot{r} \sim \omega\Delta\lambda$.

The accuracies shown in Fig. 4 are obtained from a formal error analysis of the Hamilton-Melbourne Doppler representation. Formal accuracy analysis is notoriously optimistic, and hence the actual numerical results should be considered carefully. What is of use for this discussion is the relative behavior of these accuracies. The actual values of 1 and 2 m indicated in Fig. 4 as, respectfully, spin axis and longitude accuracies are not of particular interest, since these values are directly proportional to a rather arbitrarily set 1 mm/s 1-min data noise standard deviation. Nevertheless, the fact that station longitude is relatively less well determined than station spin axis and that station longitude accuracy depends heavily on the observability of spacecraft geocentric range rate can be considered as fundamental to the method of determining DSS locations using short arcs of Doppler data.

The conclusions regarding longitude and spacecraft range rate correlation can be extended to multiple passes and additional stations. Combining multiple passes alone will not affect the correlation; they will only reduce the error by a $1/\sqrt{N}$ factor. Additional stations reduce the correlation between each individual station longitude error and the spacecraft geocentric range rate, but not by a large amount. One can show, in fact, that for N individual station passes the Hamilton-Melbourne model produces a correlation between individual station longitudes and geocentric range rate that can be expressed as

$$\frac{\rho}{\sqrt{(N-1)(1-\rho^2)+1}}$$

where ρ is the individual pass λ, $\dot{r}$ correlation. The mutual correlation for longitudes of stations DSS_i DSS_j is then

$$\rho_{\lambda_i\lambda_j} = \frac{\rho^2}{(N-1)(1-\rho^2)+1}$$

Assuming $N = 8$ and $\rho = 0.96$, for example, $\rho_{\lambda_i\lambda_j}$ is still large at a value of 0.80. Hence, each of the longitude accuracies is still principally dependent on the geocentric range rate accuracy. Thus, in general, the proposed mechanism, that is, the effect of uncertain spacecraft geocentric range rate on longitude estimates provides for the observed attributes of the longitude problem. That is, the longitude instability is correlated from station to station, while the relative longitudes and spin-axis distances remain unaffected.

It was mentioned previously that longitude stability is improved if spacecraft geocentric range rate information is somehow strengthened. Such an effect can, of course, be expected for data sets including a spacecraft encounter since near-encounter trajectory bending does provide a complete orbit estimate virtually independent of Earth-based reference parameters such as station locations. Thus accurate station location estimates are possible from near-encounter data because of the accurate spacecraft velocity as well as the accurate spacecraft position determinations afforded by close-encounter radio measurements. This effect serves as an explanation for the apparent instability of and poor agreement between the Mariner 4 and Mariner 9 encounter DSS location determinations. As mentioned in the following sections these missions have incomplete metric tracking coverage post-encounter, possibly indicating degraded encounter orbit velocity estimates. In the case of Mariner 4 this is not directly shown; however, for Mariner 9 it is clearly demonstrated that an improved spacecraft velocity determination does indeed improve the agreement and hence the apparent accuracy of the DSS location estimates.

IV. Mariner 4 Encounter Data Analysis

The Mariner 4 near-encounter tracking coverage is shown in Fig. 5 in terms of station elevation profiles. The time period shown is Mars encounter, July 15, 1965, $\pm$5 days—the traditional data arc for determining DSS

[2]Minimum elevations around 15 deg are usually employed to limit atmosphere effects.

locations. As indicated, DSS 11 (Goldstone), DSS 42 (Canberra) and DSS 51 (Johannesburg) tracked Mariner 4 during this period. The coverage is seen to be nearly continuous before encounter but is sparse shortly after. This is due to picture playback activity which required reduced two-way Doppler tracking after encounter. In light of previous discussion the meager postencounter coverage of Mariner 4 possibly indicates that the encounter ±5-day data set may be inadequate in producing reliable location estimates.

Figure 6 summarizes various treatments of the encounter ±5-day data set. Longitude and spin-axis estimates are shown for two data sets: one, including all the available data, and the other including the available data for which charged particle calibrations[a] exist. The difference between these two sets is shown in Fig. 5. For the latter data set, station location solutions are shown with and without calibrations. Solutions are also shown when the GM and J_2 of Mars is estimated along with station locations and spacecraft state. It is clear from these results that the prime cause of longitude solution variation is variation in data set and not calibrations or solution vector choice. Note that spin-axis variations and relative longitude variations are less than the absolute longitude variations. The corresponding solutions for spacecraft (B plane) position are known to be essentially invariant, i.e., only sub-kilometer variations are observed. At the Mariner 4 Earth-Mars encounter distance of 200 million kilometers, the geometric interpretation of a 1-m longitude shift would imply a 42-km spacecraft position change. This indicates that the longitude solution variations are due to a more subtle error type, such as the effect of spacecraft geocentric range rate described earlier.

The possibility of solution instability due to insufficient coverage can be investigated by simply including additional data. This effect is illustrated in Figs. 7 and 8 which show station longitude change as a function of additional radio data included past Mars encounter. Indicated in each figure are the data intervals for which longitude solutions are plotted. In Fig. 7 the data set spans from encounter −5 days to encounter +5 days, and in Fig. 8 the data set spans from encounter −15 days to encounter +15 days. In both cases only spacecraft state and station location parameters are solved for. No calibrations are added for either case, since data for which calibrations are available are only contained in the encounter ±5-day interval. The calibration effect for the additional data can be assumed to be similar to the slight variations for the encounter ±5-day calibrations. The additional 20 days of radio data is seen to produce marked improvement in the Mariner 4 agreement with LS 37. Improvement occurs right after encounter and holds up throughout the remainder of the data set.

The station location solutions for the two data sets are summarized in Table 1. It is of interest that the spin axis values and relative longitudes vary by no more than 1 and 2 m, respectively, although the longitude values move by as much as 4 m.

The principal concerns accompanying a longer arc determination of station locations can be given as follows:

(1) The spacecraft position reference will become sun-centered rather than planet-centered and in the event of a planet right ascension error cause a shift in DSS longitudes.

(2) Spacecraft non-gravitational accelerations will corrupt the radio measurements to greater extent over a longer arc and hence cause erroneous variations in the DSS location estimates.

Figure 9 presents the results of analysis directed at testing the validity of the longer arc longitude estimates. The general stability of longer arc longitude estimates is shown in Fig. 9a. The solution value is seen to decrease sharply between the 10- and 30-day arcs and the value remains relatively stable for up to 90-day arcs, i.e., encounter ±45 days. Figure 9b addresses the above-stated concerns regarding the reliability of longer arc DSS location solutions. As shown, the stability of the Mars right ascension perturbation on the longitude solutions demonstrates that the location determinations remain "Mars referenced" for arcs up to 70 days in length. The perturbation is, in fact, closely approximated by a value of 2.4 m, predicted by simplified geometric reasoning. The effect of a nominal 10^{-12} km/sec^2 (bias) nongravitational acceleration perturbation also demonstrates that the longer encounter arc solutions are not unduly sensitive to spacecraft acceleration uncertainty.

In summary, the Mariner 4 solutions are seen to be unstable for the traditional encounter ±5 day arc. Longer arcs about encounter exhibit improved stability and better agreement with the reference station location set and, hence, the other Mariner encounter station location determinations. These results are not entirely satisfying, since no explicit cause for the longitude "errors" is found, only implications regarding the cause of the improved

[a]The calibrations were prepared by K. W. Yip, JPL Section 391, and are based on Faraday rotation and ionosonde measurements.

agreement can be made. Nevertheless large longitude variations are observed as a function of solution strategy, and those estimates that best agree with the other Mariner values exhibit more stability than those that do not.

V. Mariner 9 Encounter Data Analysis

The Mariner 9 spacecraft inserted into Mars orbit shortly after 0 hours GMT on November 14, 1971. Because of the large ΔV required for orbit insertion, the postencounter radio data cannot be combined with preencounter data for improving station location estimates. Thus, as in the case of Mariner 4, the Mariner 9 longitude solutions may be somewhat unstable due to an imprecise determination of the entire orbit state vector, including position and velocity.

That such an instability does occur is shown quite clearly in Fig. 10. The station longitude solutions are plotted again as functions of increasing data arc length up to the last of the usable preencounter radio data at approximately Mars orbit insertion minus 30 min; the data arc begins at 5 days before encounter on November 9. The longitude solutions are seen to vary considerably, by as much as 10 m in the last 12 hours before encounter. This behavior is not at all inconsistent with the longitude formal error also plotted in Fig. 10. Figure 11 presents an equivalent history for the station spin-axis estimates. Their values are considerably more stable, which suggests that the longitude instability is due to spacecraft geocentric range rate uncertainty as proposed.

According to the range rate uncertainty hypothesis, an improved, independent range rate determination will improve the accuracy of station longitude determination. Unlike Mariner 4 this is indeed possible for Mariner 9, since the Mariner 9 spacecraft had a ranging transponder, and range measurements were taken near Mars encounter. Since range measured over time determines the change in range, a determination of mean range rate can be obtained to almost any accuracy using range measurements over a sufficiently long time interval.

The value of this approach depends on the inherent quality of the range measurements, and more specifically the stability of ranging delay over several days. The range quality can be evaluated with orbital data fit residuals. Shown in Fig. 12 are a set of DSS 14 MU range residuals referred to a Doppler-only orbit based on a data arc extending from encounter minus five days to encounter—the same arc used for the solutions shown in Figs. 10 and 11. In using a doppler-only fit the range measurements can be evaluated against a reference that is not itself affected by the range measurements. The data shown in Fig. 12 are remarkable from two points of view. First, the range residuals exhibit a marked "ramp" indicating a significant range rate bias in the Doppler-only orbit. Secondly, accounting for the slope in the range, the range residuals show very good internal consistency, to within 10 m or better. This result does not indicate that something is particularly wrong with the Doppler orbit; it principally shows the strength of accurate range measurements in determining *mean* range rate. Indeed, 10-m ranging accuracy implies a mean range rate determination accuracy of roughly

$$\frac{10\,\text{m}}{3 \cdot 86400\,\text{s}} \sim 0.04\,\text{mm/s}$$

which is superior to the ~0.1 mm/s range-rate accuracy obtainable from 1 mm/s 1-min Doppler taken over 5 days.

Based on earlier analysis, the range rate error implied in Fig. 12 indicates that a shift in DSS longitude solutions will occur if range data are included with the Doppler. The expected shift is on the order of

$$(14\,\text{m/mm/s}) \cdot (0.36\,\text{mm/s}) = 5\,\text{m}$$

The extent of the effect that the range data have on the Doppler plus range solution depends on the assigned range data weight vis-à-vis the Doppler data weight. As indicated, a range weight that corresponds to an assumed 10-m range accuracy should be sufficient to assure that the range measurements control the range rate determination in the combined data fit. In addition to assigning proper data weights, special care should be taken when combining the range and Doppler data types in alleviating possible conflicting effects due to biases in the range measurements. Biases will not affect a range rate determination unless they are not properly accounted for, e.g., included as solve-for parameters. Biases can arise from instrumentation uncertainties or possible errors in the Earth-Mars distance as specified by the ephemeris and can be particularly troublesome, if unaccounted for, whenever very accurate, e.g., 10-m, range accuracy assumptions are used.

The notions concerning the use of range measurements have been applied to the Mariner 9 5-day preencounter data arc; the results are shown in Figs. 13 and 14, which

correspond to Figs. 10 and 11, which show Doppler-only solution variations. The results shown in Fig. 13 are striking in three particular ways:

(1) The longitude solution movement is considerably more stable than the corresponding variations shown in Fig. 10.

(2) The final solution values are shifted upward by 3 m, thereby producing better agreement with LS37.

(3) The formal error is reduced and decreases much less drastically near encounter.

Figures 13 and 14 also show that the relative longitude and spin axis solutions are not largely affected by the addition of the range measurements, which is consistent with the properties of the range-rate effect hypothesis. The spin-axis values are seen to be biased below the LS37 reference. This reflects the absence of the ionosphere calibrations which invariably shift spin-axis solutions upward approximately 2 to 3 m for this particular encounter geometry.

These results clearly show the effect of spacecraft geocentric range rate accuracy on the determination of station longitudes. In addition, the value of range measurements in estimating DSS station locations is demonstrated. The described techniques for incorporating range data into the station location solutions should be applicable and beneficial in determining not only station locations but also spacecraft orbits in general, whenever sufficiently accurate range data are available.

VI. Final Summary

The modifications of the Mariner 4 and Mariner 9 longitude solutions that are described in this article are considered to constitute the resolution of the longitude problem. The resulting status of the individual mission DSS location solutions is shown in Fig. 15. The total longitude spread is no more than 5 m and Mariner 4 and Mariner 9 solutions agree to within 2 m.

New estimates are included for the Mariner 6 data set that show the effect of applying the range measurements according to the strategy employed for Mariner 9. A comparison of Figs. 1 and 15 reveals that, as in the case of Mariner 9, properly applied range data have improved the agreement of the Mariner 6 estimates with LS37 and the other Mariner estimates as well. Recent analysis of the Mariner 5 data set, however, has not indicated any improvement in the DSS location estimates when range measurements are used. Hence, no changes in the Mariner 5 estimates are shown. All of the estimates shown in Fig. 15 have been incorporated into a latest update of the DSS location estimates, denoted LS41. This new location set is described briefly in Ref. 3.

It is seen, therefore, that LS37, which is essentially based on the Mariner 5/Mariner 6 encounter solutions, proves to be a good determination of the DSS locations. The disagreement between the Mariner 4 and the Mariner 9 longitude estimates has been shown to arise from a basic instability in these estimates. The obtained improvements in the Mariner 4/Mariner 9 solution stabilities therefore only enhances the reliability of the already accurate DSS location determinations.

References

1. Hamilton, T. W., and Melbourne, W. G., "Information Content of a Single Pass of Doppler Data From a Distant Spacecraft," in *The Deep Space Network*, Space Programs Summary 37-39, Vol. III, pp. 18–23, Jet Propulsion Laboratory, Pasadena, Calif., May 31, 1966.

2. Madrid, G. A., et al., *Tracking System Analytic Calibration Activities for the Mariner Mars 1971 Mission*, Technical Report 32-1587, Jet Propulsion Laboratory, Pasadena, Calif., March 1, 1974.

3. Rourke, K. H., and Mottinger, N. A., "LS41—Final Pre-Venus M-10 Station Location Update," Interoffice Memorandum 391.8-147, Jan. 15, 1974 (JPL internal document).

Table 1. Mariner 4 DSS location solutions

Arc	DSS	Longitude, m		Spin axis, m	
		$\lambda - \lambda_{LS37}$	σ_λ	$r_s - r_{s_{LS37}}$	σ_{r_s}
E − 5 day→ E + 5 day	11	7.7	1.8	−0.9	0.8
	42	6.3	1.7	0.3	0.8
	51	5.4	1.5	1.0	0.9
E − 15 day→ E + 15 day	11	3.3	1.2	−1.5	0.6
	42	2.8	1.1	0.2	0.6
	51	3.1	1.1	−0.2	0.6

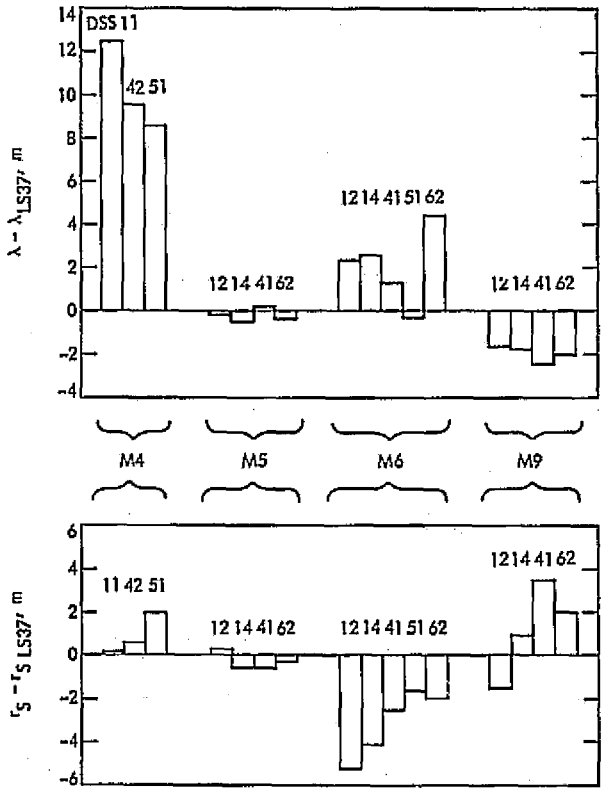

Fig. 1. Preresolution DSS location estimates

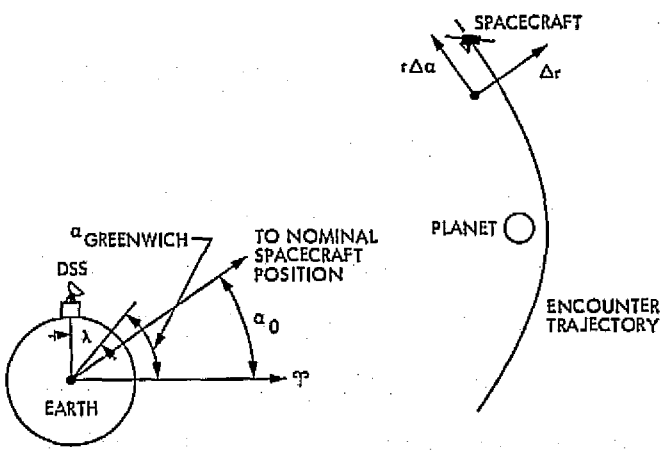

Fig. 2. Encounter geometry

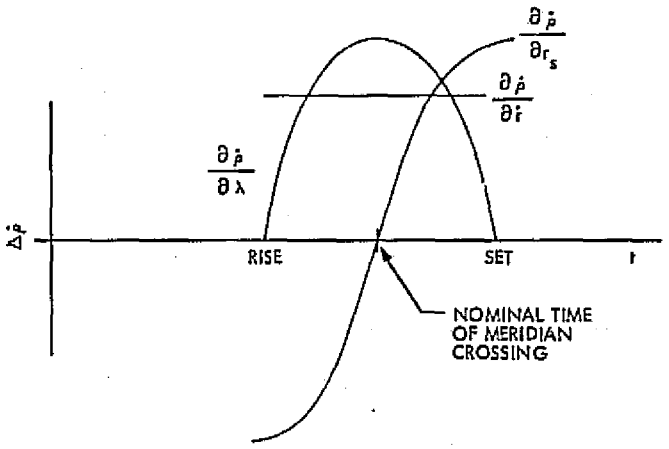

Fig. 3. Three-parameter analysis

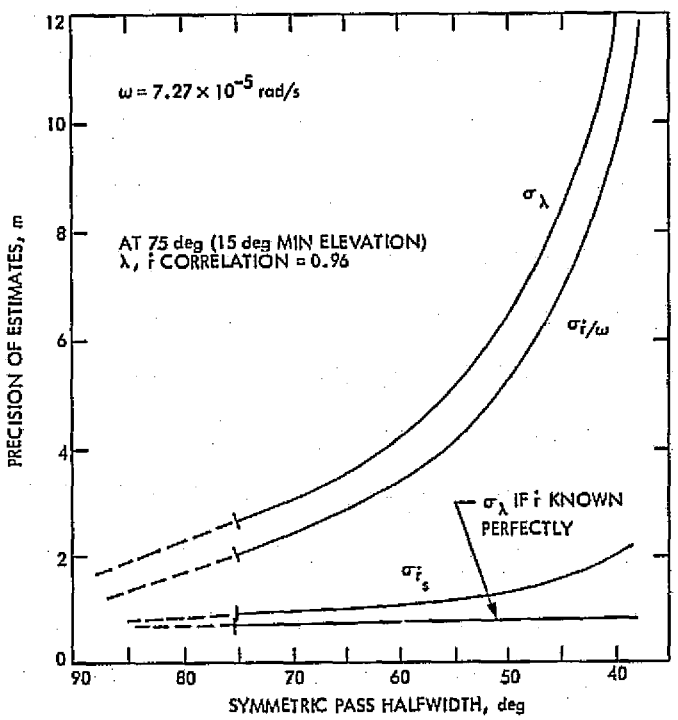

Fig. 4. Idealized one-pass accuracy

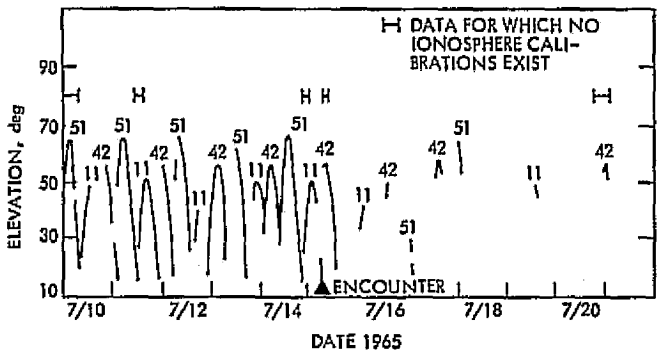

Fig. 5. Station coverage for Mariner 4 encounter

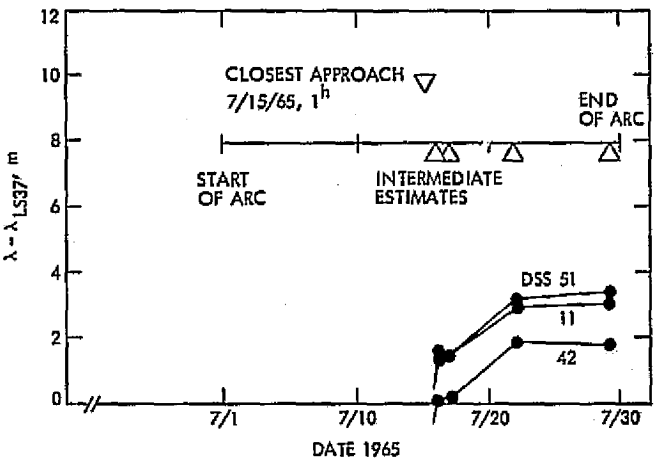

Fig. 7. Mariner 4 longitudes (data from 7-10-65)

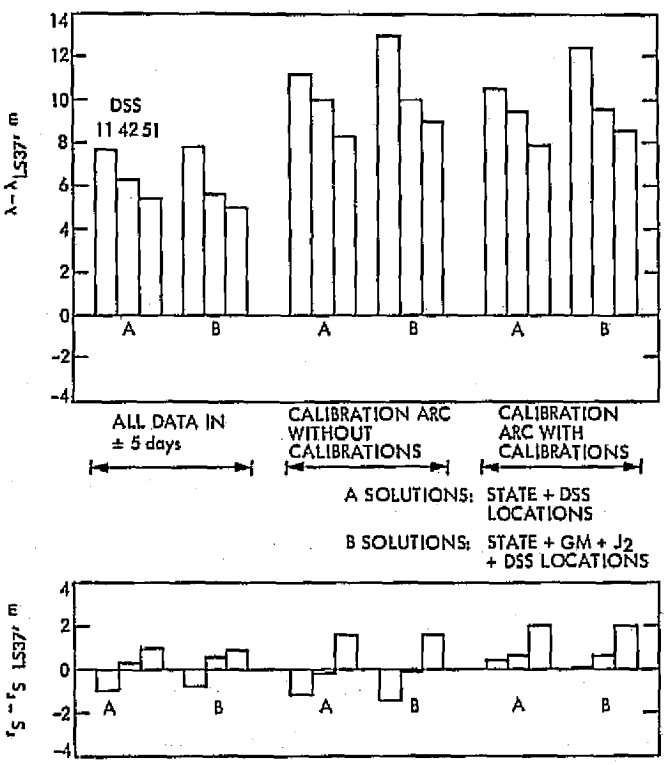

Fig. 6. Treatment variations for the Mariner 4 near-encounter data arc

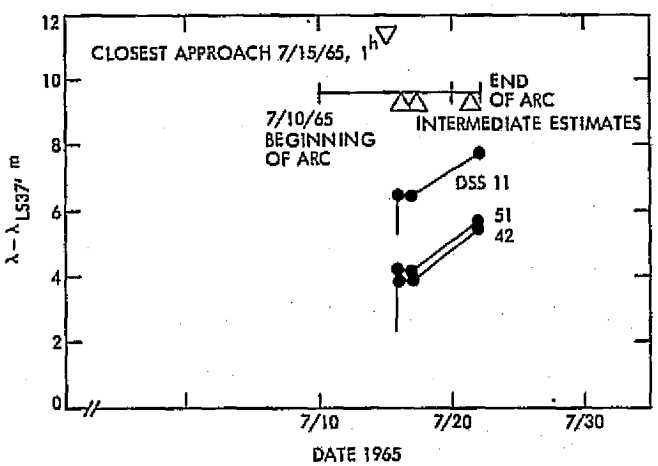

Fig. 8. Mariner 4 longitudes (data from 7-1-65)

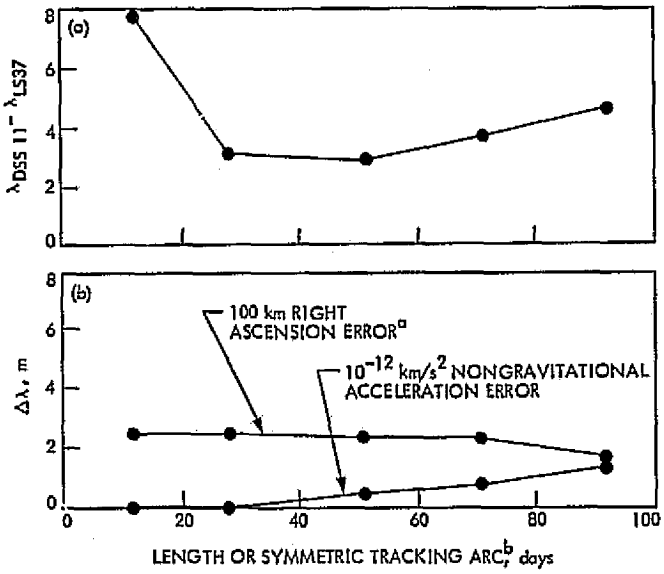

[a]CALCULATION FROM GEOMETRY YIELDS 2.4 m
[b]DATA ARC CENTERED AT ENCOUNTER

Fig. 9. Sensitivities for symmetric tracking arc: (a) Goldstone DSCC Mariner 4 longitude, (b) longitude perturbations due to Mars right ascension and spacecraft nongravitational acceleration

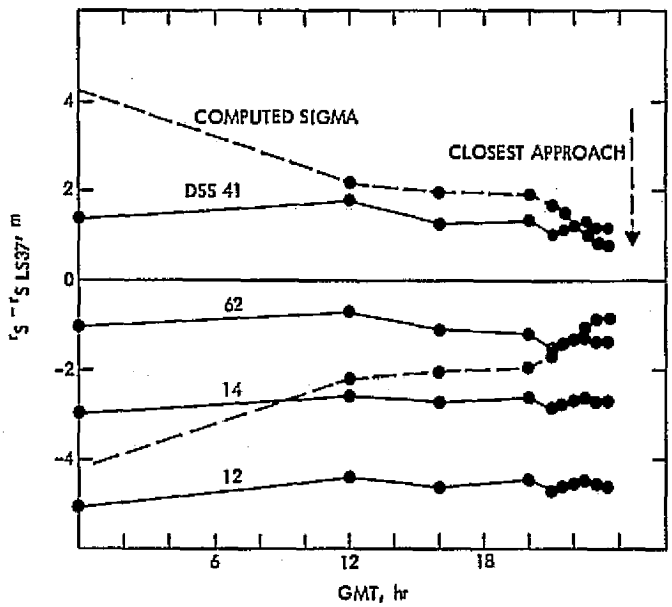

Fig. 11. Mariner 9 spin axis values on 11-13-71 uncalibrated (effect of calibrations bias solutions ~2 m positive) Doppler

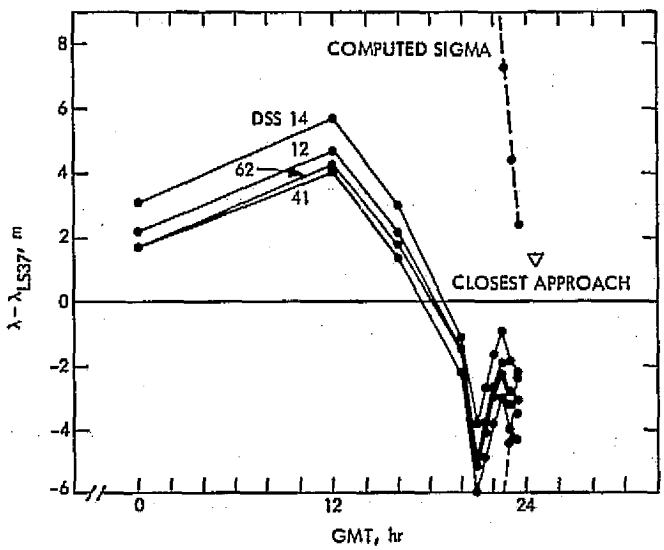

Fig. 10. Mariner 9 longitudes on 11-13-71 (Doppler only)

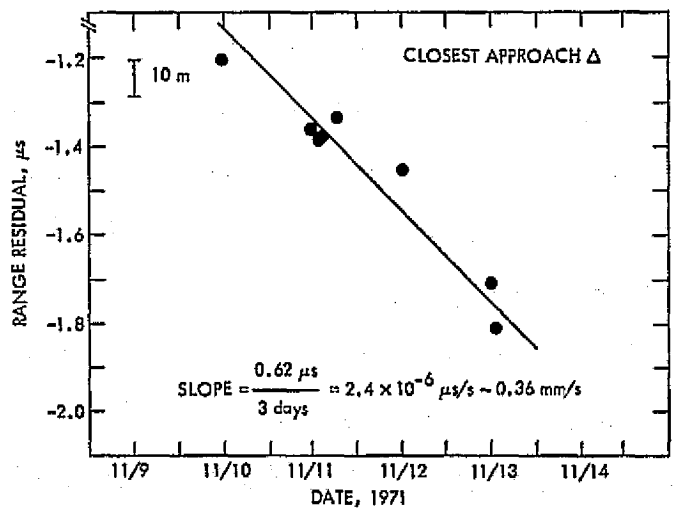

Fig. 12. Mu range with respect to encounter arc Doppler-only fit

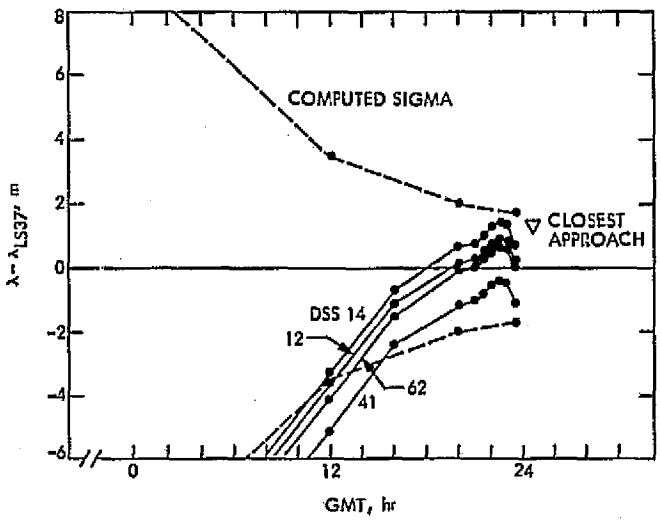

Fig. 13. Mariner 9 longitudes on 11-13-71 Doppler plus range

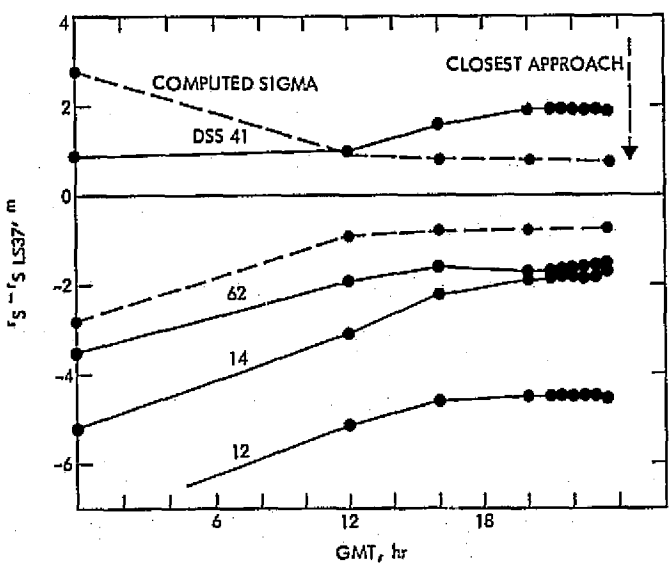

Fig. 14. Mariner 9 spin axis values on 11-13-71, uncalibrated Doppler plus range

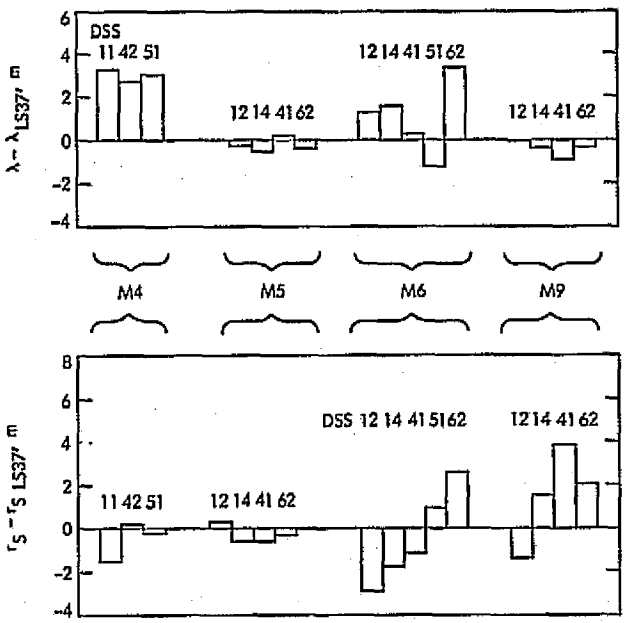

Fig. 15. Postresolution DSS location estimates

A New Angular Tropospheric Refraction Model

A. L. Berman and S. T. Rockwell[1]
Network Operations Office

As part of an effort to obtain a new angular tropospheric refraction model for use within the DSN, an empirical model has been constructed which very accurately reflects precise optical refraction data. The model developed is a single analytic function, is finite over the entire domain of elevation angle, and is highly accurate over large ranges of pressure and temperature.

I. Introduction

There exists here at the Jet Propulsion Laboratory (JPL), and particularly within the Deep Space Network (DSN), a need for an accurate, yet modestly sized, angular tropospheric refraction model. The basic angular refraction model (and several close variants) currently in use at JPL consists of three radically different analytic functions, each applicable over a different range of zenith angle (zenith angle = 90° − elevation angle) and is therefore immediately rather cumbersome. Furthermore, the accuracy of the current JPL refraction model is not well documented, and is thus subject to considerable doubt.

The present time is particularly well suited to reexamine the question of an angular refraction model for the following reasons:

(1) The remote site Antenna Pointing Subsystem (APS) is currently being redesigned, thus affording the capability to easily change the angular refraction modeling.

(2) The recent advent of X-band capability, with an antenna beamwidth of approximately 0.020°, has underscored the need for high-accuracy angular predicts.

The angular refraction model (or variants thereof) currently in use at JPL is as follows:

(1) For $Z \leq 80.26°$,

$$R = (N/10^6) \tan Z$$

(2) For $90° \geq Z > 80.26°$,

$$R = \left(\frac{N}{340}\right)\left(\frac{0.0007}{0.0589 + \left(\frac{\pi}{2} - Z^*\right)} - 0.00126\right)$$

[1]Currently graduate student in physics at the University of California at Los Angeles.

(3) For $Z > 90°$,

$$R = \left(\frac{\pi}{180}\right)\left(0.60874 - 0.201775\left\{\frac{180}{\pi}\right\}\left[Z^* - \frac{\pi}{2}\right]\right)$$

where

R = refraction correction, rad

Z = zenith angle (actual), deg

Z^* = zenith angle (actual), rad

N = "refractivity"

To gauge the degree of error inherent to the current JPL refraction model, it has been contrasted to a continuous set of refraction data as computed from the work of B. Garfinkel (see Refs. 1 and 2), and is seen in Fig. 1. The Garfinkel data is for pressure $P = 760$ mm of Hg and temperature $T = 0°C$; the JPL model data has been matched to these conditions by setting $N = 288$. The most distressingly obvious flaws in the current JPL model are the discontinuities in R at the two breakpoints, these discontinuities (and hence errors in one or the other segment) amounting to approximately 30 and 300 arc seconds (sec), respectively. (Note: For the duration of this report, refraction quantities will be dealt with in terms of arc seconds, with $0.001° = 3.6$ sec.) Further examination of the current model discloses that the first two segments are dependent upon the "refractivity" N, and hence pressure and temperature, while the third segment is not. Given that the current JPL model is inaccurate, has very large discontinuities at the segment breakpoints, and is fundamentally cumbersome because of the tri-segment construction, it would seem to be a likely candidate for a more accurate and reasonable replacement.

II. General Approach to a New Angular Refraction Model

In the previous section, the undesirability of the current JPL angular refraction model was demonstrated; in this section the general philosophy used to generate a new angular refraction model will be dealt with. One starts with the fact that angular refraction is crucially important in the effectuation of various astronomical endeavors, and hence there exists copious amounts of refraction data. The main drawback to these data is, however, that they are either in tabular form or are calculated via schemes which require large amounts of tabular inputs (for instance, see Refs. 1, 2, 3, and 4). Furthermore, the astronomical accuracy requirements are very stringent (perhaps down to about the 1-sec level), while the DSN requirements are no greater than the 10-sec level. In light of the above, it is clear that one reasonable approach would be to use empirical methods to develop a simple analytical expression to approximate the very accurate astronomical refraction data available. Since the envisioned use of the new model within the DSN includes small remote site computers as well as large central complex computers, desirable features would include:

(1) A single expression over the entire domain of Z, instead of multiple segments, each applicable over different ranges of Z.

(2) Accuracy to about the 10-sec level for reasonable ranges of Z and tropospheric conditions.

(3) Model to be designed to minimize both computer memory and run time.

III. Selection of an Angular Refraction Data Base

After a review of the literature, it became apparent that a reasonable selection for a data base would be the work of Boris Garfinkel of the Yale University Observatory (see Refs. 1 and 2). Garfinkel's original theory was published in 1944, and then reexamined in 1966. The form of his model is semi-analytical in that it is a closed function with Z, P, T as variables, but also requires tabular input in the form of Z-dependent polynomial coefficients. More importantly, his model is continued for $Z > 90°$, an aspect which is most frequently missing in other angular refraction works. Finally his work compares well with other authorities in the field. For instance, Garfinkel compares his data at $P = 760$ mm and $T = 0°C$ with those of the Radau and the Pulkova models as follows (with Z' (observed zenith angle) in degrees and R in seconds):

Z'	R Garfinkel	R Radau	R Pulkova
80	331	331	331
81	368	366	365
82	410	409	408
83	463	462	460
84	531	529	527
85	619	617	614
86	738	735	733
87	905	903	900
88	1153	1152	1147
89	1544	1545	1537
90	2206	2208	2199

Table 1 provides a detailed tabulation of Garfinkel refraction data for $0° \leq Z \leq 93°$, $P = 760$ mm, and $T = 0°C$.

IV. Derivation of a Basic Angular Refraction Model

The needs of the DSN for an angular refraction model are restricted to the following range of Z':

$$0° \leq Z' \lesssim 92°$$

where

$$Z' = Z - R(Z) = \text{observed zenith angle}$$

this range being encompassed by the Garfinkel data in Table 1. It was hoped that the data base chosen (i.e., the Garfinkel data whose selection was discussed in the previous section) could be approximately fit to a function (or functions, as necessary) via routine least squares techniques. It was planned to do all work for $P = 760$ mm and $T = 0°C$ under the assumption that P and T effects could be (multiplicatively) added at a subsequent time. The data base chosen was a slightly smaller subset of the data base displayed in Table 1. The frequency of data points was rather arbitrarily chosen as follows:

Range of Z, deg	Data frequency, deg
$0 \leq Z \leq 70$	0.5
$70 \leq Z \leq 85$	0.2
$85 \leq Z \leq 93$	0.1

with the net effect that the refraction data were increasingly "weighted" in the high Z region where the rate of change of refraction is the greatest. The computer program utilized in this study is a standardized least squares subroutine available to all UNIVAC 1108 users at JPL (see Ref. 5). Basically, it fits a data set to an nth degree polynomial such that the residuals are minimized in a least squares sense, i.e.,

$$\text{if} \quad R_i(Z_i); \qquad i = \text{data set}$$

then a function X is formulated such that

$$X = \sum_{j=0}^{n} K_{j+3} \{U(Z)\}^j$$

where

$$K_1 = \frac{1}{2}\left[(R_i)_{max} + (R_i)_{min}\right]$$

$$K_2 = \frac{1}{2}\left[(R_i)_{max} - (R_i)_{min}\right]$$

$$U(Z) = \frac{1}{K_2}\left[Z \quad K_1\right]$$

and where the conditions satisfied are the following n equations in n unknowns.

Let

$$\Delta_i = R_i(Z_i) - X(Z_i)$$

$$\sigma = \left[\sum^{i} \Delta_i^2\right]^{1/2}$$

Then, finally,

$$\frac{\partial \sigma}{\partial K_3} = 0$$

$$\frac{\partial \sigma}{\partial K_4} = 0$$

$$\vdots$$

$$\frac{\partial \sigma}{\partial K_{j+3}} = 0$$

It was originally intended to attempt a least squares curve fit to the "raw" refraction data, shown in Fig. 2. It was observed, however, that the natural log (ln) of R gave a very smooth representation and possessed, of course, far less dynamic range, as can be seen in Fig. 3. It seemed possible that it might yield a better fit for a lower order polynomial (a desirable property), i e., fitting:

$$\ln\left(R_i(Z_i)\right); \qquad X$$

Finally, it was observed that taking the inverse tangent (arctan) of ln (R) yielded a representation that appeared almost linear, as can be seen in Fig. 4. This was also felt to be worth attempting as a fit, in the form of:

$$\arctan\left\{\frac{\ln\left(R_i(Z_i)\right)}{\ln\left(R(45°)\right)}\right\}; \qquad X$$

The ln (R) fit was attempted first as the most likely candidate. The main goal established was to find the smallest order fit which would keep the maximum residual below some reasonable limit. The results of a series of different order fits appear in Fig. 5. Although it might at first seem strange that the absolute maximum residual does not decrease monotonically with degree of fit, all one should really expect is that σ decrease monotonically with degree of fit, and this was the case. At any rate, the 8th degree case was felt to be the best compromise, as one needed to go to a 14th degree fit to obtain significant improvement. The other two types of fits were attempted, with a general tradeoff expected that an increase in functional dependence (ln, arctan, etc.) should decrease the order of fit necessary. A few of the salient features of each of the three types of fits attempted are:

(1) Raw Data Fit

(a) Simple—no additional functions required for modeling.

(b) Minimum acceptable polynomial required ~12th order.

(c) Large residuals (~20 sec or higher) as $Z \rightarrow 0°$, leading to unpalatable result of refraction being applied in wrong direction at very small Z, etc.

(2) Ln(R) Fit

(a) Model would require natural exponentiation (exp).

(b) Minimum acceptable polynomial required ~8th order.

(c) Logarithmic condition of fit forces residuals to be approximately proportional to R, so residuals quite small except at very large Z.

(3) Arctan (ln(R)) Fit

(a) Model would require tangent (tan) and exp.

(b) Minimum polynomial fit required ~6th order.

(c) Extremely low residuals for $Z \lesssim 90°$ and quite high residuals for $Z \gtrsim 90°$.

A comparison of the three types of fits is seen in Fig. 6.[2] The ln R fit was assessed to be the best compromise amongst the design goals stated in Section II. Further refinement to the 8th order ln R fit was accomplished by making minor adjustments to the data set used in the fit process, until an optimum fit (in the sense of the smallest maximum residual) was achieved. For this case, the maximum residual in the interval $0° \leq Z \leq 92°$ occurred at about $Z = 91.1°$ and had a value of:

$$\Delta R = +21.6 \text{ sec}$$

V. Complete Refraction Model Determination

The refraction model, as finally determined in the previous section, is as follows:

$$R = \exp\left\{\sum_{j=0}^{8} K_{j+3}\,[U(Z)]^j\right\} - K_{12}$$

where

R = refraction, sec

Z = zenith angle, actual

$EL = 90° - Z$ = elevation angle

$$U(Z) = \left\{\frac{Z - K_1}{K_2}\right\}$$

$K_1 = 46.625$

$K_2 = 45.375$

$K_3 = 4.1572$

$K_4 = 1.4468$

$K_5 = 0.25391$

$K_6 = 2.2716$

$K_7 = -1.3465$

$K_8 = -4.3877$

$K_9 = 3.1484$

$K_{10} = 4.5201$

$K_{11} = -1.8982$

$K_{12} = 0.89000$

When this model is compared to the Garfinkel data (with $P = 760$ mm and $T = 0°$C), the following maximum residuals[3] result:

$$0° \leq Z \leq 85° \qquad \Delta R = + \quad 5.6 \text{ sec}$$

[2]This figure and Figs. 7, 9, and 10 were prepared on the basis of interim results and are at variance with the final model by as much as 5 sec at large Z. Therefore, they should be used for illustration only.

[3]All residuals (ΔR) will be Garfinkel Data — Proposed Model.

$85° \leq Z \leq 92°$ $\quad \Delta R = +\ 21.6$ sec

$92° \leq Z \leq 93°$ $\quad \Delta R = -302.6$ sec

The very large residuals between $Z = 92°$ and $Z = 93°$ are primarily a result of ending the fit at 92°. At this point there was still one point of concern and that was:

As $Z > 93°$

$|R| \rightarrow$ very large

such that at some $Z > 93°$ there exists the following condition:

$Z - R(Z) < 90°$ (or local horizon)

giving the appearance of a "false" rise. This would, of course, pose difficulties for trajectory-type programs which calculate, and examine for a rise condition, zenith angles considerably larger than 90°. Based on this undesirable feature, it was felt that the model should be modified such that shortly after $Z = 93°$ it would be required that:

$R(Z) \rightarrow 0$

At the same time, it was felt that possibly the characteristics of the model for $Z \gtrsim 90°$ could be improved upon. The residuals between $Z = 90°$ and $Z = 93°$ look like:

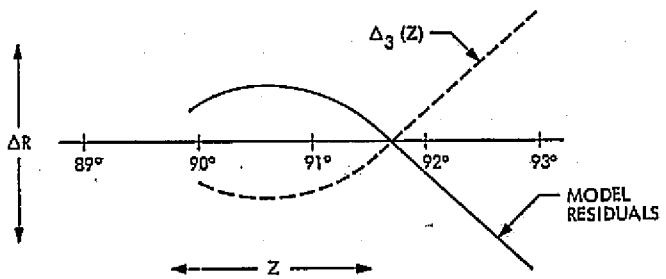

It was therefore felt that if a function (say, $\Delta_3(Z)$) could be derived with inverse characteristics to the above residuals plus possessing the following qualities:

$\Delta_3(Z) \rightarrow$ very large for $Z \gtrsim 93°$

$\Delta_3(Z) \rightarrow$ very small for $Z \lesssim 90°$

Then a model of the form:

$$R = \exp\left\{\left(\sum_{j=0}^{8} K_{j+3}[U(Z)]^j\right) \Big/ [1 + \Delta_3(Z)]\right\} - K_{12}$$

could perhaps both improve the present model between 90° and 93° and drive the model to approximately zero (actually $1 - K_{12}$) thereafter. A function to accomplish this was constructed (empirically) as follows:

$$\Delta_3(Z) = (Z - C_0)\{\exp[C_1(Z - C_2)]\}$$

where

Z = zenith angle, deg

$C_0 = 91.870$

$C_1 = 0.80000$

$C_2 = 99.344$

The improvement in the $Z = 90°$ to $Z = 93°$ region can be seen in Fig. 7, while the rapid drop off of the modified model after $Z = 93°$ can be viewed in Fig. 8. The maximum residuals after the above modification become:

$0° \leq Z \leq 85°$ $\quad \Delta R = +\ 5.6$ sec

$85° \leq Z \leq 92°$ $\quad \Delta R = -14.7$ sec

$92° \leq Z \leq 93°$ $\quad \Delta R = -15.0$ sec

VI. Refraction Model Functional Dependence Upon Pressure, Temperature, and Relative Humidity

It was originally felt that once a refraction model for standard conditions ($P = 760$ mm and $T = 0°$C) had been achieved, the usual scaling by $P/760$ and $273/(T + 273)$ could be applied. However, after examining different combinations of P and T in the Garfinkel data, this did not prove to be an adequate treatment of the pressure and temperature dependence, and additional work in this area was required.

A. Pressure Correction

Examination of the Garfinkel data at different pressures indicated that scaling of the basic model by $P/760$ was reasonable at most Z, but broke down as $Z \gtrsim 90°$. It was hoped that this could be compensated for by a correction factor (say, $\Delta_1(P, Z)$) such that the entire pressure correction factor would be of the form:

$$\frac{P}{760}\{1 - \Delta_1(P, Z)\}$$

Furthermore, it would be necessary that:

$$\Delta_1(P, Z) \to 0, \qquad Z \lesssim 90°$$

$$\Delta_1(P, Z) \to 0, \qquad Z \gtrsim 93°$$

It was noted in the examination of the Garfinkel data that the pressure effect (as different from $P/760$) was for the most part separable, i.e.:

$$\Delta_1(P, Z) \sim \Delta_p(P)\Delta_z(Z)$$

and it could be seen that further:

$$\Delta_p(P) \sim (P - 760)$$

A representation for Δ_z was then empirically constructed as follows:

$$\Delta_z(Z) \sim \exp\,[A_1(Z - A_2)]$$

so that the $\Delta_1(P, Z)$ pressure correction would be:

$$\Delta_1(P, Z) = (P - 760) \exp\,[A_1(Z - A_2)]$$

The results of using $\Delta_1(P, Z)$, above, can be seen in Fig. 9. Finally, to satisfy the conditions of a small $\Delta_1(P, Z)$ for $Z \gtrsim 93°$, the previously determined $\Delta_3(Z)$ was utilized to arrive at the following expression:

Pressure correction factor =

$$\frac{P}{760}\left\{1 - \frac{(P - 760) \exp\,[A_1(Z - A_2)]}{1 + \Delta_3(Z)}\right\}$$

where

Z = zenith angle, deg

P = pressure, mm of Hg

$A_1 = 0.40816$

$A_2 = 112.30$

$\Delta_3(Z)$ = as previously defined

B. Temperature Correction

The investigation of temperature effects proceeded along the same lines as the investigation of pressure effects in the previous section, with the goal of a total temperature correction factor in the form of:

$$\frac{273}{T + 273}\{1 - \Delta_2(T, Z)\}$$

in combination with the conditions:

$$\Delta_2(T, Z) \to 0, \qquad Z \lesssim 90°$$

$$\Delta_2(T, Z) \to 0, \qquad Z \gtrsim 93°$$

Similarly, the temperature effect was found to be approximately separable:

$$\Delta_2(T, Z) \sim \Delta_t(T)\Delta_z(Z)$$

and the following was (empirically) constructed:

$$\Delta_t \sim T$$

$$\Delta_z \sim \exp\,[B_1(Z - B_2)]$$

so that the $\Delta_2(T, Z)$ temperature correction would be:

$$\Delta_2(T, Z) = (T) \exp\,[B_1(Z - B_2)]$$

The results of using $\Delta_2(T, Z)$, above, are seen in Fig. 10. Once again, to satisfy the condition of a small $\Delta_2(T, Z)$ for $Z \gtrsim 93°$, the previously determined $\Delta_3(Z)$ is utilized to arrive at the following total expression:

Temperature correction factor =

$$\frac{273}{T + 273}\left\{1 - \frac{(T) \exp\,[B_1(Z - B_2)]}{1 + \Delta_3(Z)}\right\}$$

where

Z = zenith angle, deg

T = temperature, °C

$B_1 = 0.12820$

$B_2 = 142.88$

$\Delta_3(Z)$ = as previously determined

C. Relative Humidity Correction

Both the Garfinkel (see Ref. 2) and the Pulkova models (see Ref. 4) indicate that the correction for relative humidity is very small, perhaps on the order of several seconds, at large Z. This seems reasonable since optical refraction is generally considered to be proportional to dry refractivity:

$$R = R_{\text{optical}} \sim N_{\text{dry}}$$

where

$$N_{\text{dry}} \cong 77.6\left\{\frac{P}{T}\right\}$$

whereas radio frequency refraction is considered to be proportional to total refractivity:

$$R_{radio} \sim N_{dry} + N_{wet}$$

$$\sim N_{dry}\left\{1 + \frac{N_{wet}}{N_{dry}}\right\}$$

where

$$N_{wet} \cong 77.6\,[4810]\left\{\frac{(RH)\,e_s(T)}{T^2}\right\}$$

and

RH = relative humidity

e_s = saturation vapor pressure

If one should merely account for this difference by scaling the optical results by the following factor (as is effectively what has been done in the past):

$$\left\{1 + \frac{N_{wet}}{N_{dry}}\right\}$$

so that:

$$R_{radio}(P, T, RH, Z) \cong R_{optical}(P, T, Z)\left\{1 + \frac{N_{wet}}{N_{dry}}\right\}$$

one would immediately expect the transformed model (R_{radio}) to preserve the design features from Section II as well as to possess considerably greater accuracy than the current JPL models. However, the whole question of transforming the optical angular refraction model described in this report to the radio frequency level requires additional study before a definitive statement about the transformed model accuracies can be made.

VII. Complete Angular Refraction With Pressure and Temperature Corrections

The final refraction model with pressure and temperature accounted for is as follows:

$$R = F_p F_t\left(\exp\left\{\frac{\sum_{j=0}^{8} K_{j+3}\,[U(Z)]^j}{1 + \Delta_3(Z)}\right\} - K_{12}\right)$$

$$F_p = \left(\frac{P}{P_0}\left\{1 - \frac{\Delta_1(P, Z)}{1 + \Delta_3(Z)}\right\}\right)$$

$$F_t = \left(\frac{T_0}{T}\left\{1 - \frac{\Delta_2(T, Z)}{1 + \Delta_3(Z)}\right\}\right)$$

$$\Delta_1(P, Z) = (P - P_0)\{\exp\,[A_1(Z - A_2)]\}$$

$$\Delta_2(T, Z) = (T - T_0)\{\exp\,[B_1(Z - B_2)]\}$$

$$\Delta_3(Z) = (Z - C_0)\{\exp\,[C_1(Z - C_2)]\}$$

where

R = refraction, sec

Z = actual zenith angle, deg

$EL = 90° - Z$ = elevation angle

$$U(Z) = \left\{\frac{Z - K_1}{K_2}\right\}$$

$K_1 = 46.625$

$K_2 = 45.375$

$K_3 = 4.1572$

$K_4 = 1.4468$

$K_5 = 0.25391$

$K_6 = 2.2716$

$K_7 = 1.3465$

$K_8 = -4.3877$

$K_9 = 3.1484$

$K_{10} = 4.5201$

$K_{11} = -1.8982$

$K_{12} = 0.89000$

P = pressure, mm of Hg

$P_0 = 760.00$ mm

$A_1 = 0.40816$

$A_2 = 112.30$

T = temperature, K

$T_0 = 273.00$ K

$B_1 = 0.12820$

$B_2 = 142.88$

$C_0 = 91.870$

$C_1 = 0.80000$

$C_2 = 99.344$

The accuracy of this model for various pressures, temperatures, and ranges of Z, as compared to the Garfinkel data, can be seen in Table 2.

The signature of the residuals at large Z and with $P = 760$ mm and $T = 0°C$ can be seen in Fig. 7 (modified 8th order ln R fit). For use where simplicity is of a more urgent need than accuracy, an abbreviated version of the model can be obtained by setting:

$$\Delta_1 = \Delta_2 = \Delta_3 = 0$$

such that one has:

$$R = \left(\frac{P}{P_0}\right)\left(\frac{T_0}{T}\right)\left(\exp\left\{\sum_{j=0}^{8} K_{j+3}\,[U(Z)]^j\right\} - K_{12}\right)$$

where all quantities are as previously defined. The accuracy of this abbreviated version, once again as compared to the Garfinkel data, is seen in Table 3. Also, the effects of the deletion of Δ_1 is seen in Fig. 9, of Δ_2 in Fig. 10, and of Δ_3 in Fig. 7.

VIII. FORTRAN Subroutines of the Refraction Models

Appendix A presents a FORTRAN subroutine of the full model described in Section VII, while Appendix B presents a FORTRAN subroutine corresponding to the abbreviated model, also described in Section VII. Inputs required are as follows:

PRESS = pressure, mm of Hg

TEMP = temperature, K

ZNITH = actual zenith angle, deg

and the subroutine(s) return with:

R = refraction correction, sec

IX. Summary

An empirical model has been constructed which very accurately reflects precise optical refraction data. The salient features possessed by this model are as follows:

(1) Single analytic function.

(2) Finite over the entire domain of elevation angle.

(3) High accuracy for large ranges of pressure and temperatures.

(4) Designed to minimize computer storage and run time.

For S- and X-band applications, the model must be transformed from optical frequencies to radio frequencies. It is hoped that by considering the differences in optical refractivity versus radio frequency refractivity, a reasonably accurate method of transforming optical refraction to radio frequency refraction can be found.

References

1. Garfinkel, B., "An Investigation in the Theory of Astronomical Refraction," *Astron. J.*, Vol. 50. No. 8. 1944.

2. Garfinkel, B., "Astronomical Refraction in a Polytropic Atmosphere," *Astron J.*, Vol. 72, No. 2, 1967.

3. Mueller, I. I., *Spherical and Practical Astronomy as Applied to Geodesy*, Frederick Ungar Publishing Co., New York, 1969.

4. Orlov, B. A., *Refraction Tables of Pulkova Observatory*, 4th Edition, 1956.

5. Lawson, C. L., "Least Squares Polynomial Fit to Data, S.P.," *JPL Fortran V Subroutine Directory*, 1846-23 (JPL internal document).

Bibliography

Berman, A. L., *Adjustment of Predict Refraction Model to Prevent (Apparent) Lagrangian Interpolation Problems in Angle Predictions*, 401-2177, Aug. 13, 1971 (JPL internal document).

Rovello, R. C., *Antenna Pointing Subsystem Phase I, Computer Program, DSIF 210 ft Antennas*, 900-22, 315-R-6, Rev. 1, June 1967 (JPL internal document).

Smart, W. M., *Spherical Astronomy*, Cambridge University Press, London, 1965.

Table 1. Garfinkel refraction data[a] for $P = 760$ mm and $T = 0°C$

Z	R	R′	Z	R	R′
0.0	0.00	0.00	22.5	25.09	25.09
0.5	0.55	0.55	23.0	25.71	25.72
1.0	1.07	1.08	23.5	26.33	26.34
1.5	1.61	1.61	24.0	26.97	26.97
2.0	2.15	2.15	24.5	27.60	27.61
2.5	2.68	2.68	25.0	28.25	28.26
3.0	3.22	3.22	25.5	28.90	28.91
3.5	3.75	3.76	26.0	29.55	29.56
4.0	4.29	4.29	26.5	30.21	30.22
4.5	4.83	4.83	27.0	30.88	30.89
5.0	5.36	5.36	27.5	31.55	31.56
5.5	5.90	5.90	28.0	32.23	32.24
6.0	6.43	6.44	28.5	32.91	32.92
6.5	6.97	6.97	29.0	33.60	33.62
7.0	7.51	7.51	29.5	34.30	34.32
7.5	8.05	8.05	30.0	35.01	35.02
8.0	8.59	8.59	30.5	35.72	35.73
8.5	9.12	9.13	31.0	36.43	36.45
9.0	9.67	9.67	31.5	37.16	37.17
9.5	10.21	10.21	32.0	37.89	37.91
10.0	10.75	10.75	32.5	38.63	38.65
10.5	11.30	11.30	33.0	39.38	39.40
11.0	11.84	11.84	33.5	40.14	40.16
11.5	12.39	12.39	34.0	40.90	40.92
12.0	12.94	12.94	34.5	41.68	41.70
12.5	13.49	13.49	35.0	42.46	42.48
13.0	14.04	14.05	35.5	43.26	43.27
13.5	14.60	14.60	36.0	44.06	44.08
14.0	15.15	15.16	36.5	44.87	44.89
14.5	15.71	15.72	37.0	45.69	45.71
15.0	16.28	16.28	37.5	46.53	46.55
15.5	16.84	16.85	38.0	47.37	47.39
16.0	17.41	17.41	38.5	48.23	48.25
16.5	17.98	17.98	39.0	49.10	49.12
17.0	18.55	18.56	39.5	49.98	50.00
17.5	19.13	19.13	40.0	50.87	50.89
18.0	19.70	19.71	40.5	51.77	51.80
18.5	20.29	20.29	41.0	52.69	52.72
19.0	20.87	20.88	41.5	53.62	53.65
19.5	21.46	21.47	42.0	54.56	54.59
20.0	22.06	22.06	42.5	55.52	55.55
20.5	22.65	22.66	43.0	56.50	56.53
21.0	23.26	23.66	43.5	57.49	57.52
21.5	23.86	23.87	44.0	58.50	58.53
22.0	24.47	24.48	44.5	59.52	59.56

[a]R gives the refraction correction if Z = actual while R' gives the refraction correction if Z = observed.

Table 1 (contd)

Z	R	R′	Z	R	R′
45.0	60.56	60.60	69.0	156.61	156.97
45.5	61.63	61.67	69.5	160.75	161.13
46.0	62.72	62.76	70.0	165.06	165.46
46.5	63.83	63.87	70.2	166.83	167.25
47.0	64.95	64.99	70.4	168.63	169.06
47.5	66.10	66.15	70.6	170.47	170.91
48.0	67.28	67.32	70.8	172.33	172.78
48.5	68.47	68.52	71.0	174.23	174.69
49.0	69.69	69.73	71.2	176.16	176.64
49.5	70.93	70.97	71.4	178.13	178.63
50.0	72.19	72.24	71.6	180.15	180.66
50.5	73.48	73.53	71.8	182.20	182.73
51.0	74.79	74.85	72.0	184.30	184.85
51.5	76.14	76.19	72.2	186.44	187.01
52.0	77.51	77.57	72.4	188.64	189.23
52.5	78.91	78.97	72.6	190.90	191.51
53.0	80.34	80.40	72.8	193.21	193.84
53.5	81.80	81.87	73.0	195.57	196.22
54.0	83.30	83.37	73.2	197.97	198.64
54.5	84.83	84.91	73.4	200.41	201.10
55.0	86.40	86.48	73.6	202.90	203.62
55.5	88.02	88.10	73.8	205.45	206.19
56.0	89.68	89.77	74.0	208.07	208.84
56.5	91.39	91.48	74.2	210.75	211.56
57.0	93.14	93.23	74.4	213.51	214.35
57.5	94.94	95.03	74.6	216.34	217.20
58.0	96.78	96.88	74.8	219.23	220.12
58.5	98.67	98.78	75.0	222.18	223.11
59.0	100.61	100.72	75.2	225.21	226.18
59.5	102.61	102.72	75.4	228.33	229.34
60.0	104.66	104.78	75.6	231.54	232.60
60.5	106.76	106.89	75.8	234.84	235.94
61.0	108.93	109.06	76.0	238.20	239.34
61.5	111.17	111.31	76.2	241.64	242.81
62.0	113.49	113.64	76.4	245.15	246.37
62.5	115.93	116.10	76.6	248.77	250.05
63.0	118.47	118.64	76.8	252.50	253.85
63.5	121.10	121.28	77.0	256.35	257.75
64.0	123.79	123.98	77.2	260.29	261.74
64.5	126.53	126.72	77.4	264.33	265.85
65.0	129.35	129.56	77.6	268.50	270.10
65.5	132.28	132.50	77.8	272.80	274.48
66.0	135.33	135.57	78.0	277.24	279.00
66.5	138.51	138.76	78.2	281.80	283.63
67.0	141.82	142.09	78.4	286.49	288.41
67.5	145.26	145.55	78.6	291.32	293.34
68.0	148.86	149.17	78.8	296.33	298.45
68.5	152.64	152.97	79.0	301.50	303.73

Table 1 (contd)

Z	R	R′	Z	R	R′
79.2	306.85	309.20	86.9	842.56	885.73
79.4	312.36	314.82	87.0	859.68	905.41
79.6	318.03	320.62	87.1	877.38	925.93
79.8	323.92	326.68	87.2	895.71	947.24
80.0	330.09	333.02	87.3	914.73	969.38
80.2	336.46	339.52	87.4	934.45	992.51
80.4	342.99	346.20	87.5	954.84	1016.58
80.6	349.75	353.18	87.6	975.96	1041.62
80.8	356.81	360.45	87.7	997.91	1067.68
81.0	364.17	368.05	87.8	1020.64	1095.01
81.2	371.82	375.93	87.9	1044.16	1123.53
81.4	379.76	384.12	88.0	1068.53	1153.28
81.6	387.99	392.61	88.1	1093.93	1184.47
81.8	396.55	401.48	88.2	1120.27	1217.10
82.0	405.48	410.74	88.3	1147.59	1251.29
82.2	414.76	420.35	88.4	1176.01	1287.15
82.4	424.44	430.45	88.5	1205.55	1324.68
82.6	434.59	441.05	88.6	1236.25	1364.16
82.8	445.21	452.12	88.7	1268.19	1405.55
83.0	456.30	463.71	88.8	1301.38	1449.01
83.2	467.87	475.82	88.9	1335.90	1494.78
83.4	480.03	488.71	89.0	1371.84	1543.13
83.6	492.90	502.21	89.1	1409.18	1594.01
83.8	506.32	516.28	89.2	1448.01	1647.64
84.0	520.31	531.10	89.3	1488.47	1704.25
84.2	535.04	546.76	89.4	1530.70	1764.12
84.4	550.57	563.28	89.5	1574.66	1827.44
84.6	566.91	580.76	89.6	1620.40	1894.34
84.8	584.18	599.35	89.7	1668.02	1965.25
85.0	602.50	619.11	89.8	1717.65	2040.56
85.1	612.07	629.38	89.9	1769.36	2123.12
85.2	621.88	639.99	90.0	1823.24	2205.54
85.3	631.94	650.89	90.1	1879.28	2298.34
85.4	642.32	662.10	90.2	1937.63	2392.18
85.5	652.95	673.70	90.3	1998.35	2495.00
85.6	663.88	685.73	90.4	2062.49	2604.75
85.7	675.18	698.15	90.5	2130.07	2722.08
85.8	686.86	710.99	90.6	2196.81	2847.58
85.9	698.89	724.30	90.7	2269.53	2982.06
86.0	711.31	738.00	90.8	2343.68	3126.84
86.1	724.15	752.11	90.9	2419.93	3282.69
86.2	737.33	766.87	91.0	2500.71	3450.46
86.3	750.87	782.12	91.1	2584.52	3632.11
86.4	764.99	797.78	91.2	2671.66	3827.51
86.5	779.57	814.09	91.3	2762.19	4039.04
86.6	794.50	831.04	91.4	2856.17	4269.13
86.7	809.95	848.62	91.5	2953.70	4519.72
86.8	825.98	866.83	91.6	3055.07	4792.26

Table 1 (contd)

Z	R	R′	Z	R	R′
91.7	3160.32	5090.87	92.4	4009.10	8246.36
91.8	3269.46	5418.31	92.5	4147.07	8926.70
91.9	3382.48	5777.87	92.6	4289.48	9692.48
92.0	3499.59	6174.23	92.7	4436.33	10560.24
92.1	3621.06	6612.15	92.8	4587.50	11551.26
92.2	3746.26	7097.56	92.9	4742.84	12684.70
92.3	3875.53	7638.78	93.0	4902.77	13986.89

Table 2. Maximum refraction model residuals for selected P, T, and ranges of Z

Temperature, °C	Maximum refraction model residuals, sec		
	$P = 700$	$P = 760$	$P = 800$
a. $0° \leq Z \leq 85°$			
−10	+4.59	+4.87	+5.05
0	+5.25	+5.59	+5.82
+10	+5.83	+6.24	+6.51
+20	+6.41	+6.88	+7.18
+30	+6.98	+7.50	+7.83
b. $85° \leq Z < 93°$			
−10	−15.41	−18.36	−24.30
0	−13.56	−15.03	−17.45
+10	−11.91	−14.27	−14.02
+20	−15.16	−14.77	−12.61
+30	−19.20	−16.20	+13.94

Table 3. Maximum refraction model residuals for selected P, T, and ranges of Z: $\Delta_1, \Delta_2, \Delta_3 = 0$

Temperature, °C	Maximum refraction model residuals, sec		
	$P = 700$	$P = 760$	$P = 800$
a. $0° \leq Z \leq 85°$			
−10	+6.06	+6.38	+6.57
0	+5.33	+5.61	+5.78
+10	+4.68	+4.93	+5.08
+20	+4.11	+4.32	+4.45
+30	+3.59	−5.41	−6.06
b. $85° \leq Z < 93°$			
−10	+102.05	−188.07	−278.89
0	−130.49	−251.98	−338.33
+10	−196.42	−312.90	−395.56
+20	−258.65	−370.69	−450.09
+30	−317.28	−452.40	−501.90

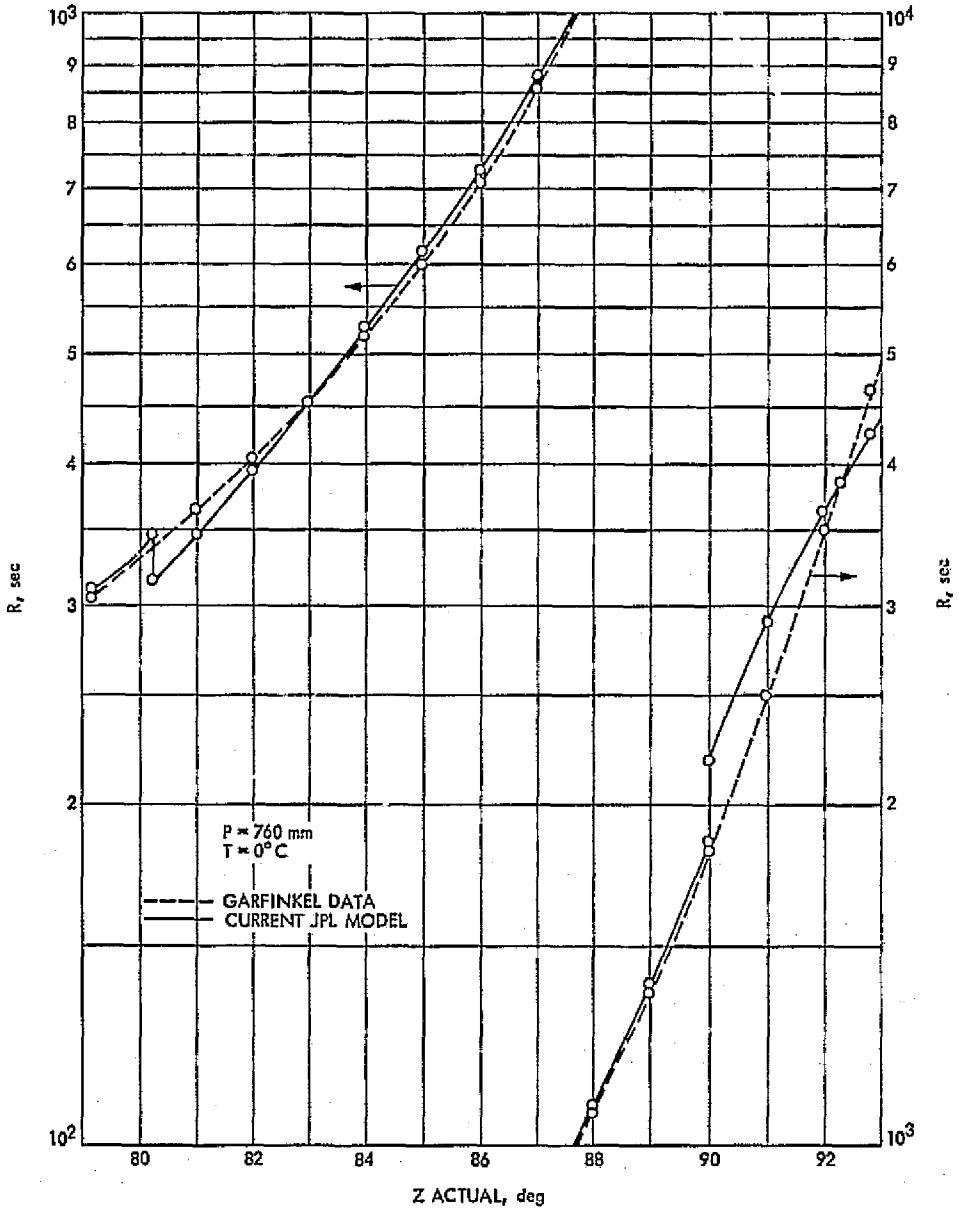

Fig. 1. Current 3-segment JPL angular refraction model versus Garfinkel refraction data

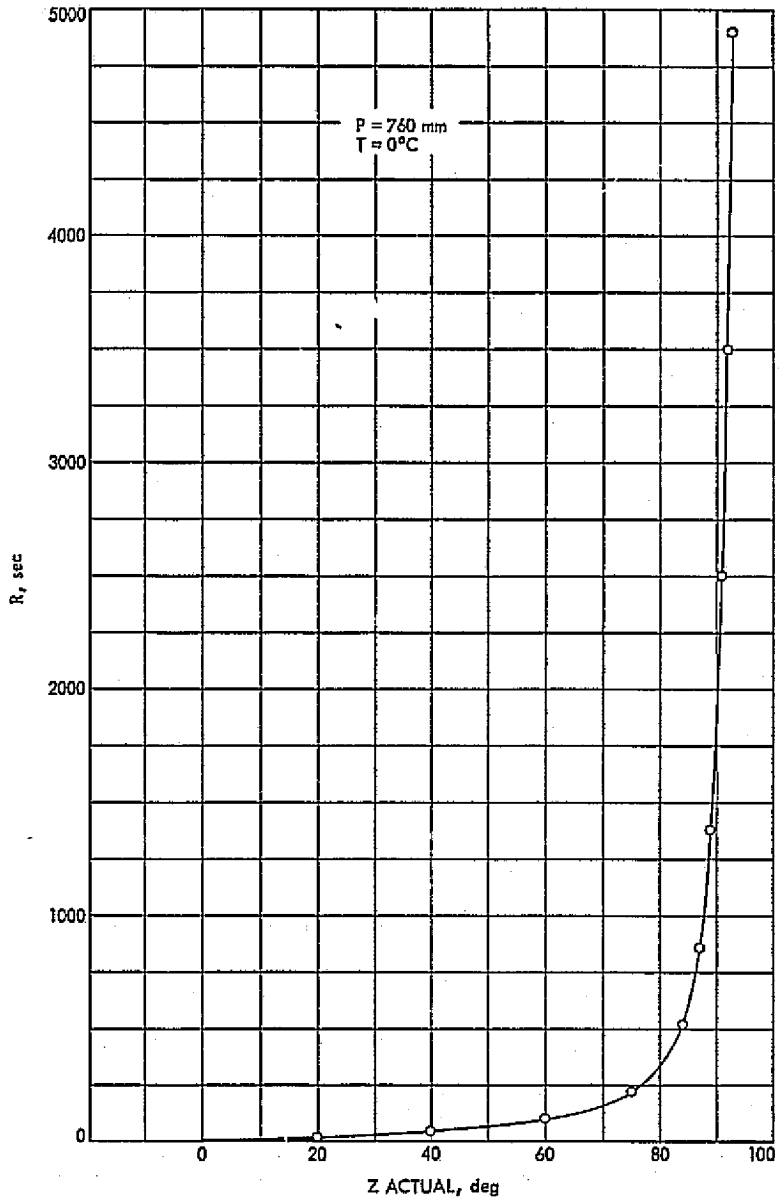

Fig. 2. Garfinkel refraction data

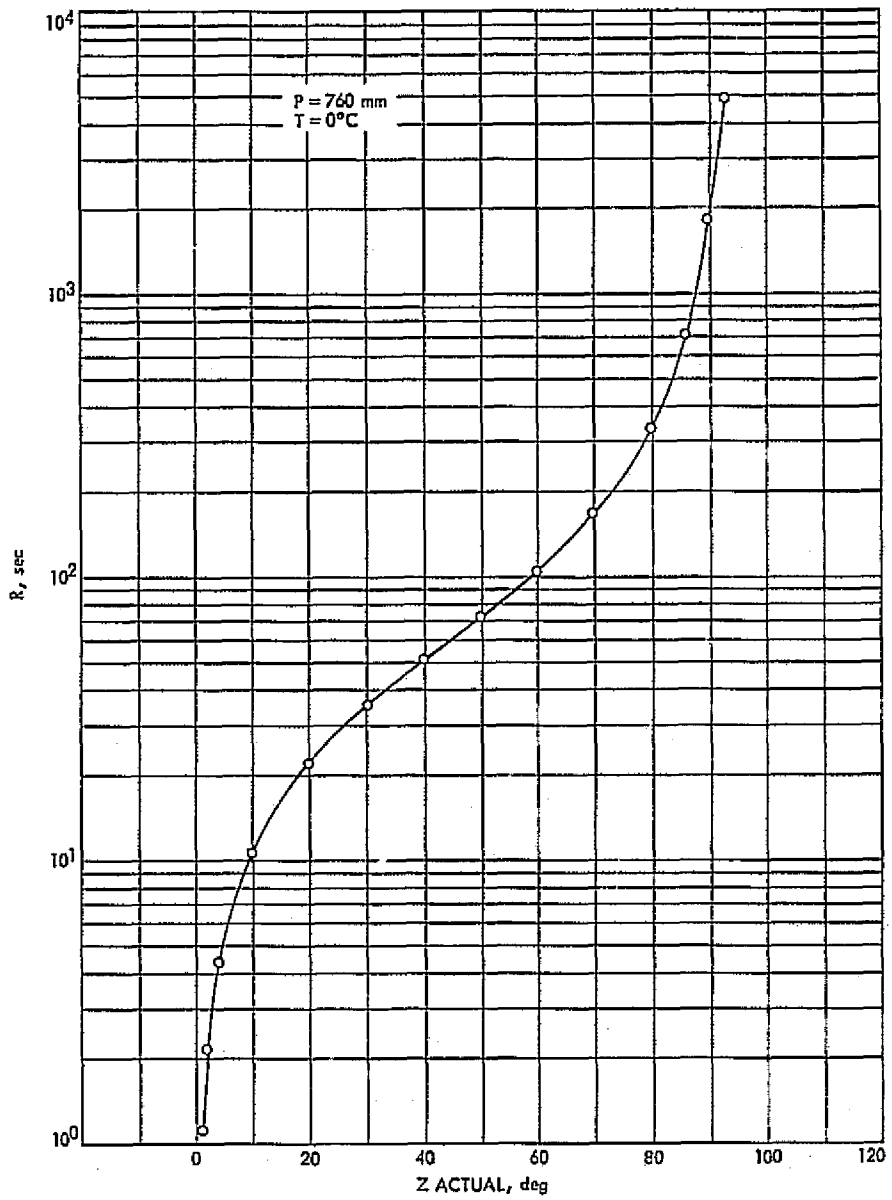

Fig. 3. Garfinkel refraction data (logarithmic)

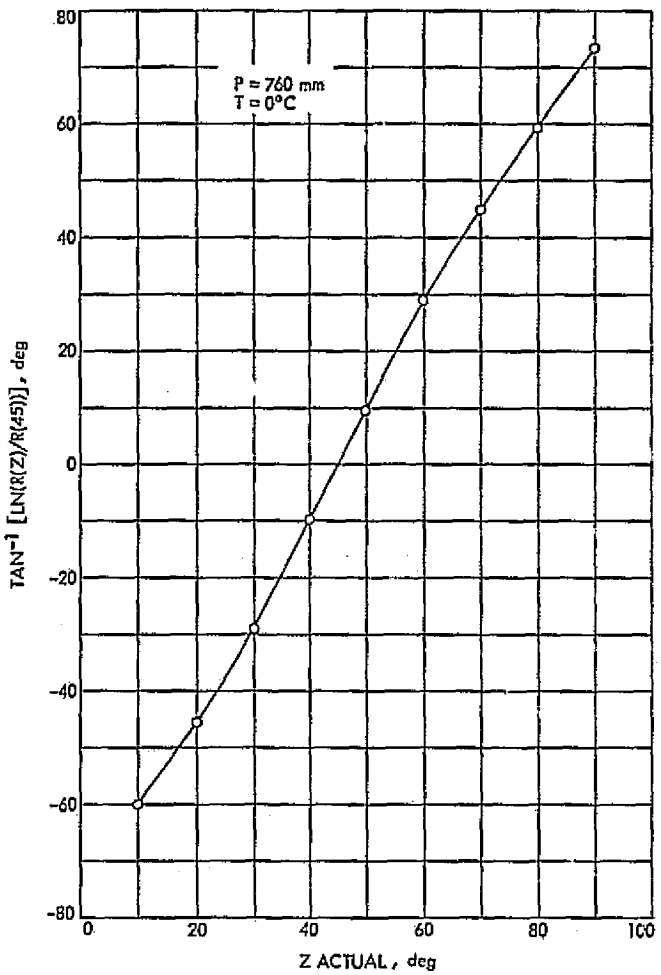

Fig. 4. Garfinkel refraction data (arctan (ln *R*))

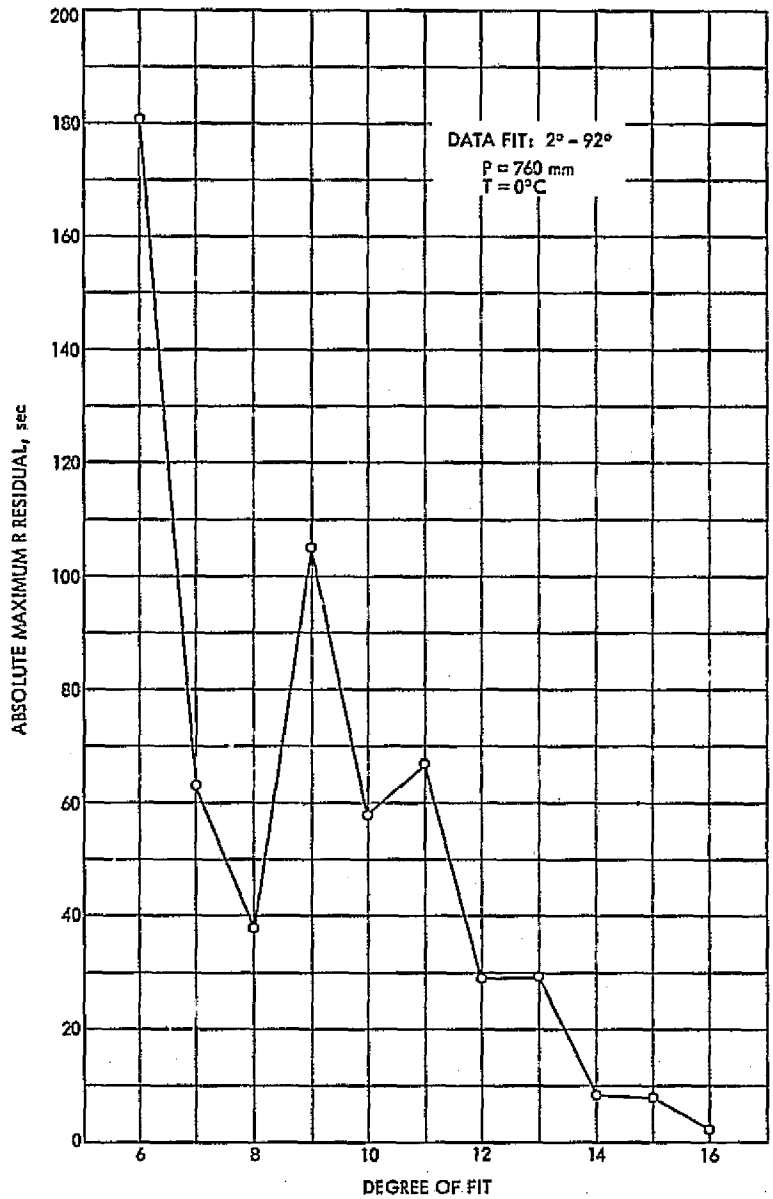

Fig. 5. Least squares fit of ln R (Garfinkel data) to an nth degree polynomial

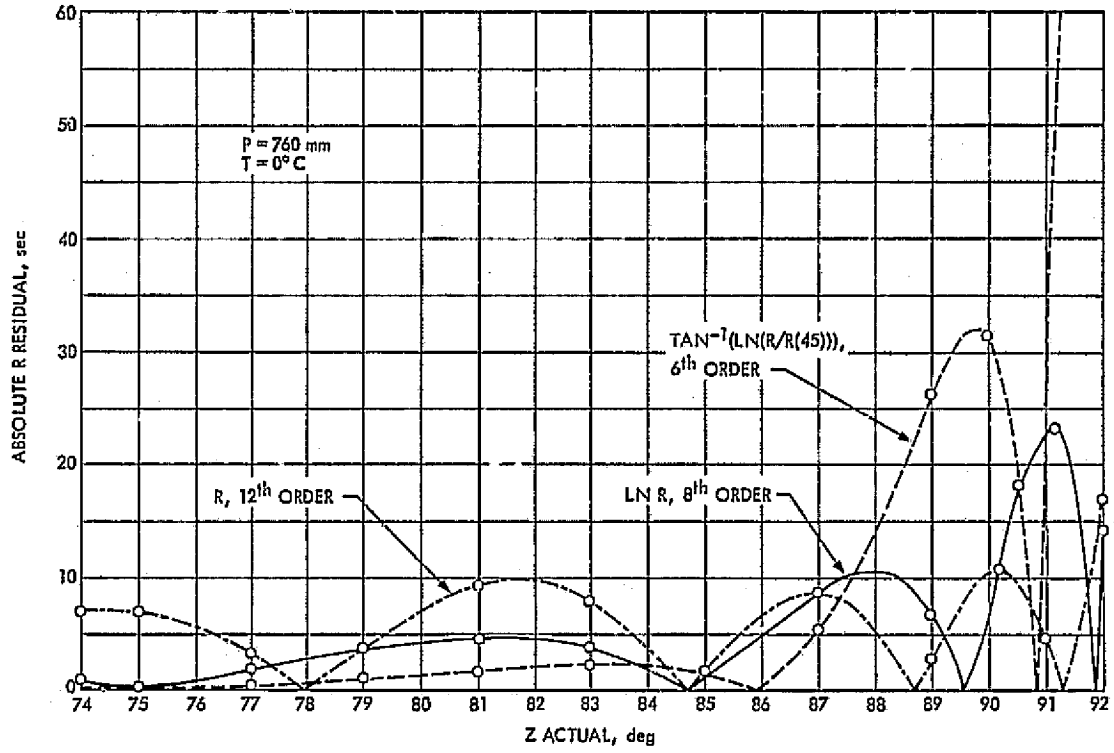

Fig. 6. Various functional forms of R fit to an nth degree polynomial

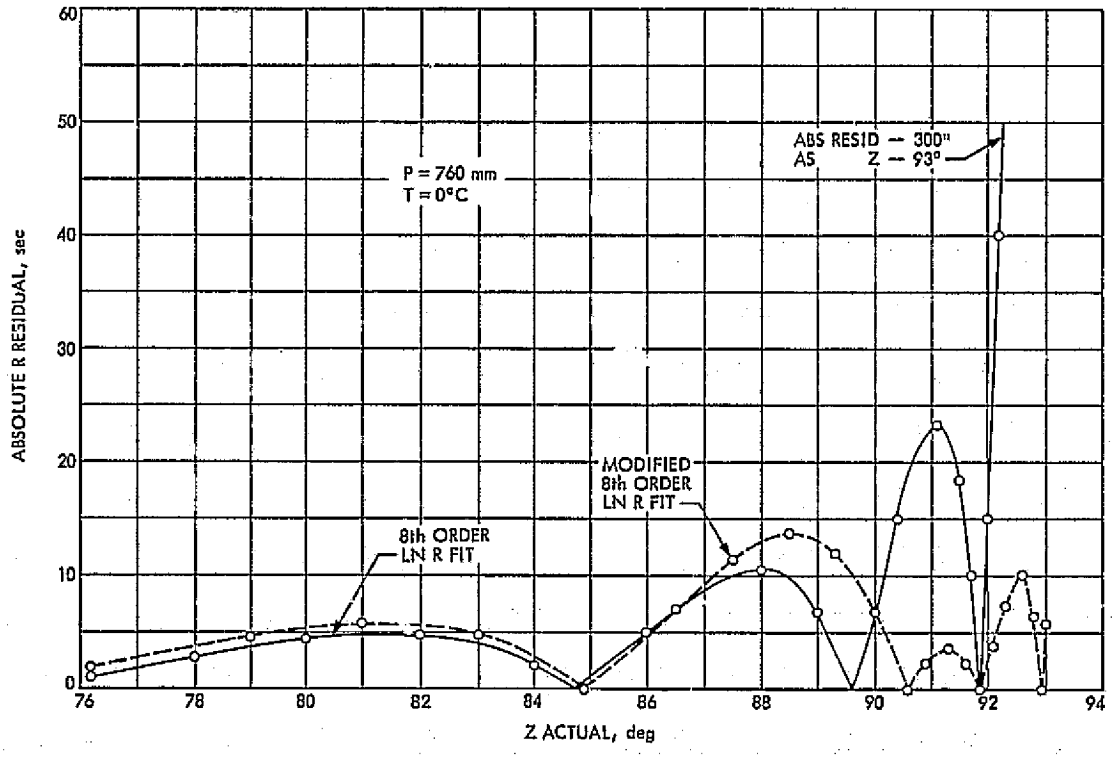

Fig. 7. 8th degree and modified 8th degree polynomial fit to ln R (Garfinkel data)

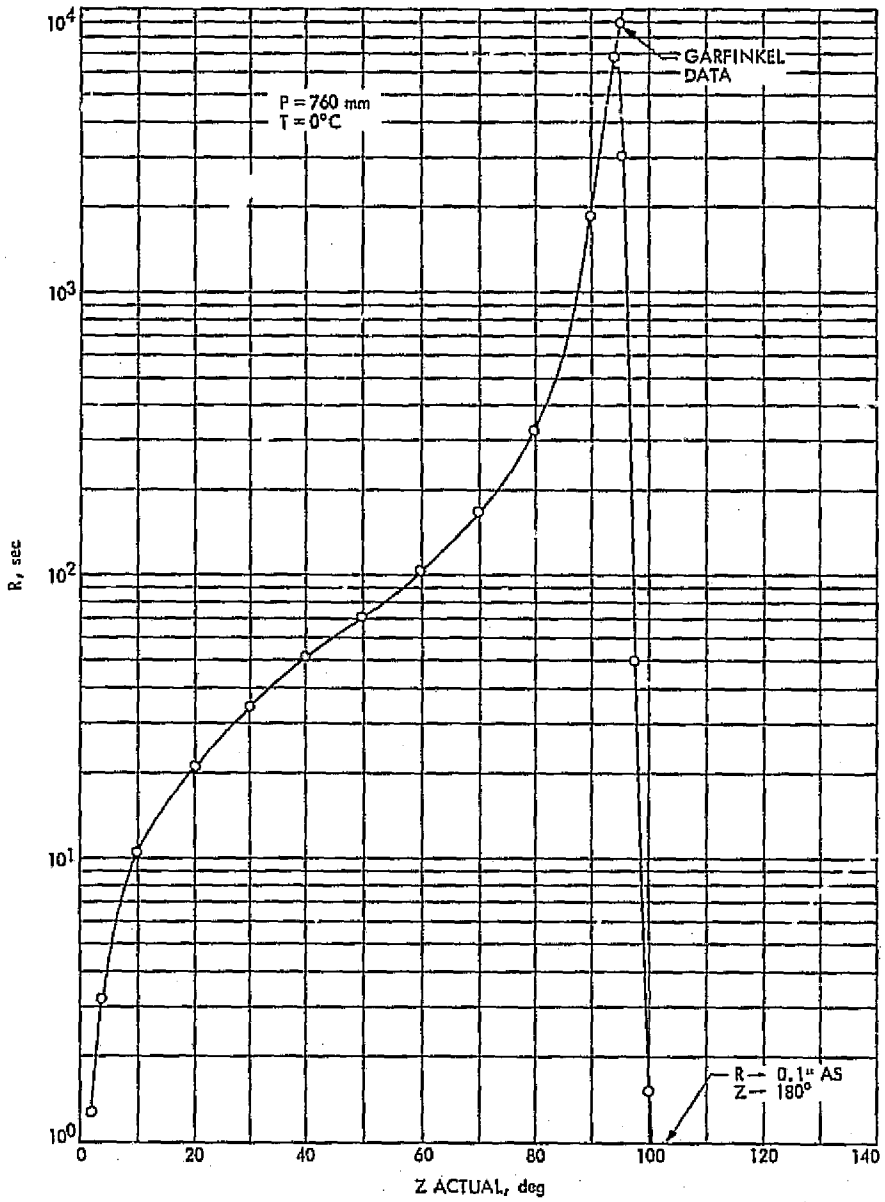

Fig. 8. Berman-Rockwell refraction model

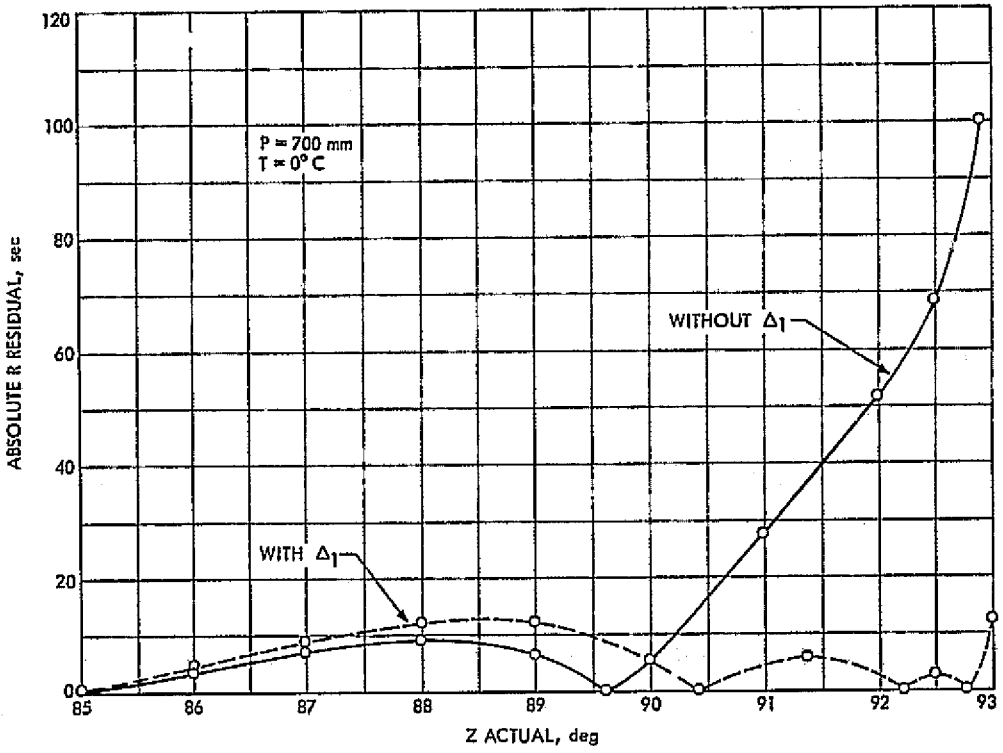

Fig. 9. Refraction model with and without Δ_1 (pressure correction factor)

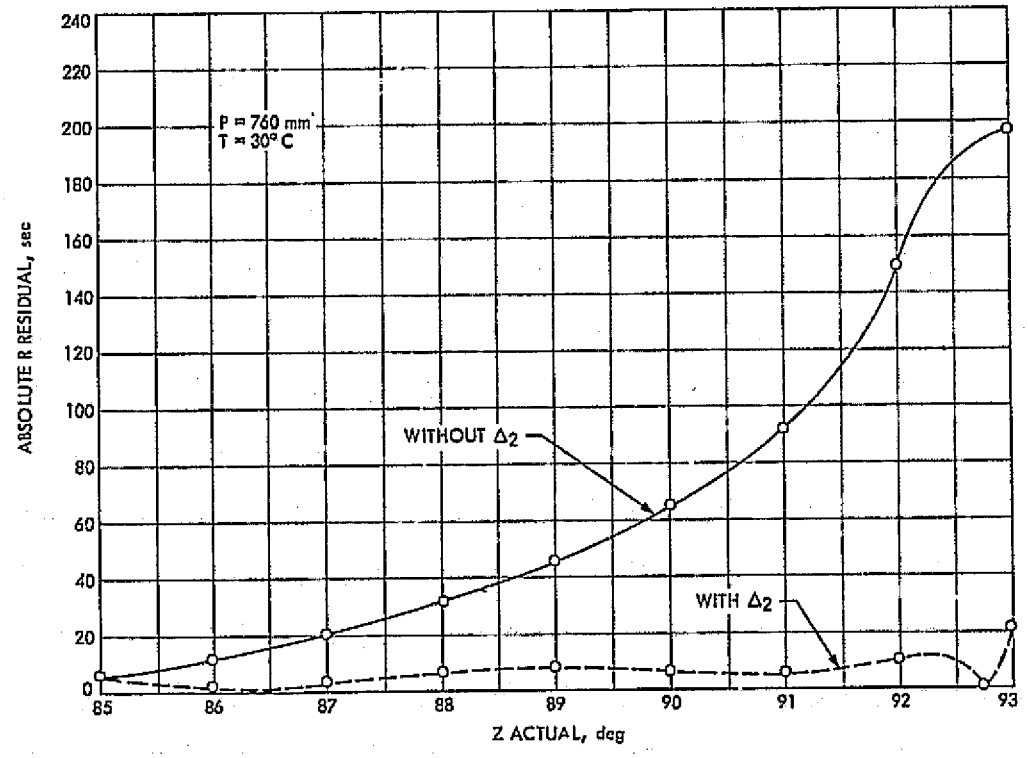

Fig. 10. Refraction model with and without Δ_2 (temperature correction factor)

Appendix A

```
00101      1*          SUBROUTINE BEND(PRESS,TEMP,ZNITH,R)
00103      2*          DIMENSION A(2),B(2),C(2),E(12),P(2),T(2),Z(2)
00104      3*          P(1) = 760.00
00105      4*          P(2) = PRESS
00106      5*          T(1) = 273.00
00107      6*          T( ) = TEMP
00110      7*          Z(1) = 91.870
00111      8*          Z(2) = ZNITH
00112      9*          A(1) = .40816
00113     10*          A(2) = 112.30
00114     11*          B(1) = .12820
00115     12*          B(2) = 142.88
00116     13*          C(1) = .80000
00117     14*          C(2) = 99.344
00120     15*          E(1) = 46.625
00121     16*          E(2) = 45.375
00122     17*          E(3) = 4.1572
00123     18*          E(4) = 1.4468
00124     19*          E(5) = .25391
00125     20*          E(6) = 2.2716
00126     21*          E(7) =-1.3465
00127     22*          E(8) =-4.3877
00130     23*          E(9) = 3.1484
00131     24*          E(10)= 4.5201
00132     25*          E(11)=-1.8982
00133     26*          E(12)= .89000
00134     27*          D3=1.+DELTA(Z,C,Z(2))
00135     28*          FP=(P(2)/P(1))*(1.-DELTA(P,A,Z(2))/D3)
00136     29*          FT=(T(1)/T(2))*(1.-DELTA(T,B,Z(2))/D3)
00137     30*          U=(Z(2)-E(1))/E(2)
00140     31*          X=E(11)
00141     32*          DO 1 I=1,8
00144     33*        1 X=E(11-I)+U*X
00146     34*          R=FT*FP*(EXP(X/D3)-E(12))
00147     35*          RETURN
00150     36*          END
```

```
00101      1*          FUNCTION DELTA(A,B,Z)
00103      2*          DIMENSION A(2),B(2)
00104      3*          DELTA=(A(2)-A(1))*EXP(B(1)*(Z-B(2)))
00105      4*          RETURN
00106      5*          END
```

Appendix B

```
00101      1*          SUBROUTINE BEND(PRESS,TEMP,ZNITH,R)
00103      2*          DIMENSION E(12)
00104      3*          P    = 760.00
00105      4*          T    = 273.00
00106      5*          E(1) = 46.625
00107      6*          E(2) = 45.375
00110      7*          E(3) = 4.1572
00111      8*          E(4) = 1.4468
00112      9*          E(5) = .25391
00113     10*          E(6) = 2.2716
00114     11*          E(7) =-1.3465
00115     12*          E(8) =-4.3877
00116     13*          E(9) = 3.1484
00117     14*          E(10)= 4.5201
00120     15*          E(11)=-1.8982
00121     16*          E(12)= .89000
00122     17*          FP=PRESS/P
00123     18*          FT=T/TEMP
00124     19*          U=(ZNITH-E(1))/E(2)
00125     20*          X=E(11)
00126     21*          DO 1 I=1,8
00131     22*        1 X=E(11-I)+U*X
00133     23*          R=FT*FP*(EXP(X)-E(12))
00134     24*          RETURN
00135     25*          END
```

Support of the Mariner 10 Television Enhancement Experiment

J. E. Allen
Network Operations

This article describes the support provided by DSN Operations for the Mariner 10 Television Enhancement Experiment that was conducted during the second Mercury encounter. The experiment included antenna arraying at the Goldstone Deep Space Stations (DSSs 12, 13, and 14) and signal combining at DSS 14 of the spacecraft's uncoded 117.6-kbps high-rate telemetry data. In addition, analog recordings of symbol synchronizer assembly outputs were made at DSSs 14 and 43 during the encounter pass view period overlap for later processing and correlation at JPL to improve the video data beyond the quality that could be obtained from a single recording.

I. Introduction

During the second Mercury encounter, more than 500 photographs were taken by the Mariner 10 spacecraft. As with the first encounter, the mission profile required real-time evaluation of video data at JPL. This required the DSN to reestablish the capability of formatting the high-rate telemetry data (117.6 kbps) at DSS 14 and transmitting the data to JPL in real-time. Additionally, in response to a Mariner 10 Project request and with TDA office concurrence, the DSN supported a research and development (R&D) TV Enhancement Experiment.

II. Wideband Data Transmission Capability

The 230-kbps wideband system, which is described in detail in Ref. 1, was removed from DSS 14 in April 1974 with the understanding that it would not be needed for the second Mercury encounter (ME II). Subsequently, however, the decision was made to provide the same support for ME II that was provided for the first encounter.

The wideband system was reinstalled at DSS 14 under the authority of Engineering Change Orders (ECO) 74.191

and 74.192. Equipment was delivered to DSS 14 on August 19, 1974, and installation and checkout were completed on September 1, 1974. Data flow tests with live spacecraft data were conducted from September 3 through September 5, 1974. In summary, the wideband system was installed and declared operational in only 15 days.

III. Television Enhancement Experiment

A. Purpose

The overall purpose of the TV enhancement experiment (Fig. 1) was to improve the quality of the television pictures received from the spacecraft during ME II. This was accomplished by arraying the antennas at Goldstone DSSs 12, 13, and 14 and combining the signals at DSS 14 for real-time transmission to JPL at Pasadena. In addition to the antenna arraying, DSS 14 and DSS 43 produced analog recordings of the Symbol Synchronizer Assembly (SSA) integral bit values for post-encounter cross-correlation of the recordings at JPL to achieve improvement in the quality of the video data.

B. Antenna Arraying and Signal Combining

DSSs 12, 13, and 14 operated in the low-noise, listen-only mode (no uplink was required during the encounter pass). The receiver baseband data from DSSs 12 and 13 were microwaved to DSS 14. The DSS 14 receiver baseband data were microwaved to the Communications Switching Center at Goldstone (GCF 10) and back to DSS 14 to realize the required signal delay. The microwaved signals were then phased and mixed at DSS 14 by using an R&D signal combiner device. The R&D signal combiner then outputted the telemetry signal to the Subcarrier Demodulator Assembly (SDA) for up-conversion and normal data handling by one of DSS 14's two data handling equipment strings to produce digital Original Data Records (ODR) and transmission to JPL. In parallel with this activity, the other data handling string was used for normal data processing and recording of telemetry data. Under the authority of ECO 74.189, the multiple antenna signal combiner and the microwave link were assembled and installed at Goldstone by September 3, 1974.

C. Results of Antenna Arraying

Pre-encounter testing took place from September 3 through September 10, 1974. In-flight testing was conducted from September 10 through September 20, 1974. During the in-flight testing, signal-to-noise ratio (SNR) improvement due to antenna arraying was observed to vary from 0.1 to 1.2 dB. The average SNR improvement was 0.60 dB. The improvement was measured by comparing the SNR from the combined signal with the SNR from the uncombined signal from DSS 14 and calculating the average difference. On encounter day, the average improvement in SNR with the combined signal was observed and reported by the Mariner project representative as being 0.35 dB.

It has been theorized that the difference between the SNR improvements obtained on encounter day (0.35 dB) and the SNR improvement obtained during the in-flight testing (0.60 dB) probably can be attributed to differences in the methods used to take the measurements. The in-flight test measurements were plotted from the bit error rate (BER) output of the Mission Test/Telemetry Computing Facility. On encounter day, the SNR was extracted directly from the telemetry data stream.

Throughout the Mariner mission, the SNR extracted from the telemetry stream has been averaging 0.2 dB lower than the SNR obtained by using the theoretical BER curves. Therefore, by adding the 0.2 dB to the SNR observed on encounter day, the telemetry SNR improvement due to antenna arraying would have been 0.55 dB, or approximately the same as was observed during the in-flight testing (0.60 dB). The SNR differences are still under investigation by the Project's telecommunication representative.

D. Real-Time Operations

The TV Enhancement Experiment operation was conducted under the direction of the experiment's team leader from Division 33. DSN Operations coordinated and controlled the overall operation and provided the following special operational capabilities for conducting the experiment:

(1) An internal voice net between the experiment team leader at DSS 14 and the receiver operators at DSSs 12 and 13.

(2) A voice net between the team leader at DSS 14 and an experiment project advisor at JPL. All operational communications between the Mariner Project and the enhancement experiment were conducted through this link.

The DSN established as a guideline that, in the event of a failure of the prime telemetry string at DSS 14, the Station Operations Supervisor, after normal coordination with the flight project via Net Control, would reconfigure the string being used for the experiment to provide operational support. This did not happen because the

operational telemetry string and the enhancement string operated without any failures.

E. Non-Real-Time TV Enhancement Experiment

In non-real-time, dedicated recorders (occultation recorders) were made available to produce special recording of SSA integral bit values during the overlap periods at DSSs 14 and 43. The output of the SSA J-2 port was cabled to the FR 1400 recorder for 7-channel recording of significant bit values. The analog tapes were delivered to the Project for processing at JPL. As of this time, the recordings have not been processed.

Equipment modifications for supporting the non-real-time portion of the TV Enhancement Experiment were completed at DSSs 14 and 43 under ECO 74.214 on 14 September 1974.

Reference

1. Hatch, J. T., and Capps, J. W., "Real-Time High-Rate Telemetry Support of Mariner 10 Operations," in *The Deep Space Network Progress Report 42-23*, pp. 125–131, Jet Propulsion Laboratory, Pasadena, California, July and August 1974.

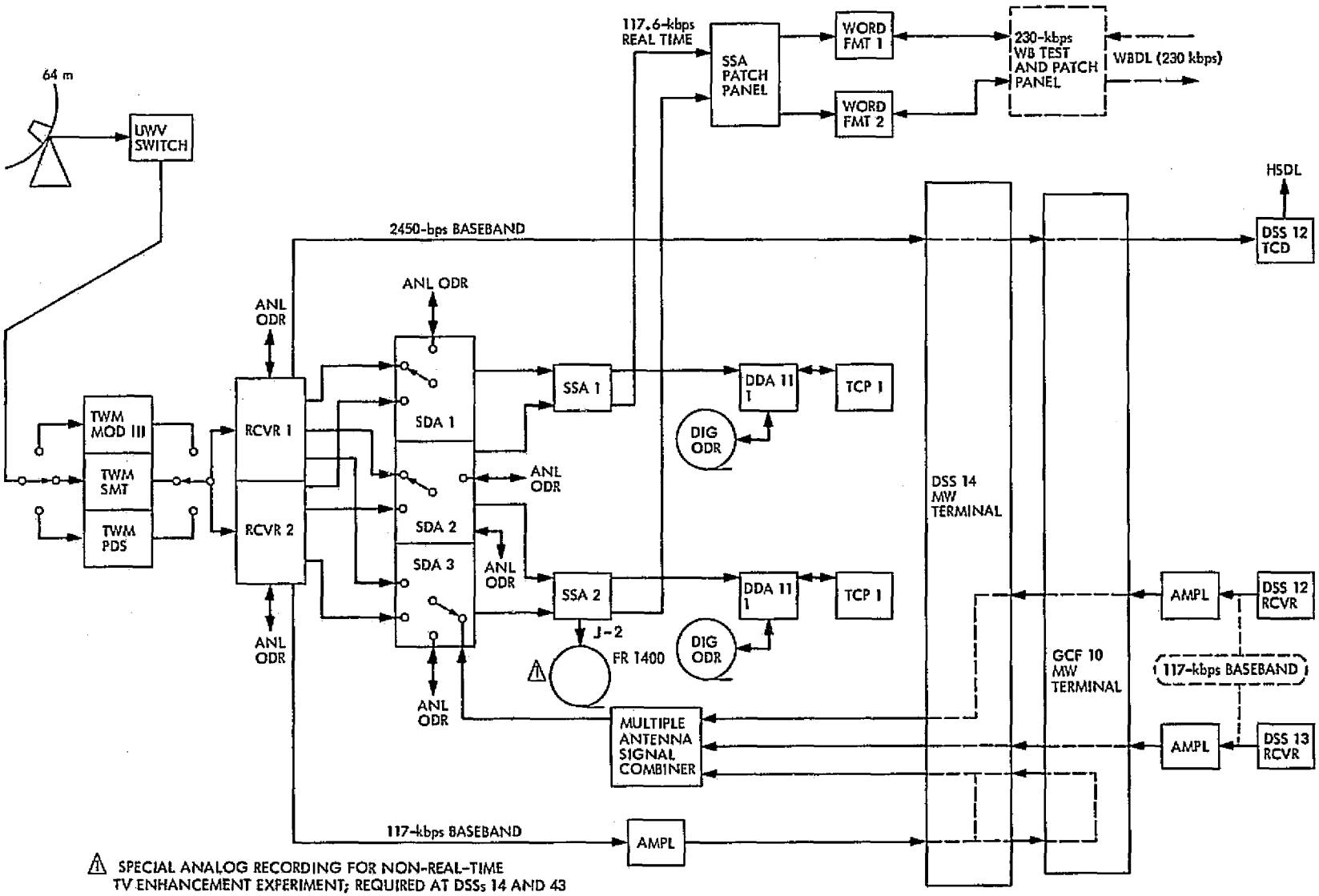

Fig. 1. DSN Mercury II TV Enhancement Experiment configuration